SCREENING AND IMPROVING THE SAFE PROVISION OF MESENCHYMAL STEM CELLS IN REGENERATIVE MEDICINE: AN *IN VITRO* STUDY

Doctor of Philosophy

by

Jonathan James Sheard

Aston University

October 2016

Aston University

SCREENING AND IMPROVING THE SAFE PROVISION OF MESENCHYMAL STEM CELLS IN REGENERATIVE MEDICINE: AN IN VITRO STUDY

Jonathan James Sheard **Doctor of Philosophy, 2016**

Thesis Summary

A number of studies have suggested that mesenchymal stem cells (MSCs) may undergo genetic alterations and spontaneous malignant transformation to form tumour cells, or at least can become contaminated with other cell types following extended periods in culture. Possible transformation or contamination of MSCs during cell culture expansion prior to their use in transplantation therapies is a risk, which should be taken into account. There is a continued need for the development of improved tools for monitoring safety and release criteria of cells intended for cell-based therapies.

In order to help address these risks, this thesis aimed to develop improved safety measures in MSC-based cell therapies. Initially, this was investigated through the use of microscopic imaging and image analysis platforms to screen, characterise and distinguish between cultures of non-transformed MSCs and MSC-derived tumour cells, i.e. the osteosarcoma cell lines, SAOS2 and MG63, as well as cells derived from a chondrosarcoma. High content screening (HCS) and live-cell imaging and analysis platforms were used to enable these experiments. Phenotypic features that distinguished the normal versus malignant cell types were identified, including immunoreactivity for the proliferation-associated Ki67 antigen and pluripotency marker Oct4, as well as significant differences in nuclear morphology. These findings help inform release criteria for therapeutic MSCs.

To further potentially improve the safety of MSC-based therapies, research was also performed to address the possibility that tumour cells in MSC cultures might remain undetected, thereby still providing a risk in MSC transplantations. Novel combinatorial regimes of potential anti-tumour drugs, i.e. bezafibrate, medroxyprogesterone, and valproic acid (termed V-BAP) were tested in vitro for their effects on MSCs versus SAOS2 and MG63 cells. At determined concentrations, these drugs were shown to significantly inhibit the growth of the osteosarcoma cells, but had little effect on MSCs.

Thus, this thesis has made inroads into improved safety of MSC-based therapies by (i) demonstrating the application of imaging-based cell screening platforms to help characterise MSC cultures intended for cell transplantation, and (ii) identifying a novel drug regime that selectively targets osteosarcoma cells whilst having little effect on MSCs. The findings on V-BAP also have application in anti-tumour treatments for osteosarcoma.

Key words: Mesenchymal stem cell; High content screening; Live cell image analysis; Osteosarcoma; Cell-based therapy.

Dedication

I would like to dedicate this thesis to my G-d, the G-d of Abraham, Isaac and Jacob and to my L-rd Yeshua Ha'Mashiah. I would also like to dedicate it to my beloved family, especially my grandmothers Lucinda Nessy Walters Hopkins Brinton Banks Nelson Kelly-Edwards and Anette Marie Sheard.

"I have set the L-RD always before me; because He is at my right hand I shall not be moved."

Psalm 16 vs 18 (NKJV).

Acknowledgements

I would like to take this opportunity to express my thanks and appreciation for all those, without whom, this thesis would not have been possible. I would like to acknowledge the patients who donated their tissue for this research and the Biotechnology and Biomedical Sciences Research Council for their funding. I would also like to thank Imagen Biotech Ltd for their collaborative contribution towards this project.

I would like to especially thank Dr Eustace Johnson for his patience, time and effort whilst supervising me through this degree, for teaching me how to balance work and a social life, for educating me in all things cheese and wine, but mostly for helping me realise my potential and priorities in life.

I would also like to thank my colleagues, Dr Merlin Walter, Htoo Wai, Nupur Kohli and Ibtesam Al-delfi for their company, companionship, constant support and unwavering friendship through these last years. I would like to thank all of my fellow PhD students, my friends, who have also been there through the good times and the bad times, the braais and the office 'meetings'. I would especially like to thank Dr Nai Yu Yeh for her amazing support, patience and friendship and for sticking with me through the busiest and most stressful days.

Finally, I would like to acknowledge and deeply thank my family, especially my parents. They have all prayed for me day and night, encouraged and supported me through each and every phase.

List of Contents

List of Abbreviations

2HG	R(-)-2-hydroxygluterate
15d-PGJ2	15-deoxy Δ12, 14prostaglandin J2
Ab	Antibody
ACI	Autologous chondrocyte implantation
ATMSC	Adipose tissue derived mesenchymal stem cell
ALP	Alkaline phosphatase
AML	Acute myeloid leukaemia
ANOVA	Analysis of variance
ATMP	Advanced therapy medicinal product
BAP	Bezafibrate with medroxyprogesterone acetate
BEZ	Bezafibrate
BMA	Bone marrow aspirate
BMMSC	Bone marrow derived mesenchymal stem cell
BMMNC	Bone marrow derived mononuclear cell
BMP	Bone morphogenic protein
BSA	Bovine serum albumin
CD	Cluster of differentiation
CFU-F	Colony forming unit fibroblast
CO_2	Carbon dioxide
CS	Chondrosarcoma derived cells
DEX	Dexamethasone
DMEM	Dulbecco's modified Eagle's medium
DMSO	Dimethyl sulphoxide
DOX	Doxorubicin
DR	Death receptor
DXT	Deep X-ray therapy
ESC	Embryonic stem cell
FACS	Flow assisted cell sorting
FAK	Focal adhesion kinase
FCS	Foetal calf serum
FSC	Forward scatter
FISH	Fluorescence *in situ* hybridisation
GAG	Glycosaminoglycan
GMP	Good Manufacturing Practice
HCl	Hydrogen chloride
HCS	High Content Screening
HDAC	Histone deacetylase
HIF 1α	Hypoxia inducible factor 1α
HSC	Haematopoietic stem cell
IBMX	3-isobutyl-1-methylxanthine
IDH	Isocitrate dehydrogenase
Ig	Immunoglobulin
iPSC	Induced pluripotent stem cell
ITS	Insulin Transferrin Selenium

LREC	Local research ethical committee
LWR	Length width ratio
MMP	Matrix metalloproteinase
MPA	Medroxyprogesterone acetate
mRNA	Messenger ribonucleic acid
MSC	Mesenchymal stem cell
MTT	3-(4,5-dimethylthiazol-2-yl)-2,5-diphenyltetrazolium bromide
NAD	Nicotinamide adenine dinucleotide
NADP	Nicotinamide adenine dinucleotide phosphate
NSC	Neuronal stem cell
OA	Osteoarthritis
OEC	Olfactory ensheathing cell
OS	Osteosarcoma
P	Passage
P2A	Perimeter to area ratio
pHH3	Phosphorylated histone H3
PBS	Phosphate buffered saline
PCR	Polymerase chain reaction
PE	Phycoerythrin
pFAK	Phosphorylated focal adhesion kinase
PGD2	Prostaglandin D2
PL	Platelet lysate
PPARγ	Proliferator-activated receptor-γ
pRb	Phosphorylated retinoblastoma protein
PS	Penicillin streptomycin
Rb	Retinoblastoma protein
RJAH	Robert Jones and Agnes Hunt
ROH	Royal Orthopaedic Hospital
ROI	Region of interest
ROS	Reactive oxygen species
RT PCR	Reverse transcription polymerase chain reaction
SCI	Spinal cord injury
SD	Standard deviation of the mean
SEM	Standard error of the mean
SFM	Serum free media
SSC	Side scatter
TBS-T	Tris-phosphate buffered saline with Tween 20
TCP	Tissue culture plastic
TGF	Transforming growth factor
TNF	Tumour necrosis factor
TRAIL	Tumour necrosis factor-related apoptosis-inducing ligand
Tris-HCl	Tris-buffered saline
V-BAP	Bezafibrate, Medroxyprogesterone acetate and Valproic Acid
VPA	Valproic acid

List of Tables

List of Figures

Chapter 1: General Introduction

Chapter 1: General Introduction

1.1 Regenerative Medicine

The focus of regenerative medicine is replacing or regenerating damaged or impaired tissues, to restore and establish normal function (Daar and Greenwood, 2007). Wound healing involves the recruitment and proliferation of cells capable of restoring tissues and even organs to their original form and function. This happens naturally within the body often without our knowledge; however, ageing, tissue loss and damage due to trauma or disease can take the body beyond the point of self-repair (Rosenthal, 2003). In these circumstances, cell therapies and tissue engineering, which are part of the broader remit of regenerative medicine, aim to deliver safe, effective and consistent therapies (Polak, 2009).

Cell based therapies include the use of somatic cells, such as the treatment of deep cartilage defects by autologous chondrocyte implantation (ACI) (Brittberg *et al.*, 1994, Roberts *et al.*, 2003); skin cells, such as the treatment of full-thickness wounds with cultured keratinocytes (Wright *et al.*, 1998); or stem cells. The use of these cells for cell-based therapies will be discussed in more detail in context of specific clinical applications further along in this review.

Broadly speaking, there are two main types of stem cells - embryonic and non-embryonic (also termed adult-derived stem cells). Embryonic stem cells (ESC) are derived from the inner cell mass of mammalian blastocysts and have the ability to grow indefinitely while maintaining pluripotency, that is, the ability to differentiate into cells of all three germ layers (Evans and Kaufman, 1981, Martin, 1981).

Non-embryonic stem cells include:

(i) induced pluripotent stem cells (iPSCs), which are differentiated somatic-derived cells reprogrammed into an undifferentiated pluripotent state by the introduction of four transcription factors (Oct-3/4, Sox2, c-Myc and KLF4) (Takahashi and Yamanaka, 2006, Takahashi *et al.*, 2007);

(ii) umbilical cord derived stem cells, which contain multipotent haematopoietic stem cells (Gluckman *et al.*, 1989) and mesenchymal progenitor cells isolated from the umbilical cord blood (Erices, Conget and Minguell, 2000), as well as mesenchymal stem cells isolated from the Wharton's Jelly (Wang *et al.*, 2004);

(iii) bone-marrow derived haematopoietic stem cells (HSCs), which are the multipotent self-renewing stem cells of the blood system and have the ability to differentiate into all the distinct mature blood cell types, as reviewed by Seita and Weissman, (2010);

(iv) mesenchymal stem cells (MSCs), which are multipotent plastic adherent stromal cells, typically isolated from the bone marrow and partially defined by their ability to differentiate into bone, fat and cartilage (Pittenger, 1999). MSCs are a common cell type used in orthopaedic disease and injury and were the stem cell used throughout this thesis.

This review will briefly discuss the history, isolation, identification and differentiation of adult human derived MSCs, whilst focusing on the safe use and provision of MSCs within clinical applications, notably within orthopaedic pathologies, spinal cord injury (SCI) and its sequalea, namely pressure ulcers and finally skin wound healing. Issues surrounding these clinical applications and the safe GMP culture expansion and manufacturing of MSCs will also be considered. Lastly, the proposed use of a high content screening (HCS) and live-cell imaging platform to facilitate the safe provision, characterisation and screening of MSCs for cell-based therapies, will be discussed in relation to known and current technologies, such as flow cytometry and selective cell sorting.

1.2 Mesenchymal Stem Cells

The history of MSCs:

The suggestion of a stem cell population as the origin of non-haematopoietic bone marrow cells, which contribute to wound repair and have a fibroblastic-like morphology, was made almost 150 years ago by the German-Jewish Pathologist, Julius Friedrich Cohnheim (Cohnheim, 1867, Prockop, 1997). The subsequent work conducted by the Russian Scientist, Alexander Friedenstein, from the late 1960s through the 1970s, credited him with the discovery of MSCs. He showed the critical observation that the bone marrow, in postnatal life, is a reservoir of stem cells for mesenchymal tissues. From rodent bone marrow, Friedenstein and colleagues isolated adherent, fibroblast-like clonogenic cells, termed colony forming unit-fibroblastic (CFU-F), which have a high replicative capacity *in vitro* (Friedenstein *et al.*, 1968, Chailakhyan, Fridenshtein and Vasil'ev, 1970, Friedenstein, Chailakhjan and Lalykina, 1970, Friedenstein *et al.*, 1974b).

From the late 1970s through 1990s, Friedenstein, amongst many others, went on to show that these bone marrow-derived stromal cells were responsible for transferring the microenvironment of the haemopoietic tissues (Friedenstein *et al.*, 1974a) and that there were fibroblast precursor cells in and amongst this heterogeneous population (Friedenstein *et al.*, 1974b). They examined *in vitro* cloning of the CFU-F and re-transplantation of the cells *in vivo* (Friedenstein, 1980) and found that the marrow microenvironment was able to be transferred by heterotropic transplantation of freshly isolated and cultured cells into porous sponges (Friedenstein *et al.*, 1982). Soon after, CFU-F were shown to have osteogenic differentiation potential *in vivo* (Ashton *et al.*, 1984) and mineralised *in vitro* (Howlett *et al.*, 1986, Friedenstein, Chailakhyan and Gerasimov, 1987). The cells were described as a heterogeneous stem and progenitor population of cells based on observed variations in colony size, morphology and alkaline phosphatase (ALP) activity (Owen, Cave and Joyner, 1987). Bab *et al.*, (1988) went on to isolate human marrow derived CFU-F, which formed

osteogenic tissue consisting of a mineralizing fibrous component as well as cartilage, when incubated in intraperitoneal implanted diffusion chambers within athymic mice (Bab *et al.*, 1988).

In Owen and Friedenstein's (1988) review, they recounted that some CFU-F demonstrated self-renewal and multipotency *in vivo* and when examined *in vitro*, studies showed that CFU-F were a heterogeneous population of stem and progenitor cells whose differentiation could be modified at the colony level by the addition of different factors to the culture medium. They concluded that the number and hierarchy of cell lines belonging to the stromal fibroblastic system had not yet been fully elucidated (Owen and Friedenstein, 1988).

Based on the embryonic perspective of multipotent progenitor cells located within the mesodermal layer, Caplan (1991) posed a hypothetical and comprehensive scheme. He proposed that within adult bone marrow there was a population of mesenchymal stem cells (MSCs) which could likewise give rise to a spectrum of mesenchymal tissues by differentiating along separate and distinct lineage pathways (Caplan, 1991). In 1999, Pittenger demonstrated this, by showing how cells isolated from human adult bone marrow aspirates displayed a stable phenotype in *in vitro* monolayer culture and were able to be induced to differentiate exclusively into the osteogenic, adipogenic, or chondrogenic lineages as shown in Figure 1.1 (Pittenger, 1999).

Figure 1.1: Isolated bone marrow-derived stem cells differentiate to mesenchymal lineages.

Cultured cells from donors were tested for the ability to differentiate in vitro to multiple lineages. Three donors (A through O) were each shown to differentiate appropriately to the adipogenic (Adipo), chondrogenic (Chondro), and osteogenic (Osteo) lineages. Adipogenesis was indicated by the accumulation of neutral lipid vacuoles that stain with oil red O (A, D, and G), and such changes were not evident (J) with Hs27 new-born skin fibroblasts or (M) with 1087Sk adult mammary tissue fibroblasts. Chondrogenesis was shown by staining with the C4F6 monoclonal antibody to type II collagen and by morphological changes (B, E, and H), which were not seen by similarly culturing (K) Hs27 or (N) 1087Sk cells. Osteogenesis was indicated by the increase in alkaline phosphatase (ALP) (C, F, and I) and calcium deposition, which was not seen in the (L) Hs27 or (O) 1087Sk cells (see Web Fig. 4). Figure from Pittenger, (1999).

Nearly half a century has passed since Friedenstien first described the stem cell properties of bone marrow stromal cells and the field of MSC research has thrived. The exact location of MSCs is still broadly disputed; however, as shown by Mendez-Ferrer *et al.*, (2010), MSCs have been shown to be located within the endosteal niche, where they line the bone surface and physically associate with osteoblasts, as well as within the vascular niche, where it was shown that perivascular MSCs play a critical role in maintaining a quiescent HSC pool within the bone marrow (Mendez-Ferrer *et al.*, 2010).

Some debate has occurred regarding the correct nomenclature of MSCs, proposing the cells should be known as multipotent mesenchymal stromal cells, whilst maintaining the acronym yet withholding the title 'stem cells' until they have been shown to meet specific stem cell criteria (Horwitz *et al.*, 2005). In 2008, Caplan called into question whether MSCs and perivascular cells (termed pericytes) are synonymous (Caplan, 2008). This was in response to a study that showed the perivascular niche as a possible location for MSCs. The study also showed that pericytes exhibited osteogenic, adipogenic, and chondrogenic potentials at the clonal level, expressed MSC markers of identification and migrated in a culture model of chemotaxis (Crisan *et al.*, 2008). Caplan concluded that this team, led by Bruno Péault, provided a solid set of observations which clearly linked MSCs with pericytes and that all MSCs may indeed be pericytes (that is perivascular in location), however, not all pericytes can be thought of as MSCs (Caplan, 2008).

The name 'medicinal signalling cells' has also been suggested for MSCs (Caplan, 2010). MSCs function as surveyors of their microenvironments and during local injury, they are released from their perivascular location, become activated, and establish a regenerative microenvironment by secreting bioactive molecules and regulating the local immune response, as reviewed by Caplan and Dennis, (2006). These trophic and immunomodulatory activities suggest that MSCs may indeed serve as site-regulated ''drugstores'' *in vivo* (Caplan and Dennis, 2006, Caplan and Correa, 2011b).

Identification of MSCs:

Bearing in mind the heterogeneous population of stem and progenitor cells collectively termed as CFU-F, scientists wanted to differentiate between the different cell phenotypes and reduce inconsistent identification and reporting between researchers. In 2006 the Mesenchymal and Tissue Stem Cell Committee of the International Society for Cellular Therapy (ISCT) proposed three 'minimal criteria' which should be used to define human MSCs (Dominici *et al.*, 2006).

MSCs were primarily isolated from bone marrow (BMMSCs), as demonstrated by Friedenstein's work. However, MSCs have been isolated from many other tissues (Hass *et al.*, 2011), which include (but are not limited to) adipose tissue (ATMSCs) (Peroni *et al.*, 2008), umbilical cord tissue (Erices, Conget and Minguell, 2000), amniotic fluid (In 'T Anker *et al.*, 2004) and dental pulp (Perry *et al.*, 2008). However, some argue that these minimal criteria for the identification of MSCs are 'a loose set of criteria' (Bianco *et al.*, 2013) allowing MSCs to be isolated from every tissue.

The ISCT's minimal criteria are briefly discussed below.

Firstly, they proposed that MSCs must be plastic-adherent when maintained in standard culture conditions (Dominici *et al.*, 2006). Friedenstein's initial isolation of MSCs was performed based on plastic adherence (Chailakhyan, Fridenshtein and Vasil'ev, 1970, Friedenstein, Chailakhjan and Lalykina, 1970), and it was shown to be a property of the stromal cells, which were recognised to support haemopoiesis *in vitro* and regenerate it *in vivo* (Friedenstein *et al.*, 1974a).

Secondly, MSCs must express the cluster of differentiation (CD) surface antigens; CD73 (SH-3/4), CD90 (Thy-1) and CD105 (endoglin or SH-2) in greater than 95% of the culture, and lack expression of; CD11b, CD14, CD19, CD34, CD45, CD79α or human leukocyte antigen-DR (HLA-DR) in greater than 95% of the culture (Dominici *et al.*, 2006). As reviewed by Murphy, Moncivais and Caplan, (2013), the first MSC specific markers identified were CD73 and CD105, followed soon after by CD90 and CD44, which collectively discriminated these cells from those of haematopoietic origin, but not

from fibroblasts. To ensure the isolated populations of MSC are not contaminated by other cells, cells are excluded if they are positive for CD markers associated with haematopoietic cells. As reviewed by Murphy, Moncivais and Caplan, (2013), CD11b and CD14 are prominently expressed on monocytes and macrophages, the most likely haematopoietic cells to be found in a primary MSC culture; CD34 marks primitive haematopoietic progenitors and endothelial cells; CD45 is a pan-leukocyte marker; CD19 and CD79a are markers of B cells that may also adhere to MSC in culture and remain vital through stromal interactions; and HLA-DR molecules which are not expressed on MSC unless stimulated. Interestingly, Niehage *et al.*, (2011) conducted an extensive study into the cell surface proteome of human MSCs and identified over 200 plasma membrane proteins. Of these, 33 were identified as cell adhesion molecules (CAMs), 26 were signalling receptors and 41 CD markers, 5 of which (CD97, CD112, CD239, CD276 and CD316) were novel markers for MSCs (Niehage *et al.*, 2011).Likewise, Martinez *et al.*, (2007) reported the potential use of the neural ganglioside GD2 as a single surface marker unique to BMMSCs, distinguishing them from other bone marrow cells as well as foreskin fibroblasts. As shown, MSC phenotypic characterization has been widely researched and published, but unfortunately there still remains no single CD antigen marker unique to MSCs accepted by the scientific community (Murphy, Moncivais and Caplan, 2013).

Thirdly, MSCs must differentiate into osteoblasts, adipocytes and chondrocytes *in vitro* (Dominici *et al.*, 2006) since they are known to be of mesodermal origin. The *in vitro* differentiation techniques and staining of MSCs along these differentiation pathways were elegantly shown by Pittenger, (1999) (Figure 1.1). Following treatment with β-glycerophosphate, ascorbic acid and dexamethasone, osteoblastic differentiation of MSCs is commonly shown by up regulation of alkaline phosphatase (ALP) activity and deposition of a calcium-rich mineralised extracellular matrix seen with von Kossa staining (Pittenger, 1999). Janicki *et al.*, (2011) demonstrated that in contrast to *in vitro* osteogenic differentiation parameters, a doubling-time of MSCs below 43.23 hours allowed to predict ectopic bone formation at high sensitivity (81.8%) and specificity (100%). They

also showed that gene expression profiling confirmed the key role of proliferation status toward the bone forming ability (Janicki *et al.*, 2011).

Adipogenic differentiation of MSCs is commonly shown by the accumulation of lipid-rich vacuoles within cells, and then stained with the lipophilic stains, Oil-Red-O or Nile-red-O, following treatment with dexamethasone, 1-methyl-3-isobutylxanthine (IBMX), insulin and indomethacin (Pittenger, 1999).

Finally, chondrogenic differentiation of MSCs is stimulated by culturing cells in 3D micro-pellets and inducing differentiation by treating the pellets with transforming growth factor-β3 (TGF-β3) and dexamethasone (Mackay *et al.*, 1998). Safranin-O, toluidine blue monochromatic staining for glycosaminoglycan (GAG) and immunostaining with an antibody specific for type II collagen have been used to indicate the formation of cartilage matrix (Pittenger, 1999, Kohli *et al.*, 2015).

A study performed by Rasini *et al.*, (2013) endeavoured to identify and characterise MSCs within their natural bone marrow environment, by performing multi-parametric immunohistochemistry on trabecular bone biopsy specimens. Describing differences in cell morphology and micro-anatomic localisation in relationship to a precise pattern of MSC antigen expression; they were able to locate within the bone marrow, an identifiable and distinct population of progenitor cells with overlapping *in vivo* expression of antigens similarly characterised during *ex vivo* expansion of BMMSCs (Rasini *et al.*, 2013). These antigens included CD10, CD73, CD140b, CD146, GD2 and CD271. The identification of cells positive for the pluripotency markers, Oct4, Nanog and SSEA-4 revealed subpopulations of different progenitor cells within the trabecular bone and bone marrow (Rasini *et al.*, 2013).

Others have proposed a multiparameter approach to the isolations and identification of MSCs. A multiparameter flow cytometry approach to enhance characterisation of MSCs and ultimately provide a pure population of cells with a defined cell surface phenotype was demonstrated by Chan

et al., (2014). They were able to isolate a triple gated population of MSCs which had an expression phenotype of 94.5 ± 1.3% for $CD73^{+ve}$/$CD105^{+ve}$/$CD90^{+ve}$/HLA-DR^{-ve}/$CD34^{-ve}$. The combination of this multiparameter approach (Chan *et al.*, 2014) and understanding the phenotypic characterisation of MSCs located *in vivo* within trabecular bone and the bone marrow (Rasini *et al.*, 2013) will help to standardise the characterisation, research and provision of MSCs towards clinical applications in regenerative medicine.

Other differentiation potentials of MSCs: There is also literature stating that MSCs are also able to trans-differentiate into myogenic cells (Wakitani, Saito and Caplan, 1995, Toma *et al.*, 2002), as well as cells from the ectodermal (neuronal-like cells) (Jiang *et al.*, 2002, D'ippolito *et al.*, 2004) and endodermal (pancreatic islet-like cells) (D'ippolito *et al.*, 2004, Zanini *et al.*, 2011) germ layers. The derivation of MSCs and their differentiation potential has been illustrated in Figure 1.2.

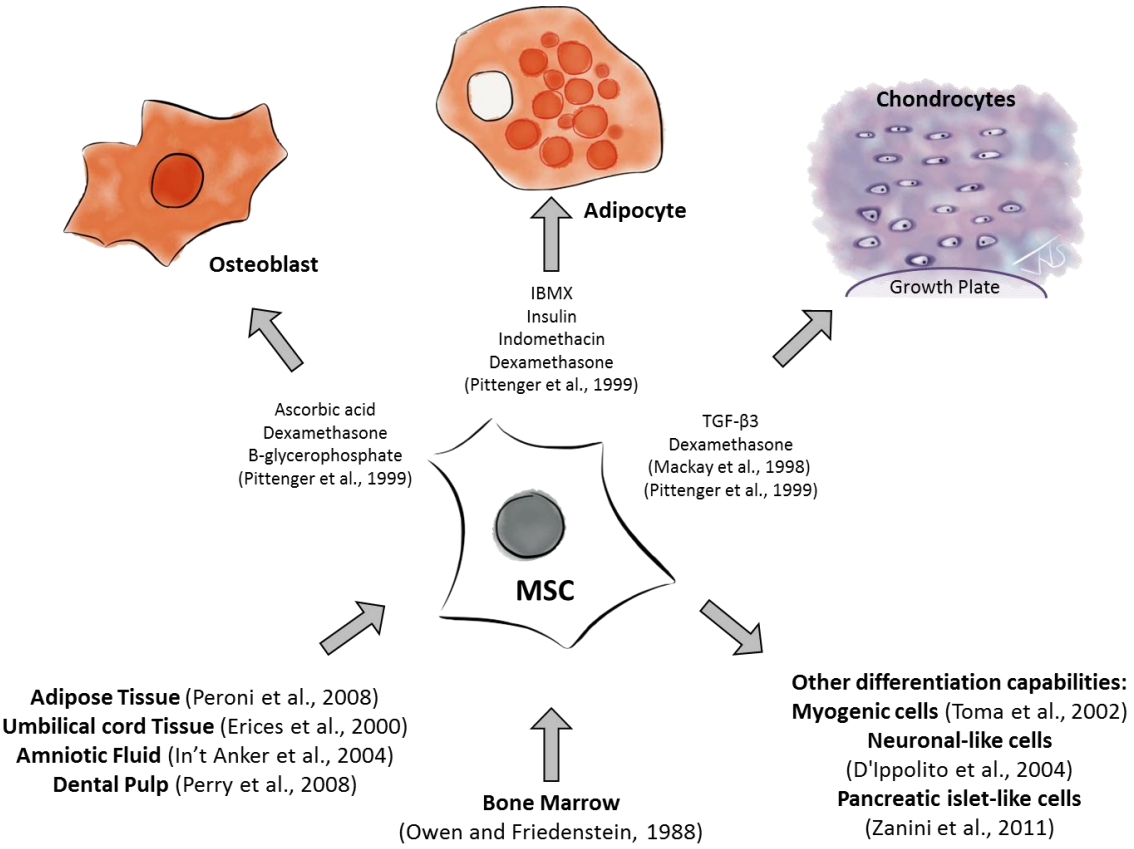

Figure 1.2: The *in vitro* differentiation potential and sites of derivation of MSCs.

A schematic illustration of the ISCT's required minimal criteria for the differentiation of MSCs. Differentiation inducing factors are shown for driving MSCs towards osteoblastic (cell with high ALP activity), adipocytic (cell with positive Oil-Red-O staining) and chondrogenic lineages (cell in matrix stained with toluidine blue) are shown here. Similarly, other differentiation capabilities and areas of isolation of MSCs are reported.

1.3 The use of MSCs in cell based therapies

As knowledge of the multipotency potential and tissue engineering capabilities of MSCs expanded, the question of MSC's intrinsic physiological role *in situ*, within the bone marrow and other tissues of origin, became more pressing. Understanding this role would help advance the use of MSCs for cell based clinical applications. Although there is great controversy with regard to the exploit of non-progenitor MSC functions to treat diseases outside of the skeletal system (Bianco *et al.*, 2013, Caplan and Ricordi, 2013, Phinney *et al.*, 2013), MSCs have exhibited a broad range of angiogenic, trophic, anti-inflammatory, and immunomodulatory activities (Caplan and Correa, 2011a) whilst being used in a variety of experimental paradigms (Dimarino, Caplan and Bonfield, 2013, Zhao *et al.*, 2014). Since MSCs are thought to be found as perivascular cells, surveying their microenvironment ready to function at various sites of tissue injury (Crisan *et al.*, 2008), their potential role in wound repair and regeneration is only just starting to be understood (Caplan and Correa, 2011b).

MSCs which have been successfully used in clinical cell based applications include, but are not limited to; (i) the successful treatment of refractory tibial non-union using calcium sulphate and bone marrow stromal cells (Bajada *et al.*, 2007); (ii) the treatment of a full thickness articular cartilage defect in the femoral chondyle of an athlete with autologous bone marrow stromal cells (Kuroda *et al.*, 2007); (iii) the use of autologous culture-expanded BMMSCs delivered in a fibrin spray which accelerated healing in human cutaneous wounds (Falanga *et al.*, 2007); (iv) culture-expanded autologous BMMSCs injected into spinal cord injury (SCI) patients, with some improved motor functions seen (Park *et al.*, 2012); (v) the treatment of severe refractory acute graft-vs-host disease (Prasad *et al.*, 2011).

It is noteworthy that as of 12th September 2016, there were 221 open recruiting studies (with known status) involving the use of "mesenchymal stem cells" in some manner, listed on ClinicalTrials.gov (www.clinicaltrials.gov). Similarly, on the EU Clinical Trial Register, there are 63

ongoing trials involving the use of "mesenchymal stem cells" (www.clinicaltrialsregister.eu). These clinical trials include the use of MSCs for the treatment of many diseases and disorders, such as cardiovascular diseases, neurological disorders, pancreatic disorders and liver diseases, skin diseases, autoimmune diseases, and bone and cartilage defects and diseases, amongst many others.

The identification and characterisation of 1342 active cell based therapies up to 1st January 2014 and the translation of these trials focusing on the clinical landscape and manufacturing challenges was recently reviewed by Heathman *et al.*, (2015a). It was reported that 382 of the cell based therapies involved the use of MSCs which had been isolated from endometrial tissue (3), placental tissue (7), unspecified locations (15), adipose tissue (59), umbilical cord (61) and bone marrow (237). The cell based therapies were divided into 18 clinical categories and the majority of these trials performed within neurological, cardiovascular, and autoimmune indications. Notably, 339 of the 382 cell based therapies were reported to be within clinical trials where 232 were Phase I, 88 trials were Phase II, 19 trials were Phase III and no trials within Phase IV. Figure 1.3 shows the four most targeted diseases according to trial phase from active cell based therapies involving the use of MSCs as described by Heathman *et al.*, (2015a).

Clinical studies detailing the use of MSCs will be discussed within this review specifically in the context of orthopaedic pathology, particularly bone and joint injury, osteoarthritis and chondral defects, spinal cord injury and its sequalea, namely pressure ulcers and skin wound healing. In these cases, disease aetiology, current treatments, as well as current or possible MSC therapies will be briefly described.

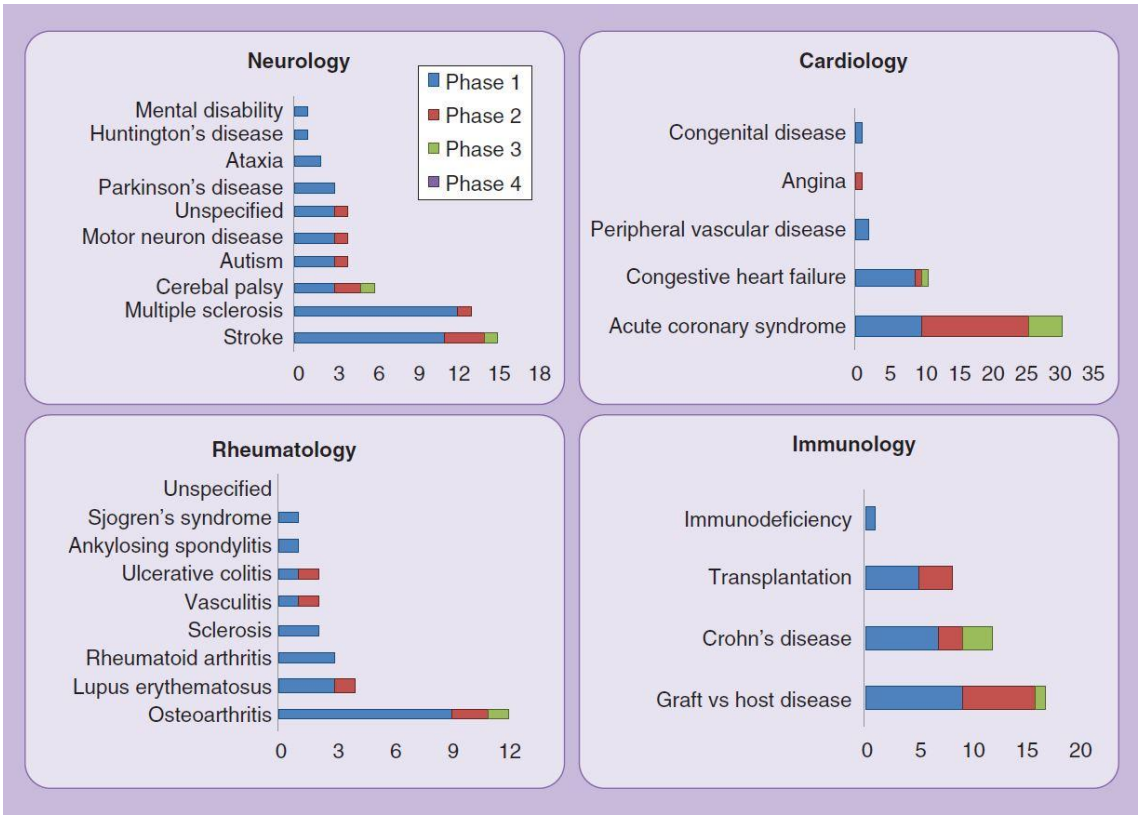

Figure 1.3: Active cell based therapy clinical trials involving MSCs.

A total of 382 of 1342 cell based therapies involved the use of MSCs. These MSCs were isolated from a variety of tissues. The cell based therapies were divided into 18 clinical categories and the four most targeted diseases are shown above according to trial phase development. Figure adapted from Heathman *et al.*, (2015a).

1.3.1 Orthopaedic Pathologies

Bone and joint injury, especially fracture non-union:

Five-20% of all bone fracture cases are associated with unsuccessful union of the fracture leading to fracture non-union or delayed healing (Tzioupis and Giannoudis, 2007). Bone repair due to fracture involves a series of complex, but well-coordinated processes. These processes are characterised by cellular and molecular events in a four-stage model as proposed by Schindeler et al (2008). These stages involve; an initial inflammatory response, soft callus formation, and hard callus formation, followed by initial bone union and remodelling (Schindeler *et al.*, 2008). The different stages and cellular participation during each stage of fracture repair are shown in Figure 1.4.

The inflammatory response details the disruption of the local tissue integrity, interruption to normal vascular function, and a distortion of the marrow architecture. This disruption is met by an influx of inflammatory cells and a plethora of cytokines and growth factors, further recruiting additional inflammatory cells. This leads to the recruitment, migration and invasion of MSCs implicated in bone formation and repair. An uncontrolled or insufficient inflammatory response or lack of reparative cells can lead to further complications at such an early stage.

The second stage of bone fracture healing sees the influx of fibroblasts and chondrocytes forming a semi-rigid soft callus. This is accompanied by three stages of tissue regeneration; replacement of cartilage matrix by mesenchymal-derived chondrocytes, the expression of growth factors and bone morphogenetic proteins (BMPs) stimulating fibroblastic proliferation and chondrogenic differentiation, as well as an increased production of extracellular matrix proteins by the chondrocytes. Vascular invasion is also observed. Reforming the bone structure and extracellular matrix is crucial at this point, thus disruption or inhibition of healing would be detrimental to the overall outcome.

The most active stage of cellular osteogenesis occurs during hard callus formation. The presence of osteogenic factors leads to osteoprogenitor cell differentiation into mature osteoblasts resulting in synthesis of mineralised extracellular bone matrix. These osteoprogenitor cells are thought to come from the periosteum, bone marrow, circulation, and vasculature. Failed recruitment of osteoprogenitor cells can therefore slow down or halt bone formation within the wound site.

The final stage of fracture healing involves remodelling the hard bony callus into cortical or trabecular bone by osteoclastic resorption and osteoblastic bone reformation. This process is a very complex balancing act of pro and inhibitory cytokines and growth factors affecting osteoclast differentiation, survival and activity. Osteoblast involvement is also crucial (Schindeler *et al.*, 2008).

There is great potential for cellular therapy throughout these different stages of wound healing and regeneration. Notably, the introduction of cells may begin the repair process earlier or facilitate recruitment of repairing cells, stimulate extracellular matrix formation, as well as increase the potential to better co-ordinate osteoblast and osteoclast function.

Figure 1.4: The four stage model of fracture repair and the cellular participants.

Representative images of histology sections of tissue during the 4 different stages of fracture healing are shown in the top four panels, from inflammation at stage 1 (left panel) through soft callus formation at stage 2 (second from left panel) and hard callus formation during stage 3 (third from left panel) to the stage of bone remodelling in stage 4 (right panel). The contributions of many different cells during the fracture repair process are shown below the panels. Notably, MSCs start to play a role within fracture repair from the end of stage 1, differentiating into osteoblasts at approximately stage 2 to 3, through to the remodelling of the bone in stage 4. Figure adapted from Schindeler *et al.*, (2008).

The use of MSCs for the treatment of fracture non-union:

According to their radiological criteria, fracture non-unions can be classified as; hypertrophic non-unions showing inadequate mobility but with sufficient blood supply, or atrophic non-unions defined as a non-union which is poorly or inadequately vascularized (Megas, 2005, Sun, Yuan and Zhang, 2011). Current treatments for fracture non-union include bone autograph to augment bone healing (which is the gold standard treatment), the use of osteoinductive or osteoconductive capabilities (such as demineralised bone matrix), the use of stimulatory proteins or growth factors (such as BMPs) to stimulate osteoblast activity at the site of non-union, as well as the use of and physical stimulation (Bajada *et al.*, 2009, Gómez-Barrena *et al.*, 2015).

Recruiting MSCs to the site of injury is crucial to the healing process, allowing regeneration of osteoblasts and re-mineralisation of the fracture site. Sun, Yuan and Zhang, (2011) reported finding MSCs at the site of atrophic non-union, though at low levels, and noting that treatment may need to focus on the reactivation of endogenous MSCs as well as transplant of autologous MSCs (Sun, Yuan and Zhang, 2011).

It should be noted that MSC are currently being used to treat patients with fracture non-unions (Bajada *et al.*, 2007, Rastegar *et al.*, 2010, Centeno *et al.*, 2011, Cox *et al.*, 2011). Treatment involves *in vitro* culture expansion of autologous MSCs or stromal cells isolated from the patient's bone marrow for a period of approximately 3 weeks, followed by transplantation into the fracture site. Successful treatment of a 9 year tibial non-union has already been demonstrated by Bajada *et al.*, (2007), when autologous MSCs were culture-expanded *in vitro* then transplanted into the fracture site mixed with calcium sulphate pellets. Two years post-operative examination showed full weight bearing capabilities, and radiography showed union across the fracture (Bajada *et al.*, 2007).

Chondral defects and autologous chondrocyte implantation:

Chondral defects usually occur after sports injuries. Following a traumatic injury, chondrocytes are irreversibly lost leading to an unbalanced articular cartilage environment and an increase in inflammation, which may ultimately lead to osteoarthritis (OA). As reported by Trattnig *et al.*, (2005) a retrospective review of over 30,000 knee arthroscopies reported that 63% of patients had chondral lesions, 20% of patients had full-thickness articular cartilage lesions with exposed bone, of which, 5% occurred in patients under 40 years old (Curl *et al.*, 1997, Trattnig *et al.*, 2005).

Symptomatic relief or repair of articular cartilage lesions include; osteochondral cylinder transplantation (mosaicplasty), marrow stimulation (microfracturing), arthroscopic lavage and debridement, or ACI following a surgical clean-up of the joint to re-establish the cartilage layer (Brittberg *et al.*, 1994, Roberts *et al.*, 2003, Noth, Steinert and Tuan, 2008, Falah *et al.*, 2010). Here this review will focus on the use of ACI for the treatment of osteochondral defects because it involves the use of chondral and culture-expanded stromal cells.

ACI is a surgical procedure performed to re-establish the chondral layer in chondral and osteochondral lesions in joints. This technique involves four stages of treatment. Firstly, the defect is cleaned by debridement of the cartilage, and then some articular cartilage is harvested from a less-weight-bearing area of the joint through a separate arthroscopic incision. Thirdly, following enzymatic digestion of the cartilage biopsy, harvested chondrocytes are culture-expanded *in vitro* to increase cell number. Finally, these culture-expanded cells are implanted back into the defect and covered with a periosteal flap or collagen membrane (Chondo-Gide®) (Marlovits *et al.*, 2006, Schulze-Tanzil, 2009). This surgical procedure is illustrated in Figure 1.5.

It is crucial to ensure the periosteal or artificial membrane is securely attached in order to prevent leakage of the injected cells (Kim and Shettey, 2011). New matrices and gel mixtures have been developed and tested to assist the successful seeding and integration of culture-expanded cells into

the injury site (Gibson, Mcdonnell and Price, 2006, Eyrich *et al.*, 2007, Kim and Shettey, 2011). The use of ACI treatment has successfully been performed in the Robert Jones and Agnes Hunt (RJAH) Orthopaedic Hospital in Oswestry (Roberts *et al.*, 2003). As a matter of fact, the mid to long term longitudinal outcome for patients who received ACI treatments at the RJAH orthopaedic hospital, reported that 81% of the treated patients presented with improved clinical outcome, with the remainder showing a decline. They also showed that the patient-reported clinical outcome at 15 months is a major predictor of the mid- to long term success of the treatment (Bhosale *et al.*, 2009).

As noted by Hourd *et al.*, (2008), there are currently two licensed cell based advanced therapy medicinal products (ATMPs) within the European market. These are MACI (matrix-induced autologous chondrocyte implantation), intended for the repair of cartilage defects (Genzyme/Sanofi, France) and ChondroCelect® (TiGenix, Belgium). Notably, since ChondroCelect® was the first ATMP to be registered, it may set the standard for the standard for the clinical development of cell based therapeutics.

The use of MSCs for the treatment of chondral defects:

As reported by Wakitani *et al.*, (2007), articular cartilage defects in the patella-femoral joint were repaired using autologous culture-expanded BMMSC. Three weeks prior to transplantation, cells were isolated from the iliac crest and culture-expanded. $5x10^6$cells/ml of single-passaged cells were embedded into a collagen solution, placed on a collagen sheet, transplanted into the defect and covered with autologous periosteum or synovium. Histological examination of one patient 12 months following the transplantation showed a fibro-cartilaginous tissue repair (Wakitani *et al.*, 2007).

Similarly, in 2010, a small study investigated the application of autologous, culture-expanded BMMSCs for full-thickness articular cartilage defects in five patients. Autologous BMMSCs were culture-expanded *in vitro,* approximately $15x10^6$ cells were placed in platelet-rich fibrin glue and

then transplanted into full-thickness cartilage defects and covered with an autologous periosteal flap. All patients experienced symptom improvement over the course of 12 months post procedure, and the two patients who consented to arthroscopy had nearly normal International Cartilage Repair Society (ICRS) arthroscopic scores (Haleem *et al.*, 2010).

Other trials are also examining the use of MSCs for the repair and regeneration of chondral defects. A phase II-III clinical trial being conducted in Cairo (NCT00891501), is examining "The Use of Autologous Bone Marrow Mesenchymal Stem Cells in the Treatment of Articular Cartilage Defects". Within this study, autologous bone marrow is aspirated from the patient's iliac crest, from which BMMSCs are isolated and culture-expanded for 2-3 weeks *in vitro*. Then these culture-expanded BMMSCs are pelleted and implanted into the osteochondral knee defect and covered with an autologous periosteal flap from the proximal tibia and finally the wound is sealed with human fibrin glue.

An investigation was performed by Kohli *et al.*, (2015), examining the incorporation, growth and chondrogenic potential of BMMSCs and ATMSCs within 2 scaffolds, Chondro-Gide and Alpha Chondro Shield. They noted that more BMMSCs and ATMSCs adhered to and were incorporated into Chondro-Gide than into Alpha Chondro Shield; although this incorporation was less than 2% of the cells seeded, a marked increase in cell proliferation of BMMSCs and chondrogenic differentiation of both BMMSCs and ATMSCs was seen (Kohli *et al.*, 2015).

Therefore, it can be seen that the clinical application of MSCs, along with the investigation for improved application of MSCs, is very much at the forefront of the treatment chondral defects.

Figure 1.5 Autologous Chondrocyte Implantation.

Articular cartilage is isolated from a non-weight baring region, enzymatically digested and culture-expanded *in vitro* for 11-21 days. $2.6x10^6$ - $5x10^6$ culture-expanded cells are then injected into the cleaned site of injury. Traditionally a harvested periosteal membrane was used to encapsulate freshly injected cells; however artificial membranes (e.g. Chondro-Gide) are now commonly used (Kohli *et al.*, 2015). Image from Brittberg *et al.*, (1994).

Osteoarthritis:

Osteoarthritis (OA) is a form of chronic arthritis, which affects mostly cartilage and bone, causing progressive loss of function leading to the eventual breakdown of articular cartilage and often inflammation. It is also a disease associated with age, affecting 70% of people over 65 years of age (Scharstuhl *et al.*, 2007). Radiological observation shows joint space narrowing, cartilage thinning and defects, subchondral bone sclerosis and osteophyte formation as seen in Figure 1.6 (Luyten, Tylzanowski and Lories, 2009, Si *et al.*, 2011). Understanding the biology of the cartilage-subchondral bone unit and cellular function within the unit will help drive the potential for cell-based regenerative therapy.

Although the exact cause of OA is unknown, there are multiple phenotypes, which can influence both the initiation, and progression of the disease. For example, OA has been characterised as a disease of mechanics, a disease with a metabolic phenotype, a disease substantially influenced by inflammatory mediators as well as a disease that is driven by aberrant joint structure, morphology and genetics, as discussed by Andriacchi *et al.*, (2014). Since chondrocytes make up only 1-2% of articular cartilage volume, regeneration is either very slow or non-existent (Glass, 2006).

As reviewed by Roughley and Mort (2014), the structure of aggrecan (a large proteoglycan bearing numerous chondroitin sulfate and keratan sulfate chains which provides articular cartilage with its ability to withstand compressive loads) is not constant throughout life, but changes due to both synthetic and degradative events. These events can be viewed as detrimental to cartilage function and are enhanced in osteoarthritic cartilage. This results in aggrecan depletion and predisposing to cartilage erosion. Likewise, the up-regulated production of matrix metalloproteinases (MMPs) and aggrecanases, which are associated with mediators of joint inflammation and overloading, play a major role in aggrecan degradation. Enhancing the production of aggrecan and inhibiting its degradation may retard the destructive process occurring during the early stages of OA (Roughley

and Mort, 2014). The structure and function of aggrecan in articular cartilage and the age related changes in its structure can be seen in Figure 1.7.

On a molecular level, the Wnt/β-catenin signalling pathway has been strongly implicated in both cartilage and bone formation and turnover in OA patients, where increased signalling leads to the loss of tissue structure and function through reprogramming of articular chondrocytes toward catabolism and unstable phenotypes (Luyten, Tylzanowski and Lories, 2009).

The treatment of OA must deal with relieving pain associated with the large degeneration of the whole joint, the prevention of any further dysfunction, and assisting in the potential regeneration of lost tissue and restoration of function to patients. This poses quite a challenge. Current non-pharmacological or surgical treatment for OA includes; a change of diet or increased exercise to encourage weight loss, ice massage, joint bracing specifically in knee OA, lateral wedge insoles, acupuncture, and a more extreme hypothetically beneficial treatment with electrical stimulation. These treatments do show some pain relief, however they do not provide a cure of OA (Glass, 2006).

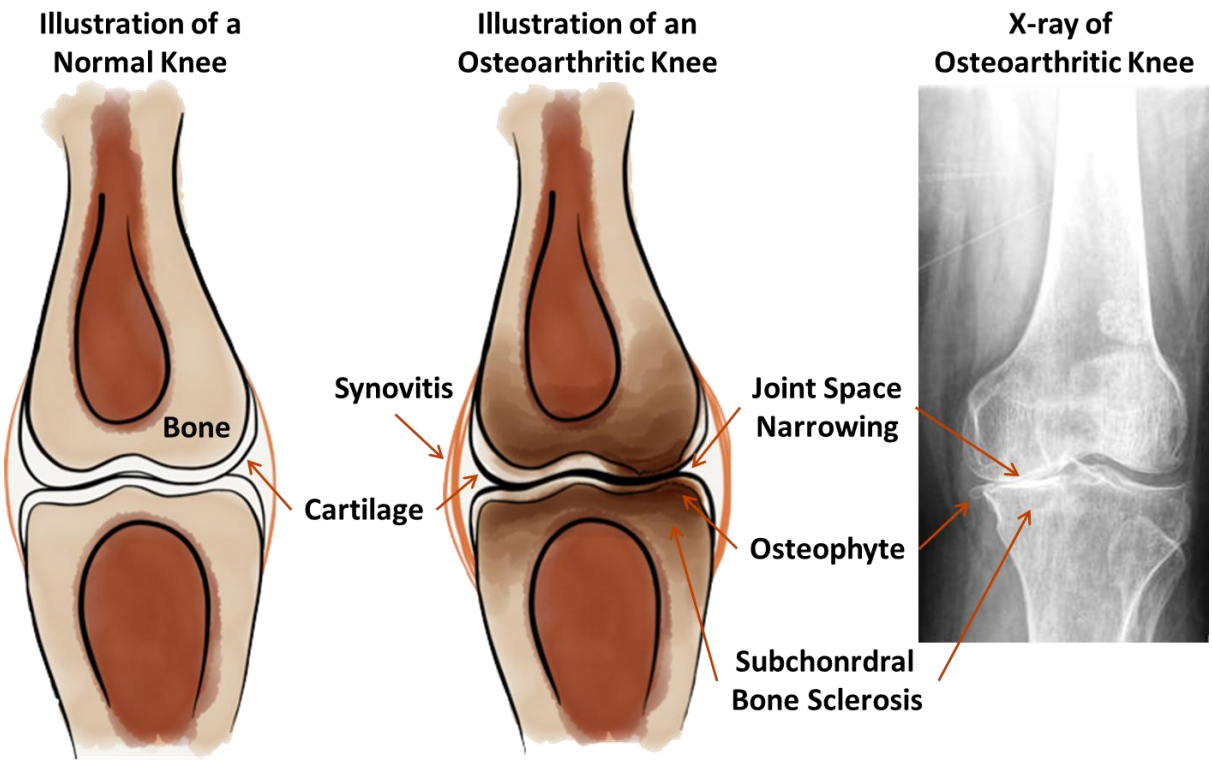

Figure 1.6: An Osteoarthritic Knee Joint.

A schematic illustration of the anatomy of a healthy knee joint compared to an osteoarthritic knee joint and an X-ray image of an osteoarthritic knee are shown, along with the typical changes associated with osteoarthritis. The illustration of the normal knee shows the bone marrow (dark brown), bone (light brown), cartilage lining the bone (clear) and the synovial membrane (orange band). The illustration of the osteoarthritic knee shows subchondral sclerosis within the bone (dark brow shading), osteophyte formation, joint space narrowing, degradation of the cartilage, as well as inflammation of the synovial membrane (synovitis). The X-ray was obtained from Radiopaedia.org care of Dr M. Osama Yonso.

Figure 1.7: The structure and function of aggrecan in articular cartilage and age related changes in its structure.

Proteoglycan aggregates with many aggrecan molecules are depicted as being entrapped by collagen fibrils (A), in the relaxed state (left panel) compared to the compressed state (right panel). Water is displaced as a result of compression. An enlarged aggrecan molecule from a proteoglycan aggregate is shown with the different domains of the aggrecan core protein (B). Changes in aggrecan structure can also be seen for the synthesis and degradation of aggrecan molecules (C). Image adapted from Roughley and Mort, (2014).

Pharmacological treatments usually function as pain management and relief for OA. Such treatments include topical applications of anti-inflammatories, oral anti-inflammatories, and the use of natural compounds for pain management or wound therapy, reviewed by Glass, (2006). One 'non-surgical' procedure reviewed by Glass (2006) is an intra-articular injection of hyaluronic acid for short-term treatment increasing the viscoelasticity of the synovial fluid in the knee providing symptomatic relief. It has been reported that following intra-articular injections of hyaluronic acid (HA) into patients with OA, that the presence of activated CD4 T cells and Th17 ($CD4^{+}CXCR3^{-}CCR6^{+}$) cells were lowered (Lurati *et al.*, Article in press, 2014). This confirms the immunological and inflammatory involvement with OA.

Surgical treatments include arthroscopic surgery to trim torn and damaged cartilage (arthroscopic debridement), realignment of a joint to alter its weight bearing properties (osteotomy), or total joint replacement. Unfortunately these treatments still do not completely cure the problem (Glass, 2006).

The use of MSCs for the treatment of osteoarthritis:

Comparative treatment of MSC transplantation for OA and ACI for chondral defects are in principle much the same, however, it is worth remembering that ACI is used for the repair of focal chondral defects within relatively healthy joints, where as an osteoarthritic joint has a hostile inflammatory environment with a much larger defect area. Therefore, MSCs may be more suitable for this treatment due to their anti-inflammatory activity (Caplan and Correa, 2011b).

The capacity of MSCs for chondrogenic and osteogenic differentiation, their proliferative potential, the ability of MSC to promote endogenous wound healing, along with their anti-inflammatory functions, makes them very attractive for use within cell based regenerative treatments of OA (Si *et al.*, 2011) . However, Noch et al., (2008) explains some of the challenges and requirements that need to be met for the successful, clinical use of MSCs to treat OA. For example, the delivery system

of the cells to the site of disease may be performed by either direct intra-articular injection or by graft of an engineered construct derived from a cell-seeded scaffold (Noth, Steinert and Tuan, 2008).

One issue facing the use of MSC transplantation for OA, is the viability and differentiation capability of MSCs isolated from elderly patients. However, Scharstuhl *et al.*, (2007), demonstrated that sufficient MSCs could be isolated from aged patients, which possessed adequate chondrogenic differentiation potential (Scharstuhl *et al.*, 2007). This was similarly reported for the osteogenic potential of MSCs *in vitro* and *in vivo* (Siddappa *et al.*, 2007). However, Choudhery *et al.*, (2014) reported contradicting results showing a significantly reduced differentiation potential for MSCs isolated from aged patients (>60 years old) when compared to those isolated from young patients (<30 years old) (Choudhery *et al.*, 2014).

According to clinicaltrails.gov, there are currently 38 open and closed studies with a known status, involving the use of MSCs for the treatment of OA. One such study conducted in Spain (NCT01586312) is a multi-centre, phase I-II clinical trial; which is randomised, blinded, and controlled. Within this study, patients in the experimental arm were given an intra-articular transplantation of $40x10^6$ autologous MSCs expanded *in vitro* for 3-4 weeks, according to GMP-compliant procedures. The clinical outcome at the first and 2nd year follow ups reported that patients exhibited rapid and progressive improvement of algofunctional indices that approached 65% to 78%, comparing favourably with the results of conventional treatments. Additionally, quantification of cartilage quality by T2 MRI relaxation measurements demonstrated a highly significant decrease of poor cartilage areas (on average, 27%), with improvement of cartilage quality in 11 of the 12 patients (Orozco *et al.*, 2013, Orozco *et al.*, 2014).

Therefore, it can be seen that MSCs are currently being used within regeneration of OA and ACI.

1.3.2 Spinal Cord Injury and its sequalea, namely pressure ulcers

Spinal Cord Injury (SCI) results in disruption of the blood brain barrier, neuronal cell death, scarring and a loss of functional mobility or sensation (Ramer, Harper and Bradbury, 2000). SCI damage can result from direct trauma (e.g. car accidents), degeneration of the surrounding bone (e.g. osteoporosis) or disease (e.g. polio). Upon axonal damage in the central nervous system, an inflammatory response is initiated accompanied by an influx of inflammatory cells (Popovich *et al.*, 2002) and expression of toxins such as matrix metalloproteinases (MMPs) (Noble *et al.*, 2002). This very high reactive response leads to secondary cell death. The inflammatory response may then lead to the formation of a cyst cavity, glial scarring involving astrocytes and oligodendrocytes, and demyelination. Subsequently axonal re-growth and neuronal function is inhibited (Willerth and Sakiyama-Elbert, 2008, Wright *et al.*, 2011).

Following injury, immediate medical attention is given and the patient immobilised, preventing further damage. After medical assessment and based on the severity of the injury, treatments may focus on targeting inflammation in the acute period with drugs such as methylprednisilone (Trivedi, Olivas and Noble-Haeusslein, 2006, Kim, Caldwell and Bellamkonda, 2009). Treatments may also target the inhibitory matrix (glial scar) in the sub-acute/chronic stage, for example, with enzyme infusion of chondroitinase ABC (Bradbury *et al.*, 2002).

Current cell therapies for SCI:

After initial mechanical injury, secondary injuries in the wound include ischaemia, inflammation, apoptosis and free radical mediated cell death. Treatment of the SCI requires therapies to address this secondary injury cascade as well as replacing lost cells, bridging gaps in the cord and inhibiting scarring of the wound (Willerth and Sakiyama-Elbert, 2008). Many cell types have been investigated in the context of SCI. As reviewed by Willerth and Sakiyama-Elbert, (2008), human and mouse BMMSCs and olfactory ensheathing cells (OECs) have been examined to reduce scar and cyst

formation in animal models, which lead to a clinical trial of human autologous OECs being performed in Australia; Schwann cells and ESC-derived oligodendrocytes have also been examined for re-myelination and possible bridging within the wound in animal models (Willerth and Sakiyama-Elbert, 2008).

Similarly, human neural stem cells (NSCs) have been examined (Enzmann *et al.*, 2005), especially to replace lost and damaged neurons. In 2009, the US Food and Drug Administration (FDA) approved the use of Geron Corporation's product - GRNOPC1 for the treatment of SCI (Alper, 2009). As a part of the clinical trial (clinicaltrials.gov, NCT01217008), recruited patients were intended to receive a single injection of $2x10^6$ GRNOPC1, which are oligodendrocytes differentiated from human ESCs (Keirstead *et al.*, 2005). However, in 2011, Geron announced that the trial was to be completely terminated owing to financial concerns (Frantz, 2012).

MSC implantation for SCI:

MSCs' immunosuppressive nature, ease of isolation and expansion, expression of growth and neurotrophic factors, as well as ability to provide a supportive environment for regeneration strongly support their use within regenerative cell therapies for SCI (Wright *et al.*, 2011). However the trans- differentiation of MSC along glial or neuronal pathways to act as replacement cells within SCI is a matter of much debate and research (Lu and Tuszynski, 2005).

Clinical trials which have been conducted on humans include the use of autologous OECs (Féron *et al.*, 2005, Mackay-Sim *et al.*, 2008), Schwann cells (Saberi *et al.*, 2008), BMMSCs (Wright *et al.*, 2011) and ATMSCs (Ra *et al.*, 2011). The long-term safety of autologous culture-expanded BMMSCs has been reported, as determined by MRI and the absence of permanent complications associated with the transplant (Park *et al.*, 2012).

Pressure ulcers associated with SCI:

Pressure ulcers (also known as decubitus ulcers) are a major complication associated with SCI, as patients with neurological deficits maybe immobilised and without sensation. Ulcers are also common amongst neuropathic, diabetic and aged patients. Pressure ulcers can be described as a breakdown of the layers of skin and underlying tissue occurring as a result of excessive pressure, compression, friction and shear forces between a bony prominence and an external surface for extended periods of time (Grey, Harding and Enoch, 2006). Sites of ulceration are usually located around the sacrum, heels, hips and other compression points experienced when patients lie in the supine, prone or lateral position, as shown in Figure 1.8. These pressure ulcers significantly increase the risk of patients developing further medical complications such as gangrene. Prevention of ulceration is the first stage of treatment, initially by regular turning of the patient, ensuring not to apply sheer stress to the areas of compromised tissue structure (Grey, Harding and Enoch, 2006, Reddy, Gill and Rochon, 2006).

Within the Consortium for Spinal Cord Medicine Clinical Practice Guidelines., (2001), surgical debridgement of necrotic or devitalised tissue should be undertaken when appropriate. It is then essential to dress the wound, maintaining a moist environment allowing the wound to heal.

The use of MSCs for the treatment of pressure ulcers

The treatment of pressure ulcers with autologous BMMNCs in patients with SCI reported that wounds treated with the cells were fully healed within an average time of 21 days. No unresolved ulcers recurred when examined during the follow-up of 19months (Sarasua *et al.*, 2011).

Likewise, a recent study performed by (Dulamea *et al.*, 2015) reported a single case study where autologous BMMSCs were used to treat a patient with two stage IV pressure ulcers on his legs due to neuromyelitis optica induced paraplegia. BMMSCs were isolated and culture expanded *in vitro* through three passages, then embedded into a tridimentiosnal collagen-rich matrix applied to the

wound. Complete epithelisation of the left lateral femoral pressure ulcer was observed within 2 months of treatment and within 5 months, the left malleolar pressure ulcer completely healed restoring normal function to the ankle. No relapse or adverse effects were reported up to 76 months following treatment. Surprisingly, the patient also experienced a sustained remission and improvement of the neuromyelitis optica associated disability, which may be explained due to the promotion and optimization of recovery mechanisms within the central nervous system (Dulamea *et al.*, 2015).

The comparison of BMMSCs with BMMNCs for treatment of diabetic critical limb ischemia and foot ulcer within a double-blind, randomised, controlled trial was recently published (Lu *et al.*, 2011). They reported that BMMSC treated wounds healed much faster than those treated with BMMNCs; likewise, the 24 week follow-up showed that BMMSCs also significantly improved limb perfusion.

Therefore, it can be seen that MSCs along with many other cell types are within clinical application or investigation towards the treatment of both SCI and pressure ulcers.

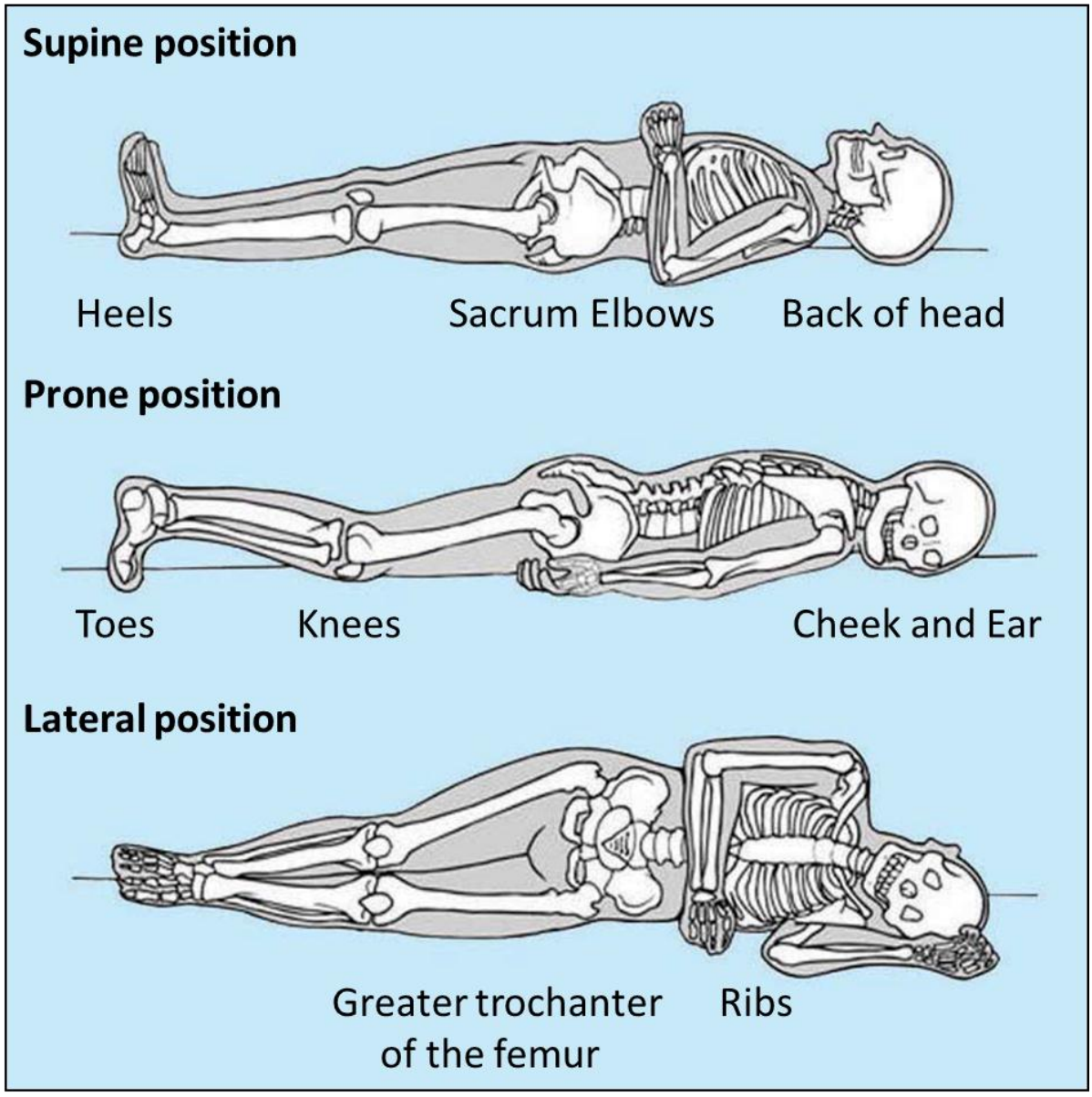

Figure 1.8: Common incidence site for pressure ulceration.

The schematic illustration shows the common areas for pressure ulcers incidence. Pressure ulcers are caused by a local breakdown of soft tissue because of compression between a bony prominence and an external surface. They usually develop on the lower half of the body. The three laying down positions shown (supine, prone and lateral) highlight bony prominences which are likely to develop into areas of ulceration. Image adapted from Grey, Harding and Enoch, (2006).

1.3.3 MSC and skin wound healing

Skin wound healing is a dynamic process classically divided into three overlapping phases; inflammation, proliferation, and remodelling which involves interactions between epidermal and dermal cells, fibroblasts, inflammatory cells, blood cells, the extracellular matrix and angiogenesis (Harding, Morris and Patel, 2002). These interactions are coordinated by an array of cytokines and growth factors. Inflammation is predominately associated with wound clean up. Proliferation focuses on restoring the barrier function of the skin, by an incredible interplay between inward migrating fibroblasts, synthesis of new extracellular matrix, degradation of old extracellular matrix, re-epithelialisation and wound closure. Remodelling of the wound occurs over time, observing a reduction in inflammation and reformation of controlled blood flow into the scar tissue (Harding, Morris and Patel, 2002, Metcalfe and Ferguson, 2007).

MSC-based therapies have shown accelerated wound closure with increased epithelialization, connective tissue formation and angiogenesis, as reviewed by Hocking and Gibran, (2010). MSCs are recruited into the wounded skin and contribute to the wound repair by trans-differentiation into multiple skin types (Sasaki *et al.*, 2008). MSCs' enhancing abilities in wound healing have been thought to occur by differentiation into epidermal keratinocytes, endothelial cells and pericytes which contribute to regeneration of damaged tissue. Their contribution towards the regulation of local responses to injury through paracrine signalling, such as the secretion of interleukin-6 (IL-6), IL-8, transforming growth factor-β (TGF-β), monocyte chemotactic protein-1 (MCP-1) and RANTES has also been shown (Hocking and Gibran, 2010, Walter *et al.*, 2010).

The uses of MSCs in skin wound healing are still being tested clinically. The Sheba Medical centre in Israel will soon be recruiting patients for a study aimed at examining the safety of allogeneic BMMSC for the treatment of diabetic foot ulcers (ClinicalTrials.gov NCT01686139). Within this study, patients who have type I or type II diabetes mellitus, with a diabetic foot ulcer will be treated with up to $20x10^6$ culture-expanded allogeneic BMMSCs.

1.4 MSCs as an ATMP and production within GMP

As shown, MSCs, as well as many other cells, are currently being used or researched for their application in cell based therapies; however, it should be noted that within the clinical studies reported, very little mention was made regarding the screening for safe provision of the cells within the clinical trials, prior to their re-transplantation.

Likewise, within a study examining the clinical application of autologous culture-expanded BMMSCs for the treatment of articular cartilage defects, the culture-expanded MSCs were characterised by their adhesive fusiform (spindle-like) shape and by flow cytometry for MSC specific markers; yet no mention was made regarding the screening method, protocol or standard release criteria of the 'characterised fusiform shaped cells' for potential tumorigenic transformation (Haleem *et al.*, 2010).

On the other hand, the phase I-II study conducted in Spain (NCT01586312), examining autologous BMMSCs for the treatment of OA within the knee, did specify that cells were produced according to current Good Manufacturing Practice (GMP) standards. Notably, that bone marrow collection from patients, mesenchymal cells' isolation and expansion under GMP conditions were conducted according to the IBGM-Valladolid protocol (Instituto de Biologia y Genetica Molecular, University of Vallavdolid, Spain); however, there is little information available regarding the specifics of these protocols. Only a brief mention of the examination of the morphology of the cells is referenced according to a previous study (Orozco *et al.*, 2011, Orozco *et al.*, 2013).

According to the 'article in press' (Soler *et al.*, 2016) reporting results from a very similar clinical study (NCT01183728), autologous MSCs were manufactured according to GMP (Banc de Sang i Teixits, Barcelona, Spain) and delivered as the product named *XCEL-M-ALPHA*, towards the treatment of osteoarthritis of the knee (Soler *et al.*, 2016). Within this study, prior to release of the cell product, the MSC suspension was only tested for bacteria and endotoxin before infusion.

MSC are now considered as Advanced Therapy Medicinal Products (ATMPs) by the European Medicines Agency (EMA) according to regulation No. [EC] 1394/2007 of the European Commission) (European Parliament, 2007); therefore, these cells must be produced in compliance with GMP standards.

The UK Medicines and Healthcare Products Agency (MHRA) participated in the production of a regulatory route map for stem cell research and manufacture, as shown in Figure 1.9. This route map was developed by the Department of Health with the support of regulatory bodies and the Gene Therapy Advisory Committee. This interim UK regulatory route map is intended to be a reference tool for those who wish to develop a program of stem cell research and manufacture ultimately leading to clinical application. As shown, non-genetically modified MSCs intended for use within humans, and manufactured into an ATMP, must be produced as GMP compliant according to a GMP license from the MHRA.

Figure 1.9: Illustrative UK regulatory route map for stem cell research and manufacture.

Abbreviations: HTA, human tissue authority; NHS, National Health Service; GLP, Good Laboratory Practice; GMP, Good Manufacturing Practice; R&D, Research and Development; HFEA, The Human Fertilisation and Embryology Authority; REC, Research Ethics Committee; ATMP, Advanced Therapy Medicinal Products; EMEA, European Medicines Agency; EudraCT, a database of all clinical trials commencing in the European Union from May 1, 2004 onward. (See http://www.mhra.gov.uk/Howweregulate/Medicines/Medicinesregulatorynews/CON041337)

Figure adapted from Goldring *et al.*, (2011).

The GMP standards are intended to ensure the provision of somatic or xenogeneic cells for cell-based therapies and tissue engineering products are produced or re-produced under the highest level of sterility, quality control and documentation following a standard operating procedure. These defining standards are listed below:

1. Where they are available, authorised sources (i.e. authorised medicinal products or CE marked medical devices) of additional substances (such as cellular products, bio-molecules, biomaterials, scaffolds, matrices) should be used in the manufacture of these products.
2. Where devices, including custom-made devices, are incorporated as part of the products:
   a. There should be written agreement between the manufacturer of the medicinal product and the manufacturer of the medical device, which should provide enough information on the medical device to avoid alteration of its properties during manufacturing of the ATMP. This should include the requirement to control changes proposed for the medical device.
   b. The technical agreement should also require the exchange of information on deviations in the manufacture of the medical device.
3. Since somatic cells are obtained either from humans (autologous or allogeneic) or from animals (xenogeneic), there is a potential risk of contamination by adventitious agents. Special considerations must be applied to the segregation of autologous materials obtained from infected donors. The robustness of the control and test measures put in place for these source materials should be ensured.
4. Manufacturing steps should be conducted aseptically where sterilisation of the finished product cannot be achieved using standard methods such as filtration.
5. Careful attention should be paid to specific requirements at any cryopreservation stages, e.g. the rate of temperature change during freezing or thawing. The type of storage chamber, placement and retrieval process should minimise the risk of cross-contamination, maintain the quality of the products and facilitate their accurate retrieval. Documented procedures should be in place for the secure handling and storage of products with positive serological markers.

6. Sterility tests should be conducted on antibiotic-free cultures of cells or cell banks to provide evidence for absence of bacterial and fungal contamination and consider the detection of fastidious organism.
7. Where relevant, a stability-monitoring programme should be in place together with reference and retain samples in sufficient quantity to permit further examination.

Similarly, for biological medicinal products with a short shelf life (a period of approximately 14 days or less, and which need batch certification before completion of all end product quality control tests (e.g. sterility tests), a suitable control strategy must be in place. “Such controls need to be built on enhanced understanding of product and process performance and take into account the controls and attributes of starting and raw materials. The exact and detailed description of the entire release procedure, including the responsibilities of the different personnel involved in assessment of production and analytical data is essential. A continuous assessment of the effectiveness of the quality assurance system must be in place including records kept in a manner which permit trend evaluation. Where end product tests are not available due to their short shelf life, alternative methods of obtaining equivalent data to permit initial batch certification should be considered (e.g. rapid microbiological methods). The procedure for batch certification and release may be carried out in two or more stages:

a) Assessment by designated person(s) of batch processing records, results from environmental monitoring (where available) which should cover production conditions, all deviations from normal procedures and the available analytical results for review in preparation for the initial certification by the Qualified Person.
b) Assessment of the final analytical tests and other information available for final certification by the Qualified Person.

A procedure should be in place to describe the measures to be taken (including liaison with clinical staff) where out of specification test results are obtained. Such events should be fully investigated and the relevant corrective and preventive actions taken to prevent recurrence documented."

These standards were taken from the document "*EudraLex, The Rules Governing Medicinal Products in the European Union, Volume 4, EU guidelines for Good Manufacturing Practice for Medicinal Products for Human and Veterinary Use, Annex 2 - Manufacture of Biological active substances and Medicinal Products for Human Use. B10. Somatic and xenogeneic cell therapy products and tissue engineering products*" The document provides guidance for the interpretation of the principles and guidelines of GMP for medicinal products as laid down in Directive 2003/94/EC for medicinal products for human use and Directive 91/412/EEC for veterinary use (http://ec.europa.eu/health/documents/eudralex/vol-4/index_en.htm).

The standard mentioned in point 7 above leaves room for ambiguity and misunderstanding. The tools for investigating the 'stability-monitoring programme' are not clearly and strictly defined, thus it is difficult to set an appropriate level of 'release criteria'.

It should also be noted that due to the quality control and release criteria depending on a 'Qualified Person', these may be seen subjectively between assessments, as well as they may vary between examiners.

1.5 The need to screen cells intended for cell therapies

Every step in the process of developing cell based therapies requires rigorous scrutiny, from the origin and isolation of the cells used through expansion, manipulation, and preclinical evaluation to eventual engraftment into the host. To achieve this, genetic and phenotypic profiling is required, along with the analysis of cell differentiation status or capacity and the cell's bio-distribution potential to ensure the clinical effects are predictable and controllable, as shown in Figure 1.10 (Goldring *et al.*, 2011).

As the passage number of cell lines increase and the culture conditions change, so too does the potential for chromosomal aberrations, therefore it is important to minimize and monitor culture time and environment. MSCs as well as human pluripotent stem cells (PSCs, i.e. iPSCs and ESCs), all of which are being investigated for clinical applications, have been reported to accumulate chromosomal aberrations during initial and extended *in vitro* culture expansion, which can lead to the accumulation of chromosomal, subchromosomal and single-base level abnormalities (Mayshar *et al.*, 2010, Ben-David, Mayshar and Benvenisty, 2011, Gore *et al.*, 2011, Hussein *et al.*, 2011, Lister *et al.*, 2011, Pera, 2011).

A study conducted by Hussein *et al.*, (2011) regarding the potential use of iPSCs towards clinical therapy, reported that significantly more copy number variations (CNVs) were present in early stage iPSCs than intermediate passage iPSCs, fibroblasts and ESCs; however, although most of the CNVs were seen to form *de novo* during the iPSC reprogramming process, the expansion of the cells selected against these mutated cells, ultimately driving the population towards a state resembling ESCs. Gore *et al.*, (2011) focused on reprogramming-associated mutation effects on iPSCs at the single nucleotide level. They reported that pre-existing and new mutations occurred during and after reprogramming of the cells, and that simply re-programming the cells may not be the cause to the observed mutations, but that selection during reprogramming, colony picking and subsequent culturing may be the contributing factors (Gore *et al.*, 2011). Similarly, Lister *et al.*,

(2011) found that the epigenome of iPSCs featured variable reprogramming, incomplete reprogramming of DNA methylation; as well as cells which retained their somatic cell memory.

Global gene expression analysis of iPSCs and ESCs chromosomal integrity reported a substantial number of cell lines examined, had full or partial chromosomal aberrations. Several of these aberrations resulted from adaptation of the cells to culture expansion. The analysis also revealed a high incidence of duplicated chromosome 12, resulting in a significant enrichment for cell cycle-regulated genes (Mayshar *et al.*, 2010).

A similar and in-depth study using global gene expression analysis of the genetic integrity of over 400 human multipotent stem cells revealed that MSCs, PSCs and NSCs acquired characteristic large chromosomal aberrations within a few passages of culture expansion, as illustrated in Figure 1.11 (Ben-David, Mayshar and Benvenisty, 2011). One such chromosomal abnormality detected in two MSC cell lines, was a monosomy of chromosome 13, which lead to the significant down-regulation of retinoblastoma (RB1) which is located on chromosome 13q14. This particular chromosomal deletion has been similarly seen in mesenchymal tumours (Yamaguchi *et al.*, 1996, Dahlen *et al.*, 2003).

Figure 1.10: Workflow for stem cell-derived therapeutic development.

Genetic and phenotypic analysis must be a continuous process throughout product development, and differentiation status and bio-distribution potential need to be tracked closely to ensure clinical effects are predictable and controllable. Figure from Goldring *et al.*, (2011).

Figure 1.11: Different types of stem cells acquire distinct chromosomal aberrations.

(A–C) Ideograms representing the chromosomal aberrations identified in (A) PSCs, (B) MSCs, and (C) NSCs. Bars to the right of the chromosome represent gains, and bars to the left of the chromosome represent deletions. In the ideogram of PSCs (A), red and orange represent human ESCs and iPSCs, respectively. (D–F) Some of the recurrent aberrations detected in stem cells are the most common aberrations in tumours of the same tissue origin. The frequency of chromosomal aberrations in various types of tumours was calculated using the National Cancer Institute ‘‘Recurrent Chromosomal Aberrations in Cancer Database. Figure from Ben-David, Mayshar and Benvenisty, (2011).

Extended culture increases the potential for cell transformation, (although, to the author's best knowledge, this has not yet been observed or reported within MSCs), or ultimately contamination by other cell types could lead to population transformation (Bernardo et al., 2007, Rubio et al., 2008a, Garcia et al., 2010). In 2005, Rubio *et al*., reported the spontaneous malignant transformation of human MSCs following extended culture *in vitro* (4-5 months), shown in Figure 1.12 (Rubio *et al.*, 2005). This report was followed by a counter-report, arguing and reporting the safety of BMMSCs through extended culture expansion (Bernardo *et al.*, 2007). Rubio and co-workers subsequently published two more reports supporting the earlier finding of spontaneous MSC transformation by characterising the genetic changes of the transformed cells using microarrays (Rubio *et al.*, 2008b) and protein analysis (Rubio *et al.*, 2008a). ,A two-centred study conducted by other researchers, i.e. Rosland *et al.*, (2009) also reported the spontaneous transformation of MSCs, which was characterised by increased proliferation rate, altered morphology and a malignant phenotype (Rosland *et al.*, 2009). However, after a more extensive examination of these cells, it was discovered that the MSC population had been contaminated with the human fibrosarcoma connective tissue cell line, HT1080 cells (Garcia *et al.*, 2010). This finding of contamination of MSC cultures with tumour cell lines was also suggested to be the case in the initial study by (Rubio *et al.*, 2005), ultimately leading to retractions of these previously published findings (Torsvik *et al.*, 2010).

There are distinct categories of malignant bone tumours: osteosarcoma, chondrosarcoma, Ewing's sarcoma, spindle cell sarcoma, sarcoma (not otherwise specified), chordoma, with the remainder composed of rare variants. Osteosarcoma, chondrosarcoma and Ewing's sarcoma collectively represent approximately 75% of the cases. Evidence exists to support an MSC as well as committed osteoblast precursors as the cell of origin for osteosarcoma. Increasing numbers of experimental models have begun to shed light on to the likely cell population that gives rise to osteosarcoma *in vivo* with the weight of evidence favouring an osteoblastic population as the cell of origin rather than an undifferentiated MSC (Gibbs *et al.*, 2005, Mutsaers and Walkley, 2014).

Figure 1.12: Transformed Mesenchymal Cell (TMC) Characterization.

The evolution of MSC morphology (A) is shown during in vitro culture (left to right), from a normal morphological appearance, through a cell crisis phase, to a transformed mesenchymal cell (TMC). G-banded karyotype analysis (B) of a normal MSC line (left) presented with a normal 2n karyotype, i.e. 46 chromosomes, including the XY chromosomes; whereas, 30% of post-senescence/pre-crisis MSC line presented with 47 chromosomes, including the XY chromosomes, and trisomy of chromosome 8. Figure from Rubio *et al.*, (2005) (article retracted (Torsvik *et al.*, 2010).

An interesting study showed that induced expression of the Ewing's sarcoma EWS-FLI-1 fusion gene within human MSCs was stably maintained by the cells and induced a gene expression profile bearing striking similarity to that of Ewing's sarcomas. They further hypothesised that this expression of EWS-FLI-1 in the MSCs may recapitulate the early steps in Ewing's sarcoma development and pathogenesis (Riggi *et al.*, 2008).

Although it was shown that the supposed transformed MSCs observed by Rubio *et al.*, (2005) (article retracted (Torsvik *et al.*, 2010)) had not in fact transformed, but had rather been contaminated; and although it has also been reported and shown that MSCs do not undergo spontaneous transformation and are safe for clinical cell based therapies (Prockop and Keating, 2012, Sensebé *et al.*, 2012), these studies have highlighted the need to safely monitor and screen cells during *in vitro* culture expansion.

Bearing this in mind, some exemplary studies addressing the safety of MSCs were performed by Fekete *et al.*, (2012a). Initially, they established an animal-free expansion protocol using haemo-derivate platelet lysate (PL) as a medium supplement rather than xenogeneic additives, such as foetal calf serum (FCS) which is still widely utilised for cell culture and associated with many risks regarding its use in the clinical context (Fekete *et al.*, 2012a). They were able to confirm the safety and feasibility of PL intended for large-scale MSC isolation and expansion. Then, having eliminated animal products from their cultivation system, they further optimised their procedural-steps and developed five GMP-compliant standardized protocols, which were designed for the safe, reliable, efficient and economical isolation and expansion of BMMSCs for clinical application (Fekete *et al.*, 2012b). When they performed sterility tests and monitored cell stability, they reported that all samples (freshly isolated BM, intermediate cultured cells, and final harvested cells), were negative following BacT/ALERT testing, endotoxin concentrations of all samples were less than 1 I.U./mL and no chromosomal abnormalities were found by karyotyping in any of the large-scale expansions of cultures analysed.

Within this study Fekete *et al.*, (2012b) did determine clonogenicity by performing the CFU-F assays, performed quality controls on starting, intermediate and final products by testing sterility and endotoxin concentrations, characterised the cells intended for clinical application by examining the chemokine and integrin receptor and characterised the MSCs by flow cytometry for specific phenotypic expression. This suggests that the MSCs produced from the examined systems were safe, truly MSCs and showed equal characteristics of homing and adhesion. However, visualisation of the cell throughout the culture period would have provided further colony characterisation, cell specific behaviour, as well as identifying potential tumorigenesis or abnormal cell behaviour.

Similar studies were performed by Heathman *et al.*, (2015b) and (2016b) examining the use of human PL or serum free media (SFM) as an alternative to FCS, improving product yield and highlighting the need for consistency of MSCs towards a manufacturing process in monolayer and micro carrier culture conditions, especially considering donor to donor and colony heterogeneity which may be seen (Phinney *et al.*, 1999, Phinney and Prockop, 2007, Heathman *et al.*, 2015b, Heathman *et al.*, 2016b). Within each study; the cells were characterised using flow cytometry for MSC specific markers, observed with phase contrast microscopy and the cumulative population doublings were reported along with the mean cell diameter of cells in suspension during cell counting. However, continuous imaging and image analysis could have provided additional cell and clonal characterisation of cells in monocultures, as well as the potential identification of abnormal or tumorigenic behaviour.

1.6 Technologies for screening cells intended for cell therapies

Flow cytometry involves the examination of cells in a single cell suspension passing through a laser either as a continuous stream, or as a series of small single cell droplets. The flow of the cell stream of single cell droplets through a laser allows the detection and measurement of light scattered forward through the cells (FSC) and orthogonal to the cells as a side scatter (SSC). Additionally, cells fluorescently labelled with monoclonal antibodies (Abs) can be detected. A flow assisted cell sorting (FACS) system loads the single cell droplets with a slight positive of negative electrostatic charge and as they pass some highly charged metal plates, the droplets are sorted accordingly into collection tubes. A schematic diagram of FACS and a traditional scatter plot of obtained results can be seen in Figure 1.13.

As previously mentioned, flow cytometry has been adopted by the ISCT as the standard technique to immunophenotype MSCs based on the presence or absence of cell surface antigens (Dominici *et al.*, 2006). Similarly, flow cytometry and FACS are currently being implemented as screening tools and as treatment strategies respectively, within clinical practice (Jaye *et al.*, 2012). Namely, they have been used within cancer diagnosis and prognosis, immunologic diseases, as well as within cell therapy and transplantation, such as transplant of haematopoietic stem cells (HSCT) (Appelbaum, 2002). Notably, the World Health Organisation (WHO) released a worldwide consensus on the diagnosis and classification of hematolymphoid neoplasms using a multidisciplinary approach where flow cytometric immunophentyping of cells is integrated alongside morphologic, cytogenetic and molecular genetic data for the provision of an accurate diagnosis (Campo *et al.*, 2011).

Figure 1.13: Schematic of FACS and an example of data.

(A) Cells suspended in a core stream (green) are carried in sheath fluid (light grey) to the flow cell (yellow sphere) where they are interrogated by an excitation laser beam. Cells in the stream are detected by light scattered through the cells forward scatter (FSC) and orthogonal to the cells side scatter (SSC); cells labelled with fluorescently labelled monoclonal Abs are detected by emitted fluorescent light (FL1). Following detection of FSC, SSC, and FL1 signals, droplets are formed and loaded with positive or negative electrostatic charges. Droplets containing single cells are deflected to the left or right by highly charged metal plates, and sorted cells are collected into tubes. (B) FOXP31 CD41 regulatory T cells are identified from a mixture of lymphocytes using multiparameter flow cytometry. Figure adapted from Jaye *et al.*, (2012).

It should be noted that the use of flow cytometry and FACS in clinical therapy or screening, is mostly associated with haematological diseases, dealing with cells within serum suspension. Likewise, apart from phenotypic classification of MSCs for antigen profiling by flow cytometry, these same cells must be plastic adherent with a fibroblastic appearance in order to be classified as MSCs (Dominici *et al.*, 2006). However, there does not appear to be a screening tool specific to this step of cell identification and classification.

The use of high content screening (HCS) imaging and live-cell imaging, along with the appropriate image analysis may facilitate the provision of tools needed to set clear and strict release criteria along with and similarly to those set by flow cytometry.

The aptly named HCS supplies large amounts of data following analysis of acquired images of cells in culture. HCS platforms collect images of formalin fixed fluorescent immunocytochemistry (ICC) labelled cells (e.g. Cellomics ArrayScan, Thermo Fisher); however, this platform can also be used to collect phase contrast and bright field images of cells in live-cell culture. The HCS platform collects images of the cells, traditionally cultured within 6 to 384 well multiwell plates; then uses complex algorithms to analyse the images on a pixel-by-pixel basis, finally reporting differences between individual cells within populations as well as whole cell populations which have been analysed. The imaging and analysis is robust and reproducible.

HCS was initially introduced to meet the need for automation of information-rich cellular assays within pharmaceutical industry mostly towards drug discovery as reviewed by Zanella, Lorens and Link, (2010). Figure 1.14 shows a detailed explanation of the use of HCS towards the interrogation of FOXO3a nuclear translocation as an identifier of potent and selective inhibitors of phosphoinositide 3-kinases.

HCS has also become closely associated with academic research into stem cell biology (Wright, Griffiths and Johnson, 2010, Matsuoka *et al.*, 2013). One such study conducted by Wright, Griffiths

and Johnson, (2010) compared the use of HCS and manual analysis to measure the effects of MSC-conditioned media (MSC-CM) on neurite outgrowths from both the human SHSY5Y neuroblastoma cell line and chick dorsal root ganglia (DRG) explants. They concluded that MSC-CM significantly increased neurite outgrowth, and HCS was able to gather these results from multiple samples within minutes, compared to the manual analysis which would take over an hour per sample; however, they also noted that optimization of the analysis algorithm is essential for the desired result.

A HCS study performed by Matsuoka *et al.*, (2013) reported a morphology-based prediction of osteogenic differentiation potential of MSCs. Within the study they applied computational machine learning, combining cell morphology features with corresponding biochemical osteogenic assay results (ALP activity and calcium deposition), and developed a prediction model of osteogenic differentiation. Using a dataset of 9,990 images automatically acquired by the BioStation CT during osteogenic differentiation culture of MSCs, 666 morphometric features were extracted as parameters. Using time-course morphological features throughout differentiation culture, the prediction results highly correlated with the experimentally defined differentiation marker values (Matsuoka *et al.*, 2013).

The collection of very large data sets following HCS presents a challenge to users in two ways; (i) firstly, users must sort through the data to identify the specific results applicable to the research or application at hand; (ii) secondly, progress in data sharing is hampered by the lack of standardisation in ICC techniques, image collection, data analysis and reporting, all challenges similarly faced by the flow cytometry community (Jaye *et al.*, 2012). Another challenge to the use of HCS based on ICC techniques is the permanent removal of cells from the culture, giving quantitative data on a subset of the population of cells intended for clinical research or application. As expressed by Gore *et al.*, (2011), determining significant cell functions still remain to be

determined even after the identification of characterising reprogramming-associated mutations were identified within iPSCs. This may be facilitated by the use of live-cell imaging.

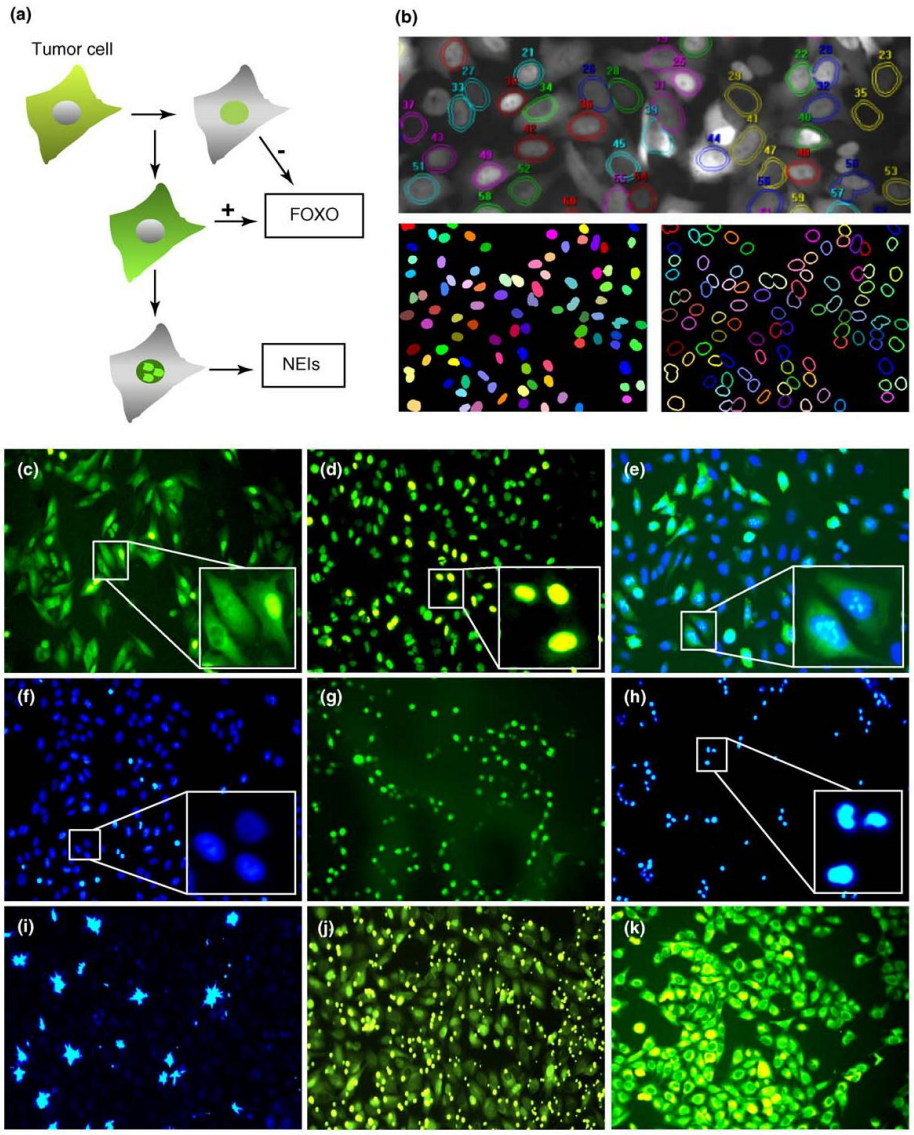

Figure 1.14: HCS on a compound library of small molecules.

(a) High-throughput cellular imaging assay that follows the intracellular location of the FOXO3a protein (FOXO) in tumour cells has been used as a primary filter to screen a collection of 33,992 small molecules. (b) The DAPI-stained nucleus was used as a seed for segmentation. The cytoplasm was defined independently of the cell size by an outer ring region with user-specified pixel width around the nucleus. (c–k) Original images from the primary compound library screen. Figure adapted from Zanella, Lorens and Link, (2010).

Alternatively, continuous live-cell imaging allows user defined identification and intermittent imaging of regions of interest (ROIs) via bright field, phase contrast or fluorescence imaging for a defined period of time. Depending on the platform, this can be done within large t-flasks to multi-well cell culture plates. Continuous imaging allows the rapid review of characteristic cell behaviour; however, it is important to obtain quantitative data from the images to correlate and compare cell behaviour. The Cell-IQ live-cell imaging and analysis platform (CM Technologies Oy, Finland) enables the imaging of cells in bright field, phase contrast and up to three fluorescent channels, during culture periods determined by the user. Work performed by Smith, (2014) demonstrated the use of this non-invasive imaging by the Cell-IQ platform towards the process monitoring and control for the manufacture of ESCs and HSCs within cell therapies.

As expressed by Heathman *et al.*, (2015a), the safe and consistent provision of MSCs for large scale manufacture is essential to provide a consistent product, as well as the need for potency assays for batch release tests to validate the quality and quantity of the cell product. Screening of cells prior to their use in clinical application and the manufacture process is therefore essential. Live-cell imaging system allows simple automated non-invasive assessment of cells during their initial stages of culture, where cell confluence, the number of cells, as well as other behavioural characteristics can be determined.

1.7 Aims of the thesis

The overriding aim of this study was to investigate the use of the Cellomics ArrayScan© HCS Reader platform and the Cell-IQ Imagen™ and Analyser™ live-cell imaging platform towards phenotypic and behavioural screening of cells intended for clinical or manufacturing applications within cell-based regenerative medicine. In particular, the thesis aimed to produce a standard method of identification and safe screening of human MSCs, compared to mesenchymal-derived sarcomas. The analysis was performed in collaboration with Imagen Biotech Ltd, a HCS industrial partner specialising in the analysis of cells in culture using antibody based ICC techniques.

Specific objectives:

- To determine whether human MSCs can be distinguished from two human osteosarcoma cell lines according to their phenotypic immuno-profile for a variety of cell biomarkers related to cell proliferation, osteoblastic differentiation and stem cell characteristics. This evaluation was conducted in a 96 well plate format, which would minimize the loss of cells that has been culture-expanded to treat patients.
- To examine whether human MSCs can be distinguished from human osteosarcoma cell lines, and a primary sarcoma derived cell line, according to characteristic cell behaviours as well as their appearance under phase contrast microscopy alone using the non-invasive live-cell imaging platform Cell-IQ.
- To test whether a novel combination of drugs could be used to selectively target sarcoma cells versus MSCs, and evaluate such selective targeting using live-cell imaging and image analysis.

In this way, the thesis has set out to increase the knowledge of, and improve the screening, safe delivery and characterisation of MSCs within MSC based cell therapies.

Chapter 2: Materials and Methods

2.1 Cell culture

2.1.1 Isolation of mesenchymal stem cells

Primary human MSCs were cultured from bone marrow or adipose tissue samples kindly provided by Mr Martyn Snow at the Royal Orthopaedic Hospital, Birmingham, or were provided already culture-expanded cells from bone marrow by Dr Karina Wright at the Robert and Agnes Hunt (RJAH) Orthopaedic Hospital, Oswestry. Cells were isolated and culture-expanded from donated bone marrow or adipose tissue, following local research ethical committee (LREC) approval and with informed consent (LREC number 12/EE/0136 for ROH and 03/74RJH for RJAH). Cells were isolated from bone marrow aspirates or adipose tissue from ten donors, ranging in age from 22 to 90 years old (Table 1).

Isolation of bone marrow-derived MSCs:

For the isolation and culture expansion of BMMSCs, mononuclear cells were initially isolated from bone marrow aspirates and then MSCs selected according to preferential adhesion to tissue culture plastic, as described (Pittenger, 1999, D'ippolito *et al.*, 2006). Briefly, this was performed as follows: (i) bone marrow aspirates (2-5ml) were harvested with a Jamshedi needle and mixed with 5ml phosphate buffered saline (PBS) (PAA, Yeovil, Somerset, UK), (ii) then gently layered over an aliquot of 5ml of Ficoll-Paque^{TM} PLUS (GE Healthcare, Buckinghamshire, UK) in a sterile 15ml conical centrifuge tube (SLS, East Riding of Yorkshire, UK). (iii) The mononuclear cells were then isolated by density gradient centrifugation for 20mins at 900g. The “buffy coat” containing the mononucleated cells was removed with a Pasteur pipette and added to 10ml of complete media; i.e. dulbecco’s modified Eagle’s medium (DMEM)/Ham’s F12 with 10% (v/v) foetal calf serum (FCS) with 1% (v/v) penicillin (50U/ml) and streptomycin (50µg/ml) (All from PAA, Yeovil, Somerset, UK). (iv) This cell suspension was then centrifuged for 10mins at 200g, the supernatant discarded and the cell pellet re-suspended in 2ml complete media, from which a viable cell count was performed by trypan blue

exclusion (see section 2.1.6). (v) Viable cells were then seeded in 20ml of complete media at a seeding density of $2x10^7$ cells per $75cm^2$ flask. (vi) After incubating in a humidified atmosphere at 37°C with 5% CO_2 for 24hrs, the medium containing any non-adherent cells was removed and the flask was gently washed with PBS. (vii) Flasks were then fed with 20ml of complete media every 2-3 days, and maintained in a humidified atmosphere at 37°C with 5% CO_2. Upon reaching 70% confluence, cells were passaged by treatment with 0.25% trypsin-1mM EDTA (PAA, Yeovil, Somerset, UK) and routinely re-seeded into new culture flasks at $5x10^3$cells/cm^2. At passage II-III cells were characterised by CD profiling, or by assessment of their differentiation potential.

Isolation of adipose tissue-derived MSCs:

For the isolation and culture expansion of ATMSCs, human knee fat-pad tissue was washed, digested with collagenase and then MSCs selected according to preferential adhesion to tissue culture plastic, as described (Peroni *et al.*, 2008). Briefly, this was performed as follows: (i) fat-pad tissue was washed twice in sterile PBS and then manually minced in 2ml of 0.1% collagenase (Sigma-Aldrich, Gillingham, Dorset, UK) using a sterile disposable scalpel (SLS). (ii) Minced adipose tissue was then incubated in a T25 flask (upright) in 5-10ml of 0.1% collagenase for 24hrs in a humidified atmosphere at 37°C with 5% CO_2. (iii) Following incubation, 10ml of complete medium was added to neutralise the collagenase and the digested tissue was centrifuged in a 50ml BD Falcon conical centrifuge tube (SLS) at 200g for 10mins. (v) The supernatant was discarded, the cell pellet was re-suspended in 2-5ml of complete media and a cell viability count performed using trypan blue exclusion (see section 2.1.6). (vi) Viable cells were then seeded in 20ml of complete media into $75cm^2$ flasks at a seeding density of $5x10^3$cells/cm^2. (vii) Flasks were then fed with 20ml of complete media every 2-3 days, and maintained in a humidified atmosphere at 37°C with 5% CO_2. Upon reaching 70% confluence, cells were passaged by treatment with 0.25% trypsin-1mM EDTA and routinely re-seeded into new culture flasks at $5x10^3$cells/cm^2. At passage II-III cells were

characterised by CD profiling, or by assessment of their differentiation potential. Within this thesis, both BMMSCs and ATMSCs were used and collectively termed as MSCs.

Table 1: MSC donor details.

Tissue of origin	Provided by	Sex	Age	Anonymous ID	ID in Appendix	Chapter	Experiment
ATMSC: Knee fat-pad	ROH	F	78	BMS001	MSC 1	Ch3	HCS Biomarker identification
						Ch4	HCS Live-cell identification
						Ch5	MTT & Live-cell identification
ATMSC: Knee fat-pad	ROH	F	22	BMS003	MSC 7	Ch4	HCS & Live-cell identification
						Ch5	MTT & Live-cell identification
ATMSC: Knee fat-pad	ROH	F	73	BMS005	MSC 8	Ch4	HCS & Live-cell identification
						Ch5	MTT & Live-cell identification
ATMSC: Knee fat-pad	ROH	M	90	BMS006	MSC 2	Ch3	HCS Biomarker identification
						Ch4	HCS Live-cell identification
						Ch5	MTT & Live-cell identification
ATMSC: Knee fat-pad	ROH	M	57	BMS010	MSC	Ch3	HCS Biomarker identification
ATMSC: Knee fat-pad	ROH	F	27	BMS101	MSC 9	Ch5	MTT & Live-cell identification
BMMSC: Knee	RJAH	M	55	09/001	MSC	Ch3	HCS ALP Activity
BMMSC: Hip	RJAH	M	71	09/002	MSC	Ch3	HCS Biomarker identification
BMMSC: Hip	RJAH	F	68	09/005	MSC	Ch3	HCS Biomarker identification
BMMSC: Hip	RJAH	M	29	10/369	MSC 10	Ch3	HCS Biomarker identification

Abbreviations: RJAH, Robert Jones and Agnes Hunt Orthopaedic Hospital, Oswestry; ROH, Royal Orthopaedic Hospital, Birmingham; HCS, High Content Screening; MTT, 3-(4,5-dimethylthiazol-2-yl)-2,5-diphenyltetrazolium bromide; ATMSC, Adipose Tissue Derived Mesenchymal Stem Cells; BMMSC, Bone Marrow Derived Mesenchymal Stem Cell; M, Male; F, Female; Ch, Chapter; ID, Identification.

2.1.2 Isolation of primary cells from chondrosarcoma tissue samples

Cells were isolated and cultured from tissues from a single donor with chondrosarcoma, following LREC approval and informed consent (LREC number: ROH12ONC01). The surgical procedure of excision, irradiation, and re-implantation of a primary chondrosarcoma is shown in Figure 2.1. The surgical procedure was conducted as follows: (i) the central section of the humerus was excised from the left arm and the tumour was curettaged from the medulla cavity of the excised bone fragment. (ii) A sample of tumour tissue was taken from the curettaged fragment. This sample was referred to as the non-radio sample. (iii) The bone fragment and another sample of tumour tissue were treated with a single fraction of 90Gy deep X-ray therapy (DXT). This sample was referred to as the post-radio sample. (iv) Following irradiation, the bone fragment was packed with non-vascularised bone cement and fixed back into place.

Briefly, the isolation and culture expansion of cells from the two chondrosarcoma tissue samples was performed as follows: (i) under aseptic conditions, the two tissue samples (non-radio and post-radio therapy) were gently rinsed twice with PBS. (ii) Each sample was weighed (non-radio = 0.860g and post-radio = 1.103g) and then divided into two halves. (iii) One-half was manually minced and then seeded in 8mls of complete media in a 25cm^2 flask. (iv) The other half was digested using 0.1% collagenase for 24hrs in a humidified atmosphere at 37^{o}C with 5% CO_2. (v) Following incubation, 10ml of complete media was added to neutralise the collagenase and the digested tissue was centrifuged in a 15ml BD Falcon conical centrifuge tube (SLS) at 200g for 10mins. (vi) The supernatant was discarded, the cell pellet was re-suspended in 2-5ml of complete media and a viable cell count was performed by trypan blue exclusion (see section 2.1.6). (vi) All viable cells were then seeded in 10ml of complete media into 25cm^2 flasks. (vii) All flasks were fed with 10ml of complete media every 2-3 days, and maintained in a humidified atmosphere at 37^{o}C with 5% CO_2. Upon reaching 70% confluence, cells were passaged by treatment with 0.25% trypsin-1mM EDTA and routinely re-seeded into new culture flasks.

Representative phase contrast microscopy images of these isolates in culture are shown in Figure 2.2. As shown, 10-11 days post seeding, cells from the non-radio treated sample adhered to the tissue culture plastic from both the explant sample (top left panel) 11 days post seeding and the 24hr collagenase digest sample (top right panel) 10 days post seeding. These appeared as proliferative viable cultures. In contrast, from the post-radio treated sample, only debris was found within the explant prepared sample (bottom left panel) and single stressed cells were identified in the collagenase digested sample (bottom right panel). With further time in culture, the non-radio treated cells continued to proliferate and colonies increased in size. In contrast, the post-radio treated cells showed no signs of proliferation throughout the culture period where only single cells were observed from 13 through 56 days post seeding.

Two techniques discussed in previous studies (Van Oosterwijk *et al.*, 2012, Monderer *et al.*, 2013) to isolate cells from tumour tissue were used here to examine potential differences in isolation and proliferation of the isolated cells. As seen in Figure 2.3, explant cells showed slow proliferation through the first three passages, with a high proliferation between passages 3-4. In contrast, cells isolated following 24hr collagenase digestion showed a gradual fold increase through all four passages 1-4. These differences in growth kinetics may be due to the techniques used, with different populations of cells possibly being isolated, e.g. fibroblast-like cells, de-differentiated chondrocytes, or tumorigenic chondrosarcoma cells. Further characterisation of these isolated cells may help identify these differences and compare them to the parental tumour tissue. Within this thesis, cells derived from chondrosarcoma tissue were collectively termed as CS cells.

A detailed description of the diagnosis and treatment of the primary grade I chondrosarcoma can be seen in Appendix 7.2.2, illustrated within Figure 7.26 through Figure 7.29.

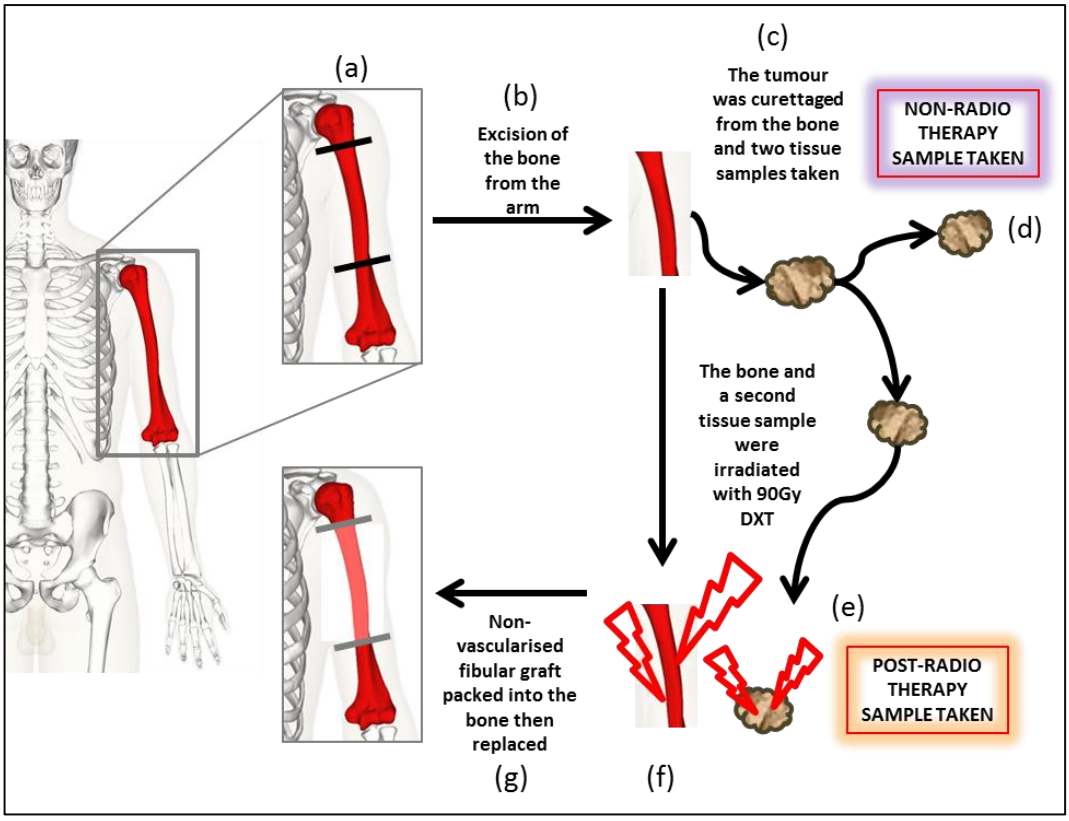

Figure 2.1: The surgical procedure of excision, irradiation and re-implantation.

Clockwise from the left. The central section of the humerus was excised from the left arm (a-b) and the tumour was curettaged from the medulla cavity of the excised bone fragment (c). A sample of tumour tissue was taken from the curettaged fragment (d). This sample is referred to as the Non-radio sample. The bone fragment and another sample of tumour tissue were treated with a single fraction of 90Gy deep X-ray therapy (DXT) (e-f). This sample is referred to as the Post-Radio sample. Following irradiation, the bone fragment was packed with non-vascularised bone cement and fixed back into place (g).

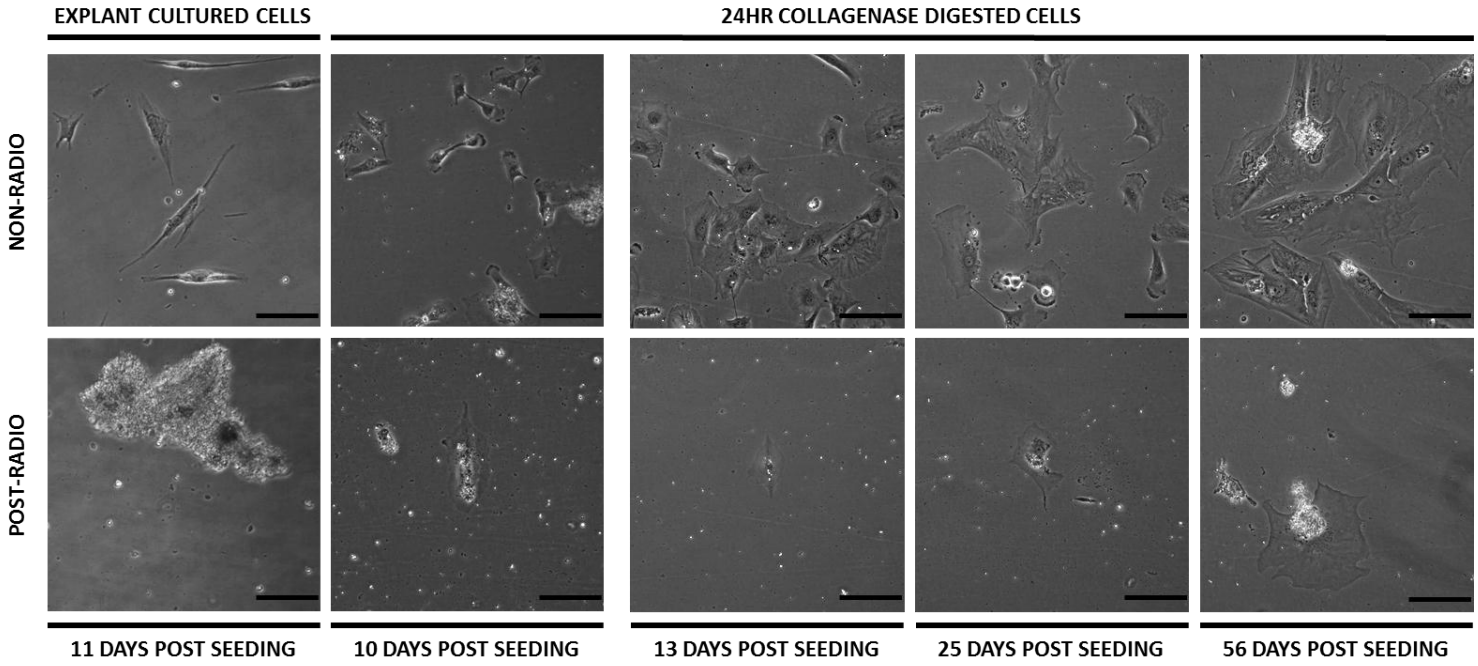

Figure 2.2: Adherent cells were isolated from both the non-radio and post-radiotherapy treated samples; however, only non-radiotherapy treated cells proliferated.

Cell adhesion of P0 cells are shown from the grade I chondrosarcoma following non-radio therapy (top panels) and post-radio therapy (bottom panels) from explant cultures (single left row panels) and 24hr digest samples (four right row panels). Cells were imaged at 10, 11, 13, 25 and 56 days post seeding as indicated below the images. Images were taken at 10 x magnification. Bar=100µm.

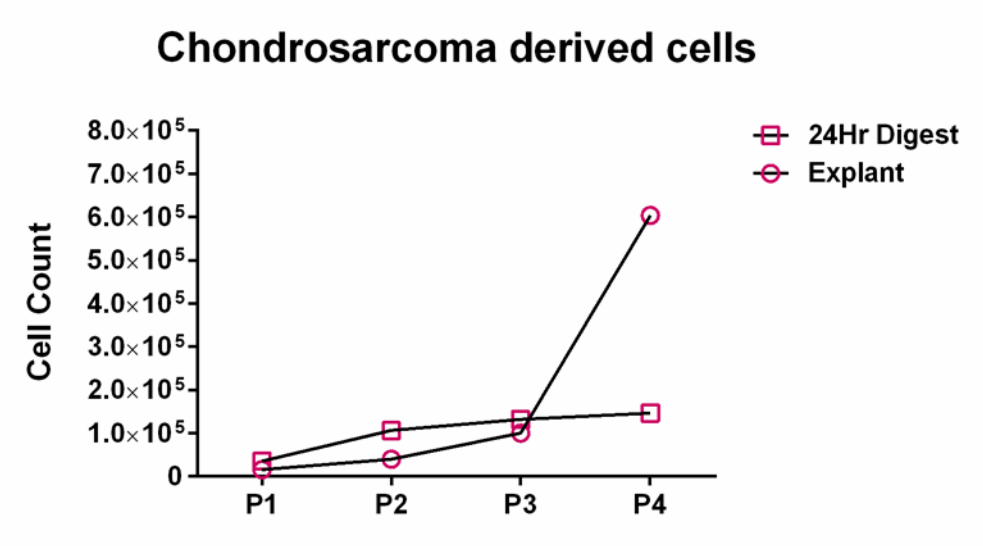

Figure 2.3: Non-radio therapy treated chondrosarcoma derived cells continued to proliferate following passage.

The graph shows the proliferation of the total viable non-radio therapy treated chondrosarcoma derived cells over a period of four passages. 24Hr digest isolated non-radio treated cells can be seen to proliferate from P1 through P4, spanning 321 days of culture. Explant isolated non-radio therapy treated explant tissue proliferated from P1 through P4, spanning 302 days of culture. Following P4, cell DNA was isolated for sequencing of IDH1/2 mutations.

2.1.3 Maintenance of all primary cells

All cells were cultured and maintained in DMEM/Ham's F12 (DMEM/F12) (PAA, Yeovil, Somerset, UK), supplemented with 10% (v/v) foetal calf serum (FCS) (PAA), and 1% (v/v) penicillin (50U/ml) and streptomycin (50µg/ml) in a humidified atmosphere at 37^0C with 5% CO_2. Upon reaching 70% confluence, cultures were passaged using 0.25% trypsin-1mM EDTA (PAA) and a viable cell count was performed by trypan blue exclusion (see section 2.1.6).

2.1.4 Maintenance of cell lines

The two cell lines used to model human osteosarcoma were the osteogenic sarcoma cell line, SAOS2, and the human osteosarcoma cell line, MG63. The SAOS2 cell line (ATCC HTB-85) was derived from an osteogenic sarcoma removed from an 11yr old Caucasian female patient who was undergoing extensive treatment with chemotherapeutic agents including methotrexate, Adriamycin, vincristine, cytoxan, and aramycin-C (Fogh, Fogh and Orfeo, 1977). The MG63 cell line (ATCC CRL-1427) was derived from an osteosarcoma removed from a 14yr old Caucasian male patient (Billiau *et al.*, 1977). Both cell types were cultured and maintained at exponential growth as described in the previous section.

2.1.5 Passage of monolayer cells by trypsinisation

Upon reaching 70% confluence, cultures were passaged using 0.25% trypsin-1mM EDTA (PAA) and a viable cell count was performed by trypan blue exclusion (see section 2.1.6). Briefly, this was performed as follows: (i) confluent monolayer cultures were washed with 5mls of PBS, which was then discarded. (ii) Cells were incubated for 5 minutes in 5mls of 0.25% trypsin-EDTA (PAA) at 37^0C until the cells became dislodged from the tissue culture plastic. (iii) When the cells had dislodged, 5mls of complete culture medium was added to neutralise the trypsin-EDTA. (iv) This cell-rich suspension was then centrifuged for 10mins at 1000rpm (1200rcf), the supernatant discarded and the cell pellet re-suspended in 2ml complete media, from which a viable cell count was performed

by trypan blue exclusion (see section 2.1.6). (v) The cell suspension was diluted appropriately and cells were seeded into new flasks or used for experiments.

2.1.6 Cell viability measured by trypan blue exclusion

Cell viability was assessed based on trypan blue exclusion. The intact membrane of a viable cell is able to exclude the trypan blue dye, giving the cell a phase bright appearance; however, when a cell membrane becomes perforated, the dye stains the nucleus of the cell making it appear blue. Briefly, the viable cell count was performed as follows: (i) 20µl of cell suspension was added to an equal volume of 0.4% (w/v) trypan blue solution (Sigma-Aldrich). (ii) The resultant cell suspension was mixed thoroughly by pipetting and then loaded onto an haemocytometer (Fisher Scientific, Loughborough, Leicester, UK). (iii) The number and proportion of viable cells (phase bright and not stained) and non-viable cells (phase dark and stained blue) were recorded after scoring a minimum of 200 cells per sample.

2.1.7 Testing for mycoplasma

Mycoplasma are a genus of bacteria which lack a cell wall and are unaffected by many common antibiotics such as penicillin or other beta-lactam antibiotics that target cell wall synthesis (reviewed by Waites and Talkington, (2004). Unfortunately, mycoplasmas have the ability to alter their host culture's cell function, growth, metabolism, morphology, attachment, membranes, chromosomal aberrations and damage. The diameter of mycoplasma is between 0.3 – 0.8µm. The EZ-PCR Mycoplasma Test Kit (Geneflow, Lichfield, Staffordshire, UK) is designed to detect the presence of mycoplasma within cell culture via polymerase chain reaction (PCR) testing.

The EZ-PCR Mycoplasma Test Kit was used to screen for contamination in all cell cultures and performed according to manufacturer's protocol as follows: (i) Test sample preparation: 0.5-1.0ml of cell culture supernatant was transferred into a 2ml micro-centrifuge tube and cellular debris was pelleted by centrifugation at 250g briefly. The supernatant was transferred into a fresh sterile

micro-centrifuge tube and centrifuged at 15,000 – 20,000g for 10 minutes to sediment any mycoplasma. The supernatant was carefully decanted and the pellet keep (the pellet may not always be visible). The pellet was re-suspended with 50µl of the Buffer Solution and mixed thoroughly with a micro-pipet and heated to 95°C for 3 minutes. (ii) Reaction mixture preparation: the following reagents were combined in a PCR tube: 35µl of H_2O, 10µl of reaction mix, 5µl of test sample. A positive template control was also prepared by adding 1µl of positive template in lieu of the 5µl sample. (iii) All tubes were placed into a DNA thermal cycler and the following parameters were set to amplify the DNA: 30 seconds at 94°C, then 35 cycles of; 30 seconds at 94°C then 120 seconds at 60°C then 60 seconds at 72°C, followed by 30 seconds at 94°C, 120 seconds at 60°C and finally 5 minutes at 72°C. (iv) Analysis of the amplified products by gel electrophoresis: a 2% agarose gel was made and allowed to set. 20µl of the PCR product (without loading buffer) was applied to the gel electrophoresis.

2.1.8 Seeding densities for experiments

Following cell culture and trypsinisation, viable cells were seeded at the following densities for respective experiments. For all Cellomics ArrayScan© HCS experiments, cells were seeded at a density of $5x10^3$ cells per well in a black clear-bottom 96 well plate (Greiner Bio-One Ltd, Gloucestershire, UK). For live-cell imaging using the Cell-IQ platform, cells were seeded at a density of $1x10^4$ cells per well in a clear 24 well plate (Corning by Appleton Woods Ltd, Birmingham, UK). For MTT viability assays, cells were seeded at a density of $5x10^3$ cells per well in a 96 well (Corning by Appleton Woods Ltd). For 3D micro pellet formation and treatment, cells were seeded at a density of $12.5x10^4$ cells per pellet in 1.5ml micro-centrifuge tubes (Fisher Scientific). For live-cell imaging of selective cell killing following drug treatments, cells were seeded at a density of $4x10^3$ cells per well in a 48 well plate (Corning by Appleton Woods Ltd).

2.1.9 Cryopreservation of cells

Cryopreservation was performed as follows: (i) upon reaching 70% confluence, cells were trypsinised, washed and pelleted by centrifugation at 1000rpm (1200rcf) for 10 minutes. (ii) The supernatant was discarded and the cell pellet was re-suspended in 1ml of freezing mix – FCS with 10% (v/v) dimethylsulphoxide (DMSO) (Sigma-Aldrich). (iii) A viable cell count was performed by trypan blue exclusion (see section 2.1.6) and then cells were placed into an appropriately labelled cryovial at a concentration of $1x10^6$ cells/ml. (iv) Cryovials were frozen overnight at -80°C in a Nalgene™ Cryo 1°C Freezing Container, 'Mr Frosty' (Fisher Scientific) containing isopropyl alcohol, then transferred and stored within a -80^0C freezer.

2.1.10 Recovery of cells from cryopreservation

The recovery of cells from cryopreservation was performed as follows: (i) cryovials were recovered from a -80^0C freezer and then rapidly thawed under a running tap of warm water. (ii) 1ml of ice cold complete media was added drop-wise over one minute. (iii) An additional 5ml of ice cold complete media was added drop wise over 5 minutes. (iv) After allowing to stand at room temperature for 5 minutes, 4ml of ice cold complete media was added drop wise. (v) The resultant cell suspension was transferred into a 15ml Falcon tube and pelleted by centrifugation at 1000rpm for 10 minutes. (vi) The cell pellet was re-suspended in 5ml of room temp culture medium, a viable cell count recorded and then cells were seeded into an appropriate culture flask and maintained in a humidified atmosphere at 37°C with 5% CO_2.

2.2 Phenotypic characterisation of primary cultures of stromal cells

Phenotypic characterisation of isolated primary cultures of stromal cells was done according to the ISCT's minimal criteria to confirm their identity as MSCs (Dominici *et al.*, 2006). CD profiling examined immunoreactivity for $CD34^{-ve}$, $CD45^{-ve}$, $CD73^{+ve}$, $CD90^{+ve}$ and $CD105^{+ve}$ and cells were

induced to differentiate along osteogenic, adipogenic and chondrogenic differentiation as shown in Figure 2.4. This work was performed in collaboration with Nupur Kohli (PhD student; Johnson laboratory, Aston University) to whom I am grateful for the provision of data and associated figures.

2.2.1 Cluster of differentiation (CD) profiling

Culture-expanded stromal cells were harvested at passage II-III by trypsinisation and suspended in PBS containing 2% bovine serum albumin (BSA) (Sigma-Aldrich). The cells were then blocked with 10% normal human immunoglobulin (Ig) (Grifols,Cambridge, UK) prior to incubation at 4 °C with the following phycoerythrin (PE) conjugated mouse monoclonal anti-human Abs: CD34, CD45, CD105 (Immunotools, Friesoythe, Germany), CD73 and CD90 (BD Biosciences, UK). Non-specific fluorescence was determined by incubating cells with isotype-matched control phycoerythrin-conjugated antibodies IgG2a and IgG1 (Immunotools). Immunoreactivity for each CD marker was assessed by flow cytometry using a Beckman Coulter FC500 Flow Cytometer and data were analysed using Kaluza® Analysis Software.

2.2.2 Osteogenic differentiation

Passage III ATMSCs were cultured in a 24-well plate and allowed to reach 70-80% confluence. The cells were then maintained under osteogenic conditions, consisting of standard culture medium supplemented with; 10mM β-glycerophosphate, 50µM ascorbic 2-phosphate and 10nM dexamethasone (DEX) (All from Sigma-Aldrich) for 28 days, as previously described (Bajada *et al.*, 2009). Control cultures were maintained in complete media alone. Both induction and control media were completely replaced every 2–3 days. Differentiation along the osteogenic lineage was evaluated by increased ALP activity.

2.2.3 Adipogenic differentiation

Passage III ATMSCs were cultured in a 24-well plate and allowed to reach 70-80% confluence. The cells were then maintained under adipogenic conditions, consisting of standard culture medium supplemented with; 1µM DEX, 0.5mM IBMX (Sigma-Aldrich), insulin, transferrin and selenium (ITS-X100 pre-mix; PAA) and 100µM indomethacin (Sigma-Aldrich), for 28 days as previously described (Bajada *et al.*, 2009). Control cells were maintained in complete media alone. Both test and control medium were completely replaced every 2–3 days. Differentiation along an adipogenic lineage was evaluated by cellular accumulation of neutral lipid vacuoles by staining with Oil Red O (Sigma-Aldrich).

2.2.4 Chondrogenic differentiation

A cell suspension of $2x10^5$ cells was prepared per 1ml of standard culture medium, following routine trypsinisation. 1ml of the cell suspension was transferred into a 1.5 ml eppendorfs and pelleted by centrifugation at 500g for 5 minutes (Johnstone *et al.*, 1998). The medium was then replaced with DMEM/High glucose with 2% FCS plus carriers in control cultures and DMEM/High glucose supplemented with 100nM DEX, 37.5µg/ml ascorbate-2-phosphate, ITS-X, 10 ng/ml TGF-β1 (PeproTech Ltd., London, UK), and 1.25µg/ml BSA and antibiotics. The pellets were maintained at 37°C and 5% CO_2 for 28 days and the medium was replaced every 2-3 days, after which the differentiation status of the pellets was examined by embedding and staining for Toluidine Blue.

2.3 Formalin fixation of cell cultures

Formalin fixation of cells was performed as follows: (i) cells were seeded into various plate formats (24, 48 or 96 well plates) and maintained for 24hrs at 37°C with 5% CO_2. (ii) Culture medium was removed from the wells and cells were washed twice with PBS. (iii) 4% formaldehyde was added to the wells and the plates were incubated for 20 minutes at room temperature. (iv) The formaldehyde was removed and the cells were washed twice with PBS, then stored in fresh sterile PBS at 0-4^{0}C.

2.4 Alkaline phosphatase staining

Alkaline phosphatase (ALP) is an ectoenzyme whose activity is used as an early marker of osteoblastic differentiation. Increased expression and subsequent activity is associated with progression along the osteoblastic lineage (Jaiswal *et al.*, 1997). The production of an insoluble red dye at the site of enzymatic activity is due to the alkaline phosphatase mediated reaction between naphthol phosphate and the diazonium salt, fast red TR. SAOS2 osteosarcoma cells were seeded as a positive control at a density of $1x10^4$cells/cm^2 24hrs prior to staining (Ali, Rowe and Teich, 1996).

ALP staining for phenotypic characterisation of stromal cells was done as follows: (i) a staining solution was prepared immediately prior to staining as described here; 10 mg of fast red TR (Sigma-Aldrich) was added to 8.4mls of 0.1M Tris-hydrochloride (Tris-HCl) buffer and 1.6mls of naphthol (Sigma-Aldrich) was added and filtered through Whatman No.1 filter paper (Maidstone, UK) just before use. (ii) Controls and test cultures were fixed with 4% formaldehyde for 1 minute and then washed twice for 1 minute at each wash with Tris-phosphate buffered saline with tween 20 (TBS-T) (Molekula, Gillingham, Dorset, UK). (iii) 500µl of staining solution was added to each well of a 24 well plate and then incubated at room temperature for 3-5 minutes. Alkaline phosphatase enzymatic activity was marked by the formation of dark red cellular precipitates (performed by Nupur Kohli).

ALP staining for HCS was done as follows: (i) following the appropriate culture period, control and test culture cells were gently washed twice with PBS then fixed in 4% formaldehyde for 1 minute at room temperature. (ii) The formaldehyde solution was removed and the cells were gently washed twice with TBS-T. (iii) A staining solution was prepared immediately prior to staining as described; for a 10ml solution, 10mg of Fast Red TR was added to 8.4ml of 0.1M Tris-HCl buffer at pH 8.6 (Molekula). 1.6ml of naphthol AS-MX phosphate solution (Sigma-Aldrich) was added to the Fast Red TR/Tris-HCl solution and gently mixed by inverting the tube. The TBS-T was removed and the cells stained for 5mins. The stain was discarded and the cells washed twice with PBS. Cells were then

fixed for a further 20mins at room temperature with 4% formaldehyde. Following fixation, cells were washed twice with PBS and stored in PBS at 4^{o}C until imaging. This protocol was adapted from Dr. N. Y. Yeh's Ph.D thesis, Aston University, 2013. Figures and results of ALP stained MSCs, SAOS2 and MG63 cells can be seen in section 7.1.3 and 7.1.4 with Figure 7.17.

2.5 Oil Red O staining

Oil red O is a dye that binds to lipids, specifically triglycerides and therefore, was used as a marker to assess adipogenic differentiation (Ramírez-Zacarías, Castro-Muñozledo and Kuri-Harcuch, 1992). The staining was performed as follows: (i) a staining solution was prepared by dissolving 60mg of oil red o powder (Sigma-Aldrich) into 20ml of isopropanol. (ii) 6ml of this stock solution was mixed with 4ml of distilled water. (iii) This staining solution was filtered through a Whatman No.1 filter paper, prior to staining. (iv) Control and test cultures were washed and fixed with 4% formaldehyde for 30 minutes at room temperature. (v) 500µl of staining solution was added to each well of the 24-well plate and the plates were incubated for 1 hour at room temperature. (vi) After this, any unbound dye was washed off with PBS and lipid accumulation was marked by orange staining of the intracellular lipid vacuoles. This protocol was adapted from thermo scientific cell culture and bioprocessing.

2.6 Toluidine blue staining

Toluidine blue is a metachromatric cationic dye that stains proteoglycans as well as glycosaminoglycans (GAGs). Use of toluidine blue in tissue sections is done with the aim to highlight components, such as mast cells granules, mucins, and cartilage (Schmitz *et al.*, 2010, Sridharan and Shankar, 2012). Toluidine blue staining was performed as follows: (i) pellets were harvested at week 4, fixed with 10% neutral buffered formalin for 24 hours and then processed in graded strengths of alcohol and paraffin embedded. For histological evaluation, 5µm thick sections were cut and

deparaffinised, rehydrated through a series of graded alcohols, and stained with 0.04% toluidine blue stain (Schmitz *et al.*, 2010).

Figure 2.4: Phenotypic characterisation of primary isolated BMMSCs and ATMSCs according to the ISCT's minimal criteria.

(A) Culture expanded cells from BM and AT differentiated along mesenchymal lineages, as indicated by the presence of ALP positive osteoblasts or Oil Red O positive adipocytes in monolayer cultures and metachromatic staining for glycosaminoglycans (GAGs) in pellet cultures (scale bars represent 100µm). (B) Representative histograms are shown for positivity for CD markers in BMMSCs (left panels) and ATMSCs (right panels). The white histogram shows immunopositivity for each indicated marker, which is only clearly apparent when the extent of immunofluorescence is greater than that detected following immunolabelling with an isotype-matched control antibody, indicated by the black histogram. Figure adapted from Kohli *et al.*, (2015).

2.7 Haematoxylin and Eosin staining of biopsy and curettage samples

Haematoxylin and Eosin (H&E) staining on paraffin embedded biopsy and curettage sections were performed according to the standard operating protocol from the Department of Musculoskeletal Pathology, Birmingham University, Birmingham, UK. Briefly, sample sections were dewaxed and rehydrated with xylene and alcohol and then washed. Sections were then stained with Ehrlich's haematoxylin, washed in tap water and differentiated in 0.3% acid alcohol (0.3%hydorchloric acid in 70% alcohol). Following this, sections were washed in running tap water and counterstained with 1% eosin, washed again with running tap water and finally dehydrated. They were then cleared and a coverslip was mounted onto the sections with DPX mounting solution. Resulting staining shows: Nuclei – Blue to black; Cytoplasm – varying shades of pink; Cartilage – purple.

2.8 DNA isolation for IDH1 and IDH2 mutation analysis

As a part of the energy generating citric acid cycle, the enzymes - isocitrate dehydrogenases (IDH) catalyze the oxidative decarboxylation of isocitrate to α-ketoglutarate and CO_2. IDH1 is found in the cytoplasm and peroxisomes, IDH2 within the mitochondria of cells. Mutations within IDH1 and IDH2 are fairly frequent events (56%) in central and peripheral chondrosarcomas. Specific point mutations commonly found in IDH1 usually result in substitutions at R132 and within IDH2 mutations may occur at R172 (analogous to IDH1 R132) and R140 (Amary *et al.*, 2011). These mutations within the active site of the IDH do not result in terminal activity of the enzyme. Rather, it has been noted that the mutation R132H (arginine to histidine) in IDH1 may lead to the enzyme's ability to further convert α-ketogluterate to R(-)-2-hydroxygluterate (2HG) an onco-metabolite (Dang, White et al. 2009). Or the mutation may lead to increased levels of hypoxia-inducible factor subunit 1α (HIF-1α), a transcription factor facilitating tumour growth under low oxygen environments (Zhao, Lin et al. 2009).

Specific point mutations within the isocitrate dehydrogenase genes, IDH1 (R132) and IDH2 (R140 and R172) were investigated following extraction of DNA from paraffin embedded biopsy samples and culture-expanded cells, RT-PCR for the IDH1 and IDH2 genes, then sequencing the cDNA for the specific point mutations. All protocols were conducted according to and by the Department of Musculoskeletal Pathology standard operating protocols.

2.8.1 DNA extraction from paraffin embedded tissue

DNA was extracted from paraffin embedded blocks of the biopsy sample according to the standard protocol from the Department of Musculoskeletal Pathology, Birmingham University, Birmingham, UK.

2.8.2 DNA extraction from culture-expanded cells

DNA extraction from culture-expanded cells was done using the QIAmp DNA Mini Kit (QIAGEN, Venlo, Netherlands) according to manufacturer's guidelines. Briefly, explant and collagenase digest cells isolated from the non-radio treated CS sample were individually harvested following trypsinisation and counted to ensure cell density $\leq 5x10^6$. Following counting, cells were centrifuged, re-suspended in PBS, protease K was added, the cells were lysed using the Buffer AL and then pulse-vortexed for 15s. Cell lysates were incubated for 10mins at 56^{o}C, pulse-vortexed for 15s, and then ethanol (96%) was added. The entire solution was added to the QIAmp Mini spin column and centrifuged at 6000g for 1min. Columns were washed with Buffer AW1 and centrifuged at 6000g for 1min, washed in Buffer AW2 and centrifuged at 20,000g for 3mins. The columns were incubated in DNA/RNA free water for 5mins then the DNA was extracted from the column by centrifugation for 1min at 6000g. Total DNA concentration and purity was checked using a nanophotometer (Implen - NanoPhotometer® Pearl, Geneflow, Lichfield, Staffordshire, UK).

2.9 RT-PCR amplification of IDH 1 and IDH2 specific genes

Reverse transcriptase-PCR (RT-PCR) for the isocitrate dehydrogenase gene mutations, IDH1 (R132) and IDH2 (R140 and R172) was carried out on formalin-fixed, paraffin-wax-embedded tissue, and culture-expanded chondrosarcoma tissue. RT-PCR was performed according to the standard protocol from the Department of Musculoskeletal Pathology, Birmingham University, Birmingham, UK. The Qiagen® OneStep RT-PCR Kit (Qiagen Ltd., Cat. No. 210212) was used according to manufacturer's protocol. Primer sequences used to identify the presence or absence of the mutations can be seen in Table 2.

2.10 Gene sequencing of IDH1 and IDH2 cDNA

Gene sequencing was outsourced and done according to the standard protocol from The Functional Genomics and Proteomics Laboratories, School of Biosciences, University of Birmingham, UK.

Table 2: Oligonucleotide primer sequences used during RT-PCR to identify the presence or absence of IDH1 and IDH2 mutations.

Mutation type	Oligonucleotide primers	Product size
R132	Left 1: AAAATATCCCCCGGCTTGT	145 bp
	Right 1: CACATACAAGTTGGAAATTTCTGG	
	Left 2: CGGTCTTCAGAGAAGCCATT	129 bp
	Right 2: GCAAAATCACATTATTGCCAAC	
R172	IDH2-R172-F: AGCCCATCATCTGCAAAAAC	102 bp
	IDH2-R172-R: CTCCACCCTGGCCTACCT	
R140	IDH2-R140-F: TGTGGAAAAGTCCCAATGGA	90 bp
	IDH2-R140-R: CTAGGCGTGGGATGTTTTTG	

Abbreviations: R, Arginine; bp, base pair; IDH, Isocitrate Dehydrogenase; F, Forward; R, Reverse. Point mutations located at R132 are specific for IDH1 and point mutations located at R140 and R172 are specific for IDH2. Sequences and table adapted from Table S4 supporting information from Amary *et al.*, (2011).

2.11 Immunocytochemistry (ICC)

Immunocytochemical staining of cells for HCS analysis was performed as follows: (i) cells were fixed in 4% formaldehyde and then washed twice with PBS. (ii) Primary antibodies (1^{o} Ab) were diluted as appropriate (detailed in Table 3) in Digitonin (500µg/ml) (Sigma-Aldrich). (iii) 50µl of 1^{o} Ab was placed into each respective wells of a 96 well plate and incubated at room temperature for 1 hour. (iv) Following incubation, the 1^{o}Ab solution was decanted and the plate was washed twice with PBS using the plate washer (Tecan UK Ltd, Theale, Reading, UK). (v) Secondary antibodies (2^{o} Ab) and the nuclei counterstained with 20µg/ml Hoechst 33342 (Invitrogen, H3570) were diluted in PBS as appropriate and added to the cells according to the species of the 1^{o}Ab used, then incubated for 1 hour at room temperature. (vi) Following this, the 2^{o}Ab/Hoechst solution was decanted and the plate was washed twice with PBS. (vii) 100µl of PBS was added to each well for imaging and storage. Due to mechanical malfunction, some wells were not washed therefore cells dried and were over stained with very high background. These wells were excluded from fluorescence intensity quantification. Immunoreactivity staining for biomarkers was done in triplicate for each independent experiment. Triplicate readings were pooled for n=3 experiments.

Table 3: ICC antibodies, concentrations and dilutions.

Antibody	Species	Concentration	Dilution	Supplier
anti-Ki67 antigen	R	30µl-Concentration cannot be disclosed due to propriety	1/500	Cellomics, Thermo Scientific
anti-phospho Retinoblastoma (pRb)	M	300µl-Concentration cannot be disclosed due to propriety	1/100	Cellomics, Thermo Scientific
anti-phospho Histone H3 (pHH3)	R	0.7mg/ml	1/600	AbCam
anti-Oct4	R	3.5µg/ml	1/200	AbCam
anti-nanog	R	0.2mg/ml	1/200	AbCam
anti-Osteopontin	R	Unavailable	1/200	Kindly donated by Dr G. Griffiths
anti-Osteocalcin	G	1.0µg/ml	1/200	Santa Cruz Biotechnology
anti-β-Catenin	R	150µl-Concentration cannot be disclosed due to propriety	1/500	Cellomics, Thermo Scientific
anti-phospho Focal Adhesion Kinase (pFAK) (Y397)	R	0.4µg/ml	1/500	AbCam
Mouse anti-αTubulin	M	1mg/ml	1/5000	Thermo Scientific
Alexa Fluor 488 Goat anti-Mouse IgG Ab	G	4µg/ml	1/500	Invitrogen
Alexa Fluor 488 Goat anti-Rabbit IgG Ab	G	4µg/ml	1/500	Invitrogen
Alexa Fluor 594 Chicken anti-Goat IgG Ab	Ch	4µg/ml	1/500	Invitrogen
Hoechst 33342		20µg/ml	1/500	Invitrogen
Whole cell green fluorescent membrane stain		50µl-Concentration cannot be disclosed due to propriety	1/100	Cellomics, Thermo Scientific

Abbreviations: R, Rabbit; M, Mouse; G, Goat; Ch, Chicken.

2.12 Cellomics HCS Reader: Compartmental Analysis Bio-Application and Morphology Explorer Bio-Application

Biomarkers of interest were labelled, visualised and the intensity quantified with the Cellomics ArrayScan© HCS Reader: Compartmental Analysis Bio-Application (V2 Version, Thermo Scientific). Indirect immunofluorescence staining was used to visualise and quantitate immunoreactivity towards proteins of interest (listed in Table 3 above). The cell morphology; area and shape (i.e. P2A - perimeter to area ratio; LWR – length to width ration) of whole cell membrane stained and α-tubulin immunostained cells were imaged and analysed with the Cellomics ArrayScan© Morphology Explorer Bio-Application (V2 Version, Thermo Scientific).

Following ICC staining of the cells, and counter staining of the nuclei with Hoechst 33342, plates of cells were loaded into the ArrayScan and ≥8 images were taken from the centre through a spiral pattern outward towards the edge of each well with no less than 5000 cells imaged within the collected images. Images were taken in three channels: channel 1 ($386nm_{EM}$), channel 2 ($488nm_{EM}$) and channel 3 ($549nm_{EM}$).

These images were then analysed through the bio-application analysis protocols to identify the immunoreactivity fluorescence intensity for the regions of interest on a per cell basis (Figure 2.5). Firstly, the platform located cells based on their Hoechst 33342 positivity designated as channel 1 (386nm). Then the platform measured the fluorescence intensity of the Hoechst 33342 as well as GFP/RFP within the nuclear area of each cell, designated the 'circ' cellular region (yellow dashed circle in Figure 2.5). Similarly, the platform measured the fluorescence intensity within the cytoplasmic ring area of each cells, designated the 'ring' region (red ring in Figure 2.5). The exact shape of the nucleus 'circ' and cytoplasmic regions of interest 'ring', were determined by the initial shape of the identified nucleus.

Next, within the 'circ' and 'ring' area, threshold values were used to identify 'spots'; these were referred to as 'circ spots' and 'ring spots' (purple rings and areas in Figure 2.5). Fluorescence immunoreactivity levels for the nuclear 'circ' and 'circ spot', cytoplasmic 'ring' and 'ring spot' regions were taken from the channel 2 (488nm) or channel 3 (549nm) fluorescence images. The results were reported on a per cell basis and include the sum of or mean intensity of the nuclear 'circ', nuclear spot 'circ spot', cytoplasmic 'ring', or cytoplasmic spot (ring spot) fluorescence intensity. The intensity is designated here as relative light units (RLU, an arbitrary annotation). Cells which measured immunoreactive fluorescence values greater than the set thresholds were counted and reported as a percentage positive (% positive) relative to all those examined within the population. An example of the distribution of and threshold values quantitated from images of Ki67 antigen immuno-stained cells can be seen in Figure 2.6. All data were corrected to values for those measured from the –ve 1^{O}Ab control. Data in Figure 2.6 is illustrated with the use of the TIBCO® Spotfire® Desktop 7.0.0 software (www.spotfire.tibco.com).

The Morphology Explorer Bio-Application protocol used in the experiments described was used to provide quantitative measurements related to whole cell morphology. The platform located cells based on the green fluorescent whole cell membrane stain designated to channel 1 (488nm). Then individual cells rather than multi-cell clusters or assemblages were located based on Hoechst 33342 positivity, and designated as channel 2 (386nm). Finally, features pertaining to the whole cell morphology were reported based on α-tubulin immunostaining, which was designated as channel 3 (549nm). Features reported within this report include; cell area, cell shape (P2A - perimeter to area ratio; LWR – length to width ratio), nuclear area, and nuclear shape P2A and LWR.

The P2A ratio was calculated using the following equation:

$$P2A = \frac{Perimeter^2}{4\pi \times Area}$$

A P2A and LWR value of 1 numerically denotes a complete circle. Therefore, objects which are more spherical have a value closer to 1, yet irregular shaped objects have values greater than 1.

The raw data showing the sum of and mean intensities on a per cell basis are shown in Appendix 7.1 within Figure 7.9 through Figure 7.16.; however, presented within this chapter is the percentage of cells positive for the biomarkers of interest, relative to a threshold value.

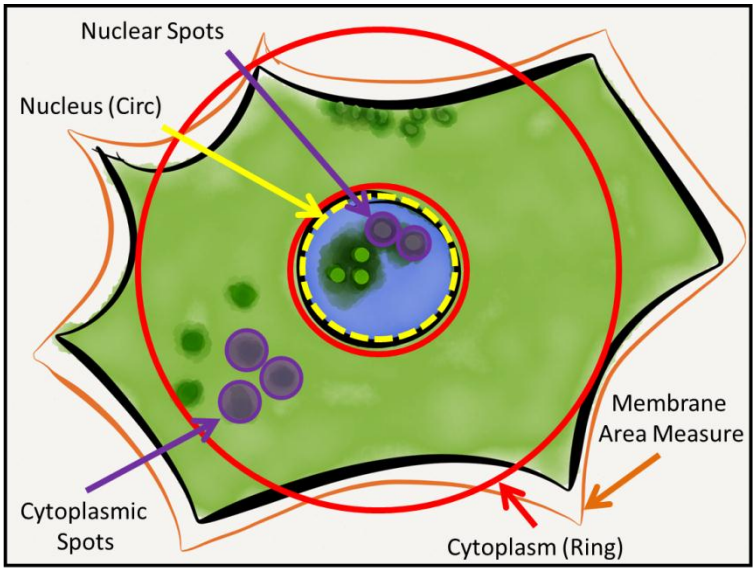

Figure 2.5: An illustration showing the different regions of interest used to identify biomarker immunoreactivity differences between cell types and regions.

The Cellomics ArrayScan© HCS and INCELL Analyser© HCS readers identify regions of interest within cells, then measure the intensity of the antibody or dye associated fluorescence of the biomarkers of interest. Fluorescence intensity was measured using the Compartmental Analysis BioApplication within the nuclear area (yellow dashed circle) or the cytoplasmic area (red ring). Using a threshold, the spot intensity was measured (purple circles) within the cytoplasm or nucleus. Cellular morphology was measured with the Morphology Explorer BioApplication based on a fluorescent membrane stain and α-tubulin staining (orange perimeter line) to reveal cell area, perimeter and shape.

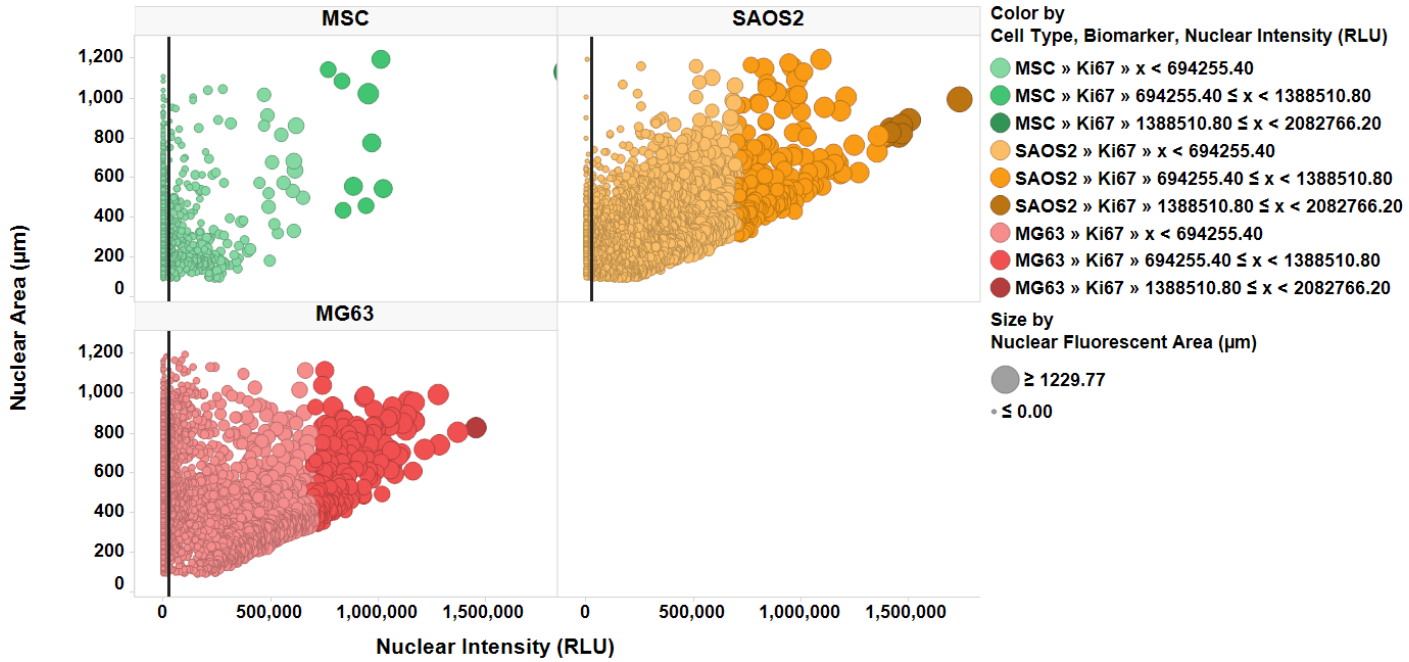

Figure 2.6: The distribution of fluorescent immunoreactive cells stained for the Ki-67 antigen.

The three graph panels detail the distribution of cells, where the nuclear intensity is shown on the x-axis and the nuclear area on the y-axis. As seen in the figure legend (right), the colour and shade of each spot varies according to cell type (MSC are green, SAOS2 are orange and MG63 cells are red) and according to fluorescence intensity (RLU) within the nucleus, categorised into three 'bins'. Likewise, the size of each spot is dependent on the area of fluorescence within each nucleus. The black line on each panel shows the mean threshold value which was used as a reference value, above which, immunoreactive cells were counted and reported as the percentage of positive cells (% positive) within the total population.

2.13 Cell labelling with Cell Tracker™ Green/Red Fluorescent Probes

To positively identify cell populations within co-cultures, MSC were labelled with Cell Tracker™ Green Fluorescent Probe Kit (Sigma-Aldrich) and SAOS2 or MG63 were labelled with Cell Tracker™ Red Fluorescent Probe Kit (Sigma-Aldrich) according to manufacturer's protocol. The fluorescent dye comprises of a lipophilic aliphatic carbon tail with a fluorochrome head group, which are incorporated and trapped within the lipid bilayer of the cell membrane (Horan and Slezak, 1989).

Cell Tracker™ Labelling was performed according to the manufacturer's protocol as follows: (i) cells in monolayer culture were trypsinised, washed three times in serum free DMEM/F-12 then centrifuged for 10mins at 1000rpm (1200rcf). (ii) After the final spin, all supernatant was removed and cells were re-suspended in 500µl of Diluent C (Mix A). (iii) In a fresh eppendorf 500µl of Diluent C and 4µl of fluorescent dye were mixed (Mix B). (iv) Mix A was then added to Mix B and thoroughly mixed by gentle pipetting. (v) This solution was allowed to stand at room temperature for 4 minutes, with regular inverting of the tube to maintain homogeneity. (vi) 1ml of complete media was added to neutralize the reaction. (vii) The solution was mixed by gentle pipetting and pelleted by centrifugation for 10 minutes at 1000rpm (1200rcf). (viii) Cells were washed and re-suspended twice in complete media. (ix) Cells were finally re-suspended in complete media, a viable cell count recorded and positive fluorescence staining was checked by fluorescence microscopy. Cells were then diluted accordingly and seeded appropriately.

2.14 Cell-IQ live-cell imaging

Live-cell imaging and analysis were conducted with the Cell-IQ Imagen^{TM} live-cell imaging platform and Cell-IQ Analyser^{TM} image analysis software (Cell-IQ version 2, CM Technologies Oy, Tampere, Finland). The Cell-IQ is a fully integrated continuous live-cell imaging platform with phase contrast and fluorescence imaging capabilities; an internal incubator, which allows continues culture of cells within any desired plate or flask format; and direct gas supply to the cultured cells. Upon selection

of the desired regions of interest (ROI), the system will image in phase contrast and fluorescence the exact X and Y coordinates of all ROIs throughout the whole plate format sequentially until stopped. The system also takes a series of Z-stack images over a desired distance, then compresses all Z-stack images into a 'snap all in focus' image. This snap all in focus image is then saved as a raw digitised image.

2.14.1 Imaging experimental setup

All images presented here were gathered with a 10x objective; at a resolution of 1392 x 1040 pixels, with a pixel to µm ratio of 0.710, therefore each image gathered is 988.3 x 738.4µm. Two - 3 ROIs were placed within each well and duplicate or triplicate wells were seeded at $4x10^3$ cells/cm^3; then the cells were fed with either control media or treatment media and then imaged. Therefore, no less than 4 ROIs were imaged per cell type or condition. Intervals between each image were set as the minimum imaging cycle time, where a complete cycle is the time needed for all positions within the whole culture format to be imaged i.e. plate or flask. Each image was analysed individually and readouts were pooled and reported as the mean ± standard deviation of the mean per repeat experiment. All ROIs were imaged with phase contrast, and where cells were stained with fluorescent membrane stains (discussed in section 2.13); a GFP filter for green fluorescence marked cells was used, a Cy3 filter for red fluorescence, and a Cy 5 filter for far-red fluorescence were also used. Cell Tracker™ fluorescent probes (Sigma-Aldrich) were used to identify specific cells, where MSCs were stained fluorescent green, SAOS2 and MG63 cells were stained fluorescent red. Dead cells were stained with DRAQ 7.

2.14.2 Image analysis

Following imaging of the cells, the system used the unique Machine Vision Technology to identify, analyse and quantify morphological features of cells within the images gathered using the Cell-IQ Analyser™ Cell Finder tool. To achieve this, the Cell-IQ Imagen™ software was "taught"

distinguishing morphological features from the digitised images, creating classes of each cell type using a stamp tool. This stamp tool record the exact pixel intensities and pattern within that region. Stamps were grouped into classes, namely; MSCs, SAOS2 cells, MG63 cells, round cells, dead cells and debris (background). A sample library of these stamp features and classes were generated into pattern recognition algorithms by the software (8 representative sample library images are shown in Figure 2.7). The two bottom panels show the morphology of confluent SAOS2 and MG63 cells respectively; however, these features were not used as a separate identification feature when analysing cultures. The debris class was included in every analysis of each experiment conducted.

The algorithms were used to analyse pixel intensities/patterns within all images gathered. Identification of MSCs, SAOS2 and MG63 cells in monoculture and co-cultures are discussed in Chapter 4. Class specific "fine-tuning" of the cell identification parameters, which was done to introduce variability of each cell type, included;

(i) Cell counting threshold: Segmentation gradient threshold value in the traditional meaning - a small value results more correct segmentations as it means the system is more sensitive to the intensity changes in the image. At the same time, the number of faulty segmentations may increase.

(ii) Minimum cell distance (pixels): The cell distance value defines the distance between two neighbouring cells - a small value potentially results more cells to be segmented.

(iii) Maximum cell diameter (pixels): The maximum cell diameter defines the size of the biggest cells in the population.

(iv) Cell symmetry (100 = round): With the cell symmetry parameter, the user can emphasize the importance of cell symmetry in the cell segmentation. In this terminology, an exactly round cell is the most symmetrical target.

(See Table 4 for details about the specific numerical differences between cell identification parameters).

>100 MSCs, SAOS2, MG63 cells and chondrosarcoma cells were tracked using the Cell-IQ Analyser™ Manual Cell Tracking tool, over culture periods greater than 24hrs of culture and results reported in Figure 4.9, Figure 7.30 and Figure 4.11.

For lineage tracking, the Cell-IQ Analyser™ Manual Cell Lineage Tracking tool was used and results presented in Figure 5.5 through Figure 5.9. Phase images of cells in monocultures were used and individual cells were tracked from images taken throughout the culture period, where ≥3 cells were tracked from each repeat experiment. In some cases, it was only possible to track 3 cells per repeat/condition due to their mobility and proliferation, where the proliferation of the cells into a fully confluent monolayer and therefore inhibit tracking and identification of the cell. The numbers of cells tracked between the different cell types and within each treatment condition are detailed in Table 5. Comparisons between the trajectory distance and speed of cells within the different treatment conditions in Chapter 5, >10 cells were tracked per cell type, per treatment condition. In depth details on live-cell imaging and analysis protocol development can be seen in Appendix 7.2.1 within Figure 7.18 through Figure 7.25. Donor to donor variability for manual cell lineage tracking is discussed in Appendix 7.2.3 and graphed in Figure 7.30.

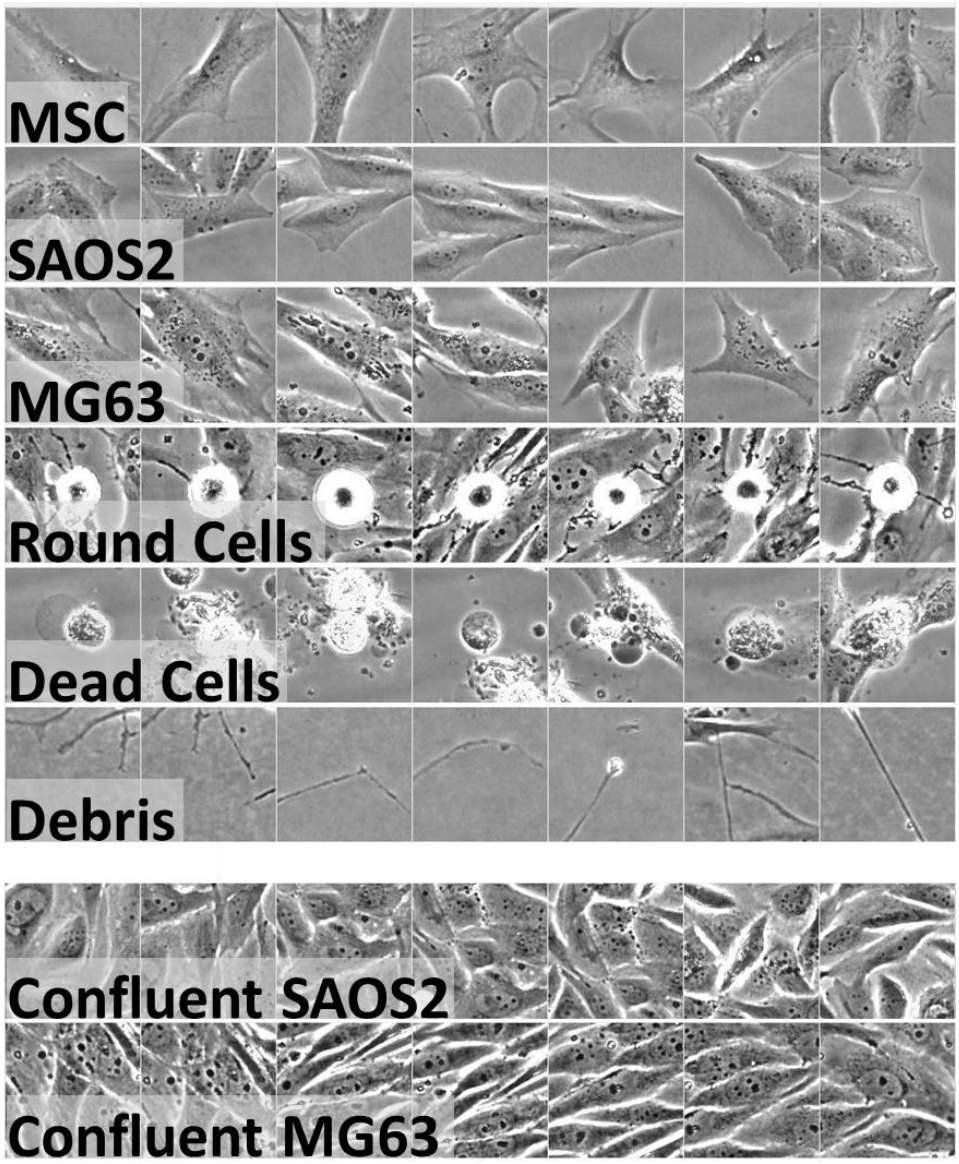

Figure 2.7: The Cell-IQ library 'stamps' which were obtained from phase contrast microscopy images showing different cell classes.

Eight representative images are shown making up the library of cell specific morphological features which were used to teach the pattern recognition software thus creating the different Algorithms. Classes shown (from the top panels) include: MSCs, SAOS2, MG63 cells, round cells, dead cells and finally debris. The two bottom panels show the morphology of confluent SAOS2 and MG63 cells respectively; however, these features were not used as a separate identification feature when analysing cultures. Original images obtained using magnification x100.

Table 4: Descriptive details for cell identification parameters: differences between class parameters.

	Cell counting threshold	Minimum cell distance (pixels)	Maximum cell diameter (pixels)	Cell symmetry (100:round)
MSCs	50	51	65	20
SAOS2	40	41	45	50
MG63	45	45	55	20
Round	65	35	48	80
Dead	35	25	45	20
Debris	35	25	45	20

Table 5: The number of cells analysed for lineage tracking are as follows:

	MSC 1	MSC 2	MSC 7	MSC 8	MSC 9	SAOS2	MG63
Con	11	46	55	21	20	60	26
BAP [Low]	18	61	53	20	14	66	44
BAP [High]	21	79	85	25	22	126	115
Con	10	73	50	18	13	78	28
V-BAP [Low]	21	38	71	23	18	71	50
V-BAP [High]	23	53	45	21	29	151	109

Abbreviations: BAP, Bezafibrate (BEZ) and Medroxyprogesterone Acetate (MPA); V-BAP, BAP supplemented with Valpoic Acid (VPA); BAP [Low], BAP concentration at [0.5mM/5µM] BEZ/MPA; BAP [High], BAP concentration at [1.0mM/10µM] BEZ/MPA; V-BAP [Low], BAP concentration at [0.5mM/5µM] BEZ/MPA supplemented with [0.6mM] VPA; V-BAP [High], BAP concentration at [1.0mM/10µM] BEZ/MPA supplemented with [0.6mM] VPA.

2.15 MTT assay

The tetrazolium dye, MTT 3-(4,5-dimethylthiazol-2-yl)-2,5-diphenyltetrazolium bromide is reduced into a purple insoluble formazan by NAD(P)H-dependent cellular oxidoreductase enzymes within viable cells. The formazan is then liberated by dissolving the cell with DMSO and the absorbance read using a spectrophotometer. MTT solution was prepared immediately prior to use and the assay was performed as follows: (i) 100µl of 5mg/ml MTT (Milford, Haarlem, Netherlands) was diluted per 1ml PBS supplemented with 4.5g/l glucose (Molekula, Gillingham, Dorset, UK). (ii) Following culture and/or treatment of samples, all media was removed from the wells and 100µl of PBS/Glucose + MTT solution was added per well in a 96 well plate. (iii) The plate was incubated in the dark for 3hrs and maintained in a humidified atmosphere at 37^{o}C with 5% CO_2. (iv) Following incubation, the solution was carefully removed and the plate was left to air dry for 10mins. (v) 100µl of DMSO (Sigma-Aldrich) was then added per well and the plate agitated until all cell debris was dissociated. (vi) The absorbance was read using a spectrophotometer at 492nm and background read at 650nm. (vii) Values were corrected for background and normalised to the mean of the control. Protocol adapted from Huang, Chen and Walker, (2004). Donor to donor variability for MTT results is discussed in Appendix 7.2.37.3.1 and graphed in Figure 7.31 and Figure 7.32.

2.16 Preparation of BEZ, MPA, VPA, BAP and V-BAP for drug treatments

Bezafibrate (BEZ) was maintained at a stock concentration of 0.5M in DMSO and used at a working concentration of 0.5mM. Medroxyprogesterone acetate (MPA) was maintained at a stock concentration of 5.0mM in ethanol and used at a working concentration of 5.0µM. Valproic acid (VPA) was maintained at a stock concentration of 0.6M in dH_2O and used at a working concentration of 0.6mM. All chemicals were purchased from Sigma-Aldrich. Stocks were stored at -20^{o}C. Combinatorial treatments with BEZ and MPA were collectively termed BAP. Treatments of BAP supplemented with VPA were collectively termed V-BAP.

The preparation of BEZ:

For a 1ml preparation of the highest working concentration [4.0mM], a 2X concentrated solution [8.0mM] was prepared as follows: (i) 8µl of BEZ stock [0.5mM] were placed into a micro-centrifuge tube, and then 1ml of warm complete media was added swiftly and mixed by pipetting. (ii) 8µl of DMSO was similarly prepared with 1ml of warm media as a negative control. (iii) Four serial doubling dilutions were then performed using 500µl of [4.0mM] solution added to 500µl of fresh complete media through to [0.25mM]. (iv) For a 96 well plate, 100µl of 2X concentrated solution was added to 100µl of complete media already within each well.

The preparation of MPA:

For a 1ml preparation of the highest working concentration [40µM], a 2X concentrated solution [80µM] was prepared as follows: (i) 8µl of MPA stock [5.0mM] were added to 1ml complete media within a 1.5ml micro-centrifuge tube and mixed by pipetting. (ii) 8µl of ethanol was similarly prepared in 1ml of warm complete media as a negative control. (iii) Four serial doubling dilutions were then performed using 500µl of [40µM] solution added to 500µl of fresh complete media through to [1.25µM]. (iv) For a 96 well plate, 100µl of 2X concentrated solution was added to 100µl of complete media already within each well.

The preparation of VPA:

For a 1ml preparation of the highest working concentration [2.4mM], a 2X concentrated solution [4.8mM] was prepared as follows: (i) 8µl of MPA stock [0.6M] were added to 1ml complete media within a 1.5ml micro-centrifuge tube and mixed by pipetting. (ii) 8µl of dH_2O was similarly prepared in 1ml of warm complete media as a negative control. (iii) Four serial doubling dilutions were then performed using 500µl of [4.8mM] solution added to 500µl of fresh complete media through to [0.3mM]. (iv) For a 96 well plate, 100µl of 2X concentrated solution was added to 100µl of complete media already within each well.

The preparation of BAP:

For a 1ml preparation of the highest working concentration of BEZ at [4.0mM] and MPA at [40µM], a 2X concentrated solution was prepared as follows: (i) 8µl of BEZ stock [0.5mM] were placed into a micro-centrifuge tube, and then 1ml of warm complete media was added swiftly and mixed by pipetting. (ii) 8µl of MPA stock [5.0mM] were added to the solution and mixed by pipetting. (iii) 8µl of DMSO and 8µl of ethanol were similarly prepared with 1ml of warm media as a negative control. (iv) Four serial doubling dilutions were then performed using 500µl of [4.0mM/40µM] solution added to 500µl of fresh complete media through to [0.25mM/2.5µM]. (v) For a 96 well plate, 100µl of 2X concentrated solution was added to 100µl of complete media already within each well. (vi) For a 24 well plate, solutions were scaled up accordingly where a final volume of 1ml at 2X concentrated solution was added per well to 1ml complete media already within the well. Results obtained from the live-cell imaging examined two concentrations of BAP; namely, [0.5mM/5µM] BEZ/MPA or [1.0mM/10µM] BEZ/MPA. For the sake of simplicity, the lower concentration was referred to as BAP [Low] and the higher concentration as BAP [High] respectively.

The preparation of V-BAP:

Preparation of a 2X concentration BAP solution with the addition of VPA was done similarly to that above and prepared as follows: (i) a solution of combined BEZ [4.0mM] and MPA [40µM] solution was made, then serially diluted. (ii) Following serial dilutions, 2µl of VPA [0.6M] were added per 1ml of all BEZ/MPA concentrations. This resulted in solutions ranging from [4.0mM/40µM] BEZ/MPA + [0.6mM] VPA to [0.25mM/2.5µM] BEZ/MPA + [0.6mM] VPA. 2µl of dH_2O were similarly added as a negative control. (iii) For a 96 well plate, 100µl of 2X concentrated solution was added to 100µl of complete media already within each well. (iv) For a 24 well plate, solutions were scaled up accordingly where a final volume of 1ml at 2X concentrated solution was added per well to 1ml complete media already within the well. Again, results obtained from the live-cell imaging examined two concentrations of V-BAP; namely, [0.5mM/5µM/0.6mM] BEZ/MPA/VPA or

[1.0mM/10µM/0.6mM] BEZ/MPA/VPA. For the sake of simplicity, the lower concentration was referred to as V-BAP [Low] and the higher concentration as V-BAP [High].

2.17 DRAQ 7 staining of dead cells

DRAQ7™ (Bio Status Ltd, Leicestershire, UK) is a far-red fluorescent DNA dye that stains the nuclei in dead and permeabilized cells, whilst showing no signs of toxic effect on the proliferation ability and rate of cells in long term culture assays. DRAQ7™ was added to control and treatment solutions for all selective killing drug-treatment experiments, to confirm cell death during live-cell imaging. 10µl of DRAQ7™ was added directly per 1.0ml of control and drug treatment solutions for a final concentration of 3µM. Fluorescence was read and imaged at $633nm_{EX}$ and $>665nm_{EM}$.

2.18 Statistical Analysis

Data from ≥3 independent experiments have been presented here as the mean ± the standard error of the mean (SEM). Data from single experiments with internal replication have been presented within the Appendix, as the mean ± the SD. All data were presumed to be normally distributed, therefore parametric statistical analysis was performed to determine and verify any significant differences between groups. For experiments that had one independent variable across 3 or more experimental groups (such as biomarker immunoreactivity between MSCs, SAOS2 and MG63 cells), a one-way analysis of variance (ANOVA) was performed with a Tukey's multiple comparison test used to identify significant differences between the means of all variables. For experiments that had two independent variables across 3 or more experimental groups (such as phase identification of MSCs, SAOS2 and MG63 cells over an extended culture period), a two-way ANOVA was performed. In such analysis, a Tukey's multiple comparison test was then performed to identify significant differences between all the variable means. A Dunnett's multiple comparison test was performed to identify significant differences between variable means when compared to an individual variable mean. In all cases; *indicates $p \leq 0.05$, **indicates $p \leq 0.01$, ***indicates $p \leq 0.001$.

Chapter 3: The use of high content screening platforms to distinguish between MSCs and osteosarcoma cell lines

3.1 Aims and Background

A number of studies have suggested that MSCs may undergo spontaneous malignant transformation to form tumour cells, or at least can become contaminated with other cell types following extended periods in culture (Rubio *et al.*, 2005, Rubio *et al.*, 2008a, Rosland *et al.*, 2009, De La Fuente *et al.*, 2010, Torsvik *et al.*, 2010). There is also substantial evidence that transformed MSCs may form the cancer stem cell for certain tumours, notably osteosarcoma, Ewing's sarcoma and chondrosarcoma (Boeuf *et al.*, 2008, Riggi *et al.*, 2008, Suva *et al.*, 2009, Lin, Wang and Lozano, 2011). Possible contamination or transformation of MSCs within culture expansion prior to transplantation therapies is a risk, which should be taken into full account, as should the need for standardized identification of MSC characteristics. In addition, there is a continued need for the development of improved tools for monitoring safety and release criteria (Heathman *et al.*, 2015a). Furthermore, automated methods of establishing MSC phenotype will enable the wide scale and regulated provision of MSCs in the developing field of regenerative medicine.

Therefore, this chapter has examined whether the computerized HCS imaging platform, Thermo Fisher Cellomics Array Scan II could provide a means of distinguishing between human MSCs and osteosarcoma cell lines, SAOS2 and MG63 cells. All fluorescence intensity measurements were performed using the Thermo Fisher^{TM} Cellomics Array Scan. This was done via quantification of fluorescent intensities of fluorescently tagged immunoreactive labelled proteins. The protein markers of interest are associated with cell cycle progression, proliferation and survival, pluripotency, osteoblastic cell differentiation, cell signalling and cell migration. In addition, the analysis included assays of cellular and nuclear morphology. All results shown within this chapter detail the percentage of cells which were positive for nuclear or cytoplasmic biomarker spot immunoreactivity relative to the total number of immunoreactive cells within each ROI, corrected for the number of -1^{0}Ab immunoreactive control cells. A detailed description of this is given in sections 2.12 and 7.1.1.

3.2 Cell cycle and cell proliferation

Representative fluorescence microscopy images and quantitation of Ki67 antigen, phosphorylated retinoblastoma protein (pRB) and phosphorylated histone H3 (pHH3) immunoreactive cells are shown in Figure 3.1, Figure 3.2 and Figure 3.3 respectively. As shown, bright nuclear immunoreactive staining for Ki67 antigen was both punctate and diffuse in appearance in many SAOS2 (91.34% ± 0.56%) and MG63 cells (65.64% ± 16.94%); in contrast, significantly fewer in MSCs (4.98% ± 3.36%, p=0.0021 and p=0.0121 respectively), which exhibited a similar pattern of immuno-localisation. Images and quantitation of pRb immunoreactivity shows significantly marked immunoreactivity in MG63 cells (55.51% ± 12.78%) rather than in MSCs (6.06% ± 7.35%, p=0.0150) and SAOS2 cells (non-detected, p=0.0077). Images and quantitation of pHH3 immunoreactivity show bright, punctate and diffuse nuclear staining seen in many MG63 cells; in contrast but non-significantly, fewer MSCs and SAOS2 cells were pHH3 immunoreactive, which exhibited a similar pattern of immuno-localisation.

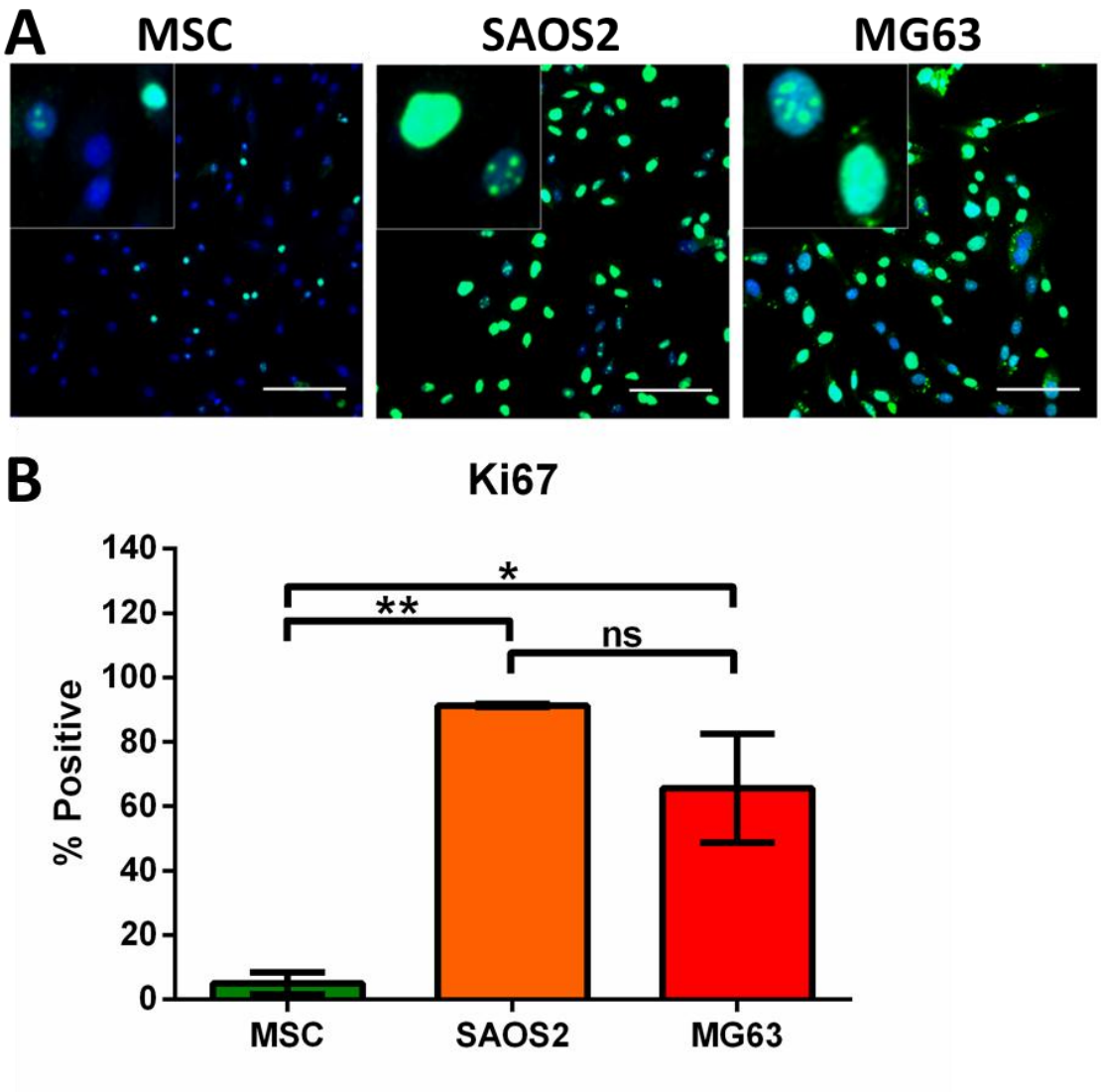

Figure 3.1: Immunoreactivity for the proliferation associated Ki67 antigen within primary human MSCs, SAOS2 and MG63 cells.

(A) Representative images showing Hoechst 33342 and fluorescent Ki67 antigen immunoreactivity in MSC, SAOS2 and MG63 cells (Bar = 100µm). Inset is 4.8x magnified. (B) Bar graph showing the percentage of cells positive relative to threshold values for nuclear intensity for the biomarker Ki-67 antigen within MSCs, SAOS2 and MG63 cells. Data shown are means ± SEM from n=3 independent experiments. **indicates $p \leq 0.01$, *indicates $p \leq 0.05$, and *ns* indicates there is no significant difference. All; one-way ANOVA with a Tukey's multiple comparisons test.

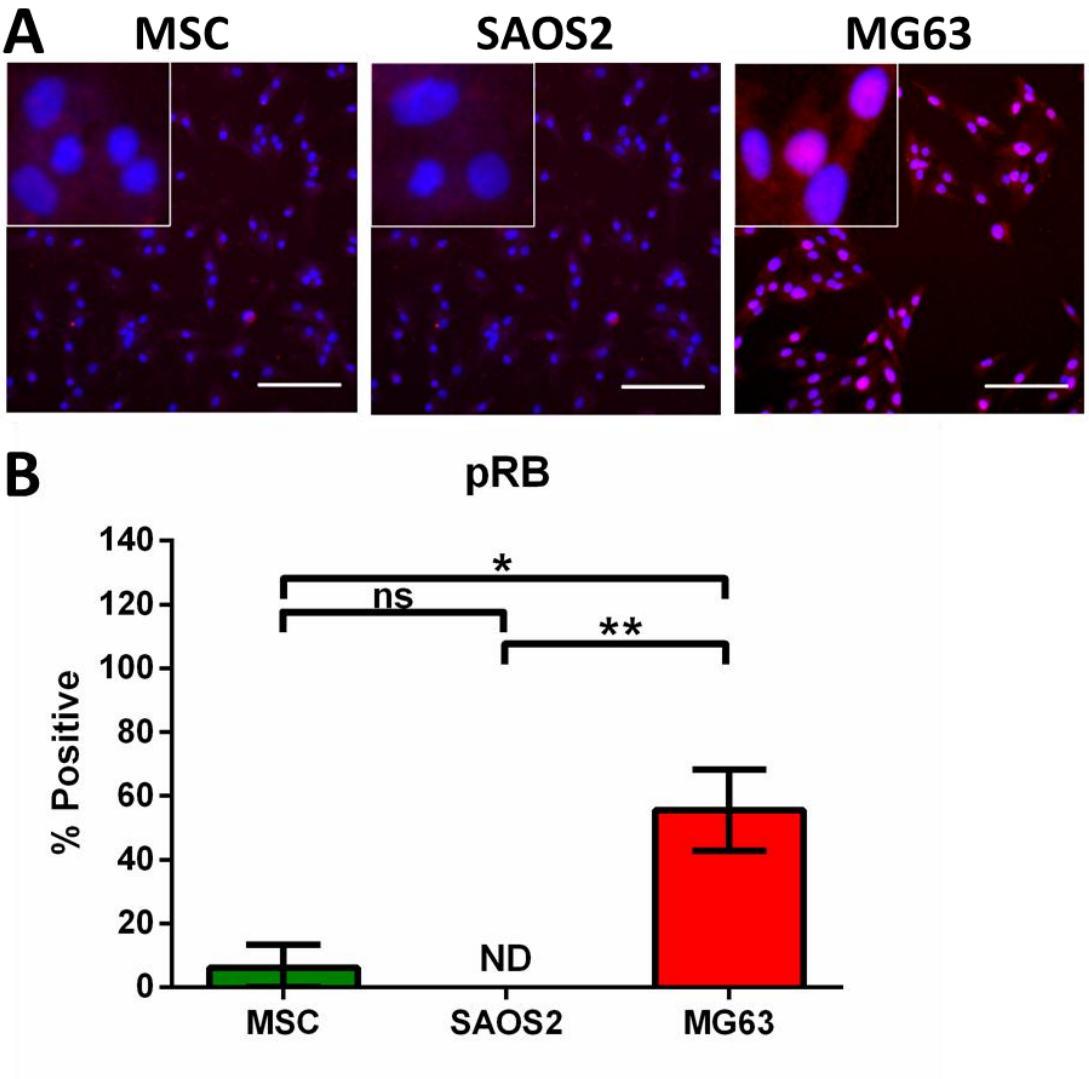

Figure 3.2: Immunoreactivity for the phosphorylated form of the tumour suppressor retinoblastoma protein (pRb) within primary human MSCs, SAOS2 and MG63 cells.

(A) Representative images showing Hoechst 33342 and fluorescent pRb immunoreactivity in MSC, SAOS2 and MG63 cells (Bar = 100µm). Inset is 4.8x magnified. (B) Bar graph showing the percentage of cells positive relative to threshold values for nuclear intensity for the biomarker pRB within MSCs, SAOS2 and MG63 cells. Data shown are means ± SEM from n=3 independent experiments. **indicates $p \leq 0.01$, *indicates $p \leq 0.05$, ND indicates non-detected and *ns* indicates there is no significant difference. All; one-way ANOVA with a Tukey's multiple comparisons test.

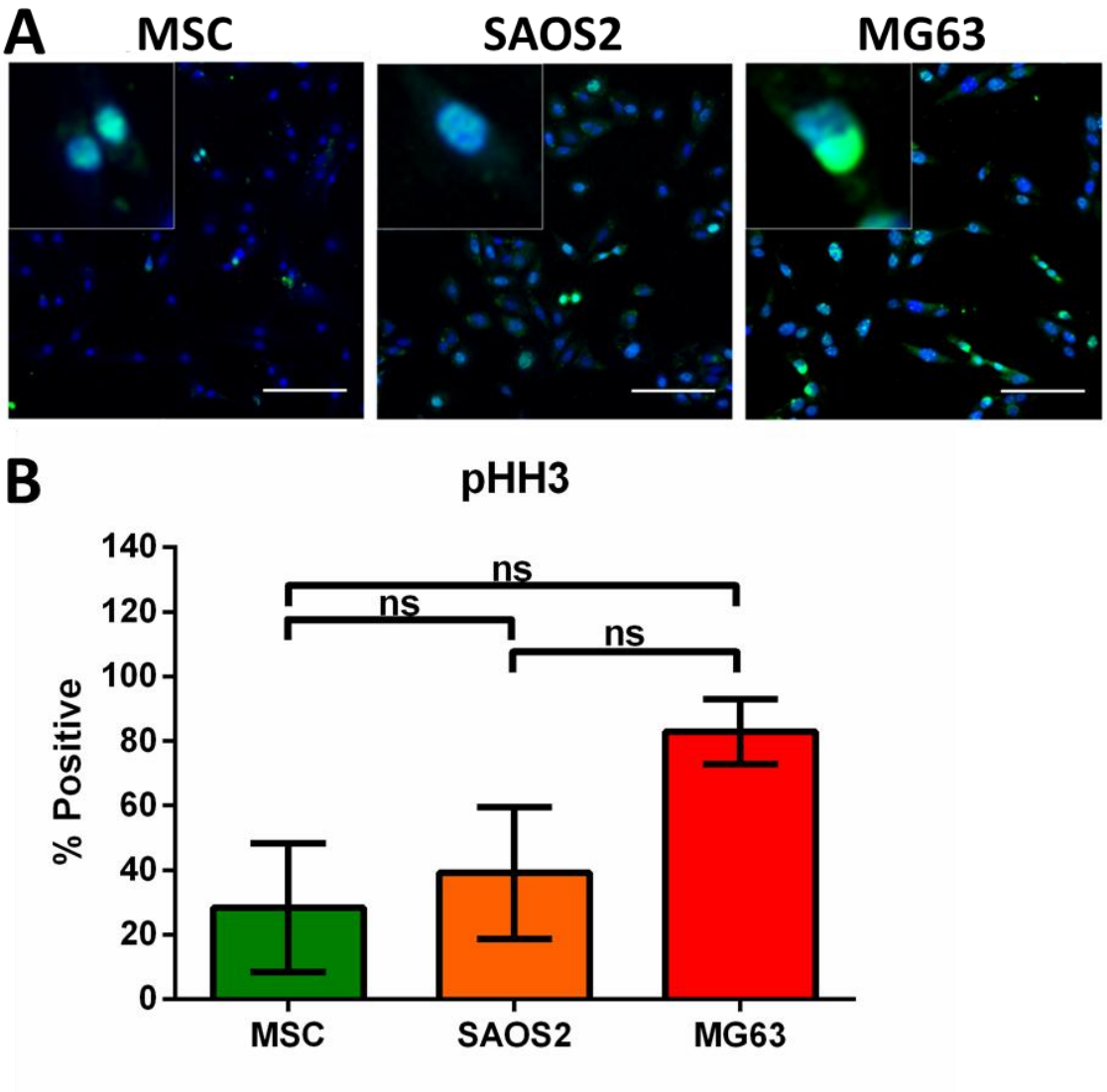

Figure 3.3: Immunoreactivity for the phosphorylated nuclear histone protein H3 (pHH3) within primary human MSCs, SAOS2 and MG63 cells.

(A) Representative images showing Hoechst 33342 and fluorescent pHH3 immunoreactivity in MSC, SAOS2 and MG63 cells (Bar = 100µm). Inset is 4.8x magnified. (B) Bar graph showing the percentage of cells positive relative to threshold values for nuclear intensity for the biomarker pHH3 within MSCs, SAOS2 and MG63 cells. Data shown are means ± SEM from n=3 independent experiments. *ns* indicates there is no significant difference. All; one-way ANOVA with a Tukey's multiple comparisons test.

3.3 Pluripotency markers

Representative fluorescent microscopy images and quantitation of the immunoreactivity of the pluripotency and transcription factors, Oct4 and nanog, are shown in Figure 3.4 and Figure 3.5 respectively. As shown, bright and diffuse nuclear staining for Oct4 was seen in many SAOS2 (68.75% ± 18.61) and MG63 cells (71.39% ± 10.34%); in contrast, significantly fewer MSCs exhibited nuclear positivity (7.92% ± 5.76%, p=0.0344 and p=0.0289 respectively), but rather showed a diffuse cytoplasmic pattern of immuno-localisation. Immunoreactivity for nanog showed punctate nuclear staining in MG63 cells (53.45% ± 8.72%); in contrast, significantly fewer MSCs (0.47% ± 0.72, p=0.0103) were immunoreactive. However, there was no significant difference seen in the number of nanog immunoreactive SAOS2 cells (23.67% ± 11.67%, p=0.102).

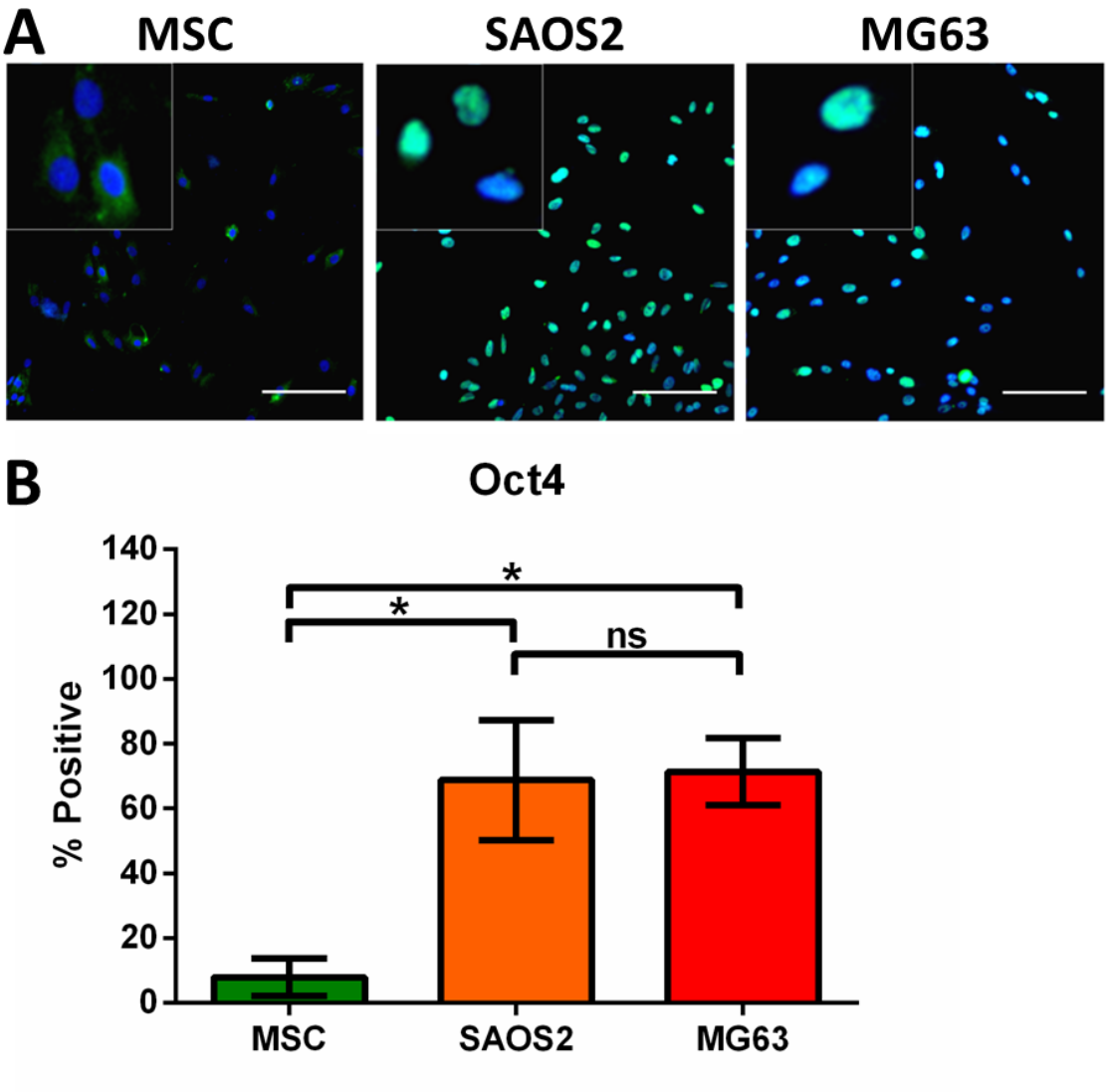

Figure 3.4: Immunoreactivity for the pluripotency marker Oct4 within primary human MSCs, SAOS2 and MG63 cells.

(A) Representative images showing Hoechst 33342 and fluorescent Oct4 immunoreactivity in MSC, SAOS2 and MG63 cells (Bar = 100µm). Inset is 4.8x magnified. (B) Bar graph showing the percentage of cells positive relative to threshold values for nuclear intensity for the biomarker Oct4 within MSCs, SAOS2 and MG63 cells. Data shown are means ± SEM from n=3 independent experiments. *indicates $p \leq 0.05$ and *ns* indicates there is no significant difference. All; one-way ANOVA with a Tukey's multiple comparisons test.

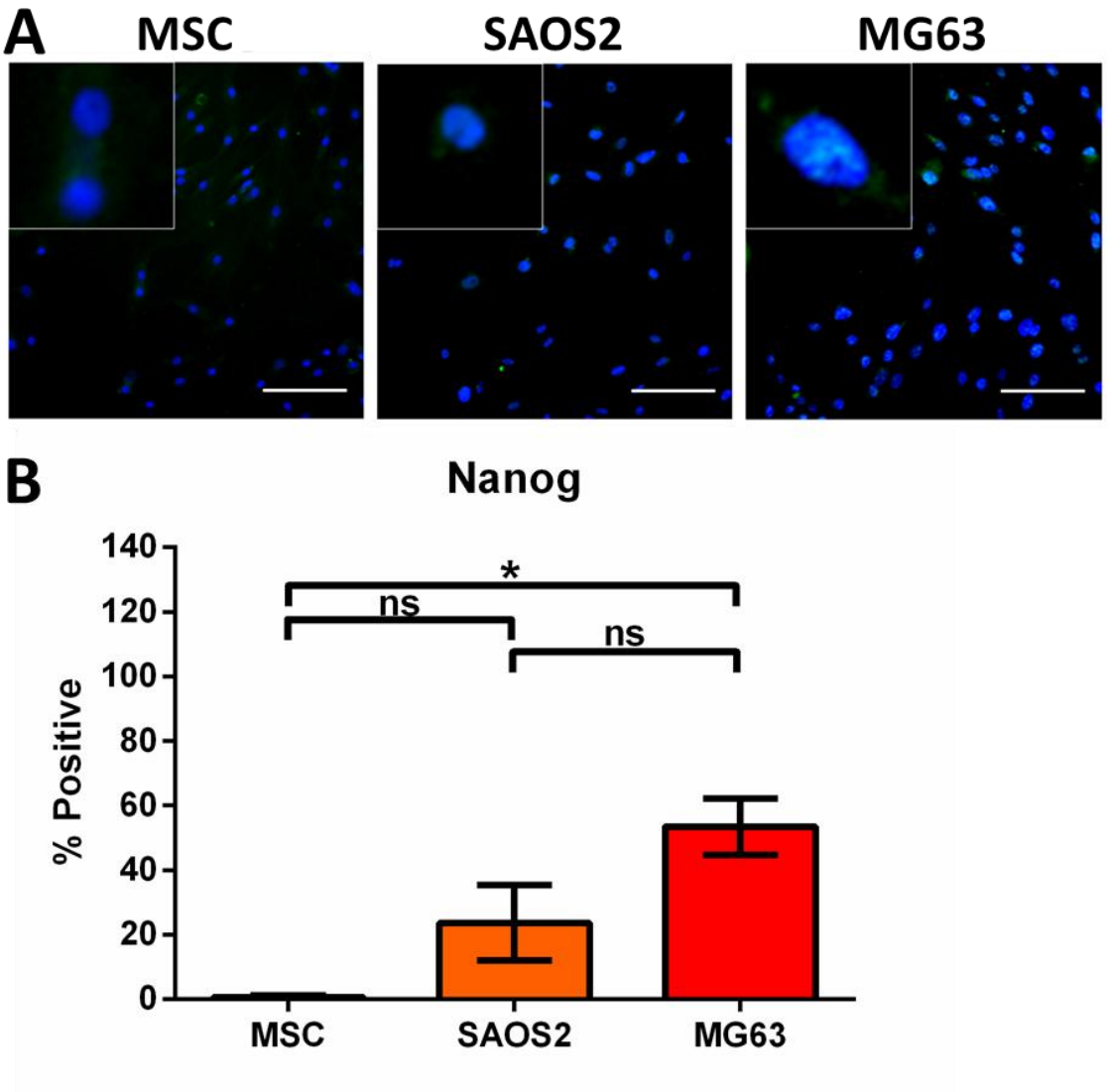

Figure 3.5: Immunoreactivity for the transcription factor nanog within primary human MSCs, SAOS2 and MG63 cells.

(A) Representative images showing Hoechst 33342 and fluorescent nanog immunoreactivity in MSC, SAOS2 and MG63 cells (Bar = 100µm). Inset is 4.8x magnified. (B) Bar graph showing the percentage of cells positive relative to threshold values for nuclear intensity for the biomarker nanog within MSCs, SAOS2 and MG63 cells. Data shown are means ± SEM from n=3 independent experiments. *indicates $p \leq 0.05$ and *ns* indicates there is no significant difference. All; one-way ANOVA with a Tukey's multiple comparisons test.

3.4 Differentiation markers

The biomarkers associated with osteoblastic differentiation, osteopontin and osteocalcin, were not able to significantly distinguish primary human MSCs from either SAOS2 or MG63 cells. Representative fluorescence microscopy images and quantitation of such, of cytoplasmic osteopontin immunoreactivity are shown in Figure 3.6. As shown, bright, perinuclear staining was seen in the MSCs and SAOS2 cells. MG63 cells exhibited a more diffuse cytoplasmic staining pattern. Similarly, fluorescence microscopy images and quantitation of the immunoreactivity for cytoplasmic osteocalcin are shown in Figure 3.7. As shown, a few MSCs exhibited bright, punctate immunoreactivity in the cytoplasm, whilst MG63 exhibited a homogenous pattern of immunoreactivity throughout the cytoplasm. In contrast, SAOS2 cells showed very little immunoreactivity throughout. No significant differences in the number of cells immunoreactive for osteopontin or osteocalcin were seen between the cell types.

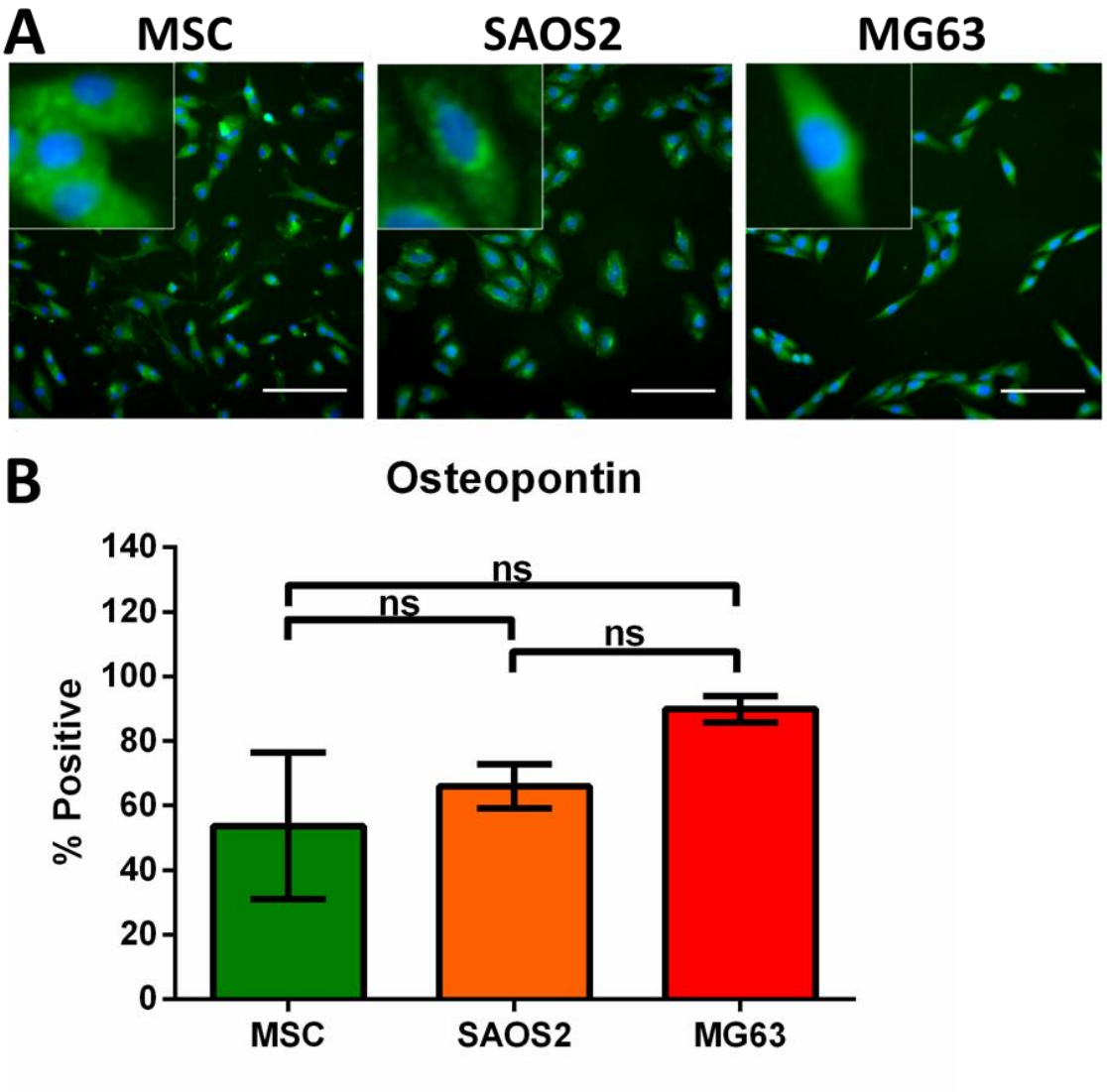

Figure 3.6: Immunoreactivity for the extracellular matrix protein osteopontin within primary human MSCs, SAOS2 and MG63 cells.

(A) Representative images showing Hoechst 33342 and fluorescent osteopontin immunoreactivity in MSC, SAOS2 and MG63 cells (Bar = 100µm). Inset is 4.8x magnified. (B) Bar graph showing the percentage of cells positive relative to threshold values for cytoplasmic intensity for the biomarker osteopontin within MSCs, SAOS2 and MG63 cells. Data shown are means ± SEM from n=3 independent experiments. *ns* indicates there is no significant difference. All; one-way ANOVA with a Tukey's multiple comparisons test.

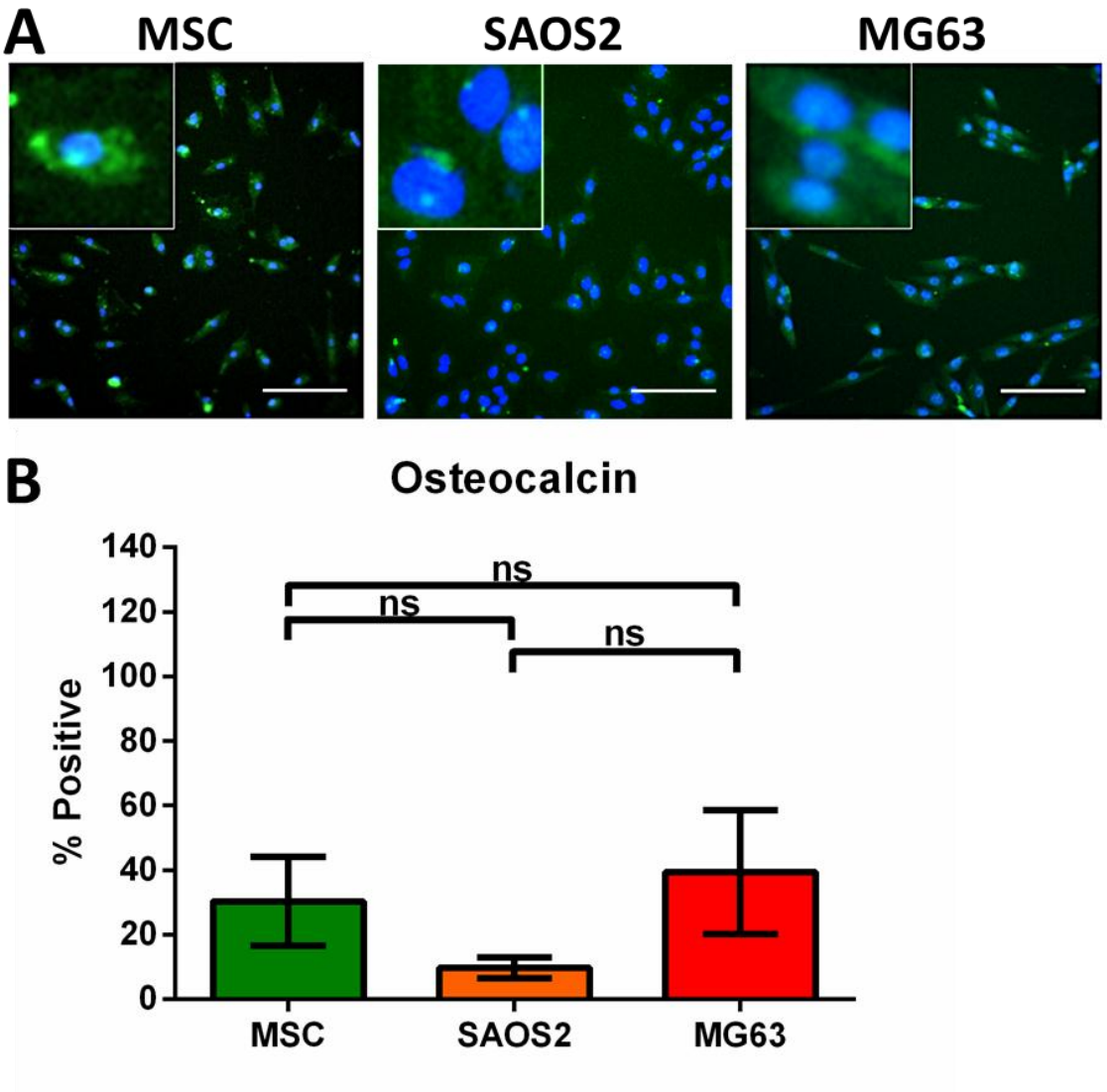

Figure 3.7: Immunoreactivity for the cytoplasmic protein osteocalcin within primary human MSCs, SAOS2 and MG63 cells.

(A) Representative images showing Hoechst 33342 and fluorescent osteocalcin immunoreactivity in MSC, SAOS2 and MG63 cells (Bar = 100µm). Inset is 4.8x magnified. (B) Bar graph showing the percentage of cells positive relative to threshold values for cytoplasmic intensity for the biomarker osteocalcin within MSCs, SAOS2 and MG63 cells. Data shown are means ± SEM from n=3 independent experiments. *ns* indicates there is no significant difference. All; one-way ANOVA with a Tukey's multiple comparisons test.

3.5 Cell signalling and migration

Imaging and quantitation of immunoreactivity for the intracellular signalling protein, β-Catenin, identified within the nuclear (Figure 3.8) or cytoplasmic areas (Figure 3.9), was only able to distinguish MG63 cells from MSCs with no significant difference seen between MSCs and SAOS2 cells, or SAOS2 and MG63 cells. As shown, diffuse cytoplasmic staining can be seen within MSCs and SAOS2 cells. In contrast, MG63 cells showed a mixture of bright, diffuse and punctate cytoplasmic staining. A similar pattern to the cytoplasmic staining was seen within the nuclei of the cells, where SAOS2 and MSCs showed bright diffuse immunoreactivity and MG63 showed a mixture of bright diffuse and punctate nuclear immunoreactivity. MG63 cells were significantly more immunoreactive for cytoplasmic and nuclear β-catenin (91.77% ± 3.07% and 89.34% ± 1.66% respectively) compared to the immunoreactivity of MSCs (31.14% ± 22.60%, p=0.0419 and 28.97% ± 16.17%, p=0.0099 respectively).

Imaging and quantitation of immunoreactivity for the biomarkers associated with cell migration, pFAK shown in Figure 3.10, presented a distinctly unique staining pattern between each cell type. MSCs showed a dull diffuse cytoplasmic staining. In contrast, SAOS2 cells stained with a bright puncta along the outer edge of their cytoplasm and dull diffuse cytoplasmic staining. MG63 cells contrasted to both MSCs and SAOS2, where bright, punctate and diffuse stained was seen within the cytoplasm. However, quantitation of the number of immunoreactive cells was not significantly different between cell types.

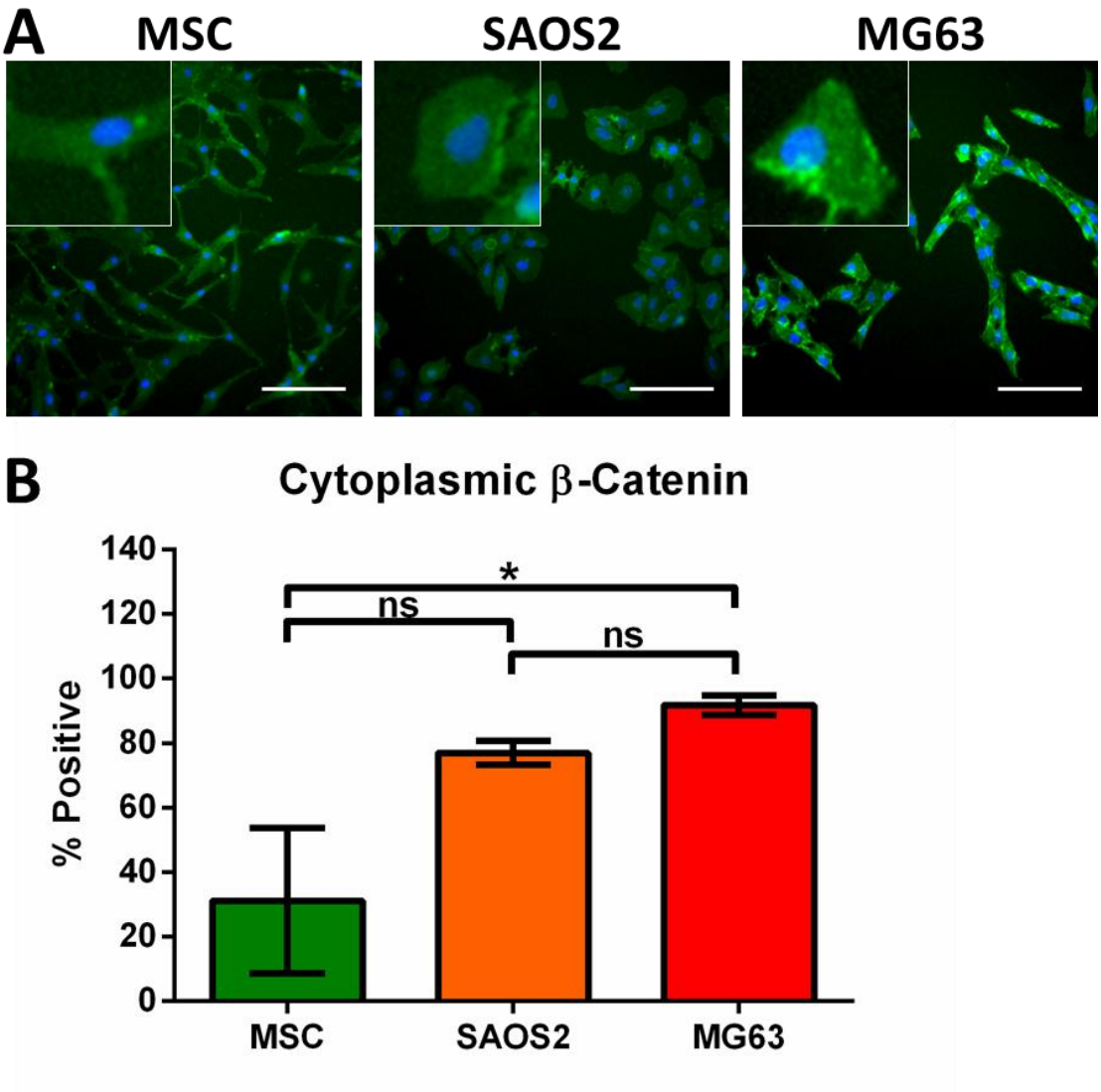

Figure 3.8: Immunoreactivity for the signalling protein β-Catenin within the cytoplasm of primary human MSCs, SAOS2 and MG63 cells.

(A) Representative images showing Hoechst 33342 and fluorescent cytoplasmic β-Catenin immunoreactivity in MSC, SAOS2 and MG63 cells (Bar = 100µm). Inset is 4.8x magnified. (B) Bar graph showing the percentage of cells positive relative to threshold values for cytoplasmic intensity for the biomarker β-catenin within MSCs, SAOS2 and MG63 cells. Data shown are means ± SEM from n=3 independent experiments. *indicates $p \leq 0.05$ and *ns* indicates there is no significant difference. All; one-way ANOVA with a Tukey's multiple comparisons test.

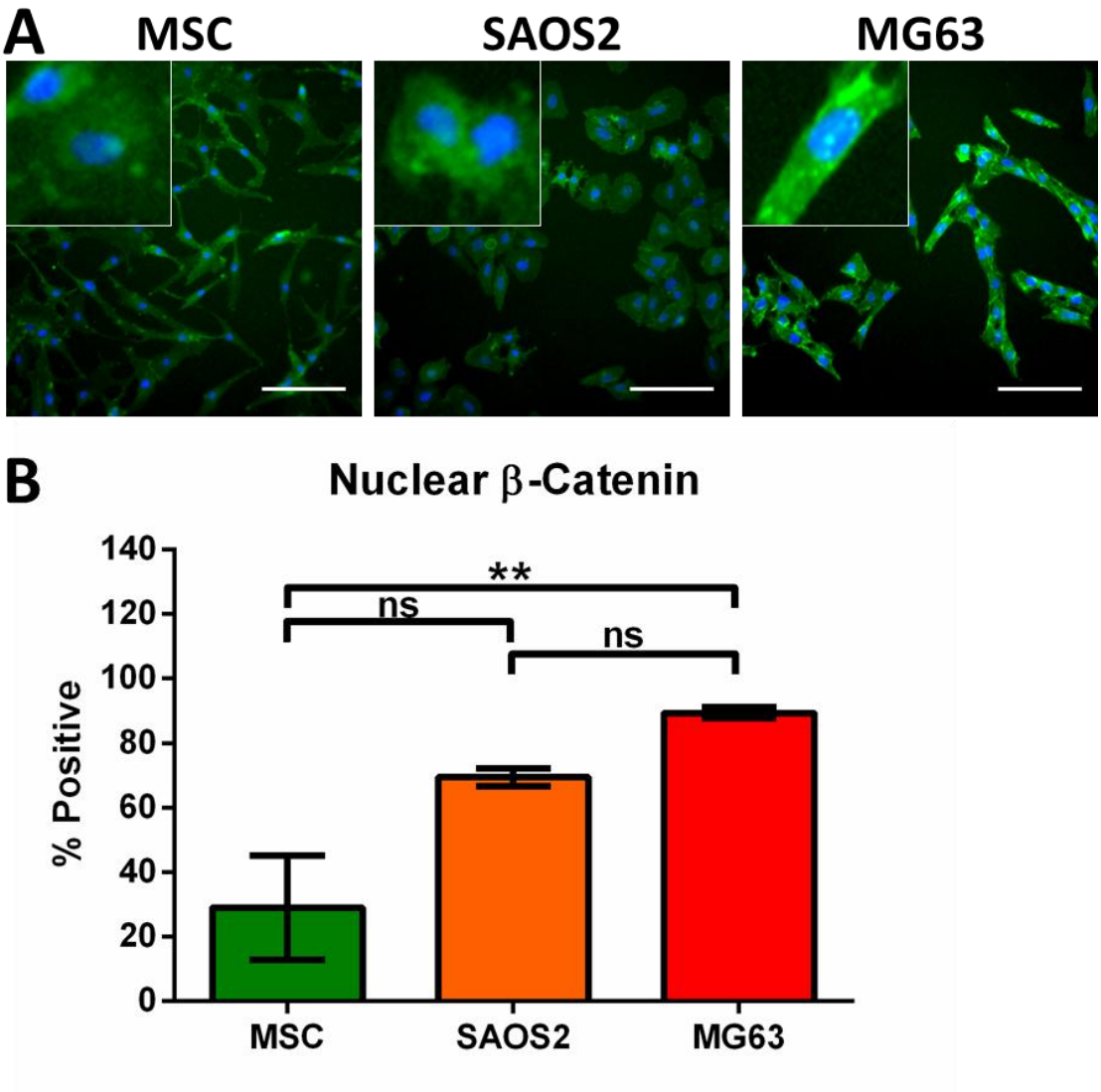

Figure 3.9: Immunoreactivity for the signalling protein β-Catenin within the nuclei of primary human MSCs, SAOS2 and MG63 cells.

(A) Representative images showing Hoechst 33342 and fluorescent nuclear β-Catenin immunoreactivity in MSC, SAOS2 and MG63 cells (Bar = 100µm). Inset is 4.8x magnified. (B) Bar graph showing the percentage of cells positive relative to threshold values for nuclear intensity for the biomarker β-catenin within MSCs, SAOS2 and MG63 cells. Data shown are means ± SEM from n=3 independent experiments. **indicates $p \leq 0.01$ and *ns* indicates there is no significant difference. All; one-way ANOVA with a Tukey's multiple comparisons test.

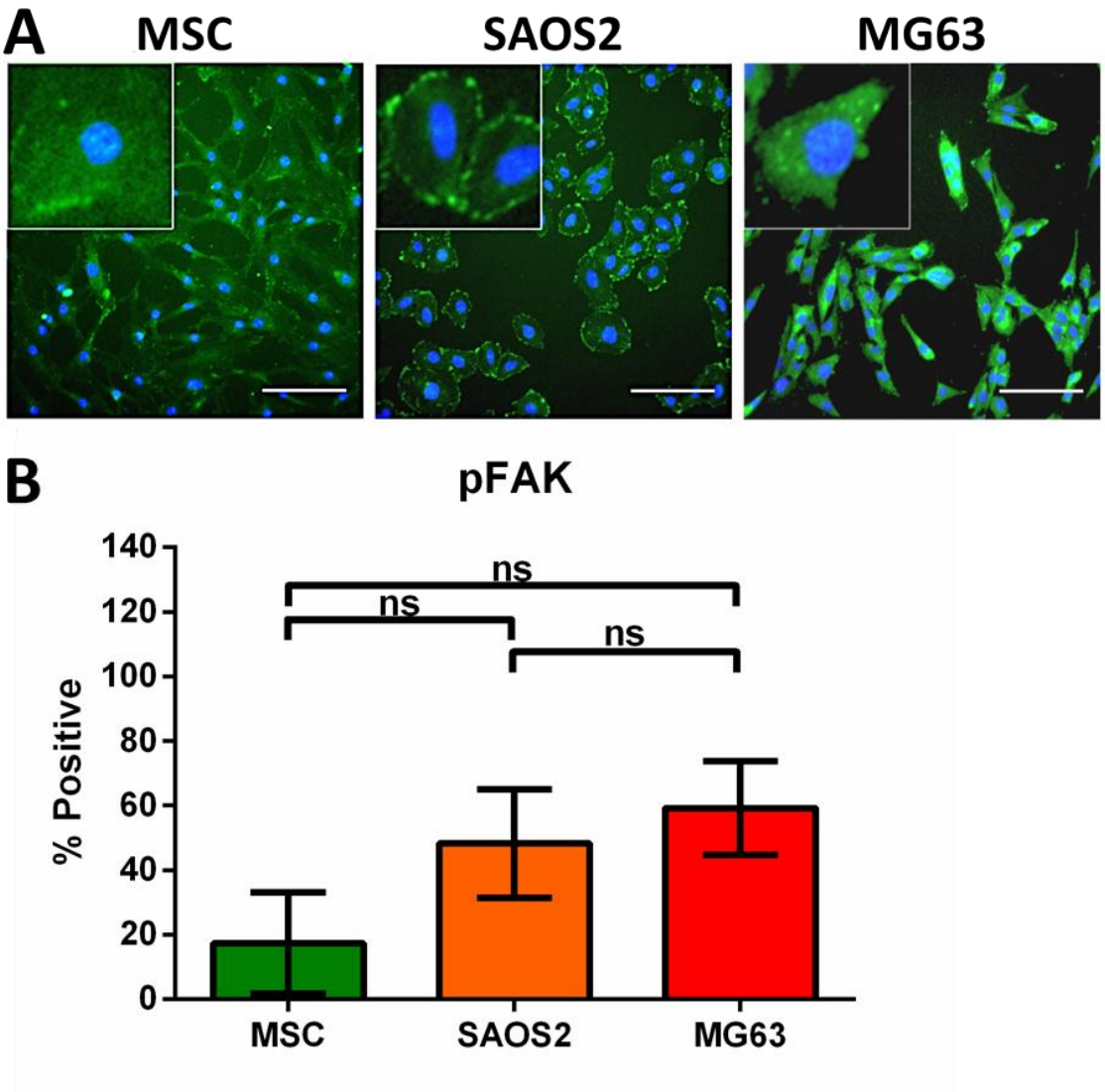

Figure 3.10: Immunoreactivity for the phosphorylated cytoplasmic protein focal adhesion kinase (pFAK) within primary human MSCs, SAOS2 and MG63 cells.

(A) Representative images showing Hoechst 33342 and fluorescent pFAK immunoreactivity in MSC, SAOS2 and MG63 cells (Bar = 100µm). Inset is 4.8x magnified. (B) Bar graph showing the percentage of cells positive relative to threshold values for nuclear intensity for the biomarker pFAK within MSCs, SAOS2 and MG63 cells. Data shown are means ± SEM from n=3 independent experiments. *ns* indicates there is no significant difference. All; one-way ANOVA with a Tukey's multiple comparisons test.

3.6 Nuclear and Cytoplasmic Biomarker Summary

The summary heat map of nuclear biomarkers examined within this chapter is shown in Figure 3.11, where the average nuclear fluorescent intensity (RLU arbitrary units) for all the biomarkers are compared and grouped according to cell type. The area of each rectangle is relative to the average biomarker fluorescence area measured (μm^2) within each nucleus. It can easily be seen that the SAOS2 and MG63 cells presented the most immunoreactive labelled cells for Ki67 antigen, nuclear β-catenin and pHH3 compared to the MSCs.

Similarly, the cytoplasmic biomarkers shown in Figure 3.12 were compared, and it easily can be seen that β-catenin was the most immunoreactive biomarker, followed by osteopontin, pFAK and osteocalcin within MG63 cells; less so within MSCs and SAOS2 cells.

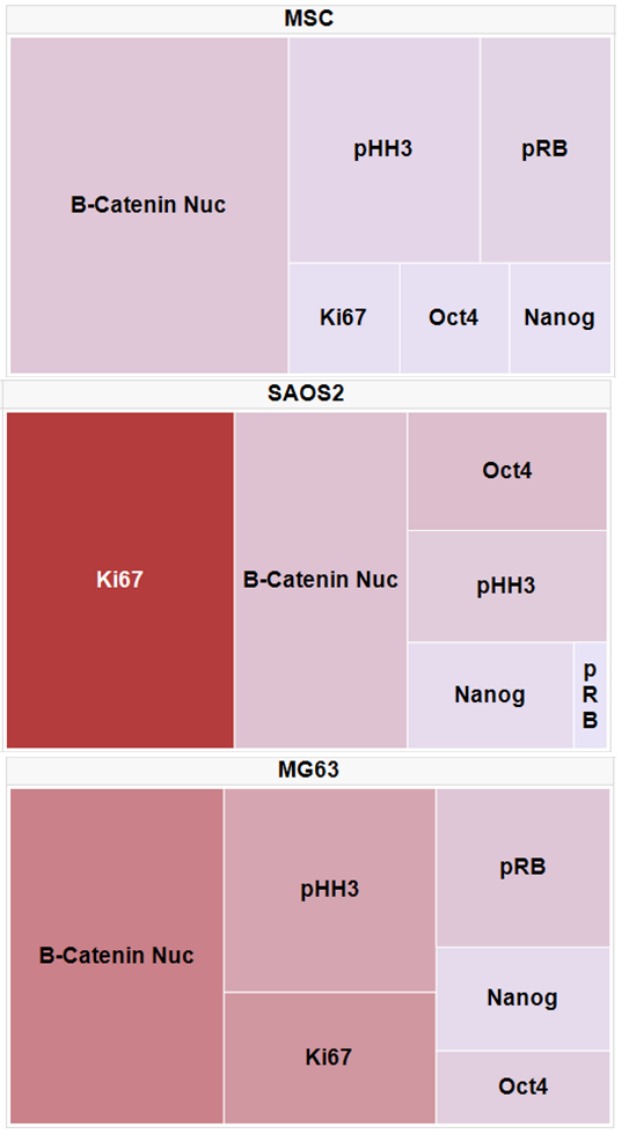

Figure 3.11: A heat map comparing the nuclear fluorescent intensity with the nuclear fluorescent area for a broad range of nuclear biomarkers within primary human MSCs, SAOS2 and MG63 cells. The heat map illustrates the range of fluorescently immunoreactive nuclear intensities (intensity of the red rectangles; min 5,259 RLU to max 205,847 RLU) and nuclear fluorescent area (area of rectangles; μm^2) for all nuclear biomarkers; β-catenin, pHH3, Ki67 antigen, nanog and Oct4 within the primary MSCs, SAOS2 and MG63 cells. Data used are from 3 independent experiments. The heat map is firstly grouped by cell type, then by biomarker.

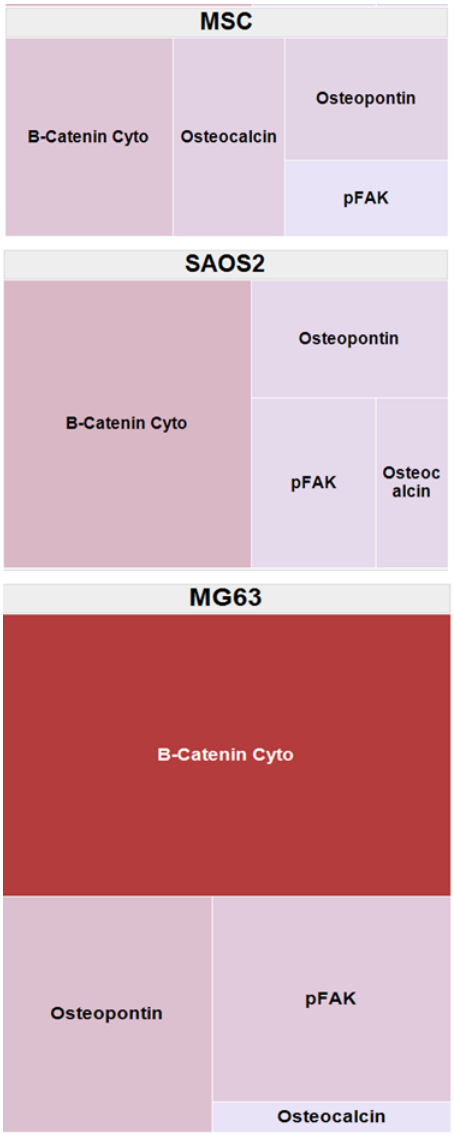

Figure 3.12: A heat map comparing the cytoplasmic fluorescent intensity with the cytoplasmic fluorescent area for a broad range of cytoplasmic biomarkers within primary human MSCs, SAOS2 and MG63 cells.

The heat map illustrates the fluorescently stained cytoplasmic intensities (intensity of the red rectangles; min 19,408 RLU to max 330,593 RLU) and cytoplasmic fluorescent area (area of rectangle; μm^2) for all cytoplasmic biomarkers; β-catenin, osteocalcin, osteopontin and pFAK within the primary MSCs, SAOS2 and MG63 cells. Data used are from 3 independent experiments. The heat map is firstly grouped by cell type, then by biomarker.

3.7 Cell and Nuclear Morphology

Measurements of cell and nuclear morphological features were only able to significantly distinguish human MSCs from both SAOS2 and MG63 cells based on nuclear area. Images of α-tubulin stained cells and the quantitation of cell area, perimeter to area (P2A) shape and length to width ratio (LWR) shapes of MSCs, SAOS2 and MG63 cells are shown in Figure 3.13 and Figure 3.14 respectively. The immunoreactivity of α-tubulin demonstrated that MSCs exhibited a fibroblastic appearance, with some stellate cells extending multiple slender cytoplasmic processes. In contrast, SAOS2 and MG63 cells were more polygonal and exhibited morphological shapes which were bipolar, triangular or circular. Quantitation of the morphology showed that MG63 cells had an average area of 2119 ± 347μm^2, significantly greater than that of SAOS2 cells (1196 ± 284μm^2, p=0.0284), but not significantly greater than the area of MSCs (1763 ± 83μm^2). The P2A and LWR measurements are a numerical representation of the 'roundness' of a cell's shape determined by the perimeter to area (P2A) ratio or the Length to Width ratio (LWR), where 1.0 is a perfectly circular object. As shown, the P2A of SAOS2 cells (1.49 ± 0.05) were significantly less than MSCs (2.44 ± 0.10, p<0.001) and MG63 cells (2.18 ± 0.23, p=0.0166). Similarly, the LWR of SAOS2 cells (1 1.66 ± 0.04) were significantly less than MSCs (2.46 ± 0.09, p<0.001) and MG63 cells (2.13 ± 0.04, p=0.0275).

Representative fluorescence microscopy images and quantitation of the area and shapes of Hoechst 33342 nuclear staining of MSCs, SAOS2 and MG63 cells are shown in Figure 3.15 and Figure 3.16 respectively. As shown, MSCs had significantly smaller nuclei (270 ± 4.96μm^2) than SAOS2 cells (358 ± 9.96 μm^2, p<0.001) and MG63 cells (460 ± 4.50 μm^2, p<0.001). Similarly, the nuclei of the SAOS2 cells were significantly smaller than the MG63 cells (p<0.001). However, there were no significant differences in nuclear P2A or LWR between the MSCs, SAOS2 or MG63 cells.

The quantitation of the total and mean fluorescence intensity of Hoechst 33342 stained nuclei significantly distinguished between all cell types; where the average intensity of MSCs (1179 ± 13 RLU) was significantly less than SAOS2 cells (1329 ± 25 RLU, p=0.0023) and MG63 cells (1665 ± 10.6

RLU, $p<0.001$). SAOS2 cell's average intensity was also significantly less than MG63 cells ($p<0.001$). Likewise, the significant differences in the total fluorescent intensities between the cell types were all significant ($p<0.001$) where MSCs had the lowest total intensity (193510 ± 5229 RLU) then SAOS2 cells (300258 ± 12733 RLU), and MG63 cells showing the greatest intensity (477373 ± 2903 RLU).

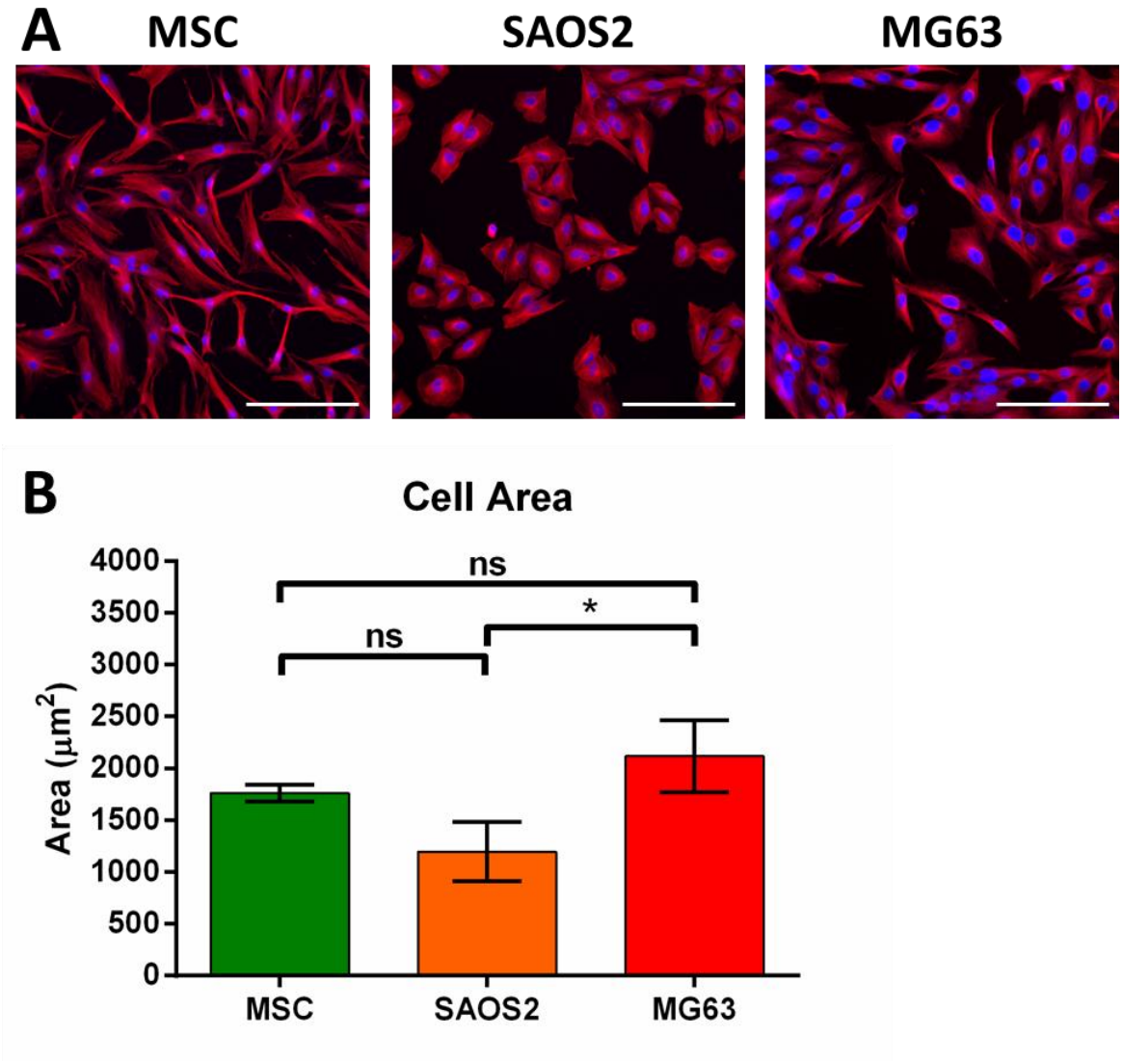

Figure 3.13: Morphological analysis of α-Tubulin immunoreactive primary human MSCs, SAOS2 and MG63 cells.

(A) Representative images showing α-tubulin immunoreactive staining in MSCs, SAOS2 and MG63 cells (Bar = 100µm). (B) Quantitative measure of average cell area of MSCs, SAOS2 and MG63 cells. Data shown are means ± SEM from n=9 MSCs and n≥3 osteosarcoma cells from ≥3 independent experiments. *ns* indicates no significant difference. All; one-way ANOVA with a Tukey's multiple comparisons test.

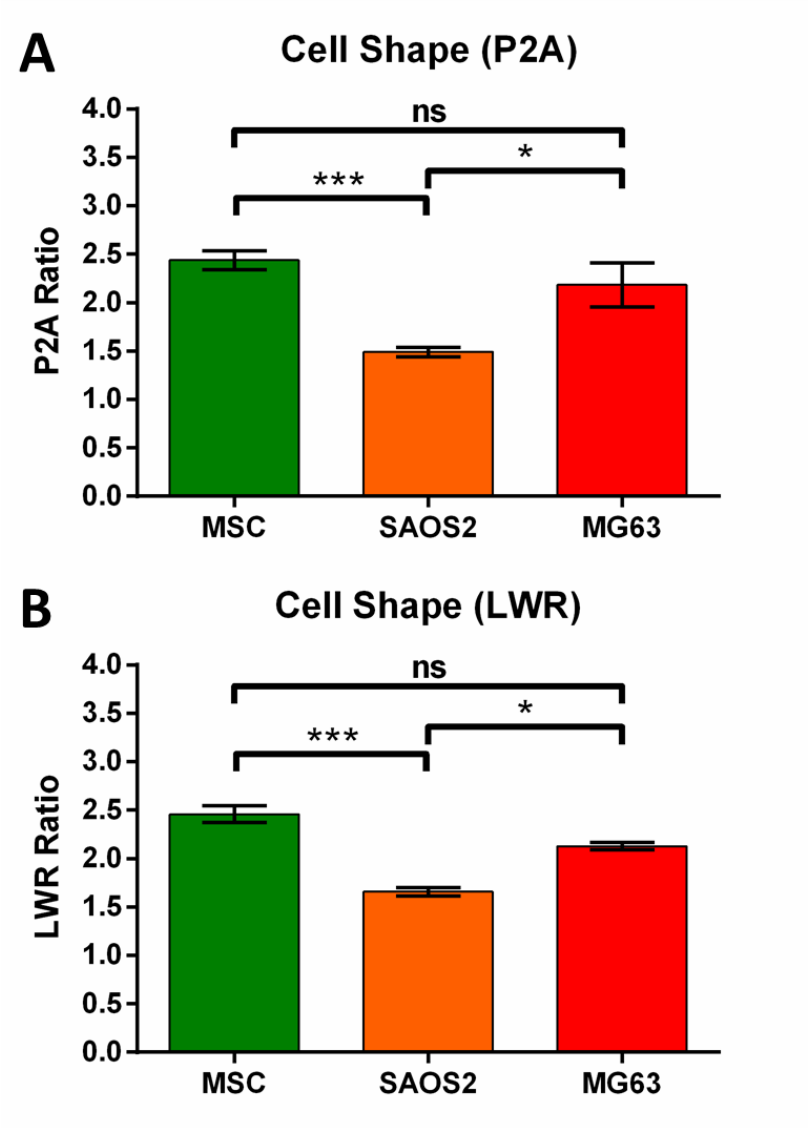

Figure 3.14: Morphological analysis of α-Tubulin immunoreactive primary human MSCs, SAOS2 and MG63 cells.

Quantitative measure of the average cell shapes defined as the perimeter to area ratio (P2A) (A) and length to width ratio (LWR) (B) of MSCs, SAOS2 and MG63 cells. Perfectly spherical objects have a ratio of 1. Data shown are means ± SEM from n=9 MSCs and n≥3 osteosarcoma cells from ≥3 independent experiments. ***indicates $p \leq 0.001$, *indicated $p \leq 0.01$, and *ns* indicates no significant difference. All; one-way ANOVA with a Tukey's multiple comparisons test.

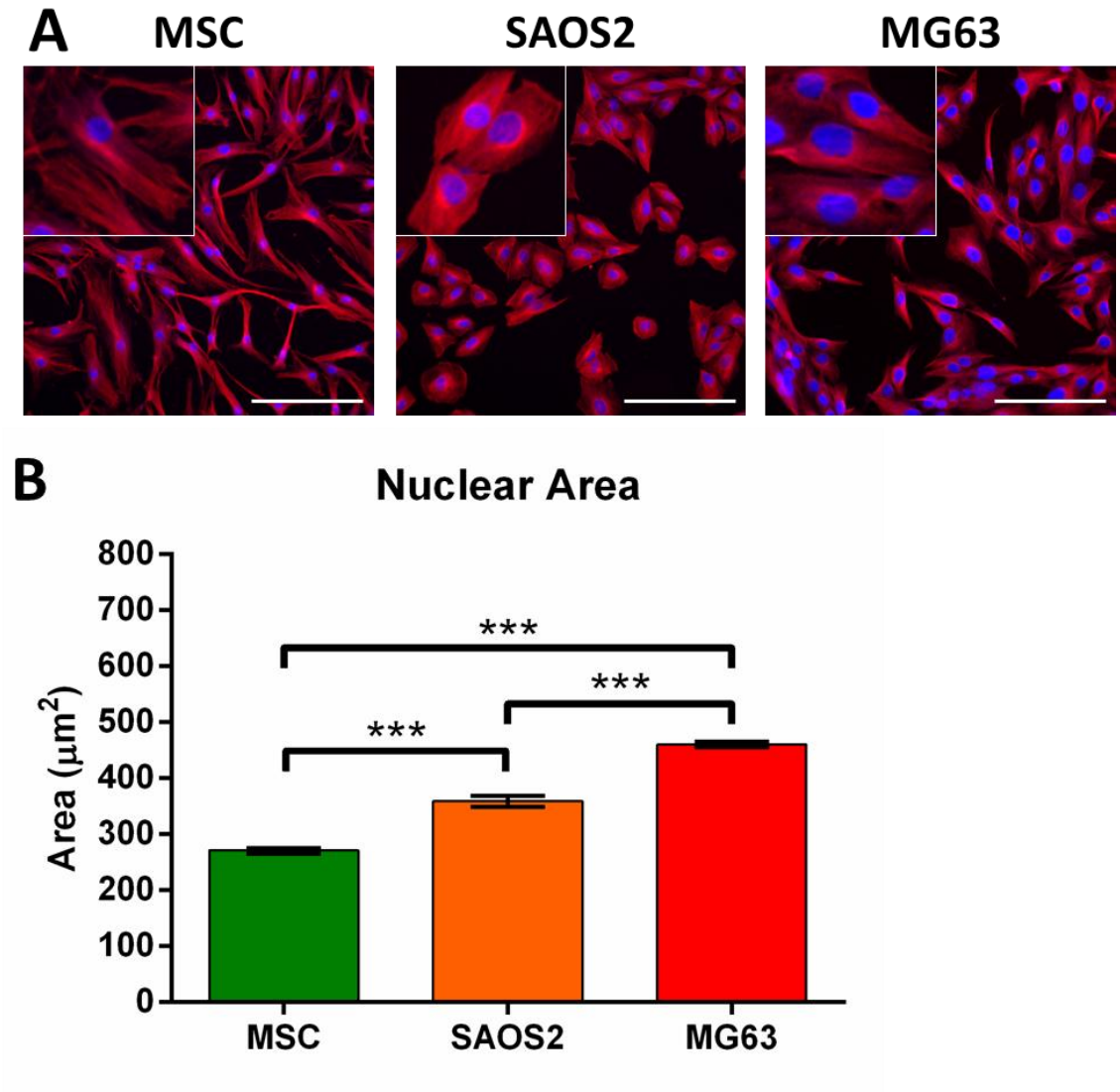

Figure 3.15: Morphological analysis of Hoechst 33342 stained nuclei distinguished between primary human MSCs, SAOS2 and MG63 cells based on nuclear area.

(A) Representative images showing Hoechst 33342 staining of nuclei from MSC, SAOS2 and MG63 cells (Bar = 100µm). Inset is 2.5x magnified. (B) Quantitation of the mean nuclear area of MSCs, SAOS2 and MG63 cells. Data shown are means ± SEM from n=3 independent experiments. ***indicates $p \leq 0.001$. All; one-way ANOVA with a Tukey's multiple comparisons test.

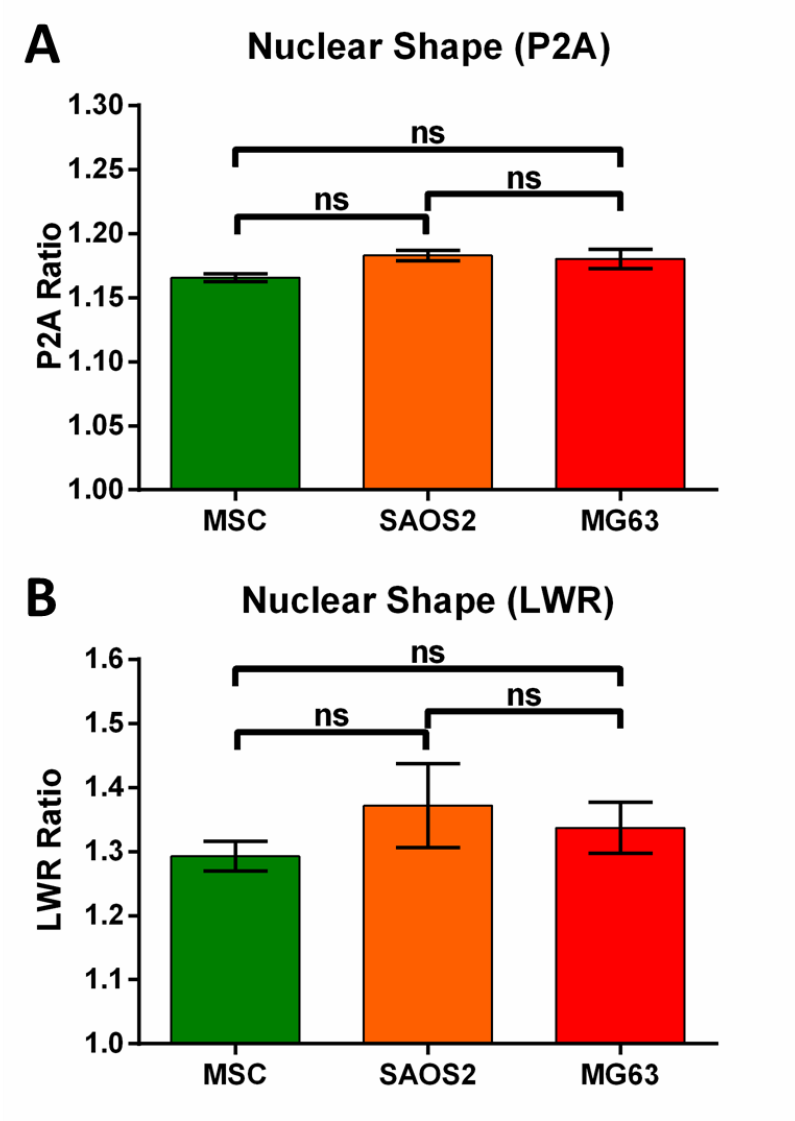

Figure 3.16: Morphological analysis of Hoechst 33342 stained nuclei did not distinguish between primary human MSCs, SAOS2 or MG63 cells based on nuclear shape.

Quantitative measure of the average nuclear shapes defined as the perimeter to area ratio (P2A) (A) and length to width ratio (LWR) (B) of MSCs, SAOS2 and MG63 cell nuclei. Perfectly spherical objects have a ratio of 1. Data shown are means ± SEM from n=3 independent experiments. *ns* indicates there is no significant difference seen. All; one-way ANOVA with a Tukey's multiple comparisons test.

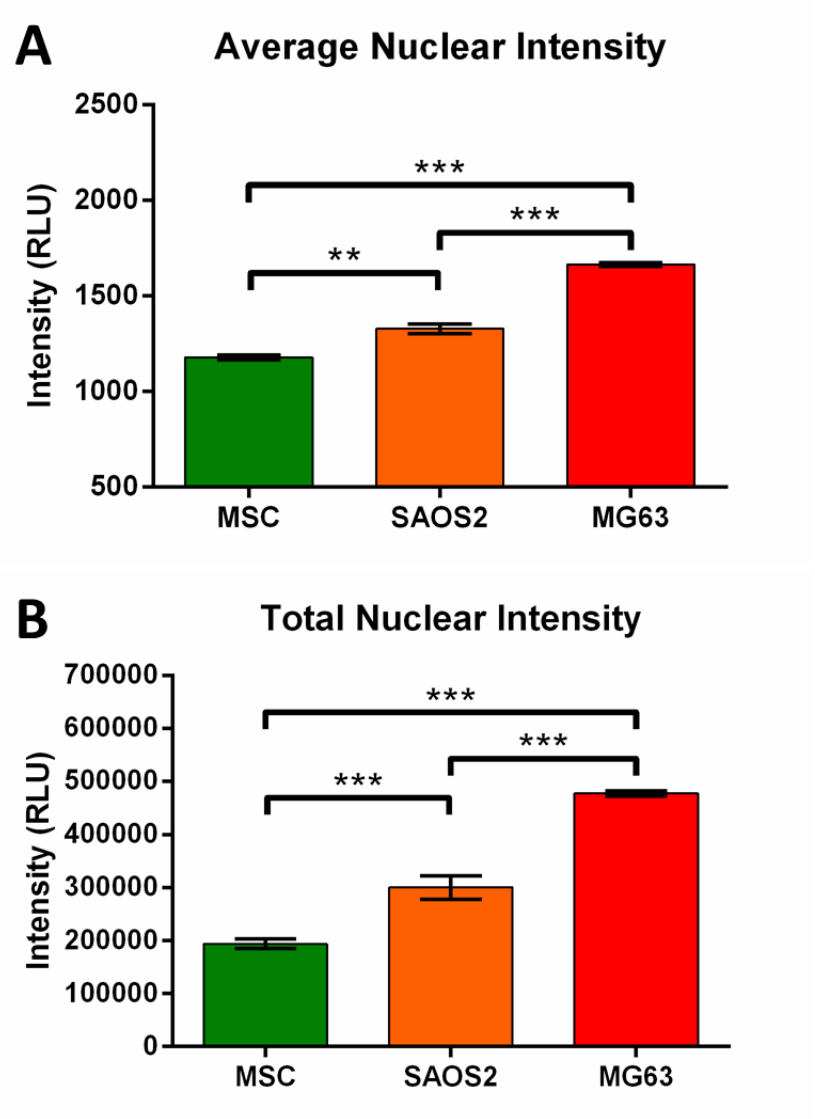

Figure 3.17: Quantitation of Hoechst 33342 stained nuclear intensity distinguished between primary human MSCs, SAOS2 or MG63 cells based on average and total nuclear intensity.

Quantitation is shown for the average (A) and total (B) nuclear intensity of MSCs, SAOS2 and MG63 cells based on Hoechst 33342 staining. Data shown are means ± SEM from n=3 independent experiments. ***indicates $p \leq 0.001$, **indicates $p \leq 0.01$. All; one-way ANOVA with a Tukey's multiple comparisons test.

3.8 Discussion

MSCs are an attractive candidate cell type for therapies in regenerative medicine on account of their ease of isolation from bone marrow throughout adult life, their evident differentiation potential to form bone and cartilage and a capacity to stimulate wound healing responses in other endogenous cells (Pittenger, 1999, D'ippolito *et al.*, 2006, Bajada *et al.*, 2008, Walter *et al.*, 2010). This requires *in vitro* monolayer culture expansion to increase the number of cells. However, a number of studies have suggested that MSCs may undergo spontaneous malignant transformation to form tumour cells, or become contaminated with other cell types following extended periods in culture (Rubio *et al.*, 2005, Mohseny *et al.*, 2009, Rosland *et al.*, 2009, Siclari and Qin, 2010, Torsvik *et al.*, 2010). Therefore, this study has examined whether the computerized HCS and imaging platform, Thermo Fisher Cellomics Array Scan (II), may provide a means of identifying biomarker differences between MSCs and tumour cells, namely the human osteosarcoma cell lines SAOS2 and MG63.

This HCS platform examined a wide range of fluorescently immunoreactive protein biomarkers. These proteins of interest are associated with cell cycle and proliferation, pluripotency, osteoblastic differentiation and cell signalling. In addition, the analysis included assays of cellular and nuclear morphology. Notable differences in immunoreactivity were seen between the MSCs compared to SAOS2 and MG63 cells. The biomarkers that significantly identified both SAOS2 and MG63 cells as different to MSCs were the Ki-67 antigen and Oct4. MG63 cells were also significantly more immunoreactive for pRB compared with SAOS2 and MSCs and more immunoreactive for nanog and β-catenin compared with MSCs alone. However, when the nuclear or cytoplasmic biomarker immunoreactivity intensities were compared alongside each-other as 'heat maps', it was clear that the osteosarcoma cell lines were distinctly more immunoreactive compared to the MSCs. Cellular and nuclear morphology distinguished MSC from SAOS2 and MG63 cells, where MSCs had a smaller nuclear area than SAOS2 and MG63 cells.

Considering the nuclear area and intensities were the most distinguishing feature between the MSCs and osteosarcoma cell lines, the need for further biomarker analysis may be seen as unnecessary. Further imaging and analysis of more patient MSC samples, transformed MSC cell lines as well as primary cancer cell lines may help elucidate whether the nuclear area could be a viable and determinant cell feature for identification. These differences between the MSCs and the osteosarcoma cell lines have been summarised in Table 6.

Table 6: Cell type specific identification by fluorescent immunoreactive labelling and high content screening.

Cell Type	Distinguishing Features	
MSC	Small nuclear area cf SAOS2 and MG63	
SAOS2	Lowest P2A and LWR cf MSC and MG63	High Ki-67 cf MSC High Oct4 cf MSC
MG63	High pRb cf MSC and SAOS2 High β-catenin and Nanog cf MSC	
All Cells	Significantly different fluorescent nuclear intensities	

Abbreviations: MSC, Mesenchymal stem cells; cf, compared with; pRb, phosphorylated retinoblastoma protein.

(Green) Cell type specific features unique to primary human MSCs was a small nuclear area compared with those of SAOS2 and MG63 cells. (Orange) The most spherically shaped cell type, hence the lowest P2A and LWR value was unique to SAOS2 cells when compared to the more complex shapes of the primary human MSCs and MG63 cells. (Red) High immunoreactivity for pRb, β-catenin and Nanog was unique to MG63 cells compared to low immunoreactive labelling in primary human MSCs and SAOS2 cells. (Blue) High immunoreactive labelling for the Ki-67 antigen and Oct4 were unique to both the SAOS2 and MG63 cells compared to low immunoreactive labelling in MSCs. (Yellow) However, the most significantly distinguishing feature between all cell types was the difference in the average or total nuclear fluorescence intensity.

Each of the biomarkers examined, have been discussed briefly. β-catenin is central in the canonical Wnt/β-catenin signalling pathway, which plays an important role in the regulation of MSC self-renewal, proliferation and differentiation. Low levels of canonical Wnt signalling are associated with the maintenance of an undifferentiated state and high levels of Wnt signalling are involved in osteogenic differentiation (Gaur *et al.*, 2005, Ling, Nurcombe and Cool, 2009). Canonical Wnt signalling in osteoblastic differentiation has been shown to stimulate the proliferation of osteoprecursor cells, increasing the number of osteoprogenitor cells available for further differentiation and mineralisation (Cook *et al.*, 2014). It has been shown that β-catenin translocation into the nucleus leads to transcriptional activation of β-catenin target genes (Couffinhal, Dufourcq and Duplàa, 2006). Interestingly, abnormally high β-catenin nuclear accumulation has been used as a diagnostic tool specific to a subset of mesenchymal tumours, but not osteosarcomas (Ng *et al.*, 2004). Low β-catenin immunoreactivity was observed within the cytoplasm and nucleus in MSCs. In contrast, high β-catenin immunoreactivity was observed within the cytoplasm and nucleus of MG63 cells, which may suggest that MG63 cells are more differentiated than the MSCs and SAOS2 cells along the osteoblastic lineage. In either case, these observations demonstrate that β-catenin alone cannot be used to identify all osteosarcomas.

In contrast to β-catenin, immunoreactivity for the activated (phosphorylated) form of focal adhesion kinase (pFAK) showed no significant differences between the osteosarcoma cells compared with MSCs. A difference was seen as expected, although this difference was not significant. A difference in pFAK expression and detection is consistent with the known involvement of pFAK in cancers (Wozniak *et al.*, 2004), where its over expression and aberrant functioning is commonly associated with increased cell proliferation and cancer metastasis (Gabarra-Niecko, Schaller and Dunty, 2003, Tilghman and Parsons, 2008). The greater levels of pFAK immunoreactivity associated with significantly increased Ki-67 immunoreactivity in the osteosarcoma cell lines, compared to the MSCs, would therefore have suggested that the main difference in cell phenotypes are in their proliferative and migratory capacity. Further analysis was

performed to examine the differences in migratory behaviour between the MSCs, SAOS2 and MG63 cells as noted in the following chapter.

Immunoreactivity for Oct4 was significantly more highly seen in SAOS2 and MG63 cells than in MSCs. Oct4 is expressed at high levels in embryonic stem cells; it is a transcription factor that plays a vital role in stem cell self-renewal and pluripotency (Pierantozzi *et al.*, 2011). The high Oct4 immunoreactivity detected in SAOS2 and MG63 cells in this study is consistent with the work of Tirino *et al.*, (2008), where the presence of Oct4 within a highly proliferative $CD133^{+ve}$ sub-population of SAOS2 and MG63 cells was described as a cancer stem cell characteristic (Tirino *et al.*, 2008). Hence, Oct4 may be involved in the self-renewal of the osteosarcoma cells. In contrast, the low levels of Oct4 seen in MSCs may reflect a more restricted differentiation potential compared to embryonic stem cells. However, the role of Oct4 in osteosarcoma cells and MSCs, including any aberrant functioning in tumourigenesis, remains to be determined.

It is interesting to compare the immunoreactivity of Oct4 with that of nanog. Nanog immunoreactivity detected in the MSCs was low. Pierantozzi *et al.*, (2011) described an observation with MSCs, where they noted a lack of nanog expression in freshly isolated cells, yet increased expression detected following *in vitro* culture expansion. Additionally, they stated that this change in expression did not directly relate to MSC proliferation or differentiation capacity, but rather, it may be associated with a transition from *in vivo* quiescence to adaptation of growth *in vitro* (Pierantozzi *et al.*, 2011). High expression of both Oct4 and nanog within subpopulations of SAOS2 and MG63 cells may be a characteristic of tumour initiating cells (Huang, Dai and Guo, 2012).

The morphology of each cell type was observed following α-tubulin immunoreactivity and Hoechst 33342 nuclear counterstaining. Differences in cell and nuclear shapes were observed and quantitated. The heterogeneous population of cells commonly labelled as MSCs have been described in many ways, such as fibroblastic, spindle shaped, large and polygonal and even cuboidal when in confluent tightly packed cultures (Javazon, Beggs and Flake, 2004, Miao *et al.*, 2006,

Chamberlain *et al.*, 2007). Classically though, freshly isolated MSCs have been described as stromal and fibroblastic in appearance (Pittenger, 1999). In contrast to the fibroblast-like shape of young MSCs, aged and senescent MSCs have been described as large, flattened cells (Kim *et al.*, 2011) with a large cell surface area and volume (Toussaint, Medrano and Von Zglinicki, 2000). SAOS2 cells are large, polygonal cells with an ellipsoid nuclei (Muff *et al.*, 2007) although highly metastatic sub-clones of SAOS2 cells have a smaller cell volume, cell area and nuclear area (Jia, Worth and Kleinerman, 1999). MG63 cells are oval to spindle-shaped and do not have branching cell processes (Pautke *et al.*, 2004). In this study, the total cell area of the MSCs was not significantly different to that of the SAOS2 and MG63 cells. However, the P2A and LWR of the SAOS2 was significantly different to that of the more complex shaped MSCs and MG63 cells. The MSCs had significantly smaller nuclei than both the SAOS2 and the MG63 cells.

As shown and discussed by (Heathman *et al.*, 2015b, Heathman *et al.*, 2016a, Heathman *et al.*, 2016b) the morphology of MSCs was seen to vary considerably from donor to donor, when cultured within different culture conditions; additional, the mean diameter of the cells was seen to increase over serial passage. These observations are critical to the manufacture and characterisation of the cells intended for therapeutic applications. The mean diameter of the MSCs determined during the study by Heathman *et al.*, (2016b) was performed on cells within suspension; however, here the morphology of adherent cells in monoculture have been presented. It was shown that a full profile of morphological readouts can be simply obtained from few cells examined.

The quantitative differences in biomarker immunoreactivity and morphology provide a rationale for the development of diagnostic platforms that could identify transformed cells within an MSC culture. One such platform would include antibodies for the Ki-67 antigen, Oct-4, pFAK, pRB and β-catenin, with α tubulin and Hoechst 33342 counterstaining for morphological criteria. However, further analysis of more MSC cultures and primary osteosarcoma cells lines is required to verify such an approach. In particular, only 3 MSC cultures were tested in this series of experiments. These

were of different donor ages (57-90 years) and passage numbers (P1-P6). Similarly, a multiparametric approach, as demonstrated by (Chan *et al.*, 2014), to the HCS of the biomarkers examined within this chapter, as well as the addition of other biomarkers of interest, could render this tool to be very productive in the screening and characterisation of cells intended for clinical therapies.

This study has also seen some donor-to-donor variation in the readouts (data not shown), but it is difficult to draw any firm conclusions on the relationship between donor age or MSC age in culture with such a low number of donors tested, e.g. one MSC sample was cultured from a 90 year old donor and was tested at P1.

A second example illustrating the need to examine more MSC donors of different passages as well as samples isolated from different locations is shown in the results seen for osteopontin immunoreactivity. All MSC cultures presented here were derived from adipose tissue and it is known that high osteopontin expression is associated with osteogenesis, whereas low levels of osteopontin expression associates with adipogenic differentiation (Chen *et al.*, 2014). Hence, osteopontin immunoreactivity may relate to the "memory" that each cultures maintains of their differentiation potential and that as the MSCs cultures were passaged, they may have become less adipogenic in phenotype and gained a more osteogenic phenotype. Examining the immuno-profile or MSCs from bone marrow over increased passage would help establish whether such differences in differentiation potential over time still occur.

An additional weakness in this study is the fact that well established osteosarcoma cell lines were used rather than primary tumours. There is likely to have been significant phenotypic drift within the SAOS2 and MG63 cell lines over time, as this is well known to occur during cell culture (Barnes, Moy and Dickson, 2006). An improvement to the current analysis would be to examine either freshly isolated primary tumours of MSC derivation (see Chapter 4) or to induce transformation of normal MSCs. Ivan Stamenkovic and co-workers (Riggi *et al.*, 2008) have demonstrated that MSCs

can be induced to form Ewing's type sarcomas following induced expression of the EWS-Fli-1 oncoprotein. It would be interesting to examine the immunophenotype of these newly transformed cells compared to their non-transformed parental MSCs. Similarly, if MSCs from non-human sources (or human sources if this can occur) undergo spontaneous malignant transformation, then these would provide the most relevant target cell with which to test differences in phenotype that occur during this process.

Nonetheless, the data generated in this chapter provides details towards the potential for HCS as a useful tool to evaluate these various limitations of approach. That is to say, the immunoreactivity and morphological assays can be used repeatedly in further analysis of other cell types.

In addition, the immunoreactivity of the different cultures tested may also provide information about the nature of the tumours that have been tested. For example, the profiles observed for SAOS2 and MG63 may be useful in identifying when the process of osteoblastic differentiation may have been disrupted to give rise to osteosarcoma. Alkaline phosphatase (ALP) is an early and transient biomarker signifying commitment toward osteoblastic differentiation, increasing early in differentiation then decreasing when mineralization is well under way. Osteopontin peaks twice, during proliferation and later prior to the appearance of osteocalcin. Osteocalcin is a late marker of osteoblastic differentiation, appearing with mineralization of the cells (Aubin, 2001, Luo *et al.*, 2008, Birmingham *et al.*, 2012). Hence, osteoblastic differentiation is associated with the sequential expression of ALP followed by osteopontin and then osteocalcin. This is supported by work from Weinreb, Shinar and Rodan, (1990), who examined the expression levels of such markers in long bone formation and calvariae during bone development. They reported that ALP was present in a large number of cells, including pre-osteoblasts, which were many layers removed from the bone-forming surface; high levels of osteopontin were expressed in osteoblasts within close proximity (one to two cell layers) to the bone surface; and osteocalcin expressed within osteoblasts in direct contact with bone (Weinreb, Shinar and Rodan, 1990).

High ALP enzymatic activity (appendix Figure 7.17), low osteopontin and osteocalcin immunoreactivity were seen in SAOS2 cells. In addition, SAOS2 cells were Ki-67 immunoreactive. This pattern may signify that SAOS2 cells were committed towards osteoblastic differentiation at a stage that is prior to mineralization yet still actively proliferating (see *** in Figure 3.18), which is consistent with other published findings (Rodan *et al.*, 1987, Farley *et al.*, 1991, Aubin, 2001, Pautke *et al.*, 2004, Bullwinkel *et al.*, 2006, Luo *et al.*, 2008). The absence of RB in SAOS2 is thought to play a role in the inability of these cells to undergo terminal differentiation (Thomas *et al.*, 2001).

The relatively low ALP activity observed within the MG63 cells, consistent with other studies (Pautke *et al.*, 2004, Luo *et al.*, 2008), implies that these cells were either immature osteoprogenitor cells or that they had differentiated into a post mitotic osteocytic phenotype (Aubin, 2001). In support for a mature osteocytic phenotype, MG63 cells were more strongly immunoreactive for osteocalcin than SAOS2. However, the cells were also highly Ki-67 and pHH3 immunoreactive. MG63 cells are known to have a doubling time of between 30hrs and 47hrs (Billiau *et al.*, 1977, Pautke *et al.*, 2004). In addition, MG63 cells can be induced to become ALP positive following treatments with osteogenic reagents (Carmeliet, Nys and Bouillon, 1997). Osteopontin immunoreactivity within MG63 cells was high, although not significantly different to the other cell types; however, this immunoreactivity may be indicative of the first peak associated with proliferation, as previously mentioned (Aubin, 2001). Therefore, the immunoreactive profile of MG63 for the osteoblastic and cell cycle markers more likely indicates an immature osteoprogenitor cell that is highly proliferative (see ** in Figure 3.18), where the elevated reactivity for osteocalcin is aberrant.

In summary, as shown in Figure 3.18, the HCS platform was able to differentiate between the different cell types examined using biomarkers associated with osteogenic differentiation (A) and normal cell cycle proliferation (B). Differentiation progresses from pluripotent embryonic stem cells (ESC) through to multipotent MSCs, which under osteo-inductive signals, further differentiate into

osteoblasts as well as further differentiate into osteocytes. The MSCs (*) examined here were not seen to be committed along osteoblastic differentiation. MG63 cells (***) are shown to have transformed prior to ALP expression. Similarly SAOS2 cells (**) are shown to have transformed following the stage of high ALP expression, yet prior to mineralization.

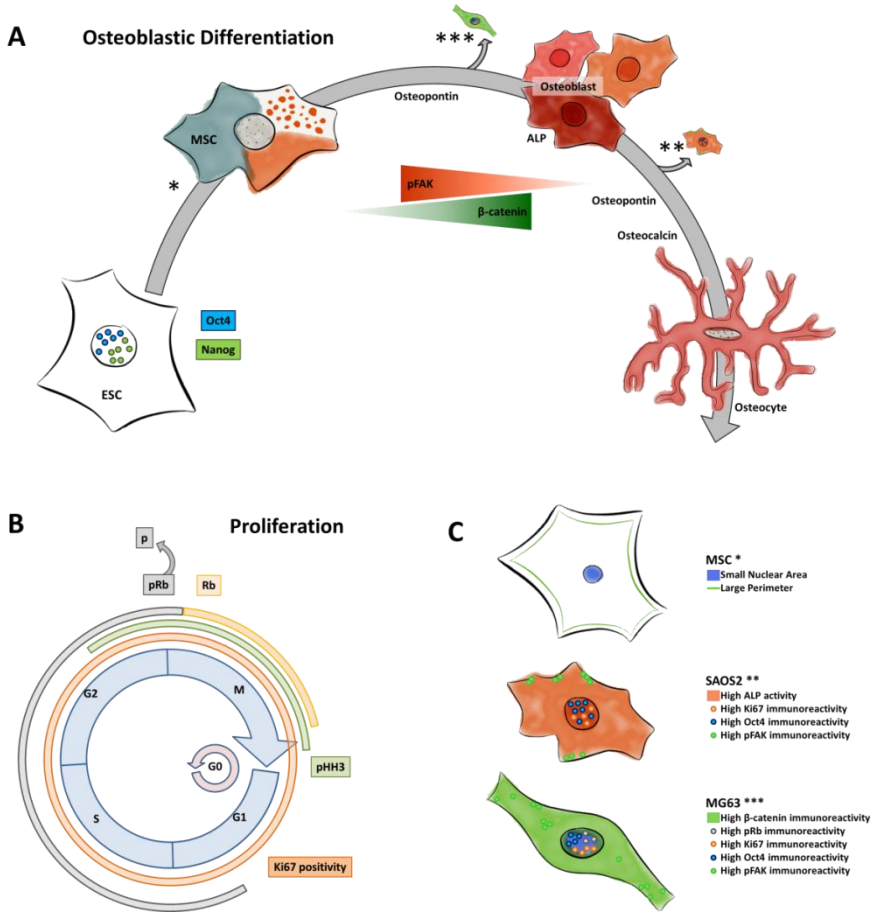

Figure 3.18: A schematic diagram showing biomarkers associated with osteoblastic differentiation and proliferation, which were distinguishing features between primary human MSCs, SAOS2 and MG63 cells.

Cells and biomarkers examined during osteoblastic differentiation (A) cell proliferation (B) from MSCs, SAOS2 and MG63 cells (C). Differentiation shown from the embryonic stem cell (ESC) through MSCs and osteoblasts (ALP +ve) then to a mineralised osteocyte (von Kossa +ve) with biomarkers associated with different stages of osteoblastic differentiation. MSC's multipotential differentiation capacities depicted with colours according to traditional colorimetric stains for chondrogenic (alcian blue), osteogenic (ALP -red) and adipogenic (oil red O - red spots) differentiation. The asterisks indicate where the cells examined here fall within the osteogenic differentiation process, where: * indicate MSCs, ** indicate SAOS2 cells and *** indicate MG63 cells.

3.9 Conclusion

This study has shown that it is possible to image and quantitate unique cellular immunoreactive biomarkers with the use of simple automated HCS of *in vitro* culture-expanded cell cultures for the purposes of cell based therapies within regenerative medicine. However, this quantitation did not significantly distinguish between the cell types examined. In contrast, the nuclear area and nuclear intensity, based on Hoechst 33342 staining, did significantly distinguish between all cell types examined.

The methods developed in this initial investigation help to enhance the understanding of MSCs' safe use; as well as the provision and description of a screening tool which is able to extract much data from few cells. Similarly, it has been shown here that normal human MSCs show a distinctly different immunoreactivity profile to the two osteosarcoma cell lines, SAOS2 and MG63 cells.

However, the need to remove and fix cells from a donor's sample is a major disadvantage for the HCS platforms used thus far. Therefore, the next chapter examines the use of the Cell-IQ live-cell imaging and analysis platform to distinguish between the same cell types based on total cell area, counting the number of total cells, as well as pattern recognition of cell morphology from phase contrast images that have been gathered during standard cell culture expansion.

Chapter 4: The use of automated live-cell imaging and image analysis characterised, identified and distinguished between primary human MSCs, SAOS2 and MG63 osteosarcoma cell lines

4.1 Aims and Background

The previous chapter presented the use of HCS to distinguish between cultured human MSCs from the osteosarcoma cell lines, SAOS2 and MG63 cells. The technique described, involved the use of ICC staining of formaldehyde-fixed samples harvested from cultures. This technique presents many advantages, such as intricate detailed examination of the cells, on a cell-to-cell basis; however, the major disadvantage of such screening is the need to permanently remove and fix cells from the primary culture. This means that not all cells are examined, only a sample there of.

Evidence of cell transformation may include changes in the rate of cell division and proliferation, cell death and cell shape in a highly localised area of a culture flask (Lowe and Lin, 2000). It is noteworthy that the live-cell imaging and image analysis platform, Cell-IQ v 2.0, can be used to develop a recognition algorithm which can identify cell features over time (Toimela, Tahti and Ylikomi, 2008). Therefore, the system can provide a dynamic evaluation of cell cultures, rather than a single end point 'snap-shot' and help to monitor the safe provision of primary human cells within clinical applications. The comparison between imaging the whole area of a culture flask, to a select representative area was investigated and elegantly demonstrated by David Smith (Smith, 2014).

Therefore, this chapter has examined the use of the Cell-IQ to provide a means of characterising and distinguishing between monolayers of cultured human MSCs compared to the osteosarcoma cell lines, SAOS2 and MG63 cells, and primary chondrosarcoma derived cells. Live-cell imaging presents many advantages over the previously discussed HCS technique. These include kinetic observation through long periods of *in vitro* culture expansion; marker-free identification and classification of cells without the need to remove cells from the culture as samples, or interfere with patient's cells; and, to a certain extent, the whole population of cells can be monitored although this was not performed in this project. Most importantly, with the use of this system, isolated cells grown within GMP facilities can be imaged and then transplanted back into the patient when necessary.

The Cell-IQ was used to continuously capture digitised phase contrast images of cells grown in traditional cell culture conditions. Initially, the confluence of each culture was measured using the Area Measurement tool based on phase contrast thresholds. Then, the Cell Finder tool counted the total number of cells within each monoculture. Following on from this, the automated pattern recognition software was "taught" distinguishing features of each cell type from the digitised images. A sample library of these features was then produced (8 representative sample library images are shown in Figure 4.3 A) and generated into a pattern recognition algorithm by the software. The algorithm was used to analyse pixel intensities/patterns within all images gathered. Differences between cell class parameters included; (i) A cell counting threshold, (ii) Minimum cell distance, (iii) Maximum cell diameter, (iv) Cell symmetry (100=round). A more detailed description of these algorithms and methods of identification can be seen in the materials and methods chapter (section 2.14.2).

Images gathered from monocultures of MSCs, SAOS2 and MG63 cells were used to generate the aforementioned algorithm. Then, this algorithm was applied to images of the aforementioned cell monocultures, mixed cell cultures grown in a 50:50 ratio co-culture and finally monocultures of cells isolated from a primary chondrosarcoma.

Finally, the Manual Cell Tracking and Manual Cell Lineage Tracking tools were used to determine migration behaviours of the MSCs, SAOS2 and MG63 cells in monoculture.

Therefore, the aim of this study was to use the Cell-IQ live-cell imaging platform to identify MSCs in culture and distinguish them from SAOS2 and MG63 cells in monocultures, as well as in co-cultures. Similarly, we used the Cell-IQ platform to characterise and compare the phenotype of adherent cells isolated from a primary Low grade I chondrosarcoma to that of MSCs, SAOS2 and MG63 cells.

4.2 The Cell-IQ Area Measurement and Cell Finder tools characterised MSCs, SAOS2 and MG63 cells in monoculture

The phase contrast images shown in Figure 4.1 are representative images of MSCs (left column panels), SAOS2 (middle column panels) and MG63 cells (right column panels) taken at a single time point 48hrs post seeding. The original images (top row panels) were taken from those collected during live imaging from 24hrs post seeding through 144hrs post seeding. These images were then analysed using the Cell-IQ Analyser^{TM} Area Measure tool (middle row panels) to measure the area and hence confluence of the cells; as well as, the Cell Finder tool (bottom row panels) to count the total number of cells within the monocultures. The graph in Figure 4.2 (A) shows the confluence of the cultured cells, where the area is shown as a percentage of the total image area of MSCs, SAOS2 and MG63 cells through 5 days of culture. It should be noted that the confluence of the MG63 cells was significantly greater ($p \leq 0.0370$) than that of the MSCs and SAOS2 cells from 80hrs of culture. Similarly, the graph in Figure 4.2 (B) shows the total number of cells counted within the same monocultures over the 5 days of culture, where the total number of MG63 cells was also significantly greater ($p \leq 0.0492$) than those counted within the MSC and SAOS2 cell monocultures from 84hrs post seeding. Videos of the original, area measure and cell count images from the ROIs shown can be seen on the supplementary DVD (Appendix 7.4).

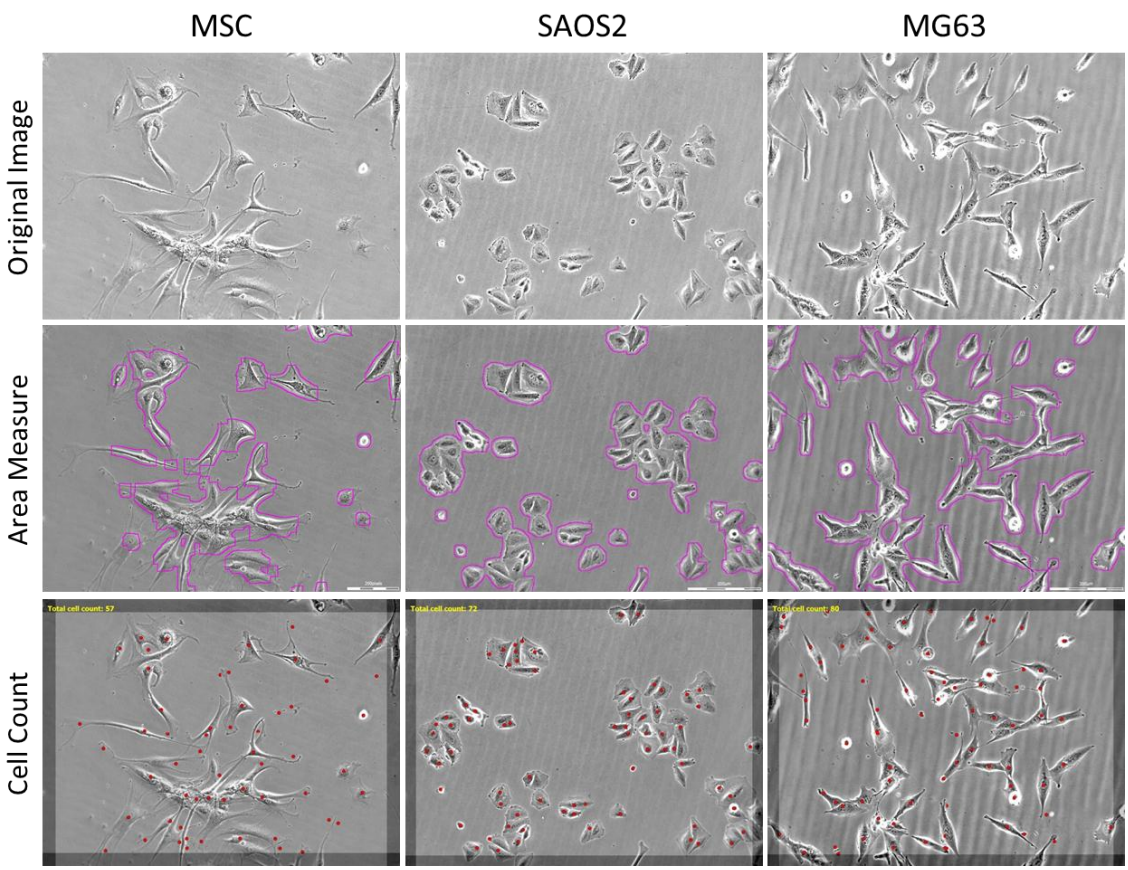

Figure 4.1: Phase contrast microscopy images of primary human MSCs, SAOS2 and MG63 osteosarcoma cells captured by the automated live-cell imaging platform, Cell-IQ.

Phase contrast images (top row panels) were gathered by the automated live-cell imaging platform, Cell-IQ of MSCs (left column panels), SAOS2 (middle column panels) and MG63 cells (right column panels) from 24hrs post seeding, through 140hrs post seeding. Images shown were taken at 48hrs post seeding. From these images, the area of the cells (middle row panels) providing the cell confluence, as well as the number of cells (bottom row panels) were measured using the Cell-IQ Analyser™ Area Measure and Cell Finder tools respectively.

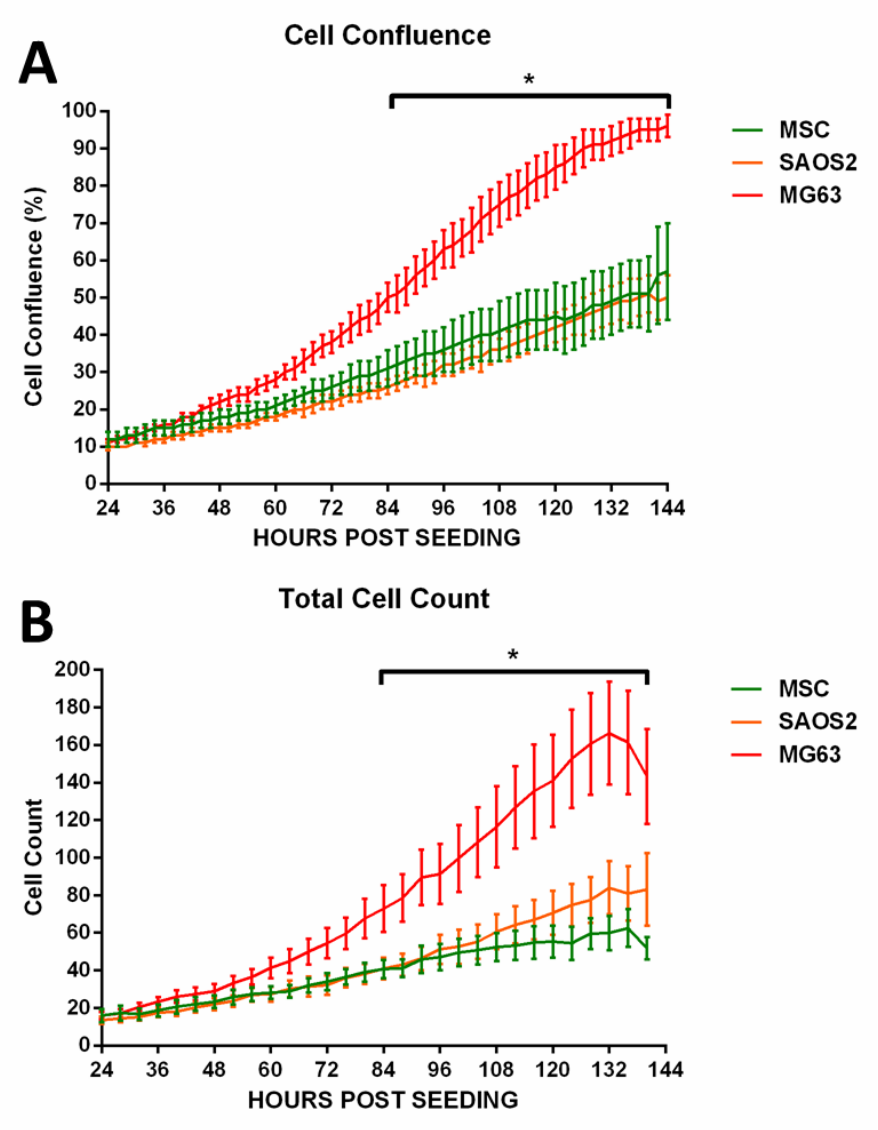

Figure 4.2: The Cell-IQ live-cell imaging platform measured the confluence of and counted the number of primary human MSCs, SAOS2 and MG63 cells cultured in the respective cell monocultures.

Cell confluence based on the area of the cells (A), and the cell counts (B) for the total number of MSCs (green), SAOS2 cells (orange), MG63 cells (red) per ROI are reported for each cell type within cell monocultures. Data shown are mean ± SEM cell counts, from MSC n=5, SAOS2 and MG63 n=4 independent experiments with ≥3 ROIs per experiment. *$p \leq 0.05$; All, Two-way ANOVA with a Dunnett's post-test where MG63 cell confluence and cell count is significantly greater than both MSCs and SAOS2 cells between the times indicated.

4.3 Digitised phase contrast images taken of distinguishing cell features provided information to create algorithms necessary for analysis

The phase contrast images shown in Figure 4.3 are representative images of each cell type which form a part of the algorithms used to identify the cells. As shown (from the top panel), MSCs, SAOS2, MG63 cells, rounded cells' unique characteristics were identified and used to form the phase contrast library. Similarly included are dead cells and debris. The two bottom panels show the morphology of confluent SAOS2 and MG63 cells observed during extended culture periods; however, these features were not used as a separate identification feature.

It can be seen that MSCs had a broad flat cell appearance, elongated fibroblastic appearance as well as irregular shapes, with some low contrasting features. That is, the cells did not show as strong contrast between the tissue culture plastic (TCP) and the edge of the cell membrane as that seen in some SAOS2 and MG63 cells.

The SAOS2 and MG63 cells were more distinctly identified apart from MSCs. Both cell types had bright and dark areas which we distinctively contrasting from the TCP. Similarly, both SAOS2 and MG63 cells had granular puncta within the nucleus, yet MG63 cells' puncta were larger and the cells also showed more granularities in the perinuclear area. SAOS2 were more commonly seen growing within colonies making cell to cell contact; however, MG63 cells would often migrate along the TCP independent of other cells.

Rounded cells were identified by a bright circular ring on the outer edge of the cells, with a dark central core. These cells were presumed to be rounded during the stages of cell division. Dead cells were identified by apoptotic blebs protruding from the edge of the cell as well as fragmentation of the cell membrane and/or organelles as described in Ziegler and Groscurth, (2004).

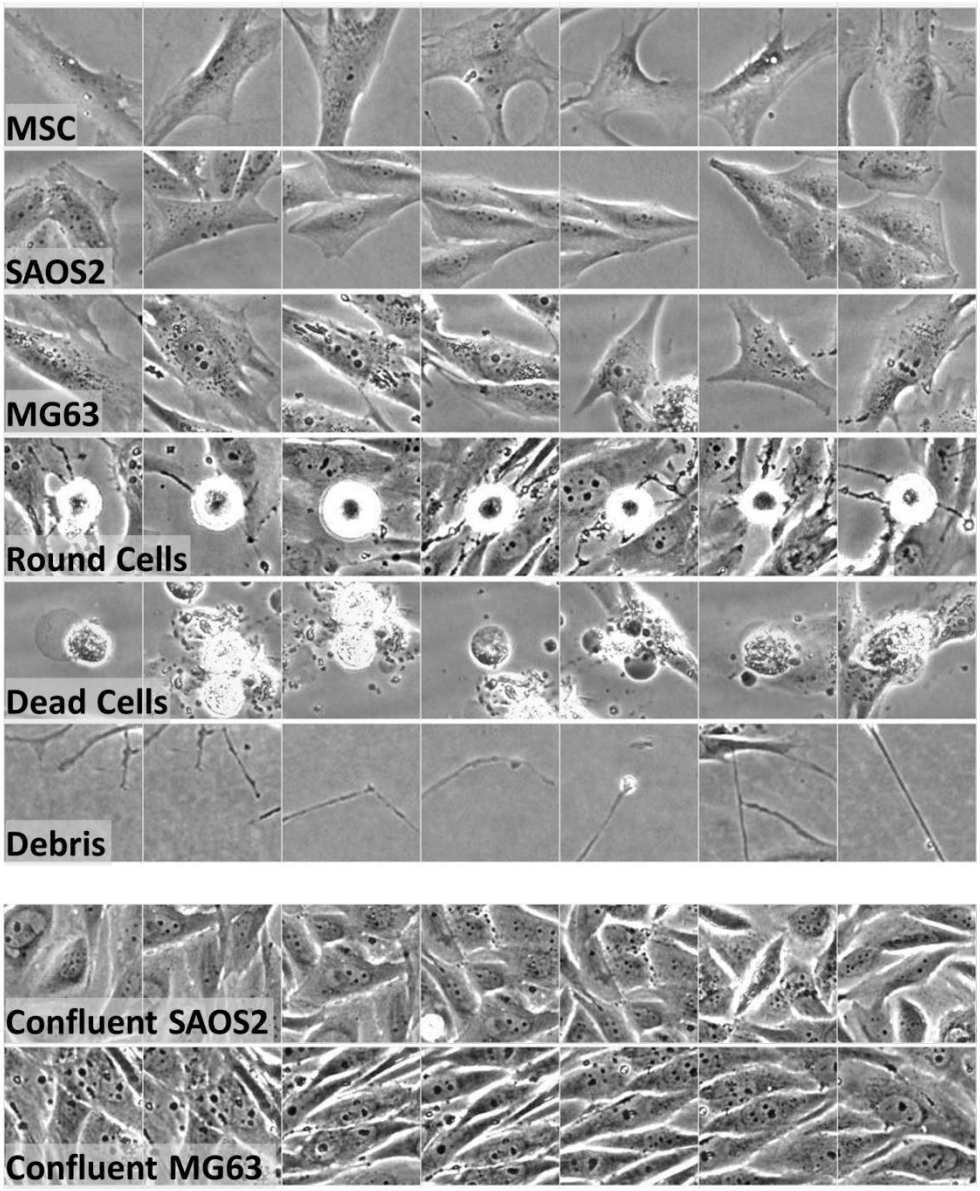

Figure 4.3: Phase contrast microscopy sample images used for the recognition of primary human MSCs, SAOS2 and MG63 cells captured by the automated live-cell imaging platform, Cell-IQ.

A library of cell specific morphological features were collected as shown above, and used to teach the pattern recognition software to identify (from the top panel to bottom panel) MSCs, SAOS2 cells, MG63 cells, Round cells, Dead Cells and Debris. The two bottom panels show the morphology of confluent SAOS2 and MG63 cells; however, these features were not used as a separate identification feature.

4.4 The identification of MSCs, SAOS2 and MG63 cells in mono and co-cultures

Identification of the three different cell types in monocultures and co-cultures using the Cell-IQ live-cell imaging Cell Finder tool, was variable between cell types. Identification of MSCs was most specific. However, identification of SAOS2 and MG63 cells was often seen with a high proportion of misidentification of MSCs.

The graphs in Figure 4.4 show the average number of cells counted per ROI imaged in MSC (A), SAOS2 (B) and MG63 (C) monocultures from 24hrs through 140hrs post seeding. Within the MSC monoculture, as seen in panel A, significantly more MSCs ($p \leq 0.0380$) were counted from 28hrs through 140hrs of culture compared to SAOS2, MG63 cells and round cells. Within the SAOS2 cell monoculture (panel B) significantly more SAOS2 cells ($p \leq 0.0053$) were counted from 136hrs of culture, apart from MSCs, MG63 cells and Round cells. Similarly, within the MG63 monoculture, significantly more MG63 cells ($p \leq 0.0223$) were counted from 124hrs through 140hrs of culture, more than MSCs, SAOS2 cells and round cells.

In Figure 4.5, the numbers of identified MSCs, SAOS2, MG63 and round cells are graphed as a percentage relative to the total number of cells shown in Figure 4.4. Within the MSC monoculture, (panel A) the cell library significantly identified the cells as MSCs ($p < 0.001$) throughout the culture period, compared to SAOS2 cells, MG63 cells and round cells. However, within the SAOS2 monoculture (panel B), the cell library significantly identified the cells as SAOS2 cells ($p \leq 0.0367$) only from 132hrs of culture, apart from MSCs, MG63 cells and round cells. Within the MG63 cell monoculture (panel C). MG63 cells were identified as such, however the identification of these MG63 cells was not significantly different to both MSCs and SAOS2 cells at any point through the culture period.

The graphs in Figure 4.6 show the average number of cells counted per ROI imaged in MSC/SAOS2 (A) and MSC/MG63 (B) co-cultures seeded at a 50/50 ratio, from 24hrs through 140hrs post seeding. Within the MSC/SAOS2 co-culture (panel A), significantly more MSCs were counted than SAOS2 cells, from 36hrs of culture through 140hrs ($p \leq 0.0370$). Throughout the culture period, the number of MSCs or SAOS2 cells were not equally identified as would be expected. Similarly within the MSC/MG63 co-culture (panel B), significantly more MSCs were counted between 68hrs ($p \leq 0.0387$) and 112hrs ($p \leq 0.0249$) of culture. At 128hrs of culture, the mean difference between the identification of MSCs and MG63 cells was the lowest at 1.00 (ϕ); however it can be seen that the identification of the MSCs or MG63 cells did not remain constant.

Figure 4.7 shows the number of identified cells graphed as a percentage relative to the total number of cells. As shown, in the MSC/SAOS2 co-culture (panel A), significantly greater MSCs were identified ($p < 0.001$) than SAOS2 cells throughout the culture period. Likewise, within the MSC/MG63 co-culture (panel B), a significantly greater proportion of MSCs were identified from 24hrs through 124hrs of culture ($p < 0.001$) than MG63 cells.

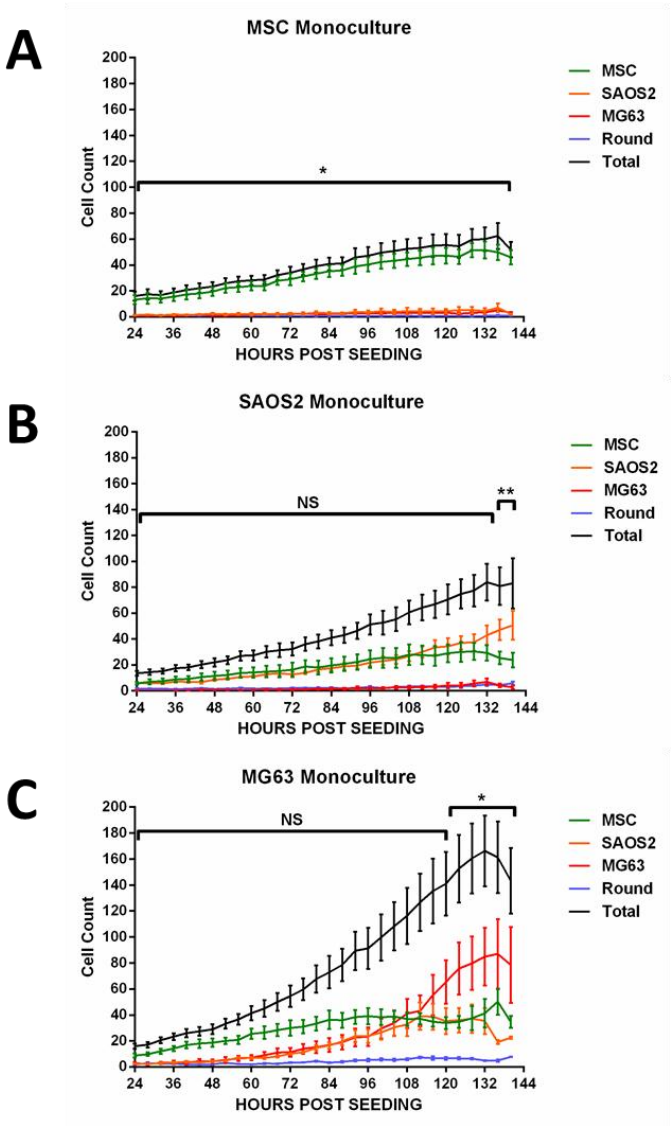

Figure 4.4: The Cell-IQ live-cell imaging platform counted the number of primary human MSCs, SAOS2 and MG63 cells cultured in the respective cell monocultures.

Cell counts for the average number and identification of MSCs (green), SAOS2 cells (orange), MG63 cells (red) and round cells (blue) per ROI are reported for each cell type within MSC (A), SAOS2 (B) and MG63 (C) cell monocultures. Data shown are mean ± SEM cell counts, from MSC n=5, SAOS2 and MG63 n=4 independent experiments with ≥3 ROIs per experiment. **indicates $p \leq 0.01$, *indicates $p \leq 0.05$ and *ns* indicates no significance; All, Two-way ANOVA with a Dunnett's post-test where the cell count within the monoculture is significantly greater than misidentification of other cell types examined, within the times indicated.

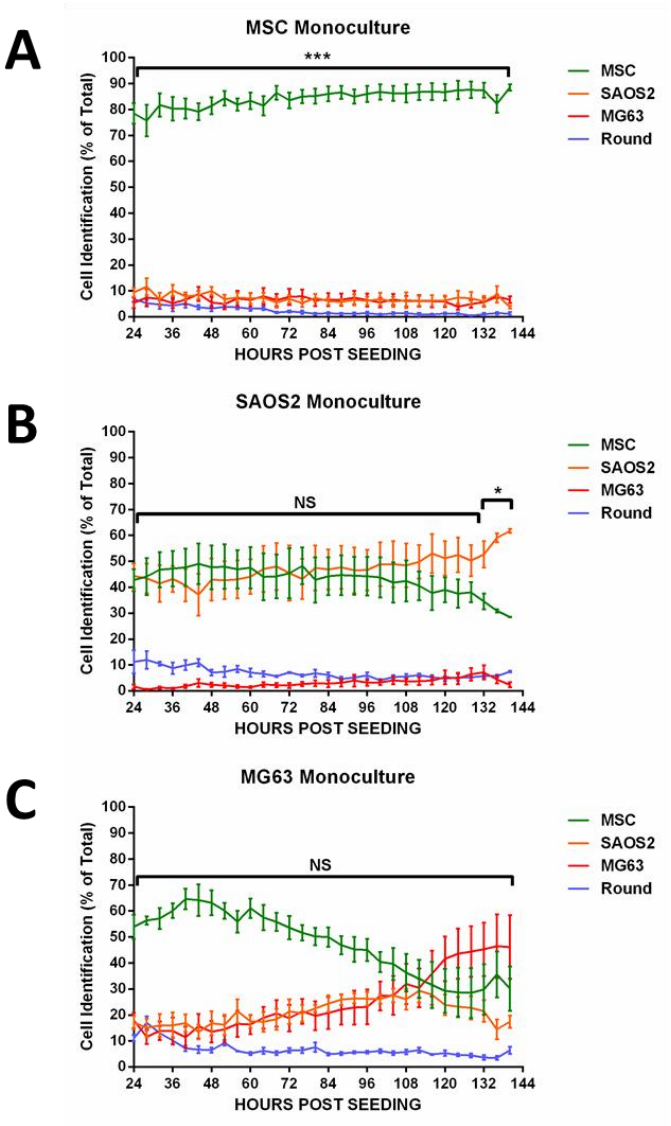

Figure 4.5: The Cell-IQ live-cell imaging platform used pattern recognition to distinguish between primary human MSCs, SAOS2 and MG63 cells cultured in monoculture.

Cell specific identification reported as a percentage of the total for MSCs (green), SAOS2 cells (orange), MG63 cells (red) and round cells (blue) per ROI are reported for each cell type within MSC (A), SAOS2 (B) and MG63 (C) cell monocultures. Data shown are mean ± SEM cell counts, from MSC n=5, SAOS2 and MG63 n=4 independent experiments with ≥3 ROIs per experiment. **indicates $p \leq 0.01$, *indicates $p \leq 0.05$ and *ns* indicates no significance; All, Two-way ANOVA with a Dunnett's post-test where the cell count within the monoculture is significantly greater than misidentification of other cell types examined, within the times indicated.

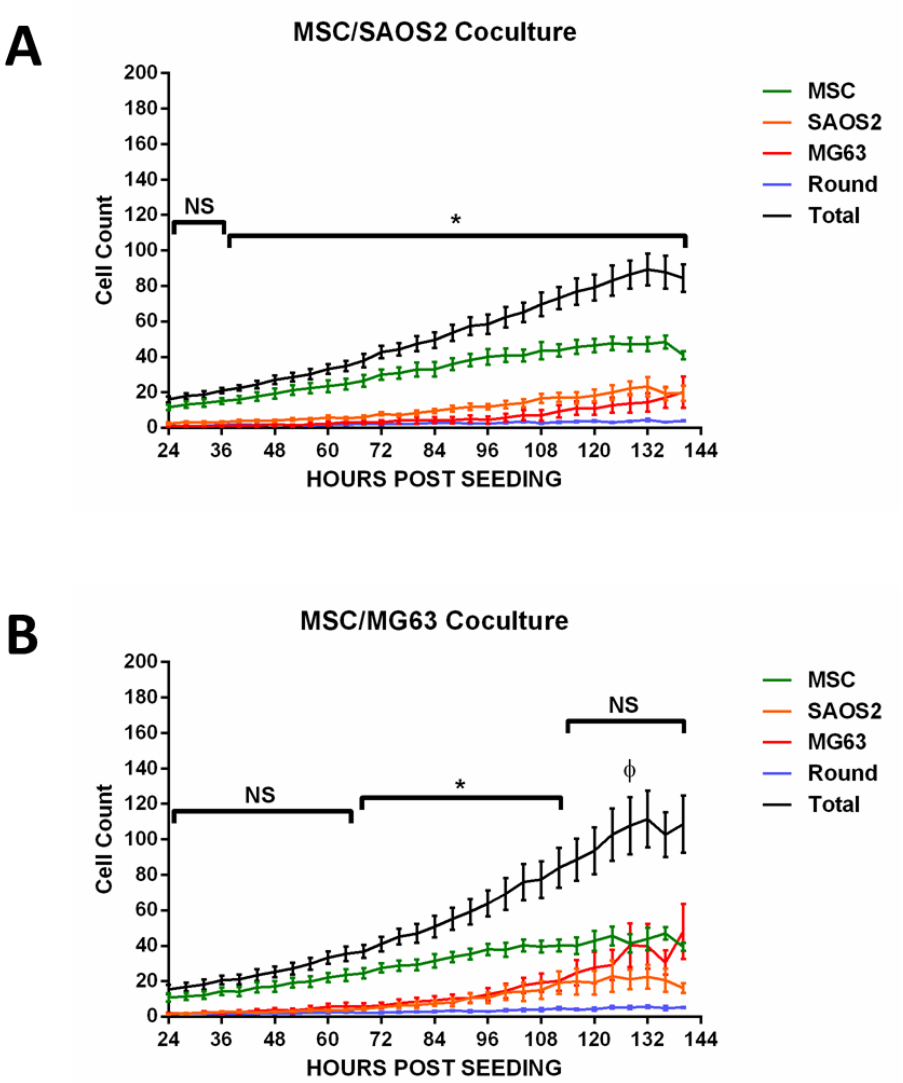

Figure 4.6: The Cell-IQ live-cell imaging platform counted the number of primary human MSCs, SAOS2 and MG63 cells cultured in the respective cell co-cultures.

Cell counts for the average number and identification of MSCs (green), SAOS2 cells (orange), MG63 cells (red) and round cells (blue) per ROI are reported for each cell type within MSC/SAOS2 (A) and MSC/MG63 (B) co-cultures. Data shown are mean ± SEM cell counts, from MSC n=5, SAOS2 and MG63 n=4 independent experiments with ≥3 ROIs per experiment. *indicates $p \leq 0.05$ and *ns* indicates no significance; the sigma sign (ϕ) indicates the least mean difference between MSC and MG63 cell identification; All, Two-way ANOVA with a Dunnett's post-test where the cell count for MSCs was significantly greater than that for SAOS2 or MG63 cells within the respective co-culture, between the times indicated.

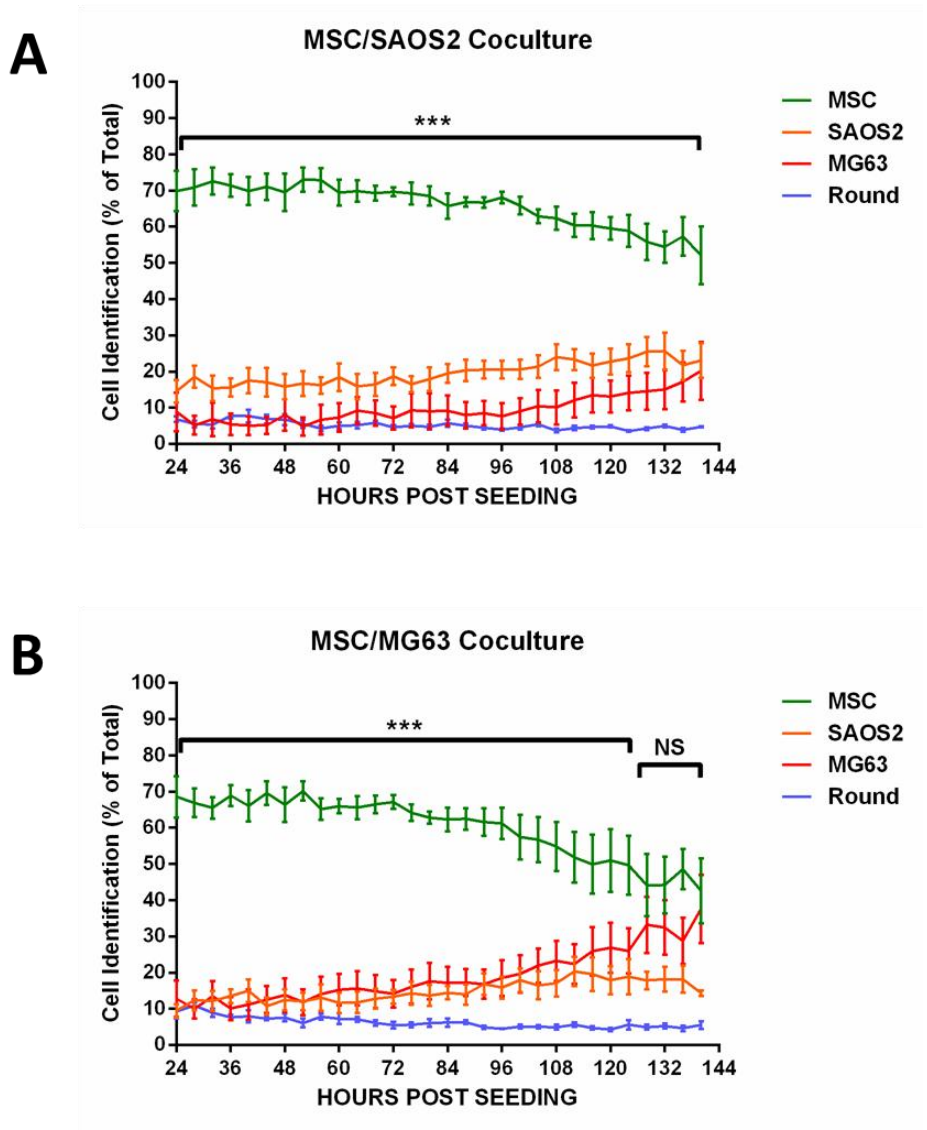

Figure 4.7: The Cell-IQ live-cell imaging platform used pattern recognition to distinguish between primary human MSCs, SAOS2 and MG63 cells cultured in co-culture.

Cell specific identification reported as a percentage of the total for MSCs (green), SAOS2 cells (orange), MG63 cells (red) and round cells (blue) per ROI are reported for each cell type within MSC/SAOS2 (A) and MSC/MG63 (B) co-cultures. Data shown are mean ± SEM cell counts, from MSC n=5, SAOS2 and MG63 n=4 independent experiments with ≥3 ROIs per experiment. ***p<0.001; All, Two-way ANOVA with a Dunnett's post-test where the cell count for MSCs was significantly greater than that for SAOS2 or MG63 cells within the respective co-culture, between the times indicated.

4.5 Cell isolation, culture and characterisation of chondrosarcoma derived cells (CS) using the Cell-IQ live-cell imaging platform

Samples of non-radiotherapy and post-radiotherapy treated chondrosarcoma were received and viable cells were isolated. A total of $17x10^6$ cells were isolated from the non-radio treated chondrosarcoma tissue sample. $14.0x10^6$ cells (82.3%) were viable and $3.0x10^6$ cells (17.7%) were non-viable. In contrast, only $12.1x10^6$ cells were isolated from the post-radio treated chondrosarcoma tissue sample. $8.6x10^6$ cells (71.1%) were viable and $3.5x10^6$ (28.9%) cells were non-viable.

Representative phase contrast microscopy images of these isolates in culture are shown in Figure 2.2. As shown, 10-11 days post seeding, cells from the non-radio treated sample adhered to the tissue culture plastic from both the explant sample (top left panel) 11 days post seeding and the 24hr collagenase digest sample (top right panel) 10 days post seeding. These appeared as proliferative viable cultures. In contrast, from the post-radio treated sample, only debris was found within the explant prepared sample (bottom left panel) and single stressed cells were identified in the collagenase digested sample (bottom right panel). With further time in culture, the non-radio treated cells continued to proliferate and colonies increased in size. In contrast, the post-radio treated cells showed no signs of proliferation throughout the culture period where only single cells were observed from 13 through 56 days post seeding.

Over 321 days of culture, the viable cell count of the 24hr digest isolated chondrosarcoma cells increased at each passage from $3.6x10^4$ cells at P1 to $14.7x10^4$ cells at P4 (Figure 2.3). In contrast, at P1, there were no post-radio treated sample chondrosarcoma cells within the culture. Over 302 days of culture, the viable cell count of non-radio treated explant isolated chondrosarcoma cells proliferated from $1.6x10^4$ cells at P1 to then $60x10^4$ cells at P4. In contrast, no viable cells were isolated from the post-radio treated culture.

The Cell-IQ platform was used to compare the isolated chondrosarcoma derived cells (CSs) with MSC, SAOS2 and MG63 osteosarcoma cells.

In terms of the appearance (i.e. Cell-IQ analysis of digitised images when compared to MSCs, SAOS2 and MG63 cells - Figure 4.8 A), the chondrosarcoma derived cells at P0, were identified as most similar to MSCs at 13 days (71.43 ± 14.51), 25 days (56.43 ± 13.89) and 56 days (49.67 ± 17.10) post seeding. However, identification as MSCs decreased between 13 to 56 days, with an increased identification of MG63 cells from 13 to 56 days, although these were not significant.

Following passage of the chondrosarcoma derived cells, no significant alteration to the identification profile was seen. The graph in Figure 4.8 B shows the cell count and classification of P1-2 chondrosarcoma derived cells from seeding through to 44hrs of culture expansion. As shown, classification of the cells from seeding, were most similar to MSCs and least similar to SAOS2, MG63 and round cells. The graph in Figure 4.8 C shows the classification of the P1-2 chondrosarcoma derived cells as a percentage relative to the total. This simply illustrates the classification of the cells as most similar to MSCs rather than SAOS2, MG63 or round cells. A video of cultured chondrosarcoma cells can be seen on the supplementary DVD (Appendix 7.4).

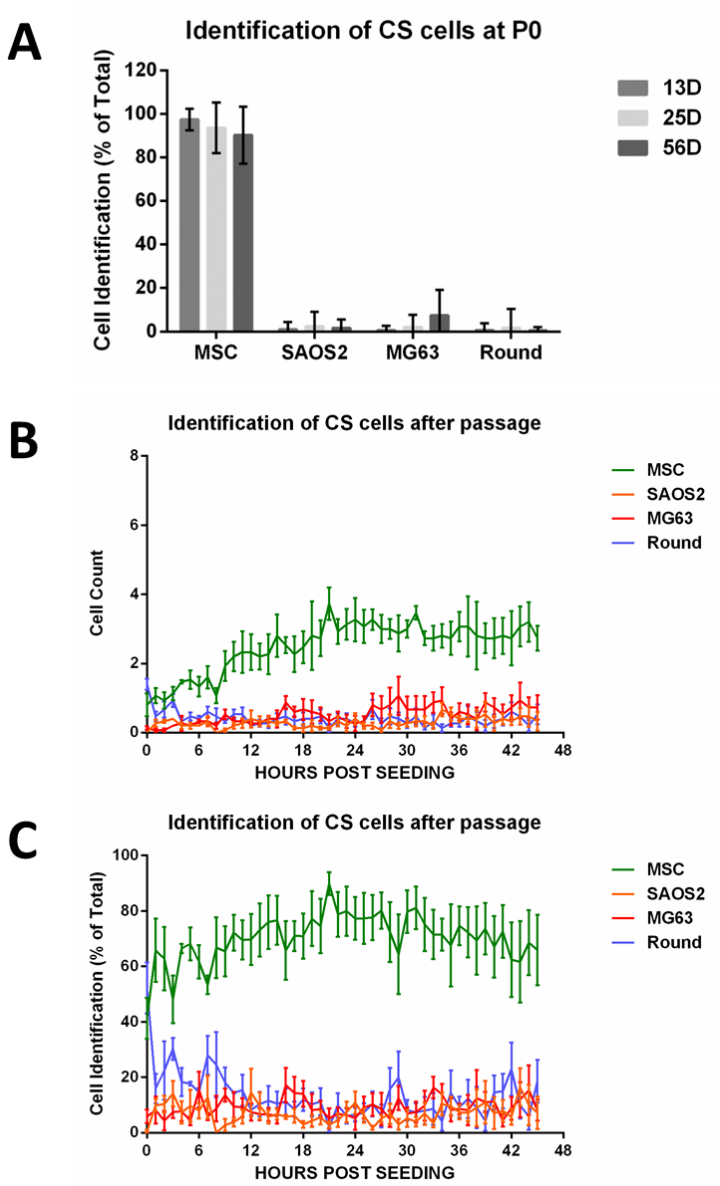

Figure 4.8: The Cell-IQ live-cell imaging platform classified non-radio chondrosarcoma derived cells according to morphological features.

Cultured chondrosarcoma derived cells (CS) prior to passage at 13, 24 and 56 days post seeding (A, P0) and following 44hrs of post seeding of subsequent passaged cells (B & C, P1-2) were imaged and identified using the sample library of MSCs, SAOS2 and MG63 cells (Figure 4.3). Identification is shown as a percentage of the total (A, C) and the number of cells counted are also shown (B) to be more morphologically similar to MSCs, (green), than SAOS2 (orange), MG63 (red) and round cells (blue). Data shown are means ± SD from n=1 CS sample imaged within n≥3 ROIs during n=3 independent experiments.

4.6 Manual cell tracking and manual lineage tracking of MSCs, SAOS2 and MG63 cells

To further characterise the different cell types examined, the Cell-IQ platform's Manual Cell Tracking tool was used to measure the trajectory length (distance of migration) and the speed via trajectory, comparing >100 of each cell type of MSCs, SAOS2, MG63 cells and P1/2 chondrosarcoma derived cells (CS), as shown in Figure 4.9 A-D respectively. It can be seen that MSCs (A) and MG63 cells (C) migrate over larger areas when compared to SAOS2 (B) and chondrosarcoma derived cells (D). The SAOS2 cells show the most compact cell migration.

Figure 4.10 illustrates lineage trees of MSCs, SAOS2 and MG63 cells obtained using the Manual Lineage Tracking tool. It can be clearly seen that SAOS2 and MG63 cells proliferated more through 120hrs of culture. Quantitation of this data is shown in Figure 4.11 where the average divisions (A), trajectory length (B) and speed via trajectory (C) are presented for each cell type. It should be noted that through the culture period, MG63 cells were in fact significantly more proliferative (18.3 ± 5.48 divisions per cell) than the MSCs (2.52±0.54 divisions per cell, $p<0.001$), SAOS2 cells (9.38 ± 0.85 divisions per cell, $p=0.0079$) and CS cells (0.03±0.03 divisions per cell, $p<0.001$). MSCs (1685 ± 533µm) and MG63 cells (1879 ± 353µm) migrated significantly more than the SAOS2 cells (407 ± 35µm, $p= 0.0238$ and $p=0.0194$ respectively) and CS cells (409 ± 24µm, $p=0.0014$ and $p=0.0024$ respectively). SAOS2 cells (3.44 ± 0.32µm/h) were the only significantly slower migrating cells compared to MSCs (14.30 ± 4.50µm/h, $p=0.0306$) and MG63 cells (15.80 ± 2.87µm/h, $p=0.0278$).

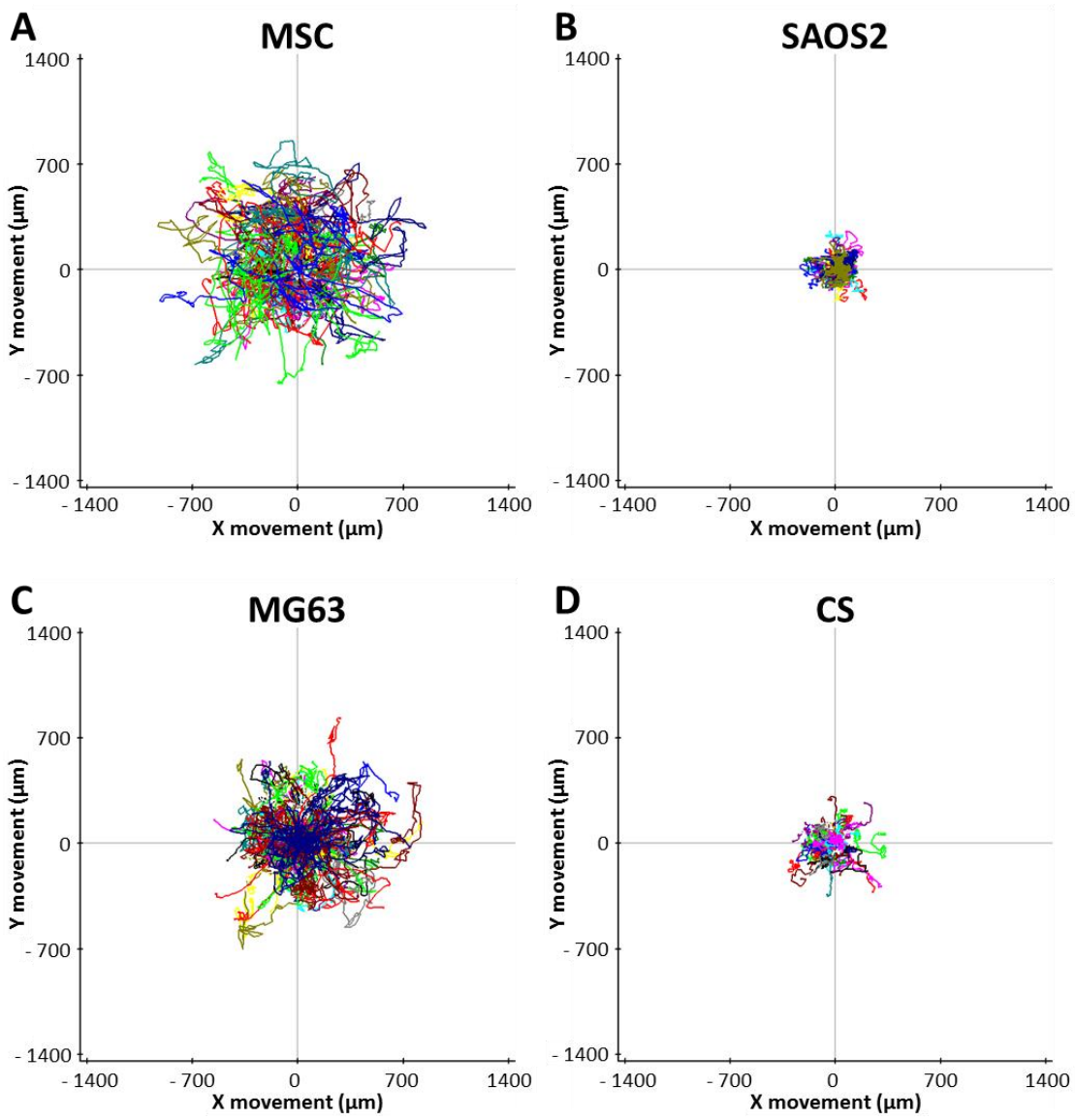

Figure 4.9: Manual Cell Tracking of live-cells using the Cell-IQ live-cell imaging platform showed the centred trajectory migration paths of primary human MSCs, SAOS2, MG63 and CS cells.

The single cell tracked lineage paths are shown for MSCs from primary human MSCs, osteosarcoma derived cell lines SAOS2 and MG63 cells, and primary chondrosarcoma derived cells (CS) tracked through ≥40hrs of culture. MSC data shown is from n=4 independent samples. Osteosarcoma data shown is from n=4 independent experiments. CS data shown is from n=1 CS sample imaged within n≥3 ROIs during n=3 independent experiments.

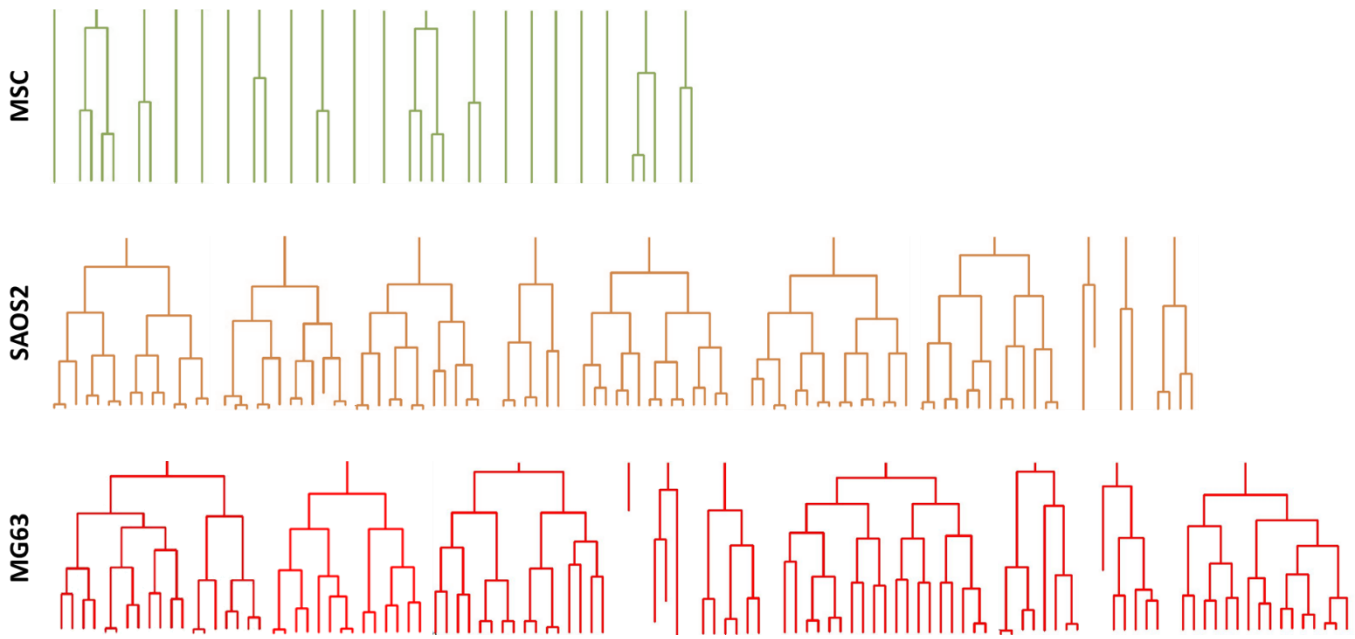

Figure 4.10: Manual cell lineage tracking of primary human MSCs, SAOS2 and MG63 cells showed differences in proliferation behaviour.

Lineage trees illustrating the proliferation of MSCs (green – top panel), SAOS2 (orange – middle panel) and MG63 cells (red – bottom panel) were gathered by tracking cells through 120hrs of culture with the Cell-IQ Manual Cell Lineage Tool. Twenty lineage trees are shown for MSCs, compared with 10 for SAOS2 and MG63 cells. Manual cell tracking data was gathered from n≥3 samples imaged during ≥3 independent experiments. The length of the lineage tree indicates cell survival through 120hrs of treatment. Interrupted or short lineage branches indicate cell death.

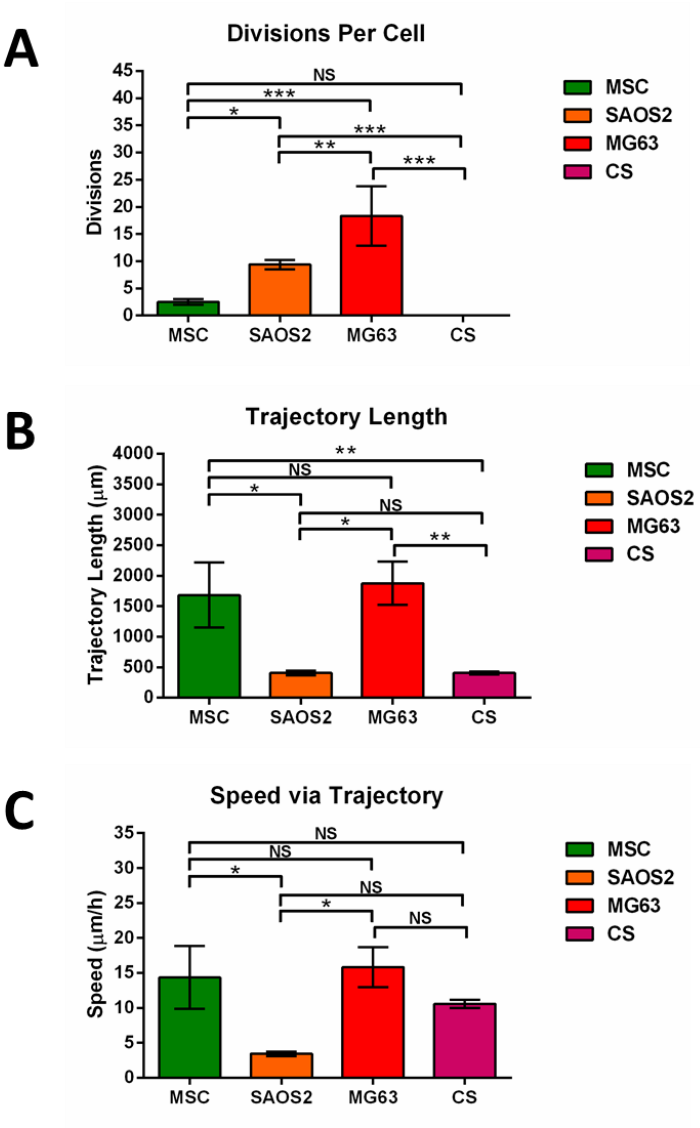

Figure 4.11: Manual Cell Tracking of live-cells significantly distinguished between primary human MSCs, SAOS2, MG63 and CS cells based on the average number of cell divisions, but not the trajectory length or speed via trajectory.

Cells from five human MSCs, SAOS2, MG63 and CS cells were tracked with the Manual Cell Lineage tracking tool. The average number of divisions (A), trajectory length (B) and speed via trajectory (C) are shown. Data shown for all call types are mean ± SEM. SAOS2 and MG63 cell data are from n≥3 independent experiments tracked through 120hrs of culture. CS data are from n=3 independent experiments tracked 60hrs of culture.

4.7 Discussion

The Cell-IQ live-cell imaging platform was able to measure the confluence of and count the total number of primary human MSCs, SAOS2 and MG63 cells within adherent monocultures; however there was a limited ability to identify and distinguish between cells in co-culture based on pattern recognition image analysis. Even in monocultures, correct identification was not exclusive to each cell type and misidentification was seen. In contrast, cell tracking markedly but not significantly distinguished cell migration patterns. Similarly, quantitation of cell proliferation, trajectory length and speed via trajectory measure by lineage tracking, significantly distinguished between some of but not all the cell types.

The identification demonstrated here, was based on a collection of images of each cell type grown in monoculture conditions and cell specific parameters were assigned to each cell class to assist the identification. This therefore allowed for heterogeneity between the cell types, yet not within the cultures.

MSCs are a phenotypically and functionally heterogeneous population of cells, which is reflected by differences in cellular morphology, differential marker expression and variable differentiation potentials, as reviewed by Pevsner-Fischer, Levin and Zipori, (2011). On the other hand, SAOS2 and MG63 cells are well-established and characterised osteosarcoma cells which show little heterogeneity (Rodan *et al.*, 1987, Pautke *et al.*, 2004). SAOS2 cells were established in 1973 and originate from a primary osteosarcoma from an 11 year old female Caucasian patient (Fogh and Trempe, 1975). Similarly, MG63 cells were first examined by Billiau *et al.*, (1977) for their mass production of human interferon (Billiau *et al.*, 1977). Although the SAOS2 and MG63 cells are not monoclonal and some phenotypic drift over long-term culture has been described (Hausser and Brenner, 2005, Barnes, Moy and Dickson, 2006), these cells can still be expected to be homogenous (Pautke *et al.*, 2004).

The identification of the MSCs, SAOS2 and MG63 cells was performed over a 120hr time period following 24hrs of cell adhesion to the TCP, through 140hrs of culture. Identification was heavily biased toward identification of the MSCs, where more specific identification of the SAOS2 and MG63 cells occurred from approximately 130hrs of culture. This stronger identification at the later culture period may be due to the specific confluent morphology of each cell type. However, the number of cells identified within the cultures clearly showed a greater and increasing number of total cells within the osteosarcoma samples compared to the slow proliferating MSCs. This was also evident within the co-cultures.

A comprehensive investigation into the heterogeneity of bone marrow stromal cells was performed by Whitfield, Lee and Van Vliet (2013). Using live-cell imaging and advanced image analysis software, they were able to track cells and record the number of cell divisions, cell migration details, as well as cell morphology and area. From these results they constructed cell lineage maps which showed that all the cells examined steadily grew larger over time, and the growth was only interrupted when a cell divided, thus producing two equally sized morphologically similar daughter cells. They also showed that these larger cells had most likely exited the cell cycle and had high levels of senescence associated β-galactosidase activity (Whitfield, Lee and Van Vliet, 2013). Their study only examined normal stromal cells, rather than what has been discussed in this chapter, i.e., the comparison of normal versus tumorigenic stromal cells; however, their approach to differentiating between cells and characterising the cells during culture expansion, provides a very powerful tool which can identify cell phenotypic differences which will assist in detecting tumorigenic transformation or aberrant cell behaviour of cells intended for cell-based therapy.

It has also been shown that the Cell-IQ live-cell imaging platform was able to identify and distinguish between cells derived from a primary low grade I chondrosarcoma compared to human MSCs and the osteosarcoma cell lines, SAOS2 and MG63 cells.

Viable cells isolated from a non-radio therapy treated primary low grade I chondrosarcoma (CS) following plastic adherence, showed clear signs of colony formation and proliferation through 13, 24 and 56 days of culture. Although it was evident that viable cells were isolated from the post-radio treated sample, and cells adhered to the plastic, there was no proliferation seen throughout the same culture period. Electromagnetic radiotherapy delivers energy through photons, which upon collision with human tissue or cells results in the release of free radicals and chemical bond breaks, leading to widespread damage throughout the cell. Single and double strand breaks to the DNA can be fatal, effecting cell division and proliferation, halting the cell cycle and ultimately leading to cell death if it is not repaired (Laval, 1980). Absorbed radiation doses, measured as joules/Kg, are expressed in the unit gray (Gy) (Ahmad *et al.*, 2012). Chondrosarcomas are highly resistant to radiotherapy, therefore to achieve local control after aggressive surgical resection, doses greater than 60 Gy are needed (Bovée *et al.*, 2005, Boeuf *et al.*, 2008, Gelderblom *et al.*, 2008).

Cell-IQ identification of the CS cells cultured at P0 between 13 through 56 days post seeding showed that the cells were most similar to MSCs. However, with time, the identification decreased non-significantly, with a slight and non-significant increase in identification as MG63 cells. Following culture expansion of the CS cells at P1/2, greater than 50% of the CS cells were still identified as most similar to MSCs, compared to SAOS2 and MG63 cells. CS cells categorised as most similar to MSCs may be due to similarities in their stromal appearance. Whole CS tissue was digested and cultured, which will most certainly contain a heterogeneous population of stromal cells; namely, cells which have a very similar appearance to MSCs. In contrast, the minor identification of CS cells as MG63 cells over time during P0 may be indicative of a clonal outgrowth of cell which are morphologically similar to MG63 cells in the chondrosarcoma sample.

Further imaging and identification of this sample and more samples of primary chondrosarcoma, or other mesenchymal derived cancer samples, over serial passages, would be needed to enhance the identification profile for these cells.

To further identify whether these cultured CS cells were in fact tumorigenic chondrosarcoma cells, specific point mutation analysis was done comparing a biopsy sample with the culture-expanded cells (data not shown).

As a part of the energy generating citric acid cycle, isocitrate dehydrogenases (IDHs) catalyse the oxidative decarboxylation of isocitrate to α-ketoglutarate and CO_2. IDH1 and IDH2 are NADP(+) dependent isocitrate dehydrogenases (compared to the other three forms IDH3α, IDH3β and IDH3γ which are NAD(+) dependant isocitrate dehydrogenases). IDH1 is found in the cytoplasm and peroxisomes, IDH2 within the mitochondria.

Mutations within IDH1 and IDH2 are fairly frequent events (56%) in central and peripheral chondrosarcomas. Specific point mutations commonly found in IDH1 usually result in substitutions at R132 and within IDH2, mutations may occur at R172 (analogous to IDH1 R132) and R140 (Amary *et al.*, 2011, Van Oosterwijk *et al.*, 2012, Monderer *et al.*, 2013). These mutations within the active site of the IDH do not result in terminal activity of the enzyme. Rather, it has been noted that the mutation R132H (arginine to histidine) in IDH1 may lead to the enzyme's ability to further convert α-ketoglutarate to *R*(-)-2-hydroxygluterate (2HG), an onco-metabolite (Dang *et al.*, 2009); or lead to increased levels of hypoxia-inducible factor subunit HIF-1α, a transcription factor facilitating tumour growth under low oxygen environments (Zhao *et al.*, 2009).

Here, the aforementioned point mutations were not observed in either the biopsy sample CS cells, nor in the culture-expanded CS cells. Unfortunately this does not confirm that the isolated culture-expanded cells were the same as the chondrosarcoma, however it does show that culture expansion does not induce these specific point mutations.

Manual cell tracking of all cell types during culture expansion showed very noticeable differences between the MSCs, SAOS2, MG63 cells and CS cells migratory behaviours when plotted on centred trajectory graphs. MSCs appeared to migrate the furthest, then MG63 cells. SAOS2 and CS cells showed little migration from their point of origin, with compact migration paths for most cells. Quantitation from the manual lineage tracking significantly differentiated between the MSCs, SAOS2 and MG63 cells based on the number of cell divisions observed through the culture period, and as expected the two osteosarcoma cell lines were significantly more proliferative than the MSCs. However, the MSCs and MG63 cells migrated significantly further throughout the culture period compared to the SAOS2 and CS cells. SAOS2 cells had the slowest migration compared to all the other cell types, notably and significantly slower than the MSCs and MG63 cells.

As discussed in Chapter 3, the SAOS2 cells are more osteoblastic than MG63 cells based on ALP positivity, thus the motility of the cells may reduce as they progress towards either a mature mineralised osteoblast, or an osteocyte. It would be interesting to examine the trajectory speed and distance of MSCs whilst being differentiated along the osteoblastic lineage, and comparing that to the trajectory speed and distance of the SAOS2 and MG63 cells.

The chondrosarcoma sample examined was diagnosed as a low grade I, thus the least metastatic of chondrosarcomas. Therefore, it would also be interesting to compare and contrast the migratory capacity of these cells *in vitro* to those from a highly metastatic grade III or dedifferentiated chondrosarcoma to see if *in vitro* cell migration is a good indicator or metastasis.

Unfortunately all of these findings do not conclusively show that the isolated chondrosarcoma derived cells are in fact chondrosarcoma cells. Therefore alternative means to identify the cultured cells as chondrosarcoma or normal cells would need to be done. This may include using the HCS platform discussed in Chapter 3. However, since there is no antibody target specifically for chondrosarcoma, primary samples would need to be compared to known chondrosarcoma cell lines (Calabuig-Fariñas *et al.*, 2012, Van Oosterwijk *et al.*, 2012, Monderer *et al.*, 2013).

4.8 Conclusion

The previous chapter showed the identification of normal human MSCs compared to SAOS2 and MG63 cells, using a HCS platform to identify biomarker immunoreactivity differences. This assay was an endpoint assay and required cells to be removed from a donor's sample, then terminally fixed, stained by ICC and analysed.

In contrast, this chapter has shown the identification of MSCs, SAOS2, MG63 and CS cells based on phase contrast images which were collected non-invasively during cell culture expansion. Both monocultures and co-cultures of MSCs and osteosarcoma cells were imaged and analysed. Analysis showed variable degrees of accuracy based on a large sample library composed of images of each cell type along with strict cell-type specific identification parameters.

The two osteosarcoma cell lines examined have been established for many years (Billiau *et al.*, 1977, Rodan *et al.*, 1987), and although they are likely to have undergone some sort of phenotypic drift as a result of this extended culture time (Hausser and Brenner, 2005), they represent a small example of MSC-derived tumours. Bearing this in mind, the phenotype of primary tumours may well be different to that of established tumour cell lines. Furthermore, the phenotype of cells which undergo spontaneous malignant transformation in culture might be considered or presumed to be more likely to resemble that of a primary tumour than an established cell line.

Here we have also shown that following excision and irradiation of a primary chondrosarcoma sample, followed by re-implantation of the humerus (Section 2.1.2), viable cells can be isolated and cultured from the excised chondrosarcoma tissue both before and after a very high dose (90Gy) of DXT radiotherapy. And, as expected, non-radiotherapy cells proliferated and post-radiotherapy cells did not. It was also demonstrated that these CS derived cells were morphologically similar to MSCs, had a low rate of proliferation to those of MSCs, and yet with a migration speed and trajectory distance similar to that of SAOS2 cells.

The first two chapters of the thesis have shown that the HCS and live-cell imaging platform may have application as screening platforms in determining whether cells that are being culture-expanded *in vitro* for regenerative cell therapies are safe, exhibit normal and expected behaviour, or may contain a malignant sub-population. There was a mixed degree of success using both platforms, which suggests that it is unlikely that these techniques, a least in the current formats and application procedures, would be able to guarantee that culture expanded MSCs do not contain transformed cells. The experiments reported in the next chapter were designed to address what could be done had such a scenario occurred. In particular, the next chapter has examined whether it may be possible to selectively inhibit the growth or kill tumour cells versus normal MSCs.

Chapter 5: Selective killing of sarcoma cell lines versus MSCs by treatment with a novel drug regime

5.1 Aims and Background

The previous chapters discussed the use of HCS and live-cell imaging to distinguish between primary human MSCs from the osteosarcoma cell lines SAOS2 and MG63 cells, and freshly isolated cells from a low grade I chondrosarcoma derived cells. These studies were performed with a view to developing improved safety and screening capabilities of cells intended for cell-based regenerative medicine. However, there remains the possibility that any tumour cells would remain undetected using the screening methods or that transformation would arise *in vivo* following transplantation. A further means of increasing the safety of MSC-based cell therapies would be the ability to eliminate any MSC-derived tumour cells, especially without affecting non-transformed MSCs to reduce harmful side-effects. Alternatively, the development and provision of an alternative treatment which can selectively target osteosarcoma cells whilst having little to no effect on resident stem cells, would help advance conventional chemotherapy.

The aim of this chapter was to identify a combination and concentration of drugs which may selectively inhibit the growth of human osteosarcoma cells, SAOS2 and MG63, compared with culture-expanded human MSCs.

A combinatorial drug regime of the lipid-regulating drug - bezafibrate (BEZ) and the sex hormone - medroxyprogesterone acetate (MPA) was recently demonstrated to target acute myeloid leukaemia cells (AML) with little effect on the survival of the normal adult myeloid progenitors (Khanim *et al.*, 2009). Following a clinical trial of these drugs within elderly patients with AML, strong evidence was shown for their safety, anti-AML activity and improved haemopoiesis in a proportion of the patients (Murray *et al.*, 2010).

Similarly, over a 5 year period, children in Malawi with relapsed or resistant endemic Burkitt lymphoma (eBL) were treated with a combination of BEZ and MPA at low, intermediate or high dose alone, or concurrently with other chemotherapies. The treatments were shown to be safe and

efficacious, and since eBL normally increases in size substantially in a week without anti-BL therapy, No Clinical Change (NCC) was seen and considered to be significant evidence of the treatment's anti-eBL activity. Comparison between the progression of the disease, NCC, partial response and a complete clinical response between the three dose cohorts showed a significant difference driven by the difference in progressive disease in the patients receiving low dose treatment (Molyneux *et al.*, 2014).

As reviewed by Činčárová *et al.,* (2013), valproic acid (VPA) has been used in clinical practice as an anticonvulsant for more than four decades, and is known to function as a histone deacetylase (HDAC) inhibitor (Gurvich *et al.*, 2004). Due to VPA's ability to; induce differentiation of a number of cancer cells *in vitro* and decrease tumour growth and metastases in animal models, restore or improve responsiveness of tumours to conventional therapeutic agents, to sensitize TRAIL-resistant tumour cells to apoptosis, and to enhance radiosensitivity of tumour cells, VPA is an attractive drug for cancer therapy (Činčárová, Zdráhal and Fajkus, 2013).

Therefore, we have hypothesised that a similar drug regime of BEZ and MPA alone (designated BAP) or supplemented with VPA (designated V-BAP), may selectively target osteosarcoma cells, whilst preserving non-transformed primary human MSCs.

To investigate this, MSCs, SAOS2 and MG63 cells were cultured in monocultures and co-cultures, then treated with a combined two fold dilution series of BAP or V-BAP, over a period of 5 days.

Viability of cells in monolayer cultures to individual drug treatments at doubling concentrations, followed by combined treatments of BAP and V-BAP were initially assessed by MTT assay. The Cell-IQ live-cell imaging platform was then used to visualise drug-induced effects in cell monolayers compared to control conditions, over time. These effects were quantitated by tracking specific cell lineages in control and treated conditions; quantitating the number of divisions, lineage trajectory length, speed via trajectory and cell survival.

5.2 The effects of BEZ, MPA and VPA treatments on single cell cultures of MSCs, SAOS2 and MG63 cells

The graphs in Figure 5.1 show the concentration-dependent effects of BEZ (A), MPA (B) and VPA (C) on the viability of five separate human MSC samples compared to SAOS2 and MG63 cells, which were tested on 3 independent occasions, by MTT assay following 5 days of treatment. The cell viability was normalised relative to the mean of the carrier-only control treated cells and reported as a percentage (%) of that control value.

There was a concentration-dependent decrease in the viability of SAOS2 and MG63 cells in response to drug treatments. The SAOS2 and MG63 cell cultures were both significantly less viable than the MSC cultures at the high concentrations of BEZ ([1.0mM], $p \leq 0.008$; [2.0mM] $p \leq 0.001$) and MPA ([20µM], $p \leq 0.0111$). VPA significantly inhibited SAOS2 cell viability compared to MSCs; however, no significant difference was seen between MG63 and MSCs cell viability, therefore no significance was indicated on the graph.

The graphs in Figure 5.2 show the concentration-dependent effects of combined treatments of BAP (A) and V-BAP (B) on the viability of five human MSC samples compared to SAOS2 and MG63 cells, where cell viability was again normalised to control levels and reported as a percentage (%).

Following combined treatments, the viability of all MSC cultures was significantly greater than that of both SAOS2 and MG63 cells following treatments with BAP and V-BAP. Specifically, MSC were significantly more viable than the SAOS2 and MG63 cells from [0.25mM]/[2.5µM] BAP ($p \leq 0.0446$) and from [0.125mM]/[1.25µM]/[0.6mM] V-BAP ($p \leq 0.0048$).

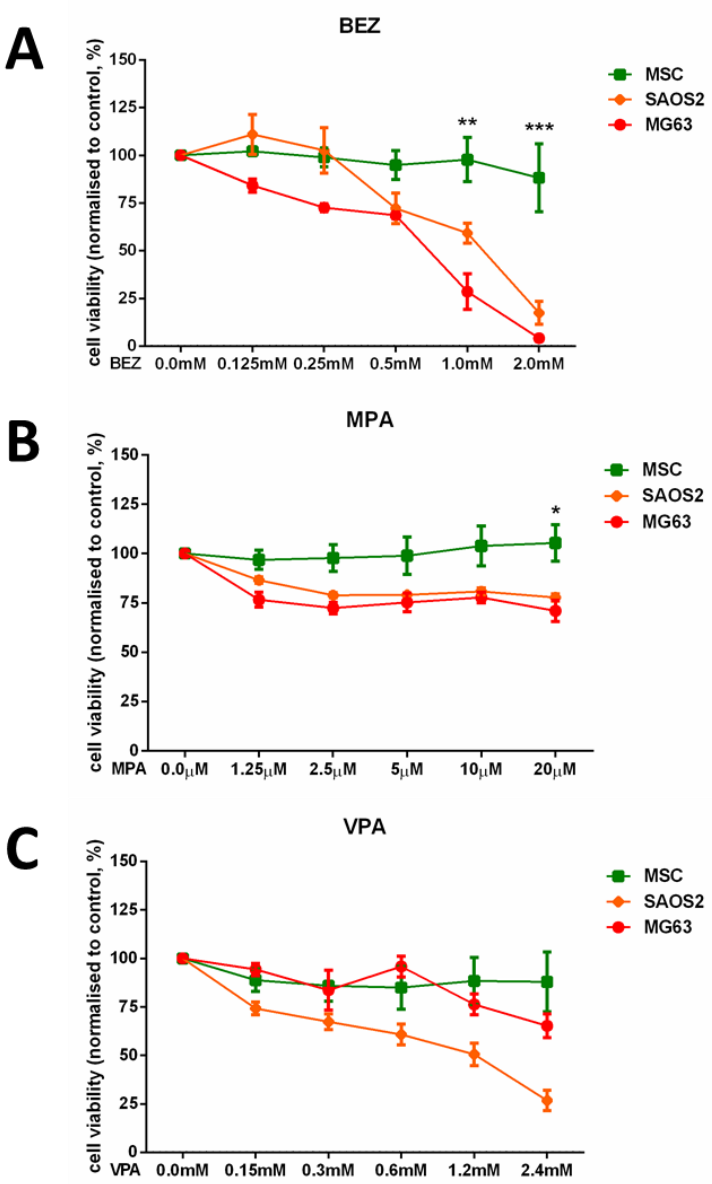

Figure 5.1: BEZ and MPA significantly inhibited SAOS2 and MG63 cells in a concentration-dependent manner compared to primary human MSCs, according to MTT assay; however, VPA did not.

The cell viability normalised to the percentage of the carrier-alone control is shown. Human MSCs, SAOS2 and MG63 osteosarcoma cell lines were treated for 5 days with two-fold increasing doses of BEZ (A), MPA (B) or VPA (C). Data shown are mean ± SEM n≥3 independent experiments. ***indicates $p \leq 0.001$, **indicates $p \leq 0.01$, *indicates $p \leq 0.05$; where MSC viability is significantly greater than both SAOS2 and MG63 cells. All; two-way ANOVA with a Tukey's post-test.

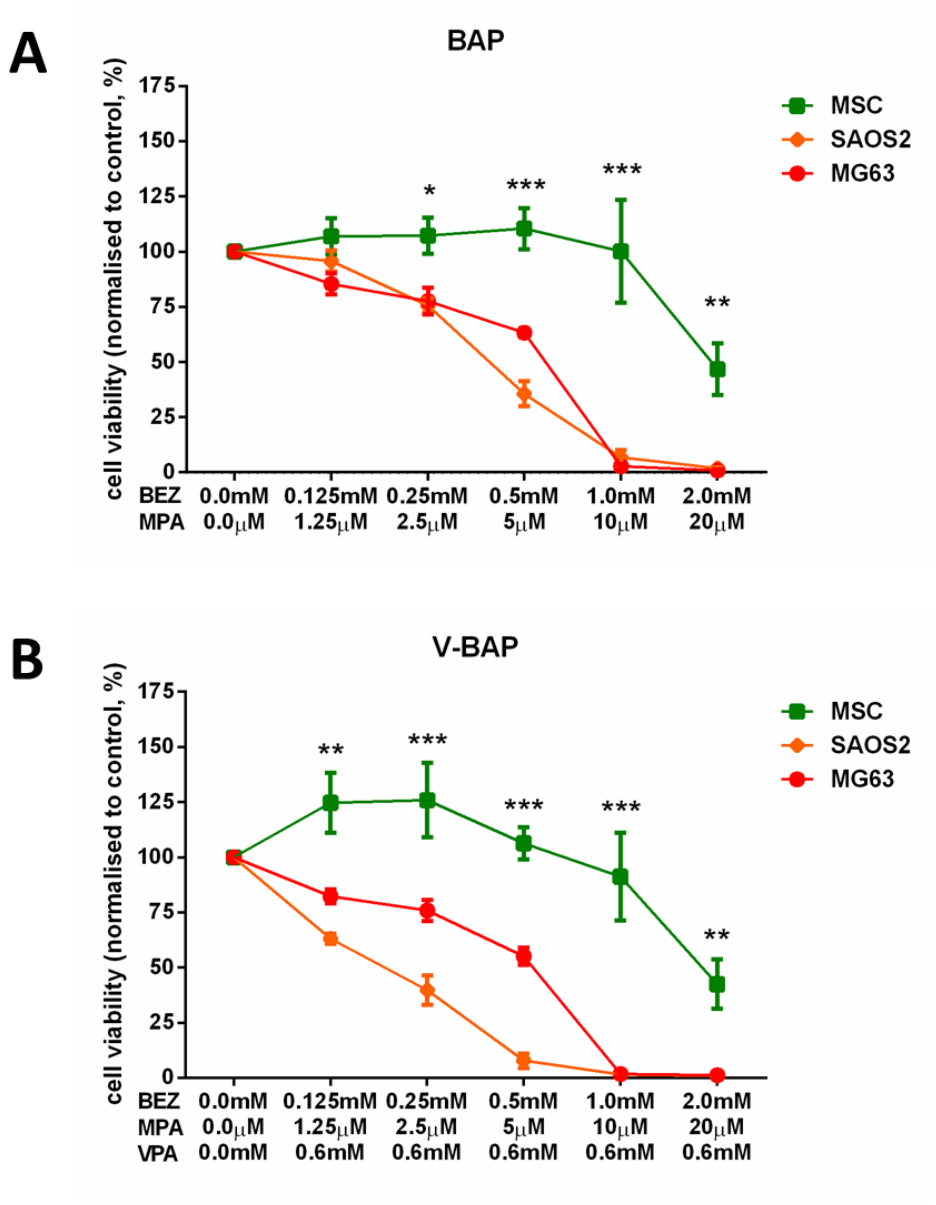

Figure 5.2: BAP and V-BAP significantly inhibited primary human MSCs, SAOS2 and MG63 cells in a concentration-dependent manner according to MTT assay.

The cell viability normalised to the percentage of the carrier-alone control is shown. Human MSCs, SAOS2 and MG63 osteosarcoma cell lines were treated for 5 days with two-fold increasing doses of BAP (A) or V-BAP (B). Cells were seeded and assayed in triplicate wells. Data shown are mean ± SEM from n≥4 independent experiments. ***indicates $p \leq 0.001$, **indicates $p \leq 0.01$, *indicates $p \leq 0.05$; where MSC viability is significantly greater than both SAOS2 and MG63 cells. All; two-way ANOVA with a Tukey's post-test.

5.3 The use of the Cell-IQ live-cell imaging HCS platform to examine combined drug treatments on five donor MSCs, SAOS2 and MG63 cells in monoculture

To quantitate the specific effects following combined treatments of BAP and V-BAP on cell behaviour using the live-cell imaging platform; monocultures of MSCs, SAOS2 and MG63 cells were seeded, then treated 24hr post seeding. Images were gathered with the Cell-IQ live-cell imaging platform from 0hrs to 120hrs post treatment. Treatment concentrations used were determined from the MTT results (Figure 5.1 and Figure 5.2) bridging the two concentrations where MG63 cell line's viability decreased more than tenfold from >50% to <5%. The concentrations were; BAP [Low] = 0.5mM/5µM, BAP [High] = 1.0mM/10µM, V-BAP [Low] = 0.5mM/5µM/0.6mM and V-BAP [High] = 1.0mM/10µM/0.6mM.

Figure 5.3 shows representative combined phase contrast and fluorescence images of MSCs, SAOS2 cells, and MG63 cells in monoculture. Images show control cells at 0hrs of treatment, and control compared to V-BAP [High] treated cells at 120hrs post treatment. All control and treatment conditions included the nuclear stain DRAQ7. When the membrane of a cell is compromised and permeable, DRAQ7 is able bind to the DNA, producing a fluorescent signal (shown as blue). White arrows indicate dead DRAQ7 positive MSCs, SAOS2 or MG63 cells. During cell death, fluorescent DRAQ7, which has bound to DNA was seen to dissipate as the DNA dissipated from the dead cell and into the media. Therefore, rather than relying on automated quantitation of dead cells, DRAQ7 positivity was instead used as a positive control whilst Manual Cell Tracking and Manual Lineage Tracking tools were used; tracking specific cell migration paths (Figure 5.4) and cell lineages (Figure 5.5); quantitating the number of cell divisions (Figure 5.6); determining cell trajectory lengths (Figure 5.7); determining cell's speed via trajectory (Figure 5.8) and the survival rate of the cells (Figure 5.9) in control and treated conditions.

Figure 5.4 graphically illustrates the cell trajectory paths of MSCs, SAOS2 and MG63 cells within control and V-BAP [High]. It can be clearly seen that there is a marked difference in cell trajectory distance and migratory behaviour between these culture conditions. Similarly, Figure 5.5 graphically illustrates up to five representative lineage trees of MSCs, SAOS2 or MG63 cells within BAP control, BAP [Low], BAP [High], V-BAP control, V-BAP [Low] and V-BAP [High] treatment conditions, from 0hrs of treatment (top of the tree) to 120hrs post treatment (bottom of the tree). It can clearly be seen that the treatments with BAP and V-BAP at both [Low] and [High], affected both the cell survival as well as capacity for division; notably more so in the SAOS2 and MG63 cells than the MSCs.

Quantitation of the number of cell divisions following BAP control treatments presented in Figure 5.6A, shows; MG63 cells as the most proliferative cell type with an average of 18.30 ± 4.47 cell divisions per cell, SAOS2 cells with significantly fewer average divisions with 9.38 ± 0.70 cell divisions per cell (p<0.001); and significantly the least proliferative cell was the MSCs with 2.52 ± 0.49 cell divisions per cell (p=0.0019 cf SAOS2, p<0.001 cf MG63). BAP [High] treatments significantly decreased SAOS2 proliferation ~4 fold to 2.64 ± 0.47 (p=0.006) divisions per cell; BAP [Low] and BAP [High] both significantly decreased the proliferative potential of MG63 cells ~3 fold to 5.71 ± 0.38, and ~8 fold 2.30 ± 0.31 (both p<0.001) divisions per cell respectively.

Similarly, following V-BAP control treatments (Figure 5.6B); MG63 cells divided 14.85 ± 4.43 times per cell, SAOS2 cells divided 9.36 ± 0.82 times (p=0.0212), and MSCs divided 2.48 ± 0.52 (p=0013 cf SAOS2, p<0.001 cf MG63) times through the culture and imaging period. V-BAP treatments also resulted in a significant decrease in both SAOS2 and MG63 cell divisions; notably following V-BAP [Low] and [High] treatments, the SAOS2 cells underwent fewer divisions than the control, decreasing ~2 fold to 4.35 ± 0.11 (p=0.368) and ~4 fold 2.16 ± 0.32 (p=0.0025) respectively. V-BAP [Low] and [High] treatment on the MG63 cells significantly decreased the number of cell divisions ~3 fold to 4.65 ± 0.17 (p<0.001) and ~7 fold to 2.033 ± 0.33 (p<0.001) divisions per cell, respectively.

The distance of trajectory of each cell type was quantitated and within the BAP and V-BAP control conditions, SAOS2 cells migrated significantly less than MSCs (p=0.0344 and p=0.0094, respectively) and MG63 cells (p=0.0289 and p=0.0060, respectively). V-BAP [High] was the only treatment which significantly reduced the migration trajectory of MG63 cells, reducing their trajectory ~3 fold from 1927 ± 549µm to 733 ± 243µm (p=0.0310).

Similarly, SAOS2 cells had the slowest speed via trajectory determined between all cell types within the BAP and V-BAP control conditions compared to that of MSCs (p=0.0267 and p=0.0107, respectively) and MG63 cells (p=0.0244 and p=0.0067, respectively).

Throughout the culture, imaging and tracking period, the death and survival of cells were noted and as shown in Figure 5.9, presented as a percentage positive relative to the control. MSC viability did not significantly decrease; however, SAOS2 cell viability significantly decreased from 98.32 ± 0.56% in control conditions to 69.32 ± 23.84% following BAP [High] treatments (p=0.0387), and MG63 cell viability significantly decreased from 98.92 ± 0.84% in control conditions to 51.63 ± 28.04% in BAP [High] treatments (p<0.001). Although the viability of MSCs within BAP [High] treatment conditions was significantly greater than that of the MG63 cells (p=0.0027), these was no significant difference of these to the viability of the SAOS2 cells at the same treatment conditions.

Similarly, V-BAP [High] treatment conditions significantly affected the viability of the SAOS2 and MG63 cells compared to the controls, where the viability of SAOS2 cells decreased from 97.30 ± 1.01% to 51.18 ± 21.84% (p=0.0018) and the viability of MG63 cells decreased from 96.16 ± 3.14% to 41.54 ± 27.70% (p<0.001). However, it should be noted that following V-BAP [High] treatments, MSCs viability was significantly greater than those of both SAOS2 (p=0.0130) and MG63 cells (p=0.0014).

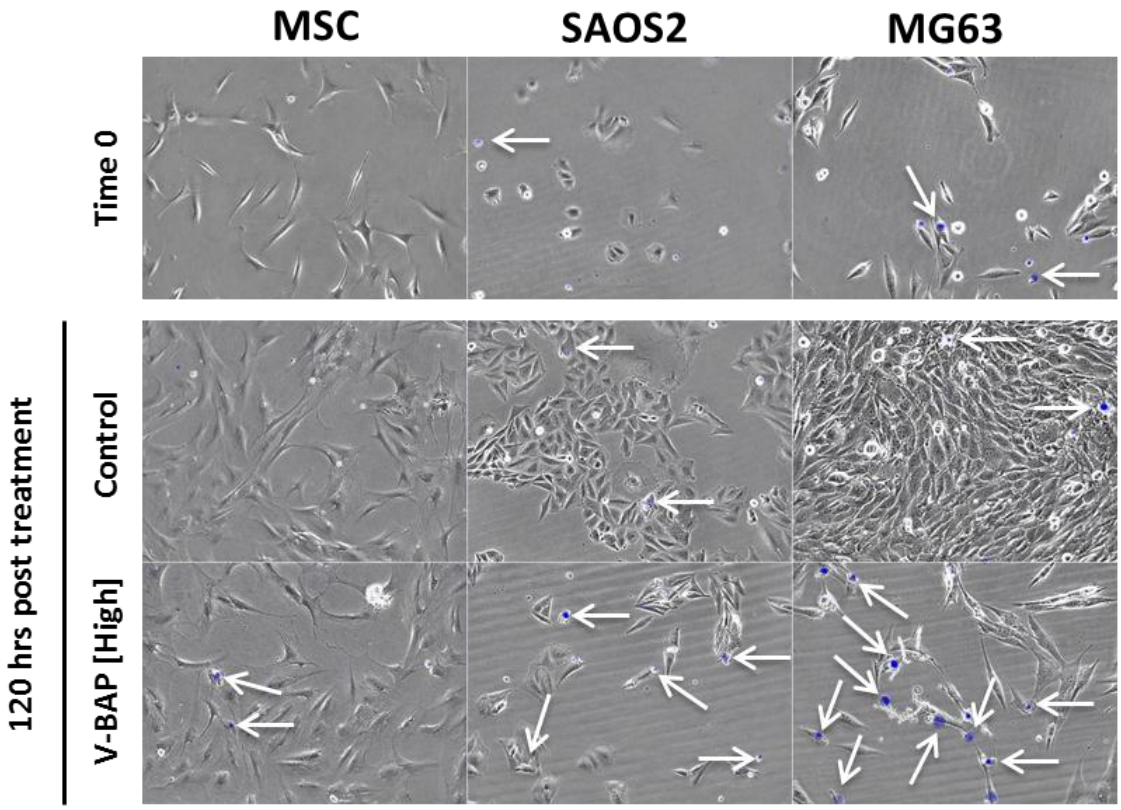

Figure 5.3: Representative phase contrast and fluorescence microscopy images of control and combined BAP treatment on monocultures of primary human MSCs, SAOS2 and MG63 cells at 0hrs and 120hrs post treatment.

Representative combined phase contrast and fluorescence images of MSCs (left column panels), SAOS2 cells (middle column panels) and MG63 cells (right column panels) grown in monocultures. Images show control cells at 0hrs of treatment (top row panels) and 120hrs post treatment (bottom two row panels) within control conditions in contrast to BAP [High] treatment conditions. White arrows indicate dead MSCs, SAOS2 and MG63 cells stained with the fluorescent DNA dye, DRAQ7 (blue).

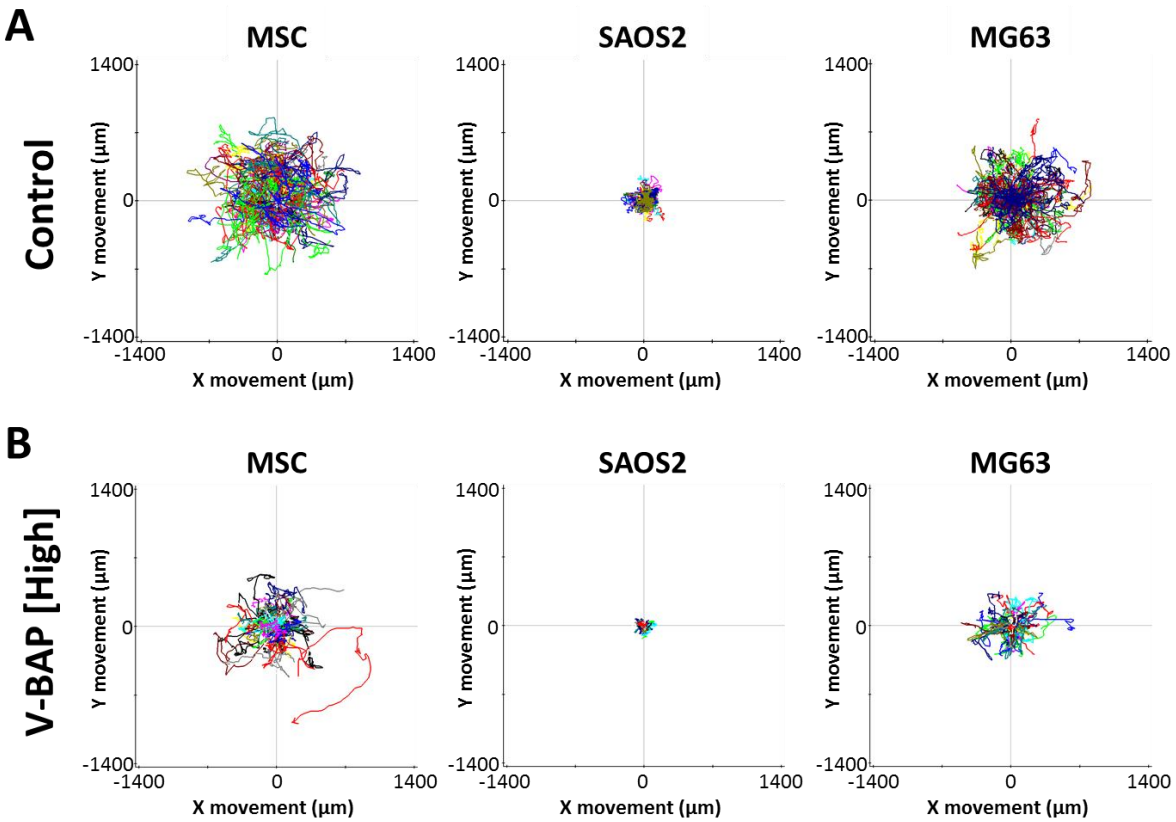

Figure 5.4: Manual Cell Tracking of live-cells using the Cell-IQ live-cell imaging platform showed the centred trajectory migration paths of primary human MSCs, SAOS2, MG63 cells in control versus V-BAP [High] treatment conditions.

The centred trajectory cell migration paths are shown for MSCs, SAOS2 and MG63 cells, tracked through 120hrs of culture within control (A) and V-BAP [High] (B) treatment conditions. Data shown was gathered from MSC n≥4 donors and SAOS2 and MG63 cells analysed over ≥3 independent experiments.

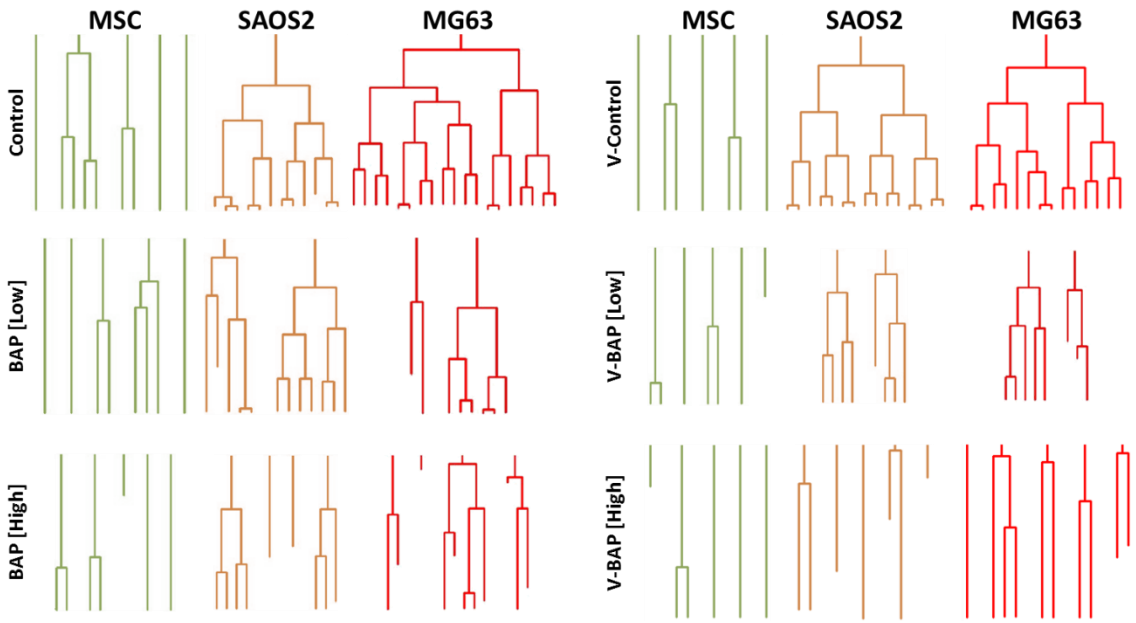

Figure 5.5: Treatments of BAP and V-BAP inhibited growth and induced cell death of primary human MSCs, SAOS2 and MG63 cells in monoculture, compared to the control.

Lineage trees of MSCs (green), SAOS2 (orange) and MG63 cells (red) following 120hrs of culture and treatment with BAP (left panels) and V-BAP (right panels) show effects of inhibited cell division and induced cell death compared to controls. Up to 5 representative lineage trees of each cell type are shown from ≥10 cells of each cell type tracked in each treatment condition. Manual cell tracking data was gathered using the Cell-IQ Manual Lineage Tracking tool from n≥3 independent experiments. The length of the lineage tree indicates cell survival through 120hrs of treatment. Interrupted or short lineage branches indicate cell death.

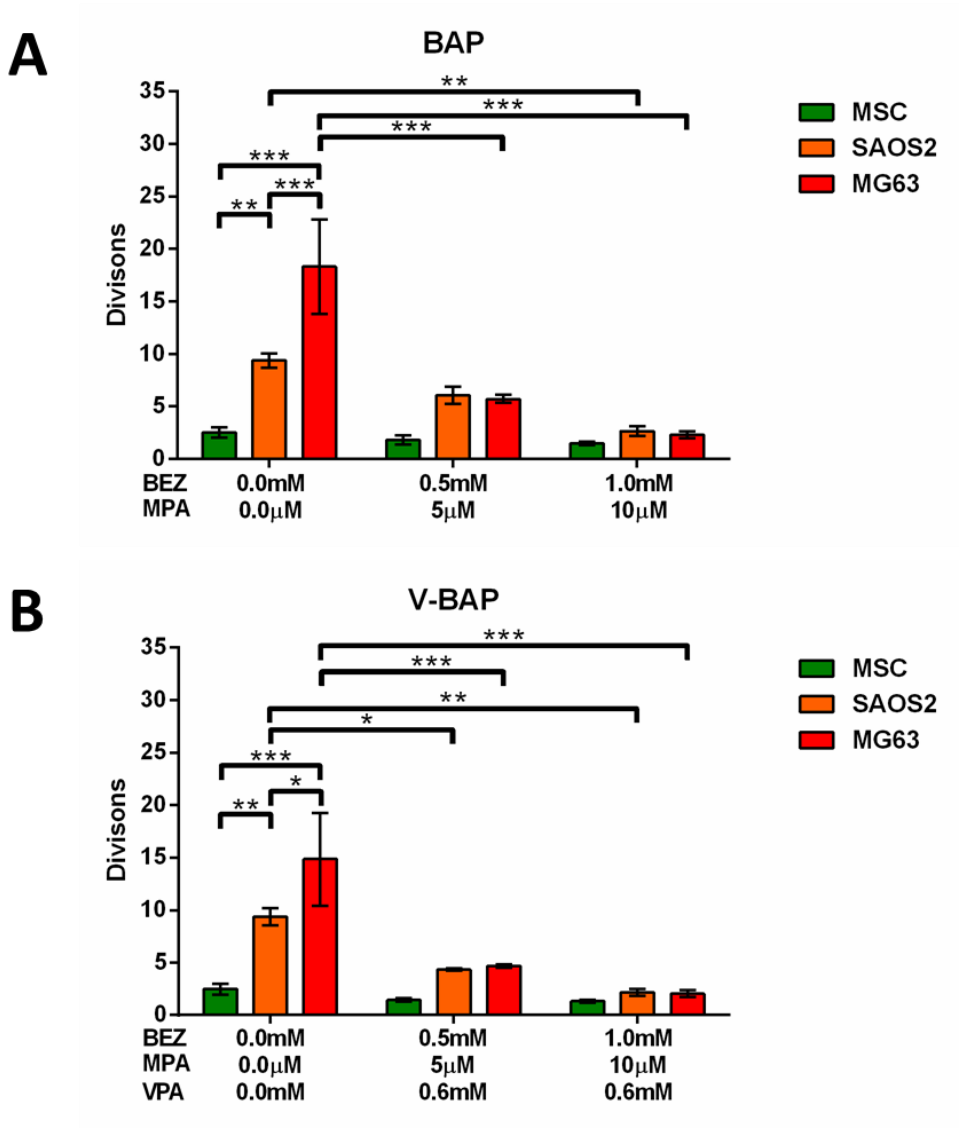

Figure 5.6: BAP and V-BAP affected the average number of cell divisions of SAOS2 and MG63 cells in a concentration-dependent manner, with little effect on MSCs, according to manual lineage tracking.

The average number of cell divisions per cell was quantitated following cell lineage tracking of MSCs, SAOS2 and MG63 cells in monoculture over 120hrs in control treatments, and doubling concentrations of BAP (A) and V-BAP (B). Data shown are means ± SEM from n≥3 independent experiments from ≥10 cells of each cell type tracked in each treatment condition. ***indicates $p \leq 0.001$, **indicates $p \leq 0.01$ and *indicates $p \leq 0.05$. All; two-way ANOVA with a Tukey's multiple comparison test.

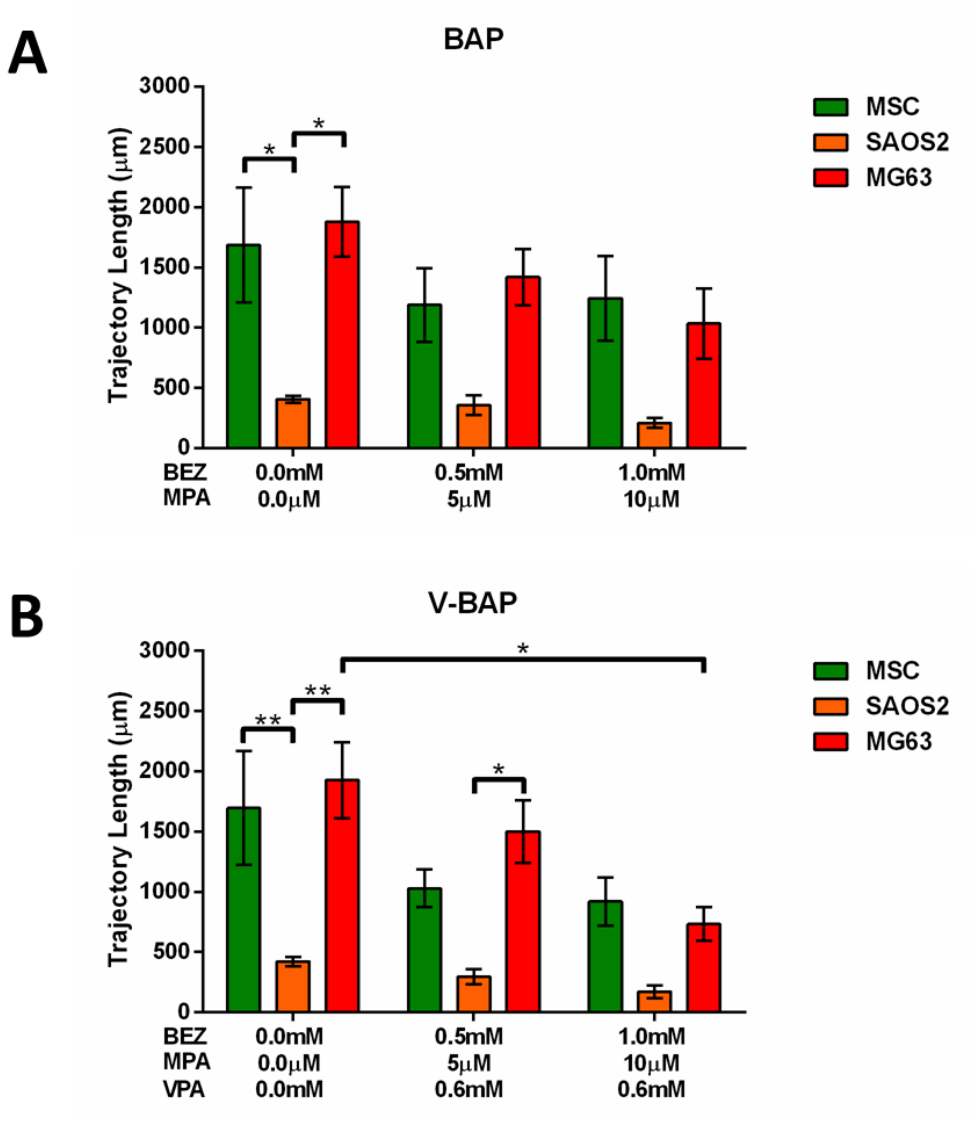

Figure 5.7: BAP and V-BAP affected the average cell trajectory length of MSCs, SAOS2 and MG63 cells in a concentration-dependent manner, according to manual lineage tracking.

The average trajectory length per cell was quantitated following cell lineage tracking of MSCs, SAOS2 and MG63 cells in monoculture over 120hrs following control treatments, and doubling concentrations of BAP (A) and V-BAP (B). Data shown are mean ± SEM from n≥3 independent experiments. **indicates $p \leq 0.01$ and *indicates $p \leq 0.05$. All; two-way ANOVA with a Tukey's multiple comparison test.

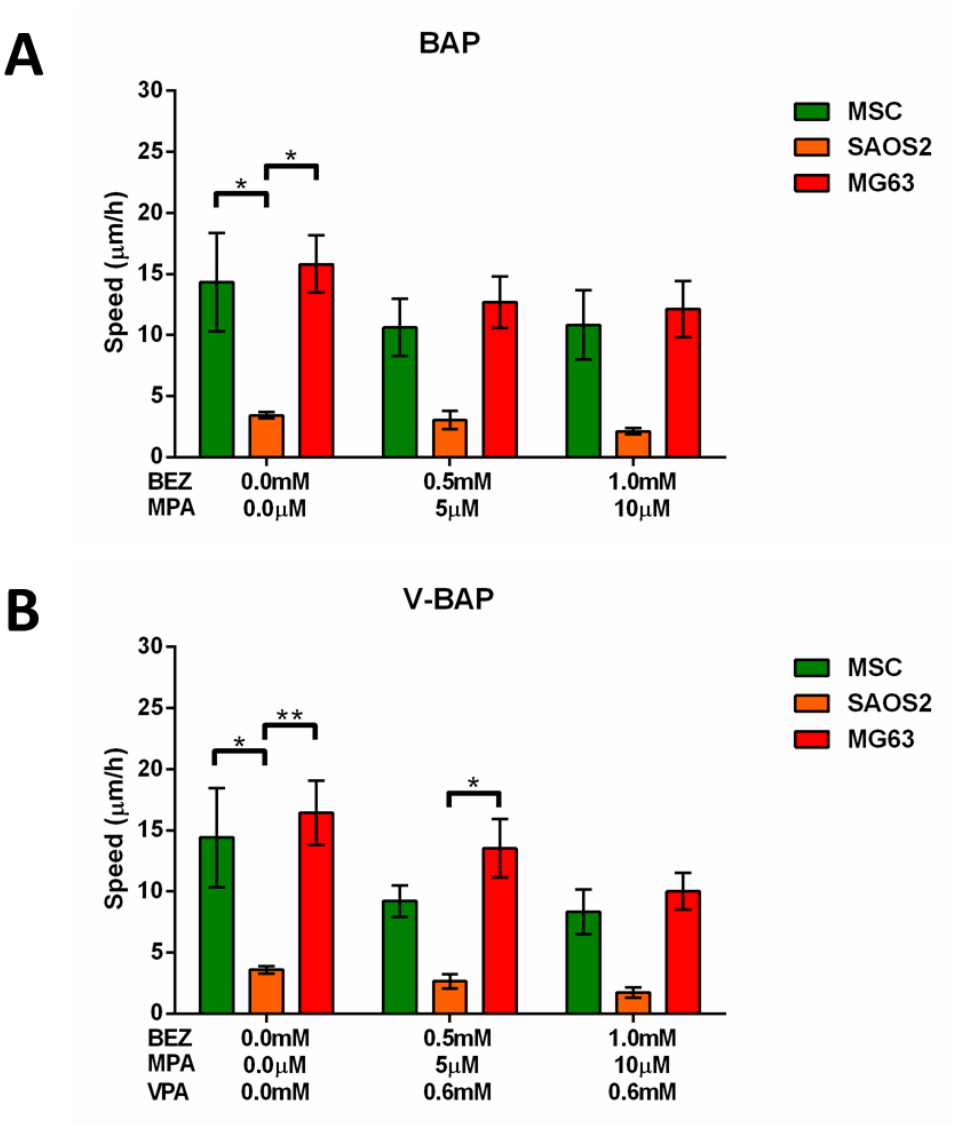

Figure 5.8: BAP and V-BAP affected the average cell speed via trajectory of MSCs, SAOS2 and MG63 cells, according to manual lineage tracking.

The average cell speed via trajectory was quantitated following cell lineage tracking of MSCs, SAOS2 and MG63 cells in monoculture over 120hrs following control treatments, and doubling concentrations of BAP (A) and V-BAP (B). Data shown are mean ± SEM from n≥3 independent experiments. **indicates $p \leq 0.01$ and *indicates $p \leq 0.05$. All; two-way ANOVA with a Tukey's multiple comparison test.

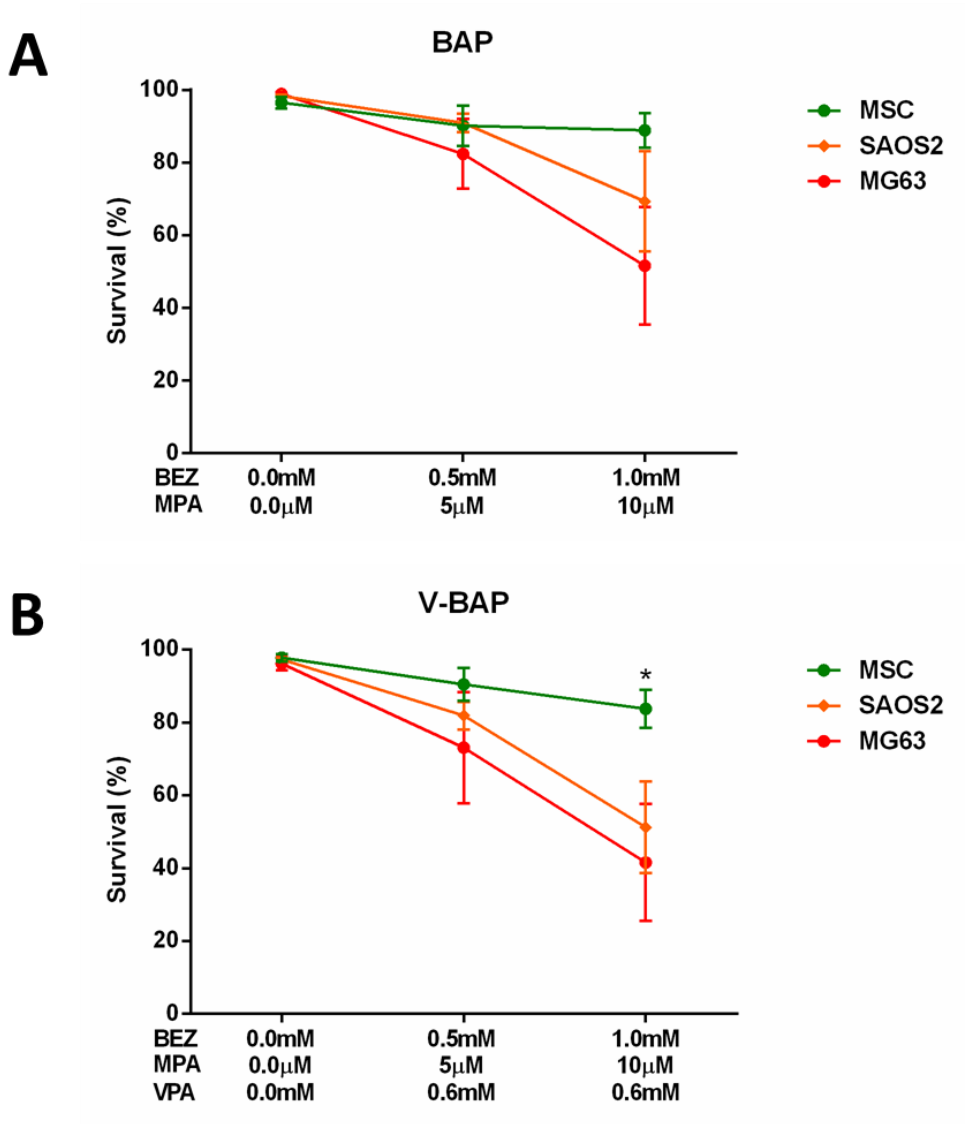

Figure 5.9: BAP and V-BAP affected the viability of MSCs, SAOS2 and MG63 cells in a concentration-dependent manner, according to manual lineage tracking.

The cell viability as a percentage (%) of the total, was determined in MSCs, SAOS2 and MG63 osteosarcoma cell lines by manual cell tracking following 120hrs of treatment with doubling concentrations of BAP (A) and V-BAP (B). Data shown are mean ± SEM from n≥3 independent experiments. * indicates p≤0.05; where MSC viability is significantly greater than both SAOS2 and MG63 cells. All; two-way ANOVA with a Tukey's multiple comparisons test.

5.4 Discussion

A combinatorial drug regime of bezafibrate (BEZ) and medroxyprogesterone acetate (MPA) designated as BAP, was recently demonstrated to target acute myeloid leukaemia (AML) with little effect on the survival of normal adult myeloid progenitor cells (Khanim *et al.*, 2009). Khanim *et al.*, (2009) proposed that the mechanism of action following combinatorial treatment of BEZ and MPA was due to increased synthesis and reduced metabolism of prostaglandin D_2 (PGD_2) resulting in elevated levels of the downstream product, 15-deoxy $\Delta^{12,14}$prostaglandin J_2 (15d-PGJ_2). 15d-PGJ_2 is an endogenous ligand for peroxisome proliferator-activated receptor-γ (PPARγ), which itself is an inducer of adipogenesis and inhibitor of osteoblastogenesis (Takada, Yogiashi and Kato, 2012).

The proposed mechanism of action was shown to be via separate and overlapping actions of reactive oxygen species (ROS), prostaglandin D_2 (PGD_2) and 15-deoxy $\Delta^{12,14}$ PGJ_2 (15d-PGJ_2), resulting in growth arrest, apoptosis and cell differentiation of AML cells with little effect on the survival of normal myeloid progenitor cells (Murray *et al.*, 2010). Later studies suggest that the critical anticancer actions of BAP disrupt lipogenesis by decreasing fatty acid and phospholipid biosynthesis from 13C D-glucose. Specifically, BAP treatments caused a decrease in stearoyl CoA desaturase 1 (SCD1) protein levels and fatty acid synthase (FASN) protein levels; therefore leading to a reduction in monounsaturated fatty acid and fatty acid synthesis (Southam *et al.*, 2015).

Previously, increased activation of PPARγ has been associated with: (i) induced growth inhibition of human hepatocellular carcinoma (Rumi *et al.*, 2001); (ii) inhibition of cell growth and induced apoptosis of human oral squamous cell carcinoma (Nikitakis *et al.*, 2002) (iii) induced apoptotic cell death in neuroblastoma cell lines (Kondo *et al.*, 2002); (iv) a differential ability to inhibit proliferation and to induce apoptosis and differentiation of human glioblastoma cell lines (Morosetti *et al.*, 2004); (v) altering the growth or invasive properties of the malignant potential of anaplastic carcinoma cell lines (Hayashi *et al.*, 2004); (vi) increased and induced apoptosis in normal

and malignant human B lymphocytes (Ray, Akbiyik and Phipps, 2006); (vii) inhibition of cell growth via apoptosis and cell cycle arrest in human colorectal cancer (Lin *et al.*, 2007).

Treatment of mesenchymal-derived chondrosarcoma cells with Pioglitazone, which is a selective ligand for PPARγ, as well as treatment with 15d-PGJ_2, the endogenous PPARγ ligand, inhibited cell proliferation and induced apoptosis in a dose-dependent manner (Nishida *et al.*, 2002). The mechanism of cytotoxic affect in the process of 15d-PGJ_2-induced apoptosis was later shown to be due to down-regulation of anti-apoptotic Bcl-xL and up-regulation of pro-apoptotic Bax and p21, a cyclin-dependent kinase inhibitor (Shen *et al.*, 2005).

15d-PGJ_2 has also been shown to induce and increase death receptor 5 (DR5) expression through mRNA stabilization independently of PPARγ, potentiating tumour necrosis factor-related apoptosis-inducing ligand (TRAIL) induced apoptosis (Nakata *et al.*, 2006). Furthermore, combined treatment with 15d-PGJ_2 and TRAIL induced apoptotic cell death in Jurkat human leukaemia calls and PC3 human prostate cancer cells (Nakata *et al.*, 2006). In a study conducted by Mitsiades *et al*., (2001), it was demonstrated that Ewing's sarcoma family tumours were sensitive to TRAIL through its binding to the DR5 (Mitsiades *et al.*, 2001).

It was therefore hypothesised that a similar drug regime of BAP may selectively target osteosarcoma cells, whilst preserving non-transformed MSCs. We determined to see if we could observe reduced viability or proliferation and increased cell death of the SAOS2 and MG63 cells, with little effect on non-transformed MSCs within monoculture conditions.

Based on the concentrations used by Khanim et al (2009) and those previously published (Bunce *et al.*, 1996, Fenton *et al.*, 1999, Fenton *et al.*, 2003, Murray *et al.*, 2010), we examined individual drug treatment effects on cell viability with MTT assay in a two-fold dilution series of BAP alone and supplemented with VPA at 0.6mM, designated V-BAP.

Following individual drug treatments for 5 days, it was seen that BEZ or VPA treatments reduced SAOS2 and MG63 cell viability to a greater extent than MPA, and in a concentration-dependent manner. Combinatorial treatments with BAP showed osteosarcoma-specific inhibitory effects from concentrations of and above 0.5mM BEZ and 5.0µM MPA. The addition of 0.6mM VPA to the BAP treatments significantly increased the osteosarcoma-specific inhibitory effects by reducing the viability of the SAOS2 and MG63 cells compared to the MSCs. This was seen for treatment conditions as low as V-BAP concentrations of 0.125mM BEZ, 1.25µM MPA, and 0.6mM VPA.

Lineage tracking of cells within monoculture showed that within control conditions, the MSCs were slow to proliferate and did not undergo many population doublings; however, they remained viable throughout the culture period with a trajectory path and speed via trajectory equal to that of MG63 cells. On the other hand, the SAOS2 and MG63 cells proliferated many times, where a single cell divided to produce many daughter cells; similarly remaining viable throughout the culture period. The SAOS2 were the least migratory cell with a short trajectory distance and a slow speed via trajectory. Following BAP [Low] and [High] treatments, the number of cell divisions and viability of MG63 cells significantly decreased. This trend was similarly seen to a greater extent following treatment with V-BAP [Low] and BAP [High]. SAOS2 cells were less affected by BAP [Low] and BAP [High] treatments; however, the number of cell divisions and viability significantly decreased following V-BAP [Low] and [High] treatments.

It should be noted that within the BAP and V-BAP treatment conditions; the MSCs' cell divisions, trajectory distance, speed via trajectory or cell survival did not significantly decrease relative to controls; as opposed to the responses seen by both the SAOS2 and MG63 cells, where proliferative and migratory potential were inhibited, and cell death was observed.

These observed concentration-dependent effects of BAP and V-BAP, alone and in combination, on the viability of SAOS2 and MG63 cells compared to the MSCs, and also that seen between MSC donors (data discussed in Appendix 7.2.3 and graphed in Figure 7.30), may be due to differences in

proliferation rate of each cell type. Fibrates and MPA were shown by Fenton *et al.,* (2003) to inhibit the proliferation and induce apoptosis of Burkitt's lymphoma (BL) cells, which are characterised by their uncontrolled proliferation, rapid growth and abnormal survival (Fenton *et al.*, 2003). SAOS2 and MG63 cells have rapid growth with doubling times of approximately 53hrs and 47hrs respectively (Pautke *et al.*, 2004), compared to that of adipose-derived MSCs which is greater than 60hrs (Choudhery *et al.*, 2014). Therefore the faster proliferating osteosarcoma cells may be more susceptible to the drug treatments than the MSCs.

A study performed by Lee *et al.*, (2008), demonstrated that 15d-PGJ_2 induced apoptotic cell death through the mitochondrial apoptotic pathway, which was mediated by ROS generation and JNK activation in osteoblastic cells (Lee *et al.*, 2008). Cytotoxic effects of 15d-PGJ_2 against SAOS2, MG63 and U2OS osteosarcoma cells through ROS-mediated AKT and cell cycle inhibition was recently reported (Yen *et al.*, 2014). 15d-PGJ_2 induced significant G2/M arrest and exerted time- and dose-dependent cytotoxic effects against the osteosarcoma cells; and, western blot analysis showed that both AKT and PKA-PLK1 were down-regulated in osteosarcoma cell lines after treatment. These reports are similar to Khanim *et al*., (2009), where BEZ increased PGD_2 synthesis via the generation of ROS and activation of the lipid peroxidation pathway, and MPA directed prostaglandin synthesis towards 15d-PGJ_2. Therefore, this may be the mechanism of action of the BAP treatments reported here; however, further investigation would need to be conducted to confirm this.

Adipogenic differentiation of the MSCs following BAP treatments may have occurred, since it has been shown that 15d-PGJ_2 binding to PPARγ induces adipogenic differentiation of the BOSC23 human kidney cell line (Forman *et al.*, 1995). However, induced adipogenic differentiation would need to be confirmed; firstly by examining if BAP in fact increased 15d-PGJ_2 production in the MSCs, then testing if there was a direct correlation with adipogenic differentiation. Bearing that in mind, a study conducted by Chi *et al*., (2013) examined the effect of 15d-PGJ_2 treatment on MSCs and reported that although the MSC underwent apoptosis and detached from the culture dish at

>20µmol/L, PPARγ mRNA levels were significantly higher within <10µmol/L treated MSCs than un-treated cells (Chi *et al.*, 2013). However, they did not report whether there was an increase in adipogenic differentiation.

As previously mentioned, VPA has been used in clinical practice as an anticonvulsant for more than four decades, and is known to function as a histone deacetylase (HDAC) inhibitor (Gurvich *et al.*, 2004). VPA has been shown to restore or improve responsiveness of tumours to conventional therapeutic agents, to sensitize TRAIL-resistant tumour cells to apoptosis, and to enhance radio sensitivity of tumour cells. However, drawbacks in the medical application of VPA include its teratogenicity and an incomplete understanding of the complexity of its effects (Činčárová, Zdráhal and Fajkus, 2013). As reviewed by de Ruijter *et al.,* (2003), HDACs remove acetyl groups from histones, creating a more compact chromatin structure. Inhibition of HDACs can result in a general hyperacetylation of histones, which is followed by the transcriptional activation of certain genes through relaxation of the DNA conformation (De Ruijter *et al.*, 2003).

The pre-treatment of BMMSC and ATMSC with increasing concentrations of VPA before induction towards osteogenic differentiation was shown to enhance the differentiation capacity of the cells in a concentration dependent manner (Cho *et al.*, 2005). Similarly, the *in vitro* effects of VPA on doxorubicin (DOX) sensitivity in canine and human osteosarcoma cell lines was examined, and treatment resulted in increased histone acetylation. Pre-incubation of osteosarcoma cells with VPA, followed by treatment with DOX resulted in significant growth inhibition of the osteosarcoma cells and potentiation of apoptosis, associated with a dose-dependent increase in nuclear DOX accumulation (Wittenburg *et al.*, 2011).

Therefore, the addition of VPA to the BAP treatments may have enhanced the PPARγ induced cytotoxic effects toward the osteosarcoma cell lines, whilst driving the MSCs along an adipogenic differentiation lineage. Further experiments would need to be conducted to examine the levels of

PPARγ and any direct correlation with osteosarcoma cell death, and adipogenic differentiation of the MSCs.

5.5 Conclusion

In summary, a combination and concentration of BEZ, MPA and VPA has been identified and shown to inhibit the growth of human osteosarcoma cells compared with culture-expanded human MSCs. Notably, the live-cell imaging platform was able to monitor and characterise the cells throughout the culture and treatment periods non-invasively, whilst showing drug induced inhibition of growth, the selective inhibition of cell proliferation and effect on cell survival of cells in monoculture.

Whilst the mechanisms of action of each of these drugs and the V-BAP drug combination remains to be resolved, as does whether the drugs induce any potential deleterious effects on the regenerative and differentiation activity of MSCs, this work provides a proof of concept that drugs re-deployed in the treatment of one type of malignancy, i.e. leukaemias and lymphomas, may also be used to treat a different type of malignancy, i.e. osteosarcomas. Furthermore, the study goes some way to further improving the safety of MSC-based cell therapies in which cell contamination or spontaneous malignant transformation are risk factors.

Chapter 6: Discussion

The work described in this thesis was aimed at improving the safety of autologous cell therapies that require cell culture in the provision of increased cell numbers, with a focus on human mesenchymal stem cells (MSCs). A high content screening (HCS) platform was employed in collaboration with an industrial partner (Imagen Therapeutics Ltd, formally Imagen Biotech Ltd) that specialises in the use of HCS to assess cell phenotype, particularly through immunological techniques that label cells in standard 2D cell cultures combined with digitised image analysis. The live-cell imaging platform, Cell-IQ was also employed to further assess cell phenotype and identification based on digitised images collected under phase contrast and fluorescence microscopy during live-cell culture.

Several key questions were addressed, all of which related to the potential risk of MSC cultures becoming transformed into MSC-derived tumours or containing tumour cells via some other route, e.g. through culture contamination. These questions were:

- Can a HCS platform be used to identify a non-transformed MSC versus a tumour cell thought to derive from MSCs during monolayer culture expansion using fixed cell samples? This was examined in Chapter 3 by quantitating immunoreactive phenotypes of MSC cultures versus established osteosarcoma cell lines, SAOS2 and MG63.

- Can live-cell imaging and analysis do the same screening procedure, i.e. correctly distinguish between a non-transformed MSC and a MSC-derived tumour cell without the need to fix cell samples? Similarly, does live-cell imaging and analysis enable the identification of non-transformed MSC versus primary tumour cells as well as established tumour cells? This was examined in Chapter 4 by using the Cell-IQ platform to analyse digitised phase contrast microscopy images captured during live-cell culture of MSCs, a primary chondrosarcoma, SAOS2 and MG63.

- In the worse-case scenario, where tumour cells are thought to be present in an MSC culture, can they be treated by drugs in such a manner that the tumour growth is inhibited or deleted

without causing harmful effects to non-transformed MSCs? This was examined in Chapter 5 by testing a novel combination of drugs known to target leukaemia and lymphoma without affecting normal haematopoietic stem cells.

6.1 HCS imaging and analysis key findings

To summarise the findings of work presented in Chapter 3, it was possible to demonstrate that the Cellomics HCS platform was able to determine to some extent an immunoreactive profile of biomarkers that distinguished osteosarcoma cells (SAOS2 and MG63) from MSCs. Immunoreactivity for protein markers associated with cell cycle progression, cell proliferation, cell survival, pluripotency, osteoblastic differentiation, cell signalling and cell migration were examined. However, significant differences between the non-transformed MSC versus the osteosarcoma cells were noted only in the proliferation associated Ki-67 antigen and the pluripotency marker, Oct4. As might be expected, significantly more of the SAOS2 cells and highly proliferative MG63 cells were immunopositive for the Ki67 antigen compared to the MSCs. Likewise, significantly more SAOS2 and MG63 cells were more immunopositive for Oct 4 compared to MSCs. In addition, significant differences between MSC versus the osteosarcoma cell lines were seen in some of the cell morphological features; namely, nuclear area and fluorescence intensity based on Hoechst 33342 staining.

The key finding of this work is that HCS is of value in determining cell phenotype, but there are possible limitations. Not least, the findings shown in this thesis would benefit from increased analysis of a great many more donors to further establish donor-donor variation in each of the parameters examined. It is generally well recognised that both the proliferative capacity and differentiation capacity of cultured MSCs can vary significantly between donors [references]. In addition, although a fairly broad range of different biomarkers were examined in this study for each MSC donor, the study may be improved by increasing the number of parameters examined by HCS. This could help to create a more in-depth immunophenotypic profile of each cell type.

Further work is required to optimise the use of HCS for MSC-based therapies, but, ultimately, it can be concluded that the adoption of HCS by cell therapy providers will provide useful additional information to improve the safety release criteria of MSCs for clinical transplantation. This is a key finding.

One potential area of improvement may be combining the immunophenotyping and morphological analysis of the Cellomics platform with other more established techniques that have been used to characterise MSCs. Indeed, it would be necessary to compare the quantitated immunoposivity data for MSC-biomarkers seen using the HCS platforms with that seen in flow cytometry, which is currently the gold standard for such MSC immunophenotyping, although usually only for cell surface markers. In order to measure risk of tumourigenesis, high throughput genotyping could be done to assess karyotypes and identify specific genetic alterations seen in MSC-derived tumours (Choy *et al.*, 2012). Similarly, fluorescence in situ hybridisation and RT-PCR have been used to identify translocations associated with MSC-derived tumours, such as the EWS1/Fli-1 translocation in Ewing's sarcoma (Riggi *et al.*, 2008, Machado *et al.*, 2009). The use of short tandem repeat analysis would help identify cross-contamination between samples should it occur, as shown previously by the identification of the HT1080 fibrosarcoma cell line within primary MSC cultures that had been reported to have spontaneously transformed (Rubio *et al.*, 2005, Torsvik *et al.*, 2010)article retracted by (Torsvik *et al.*, 2010).

It must be borne in mind, however, that all of these analyses use cells that have been sampled from the cultures that will be transplanted into a patient. Therefore, this sampling procedure reduces the number of cells available for transplantation, which could be a problem when cell number is limited and related to functional outcome, whilst also carrying a risk of not including tumour cells within the sample, or at levels below detection, e.g. if they were only present in small numbers during their initial clonal expansion.

6.2 Live-cell imaging and analysis key findings

For these reasons, live-cell imaging of MSCs and tumour cultures was undertaken using the Cell-IQ platform, because in principal this analysis can be done directly on all those cells which will be transplanted. The findings of work presented in Chapter 4 showed that following live-cell imaging and image analysis, the identification of MSCs compared to the SAOS2 and MG63 osteosarcoma cell lines by the pattern recognition algorithms had variable accuracy, depending on time in culture. This variability in accurately identifying each cell type related to the degree to which each cell type exhibited homogeneity and heterogeneity in cell morphology, as well as the confluence of the cells. Furthermore, it was clear that the variation in cell shape meant that the live-cell imaging and analysis performed was not able to distinguish between the different cell types with complete accuracy. This is a key finding and obvious limitation to the approach. The variability in MSC morphology is expected (Whitfield, Lee and Van Vliet, 2013). Further research and the additional development and refinement of algorithms to examine each cell type is needed and will likely improve the use of the Cell-IQ platform for identification of different cell types.

As described above, it would be advantageous to examine more donor-derived MSCs to gain a better understanding of morphological variation within this cell type, applying different cell-specific parameters within the algorithm developed in this thesis. This potentially would improve the correct identification of either homogeneous populations or heterogeneous sub-populations in donor-derived MSCs. However, it may be that there are only a limited number of MSC phenotypes that need to be identified, so only a limited number of algorithms or parameters are required. A similar argument can be applied to the assessment of MSC-derived tumours, where several algorithms may be needed to identify the tumour cells, e.g. one for osteosarcoma and a different one for Ewing's sarcoma.

More successfully, live-imaging and image analysis of cell division based on lineage tracking demonstrated MSCs divided significantly less frequently than the osteosarcoma cell lines. This key

finding matches the significant differences seen in Ki-67 antigen immunopositivity in Chapter 3. However, although the migratory behaviour of each cell type differed, MSCs were not significantly different to MG63 cells, with both significantly more migratory than SAOS2 cells. Whether the migratory behaviour of tumour cells *in vitro* reflects metastatic potential *in vivo* requires further work, but the findings here suggest that cell migration *per se* cannot be used reliably to distinguish MSCs from all tumour cells.

HCS and live-cell imaging has been successfully applied to assess heterogeneous populations of MSCs, where their osteogenic differentiation potential was determined based on morphological differences during live-cell culture (Matsuoka *et al.*, 2013). Therefore, it would be interesting to compare alkaline phosphatase activity with cell morphological features using the Cellomics and Cell IQ platform to see if this data might verify those previously published.

The Cell-IQ platform was also able to distinguish cells that were derived from a low grade chondrosarcoma (CS) from non-transformed MSCs, based on trajectory length of migrating cells. However, based on morphology the CS cells were more similar to MSCs compared to the osteosarcoma cells, although this drifted (albeit non-significantly) towards the identification of MG63 cells prior to the first passage of the CS cells. Following their first passage, the CS cells were still identified as being phenotypically more alike to MSCs than SAOS2 and MG63. Hence, the use of live-cell imaging and image analysis may be of limited use in identifying primary tumour cells from non-transformed cells from tissues that may well contain both cell types. This conclusion requires confirmation of whether the cells isolated and cultured from the CS tissue were actually tumorous or not. Although PCR analysis was performed using the cultured CS cells for the most common point mutations seen in chondrosarcoma, i.e. IDH1:IDH2, this was negative. Therefore, this aspects also requires further work.

This issue of identifying a primary population of tumour cells alongside a primary non-transformed cell population remains to be resolved. The outgrowth of primary chondrosarcomas has been

achieved previously (Calabuig-Fariñas *et al.*, 2012, Van Oosterwijk *et al.*, 2012), but it is a difficult process requiring multiple attempts and extended culture times. The advantage of using primary tumour cells *in vitro* goes beyond identifying how they may differ from non-transformed cells to inform the safety of cell therapy programmes, as these cells would provide a valuable resource in the development of drugs with anti-tumour activity.

A question arises as to how these screening techniques can be applied to MSC-based therapies? The primary advantage of the Cell-IQ live-cell imaging platform compared to the Cellomics HCS platform is the ability to monitor cell cultures without any interference. This makes it an invaluable tool for screening cell behaviour within a GMP compliant facility, when the cells are intended to be transplanted into the patient. On the other hand, the Cellomics platform, which can also be installed within a GMP facility, can provide substantial identification and characterisation data of cells on a single cell level. The combined provision of these two platforms towards the phenotypic profiling for the safety of cells used for cell based therapies has been shown diagrammatically in Figure 6.1.

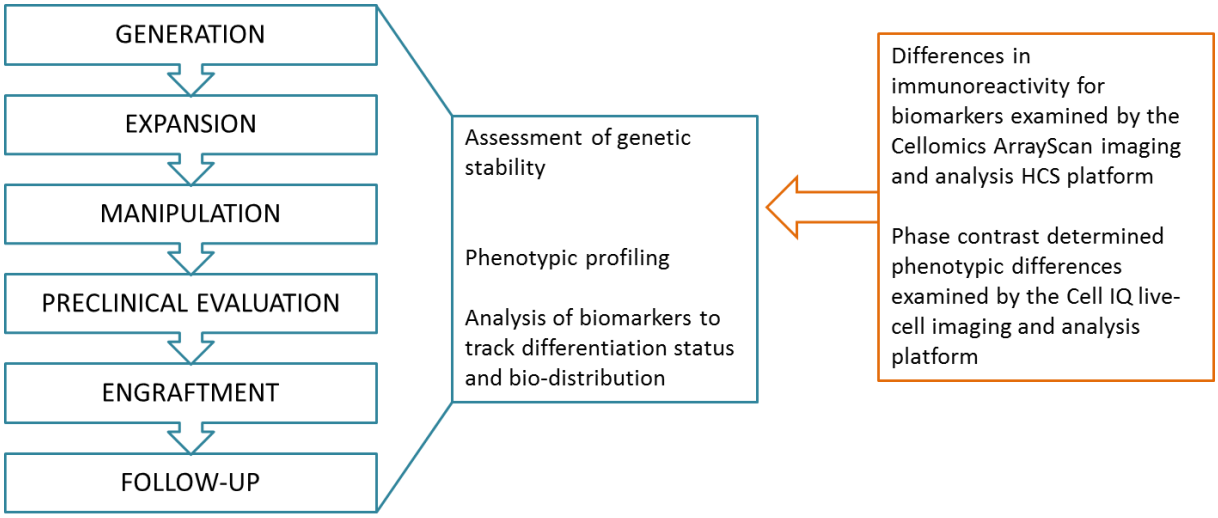

Figure 6.1: Workflow for Stem Cell-Derived Therapeutic Development

The major findings of Chapters 3-5 of this thesis (orange box) complement and enhance current GMP standards in the assessment of genetic stability and phenotypic profiling of cells to be used as "products" in cell therapies. Genetic and phenotypic analysis must be a continuous process throughout product development. After assessment of safety, the differentiation status and bio-distribution of cells within recipients also need to be assessed and tracked closely to further ensure safety and to evaluate whether clinical effects are predictable and controllable. Thus, HCS and live-cell imaging are able to screen and monitor the safety of cell intended cell therapies. Figure adapted from Goldring *et al.*, (2011).

6.3 Novel drug combination towards selective cell killing

The final aspect of the research reported in this thesis is an experimental approach to address a worse-case scenario in MSC-based therapies, where the transplanted cells may contain tumorous cells. Culture expansion of cells on tissue culture plastic *in vitro* is obviously a complete contrast to the micro environment of cells *in vivo*; this process itself causes genetic abnormalities to occur (Mayshar *et al.*, 2010, Ben-David, Mayshar and Benvenisty, 2011), hence compromising the safe provision of the cells for cell based therapy. Similarly, if a very small sample of cancer cells were amongst the primary cell isolate, the process of culture expansion may boost their proliferative capacities. Should a malignant colony arise, it would be beneficial to be able to target and kill this population of cells whilst preserving the normal cells.

To summarise and discuss the findings of the work presented in Chapter 5, a unique combination of drugs was identified, i.e., BEZ, MPA and VPA (termed V-BAP), which selectively targeted SAOS2 and MG63 osteosarcoma cells (at a specific concentration), whilst having little effect on normal MSCs. The drug combination inhibited the growth and induced cell death of the osteosarcoma cells in monocultures, as determined using a traditional method of quantitating viable cell numbers (MTT assay). Donor-to-donor variability was observed between the MSCs (discussed in Appendix 7.2.3 and7.3.1 and graphed in Figure 7.31 and Figure 7.32), where only four of five MSC cultures were resistant to drug treatment, which shows the need to screen newly emerging anti-cancer drugs in a patient-specific manner to generate personalised medicines. The Chapter also described experiments using the Cell-IQ live-cell imaging platform to analyse the effects of the same drug regime using the manual lineage tracking tool, over 5 days of treatment. This live-cell imaging and analysis platform was advantageous in that it demonstrated selective targeting of the osteosarcoma cells compared to MSCs.

The key finding of this research was that the novel combination of drugs, i.e. V-BAP has been identified as a potential therapy for the treatment of osteosarcoma. Importantly, the MSCs were

not adversely affected, suggesting minimal side effects. A similar drug redeployment of BAP has proven successful in the treatment of myeloid and lymphoid malignancy. However, much work will need to be done prior to successful clinical trials and application of this novel drug regime towards the treatment of osteosarcoma.

Further work is also needed to determine the mechanisms by which V-BAP targets osteosarcoma cells without affecting MSCs, e.g., to examine whether this differential effect may relate to the proliferative status of the different cell types (Pautke *et al.*, 2004, Choudhery *et al.*, 2014), or whether it is a result of differential effects on metabolic pathways (Lee *et al.*, 2008, Khanim *et al.*, 2009). In addition, and as described in Chapter 5, it would be particularly advantageous to test the drugs on primary MSC-derived tumours rather than established cell lines. This aspect was complicated by an inability to culture cells from the chondrosarcoma. An alternative approach might be to induce sarcoma formation in non-transformed MSCs, e.g. by EWS/Fli-1 translocation (Riggi *et al.*, 2008) and then use these cells for drug screening. Similarly, it would be very interesting to explore the relationship of drug induced effects on each cell type when cultured in co-culture conditions. Specifically, might one cell type provide protective mechanisms of behaviour towards another cell type, altering the effectiveness of the drugs?

The ISCT have stated that MSCs should be routinely characterised and identified by flow cytometry according to the presence and absence of immunolabelled cell surface antigens (Dominici *et al.*, 2006). Similarly, HSCs intended for clinical application and cell therapy are put through stringent characterisation by flow cytometry prior to transplantation. However, flow cytometry may not be the best method for spotting morphological malignant transformation of adherent cells cultured *in vitro* prior to transplantation. Morphological changes and the loss of adherence to tissue culture plastic is characteristic of the transformative process or alternatively contamination by another cell type (Riggi *et al.*, 2008, Torsvik *et al.*, 2010). Thus, this highlights the need for screening platform which provide automated and semi-automated analysis of fluorescence and phase contrast images,

both samples and non-invasively for phenotypic characterisation of cells cultured *in vitro* prior to their intended use in cell-based therapies.

Overall, this thesis has demonstrated the use of a HCS screening platform and a live-cell imaging platform to screen MSCs intended for cell-based therapies. It has compared and contrasted MSCs to two well-known osteosarcoma cell lines, as well as primary cells grown from a tumour sample. There were some interesting, novel and potentially clinically relevant findings regarding the differences between the cell types that provide a basis to improve the safety of MSC transplantation. However, larger donor groups are required to enhance the accuracy of MSC profiling and the identification of MSC specific distinguishing features. Similarly, larger donor groups of tumour tissues are required to enhance our understanding of these cells, and to help identify differential cell behaviours. The next stage of the V-BAP studies should focus on determining mechanisms of action. The HCS and live-cell platforms and approach will enable each of these overriding goals, thus improving the safe provision of MSCs in regenerative medicine, as well as targeting MSC-derived tumours.

6.4 Further Work

It is the author's opinion that the provision of cell imaging systems, including both the required software and hardware, will help improve monitoring systems of MSC cultures in traditional 2D systems. These systems would ideally be relatively easy or automated and would analyse images of cells in real time throughout the culture period in a non-invasive manner. Although such systems are or have been available, e.g. the Cell-IQ platform, IncuCyte® and Nikon BioStation CT, these systems are bulky and costly. In addition, much work has still to be undertaken to install such or similar systems within cGMP facilities. Nonetheless, their uptake by users and central pooling of the images collected could help many people involved in MSC-based research and therapies advance their recognition and analysis of MSC-specific features and behaviours. This ultimately

would help lead to the provision of a standard to which cells can be compared for their safer culture and therapeutic use.

At this point, multiparametric ICC and HCS of a sample of cells taken from a MSC culture to be used in cell therapies can be used to provide an enhanced profile of biomarkers for differentiation status, proliferation, cell morphology and cell signalling. Although, further work is required to examine how these cell-based readouts align to genetic monitoring and alterations, the adoption of these techniques in a cGMP facility would help enhance the safe provision of therapeutic MSCs. However, these measures are only indicative of safety. Additional work is also needed to clarify that cells that are predicted to be safe, through their biomarker profile, actually are safe when transplanted into model systems. In an ideal world, these transplantation studies would be using human MSCs into a humanised rodent model, so that the immune system remains engaged.

As previously noted, the mechanism of anticancer action of BAP within AML cells was reported to be a disruption of lipogenesis by decreasing fatty acid and phospholipid biosynthesis from 13C D-glucose. Specifically, BAP treatments of the AML cells caused a decrease in stearoyl CoA desaturase 1 (SCD1) protein levels and fatty acid synthase (FASN) protein levels This lead to a reduction in monounsaturated fatty acid and fatty acid synthesis ,respectively (Southam *et al.*, 2015). Therefore, it is important to investigate whether BAP and V-BAP treatments on MSCs, SAOS2 and MG63 cells similarly disrupt lipogenesis, particularly and possibly specifically within the SAOS2 and MG63 cells through the same mechanism of action, i.e. decreasing SCD1 and FASN protein levels. As detailed by Southam et al., (2015), supplementation with the SCD1 enzymatic product, oleate, rescued AML cells from the effects of BAP. Thus, rescue of the BAP and V-BAP effects on SAOS2 and MG63 cells would similarly help verify that the treatments work through a shared mechanism to that of AML cells. It would also be interesting to examine whether the effect of V-BAP treatment is consistent in co-cultures of normal MSCs with osteosarcoma cells. Examination of possible synergistic behaviours between the MSCs and osteosarcoma cells could be performed through imaging and

image analysis systems described within this thesis, e.g. to examine selective cell death in relation to ICC for SCD1 and FASN levels. Ultimately, it would be highly desirable to direct the use of BAP and V-BAP within a clinical study towards the treatment of osteosarcoma; however, the mechanism of action, potential toxicity and potential side effects still need to be firmly established through both *in vitro* and *in vivo* experiments.

References:

Ahmad, S. S., Duke, S., Jena, R., Williams, M. V. & Burnet, N. G. (2012). Advances in radiotherapy. *BMJ,* 345.

Ali, N. N., Rowe, J. & Teich, N. M. (1996). Constitutive expression of non-bone/liver/kidney alkaline phosphatase in human osteosarcoma cell lines. *J Bone Miner Res,* 11**,** 512-520.

Alper, J. (2009). Geron gets green light for human trial of ES cell-derived product. *Nat Biotech,* 27**,** 213-214.

Amary, M. F., Bacsi, K., Maggiani, F., Damato, S., Halai, D., Berisha, F., Pollock, R., O'donnell, P., Grigoriadis, A., Diss, T., Eskandarpour, M., Presneau, N., Hogendoorn, P. C. W., Futreal, A., Tirabosco, R. & Flanagan, A. M. (2011). IDH1 and IDH2 mutations are frequent events in central chondrosarcoma and central and periosteal chondromas but not in other mesenchymal tumours. *The Journal of Pathology,* 224**,** 334-343.

Andriacchi, T., Favre, J., Erhart-Hledik, J. C. & Chu, C. (2014). A Systems View of Risk Factors for Knee Osteoarthritis Reveals Insights into the Pathogenesis of the Disease. *Annals of Biomedical Engineering***,** 1-12.

Appelbaum, F. R. (2002). Hematopoietic cell transplantation beyond first remission. *Leukemia,* 16**,** 157-159.

Ashton, B. A., Eaglesom, C. C., Bab, I. & Owen, M. E. (1984). Distribution of fibroblastic colony-forming cells in rabbit bone marrow and assay of their osteogenic potential by an in vivo diffusion chamber method. *Calcif Tissue Int,* 36**,** 83-86.

Aubin, J. (2001). Regulation of Osteoblast Formation and Function. *Reviews in Endocrine and Metabolic Disorders,* 2**,** 81-94.

Bab, I., Passi-Even, L., Gazit, D., Sekeles, E., Ashton, B. A., Peylan-Ramu, N., Ziv, I. & Ulmansky, M. (1988). Osteogenesis in in vivo diffusion chamber cultures of human marrow cells. *Bone Miner,* 4**,** 373-386.

Bajada, S., Harrison, P. E., Ashton, B. A., Cassar-Pullicino, V. N., Ashammakhi, N. & Richardson, J. B. (2007). Successful treatment of refractory tibial nonunion using calcium sulphate and bone marrow stromal cell implantation. *Journal of Bone & Joint Surgery, British Volume,* 89-B**,** 1382-1386.

Bajada, S., Mazakova, I., Richardson, J. B. & Ashammakhi, N. (2008). Updates on stem cells and their applications in regenerative medicine. *Journal of Tissue Engineering and Regenerative Medicine,* 2**,** 169-183.

Bajada, S., Marshall, M. J., Wright, K. T., Richardson, J. B. & Johnson, W. E. B. (2009). Decreased osteogenesis, increased cell senescence and elevated Dickkopf-1 secretion in human fracture non union stromal cells. *Bone,* 45**,** 726-735.

Barnes, L. M., Moy, N. & Dickson, A. J. (2006). Phenotypic variation during cloning procedures: Analysis of the growth behavior of clonal cell lines. *Biotechnology and Bioengineering,* 94**,** 530-537.

Ben-David, U., Mayshar, Y. & Benvenisty, N. (2011). Large-Scale Analysis Reveals Acquisition of Lineage-Specific Chromosomal Aberrations in Human Adult Stem Cells. *Cell Stem Cell,* 9**,** 97-102.

Bernardo, M. E., Zaffaroni, N., Novara, F., Cometa, A. M., Avanzini, M. A., Moretta, A., Montagna, D., Maccario, R., Villa, R., Daidone, M. G., Zuffardi, O. & Locatelli, F. (2007). Human Bone Marrow–Derived Mesenchymal Stem Cells Do Not Undergo Transformation after Long-term In vitro Culture and Do Not Exhibit Telomere Maintenance Mechanisms. *Cancer Research,* 67**,** 9142-9149.

Bhosale, A. M., Kuiper, J. H., Johnson, W. E., Harrison, P. E. & Richardson, J. B. (2009). Midterm to long-term longitudinal outcome of autologous chondrocyte implantation in the knee joint: a multilevel analysis. *Am J Sports Med,* 37 Suppl 1**,** 131s-138s.

Bianco, P., Cao, X., Frenette, P. S., Mao, J. J., Robey, P. G., Simmons, P. J. & Wang, C.-Y. (2013). The meaning, the sense and the significance: translating the science of mesenchymal stem cells into medicine. *Nat Med,* 19**,** 35-42.

Billiau, A., Edy, V. G., Heremans, H., Van Damme, J., Desmyter, J., Georgiades, J. A. & De Somer, P. (1977). Human Interferon: Mass Production in a Newly Established Cell Line, MG-63. *Antimicrobial Agents and Chemotherapy,* 12**,** 11-15.

Birmingham, E., Niebur, G. L., Mchugh, P. E., Shaw, G., Barry, F. P. & Mcnamara, L. M. (2012). Osteogenic differentiation of mesenchymal stem cells is regulated by osteocyte and osteoblast cells in a simplified bone niche. *Eur Cell Mater,* 23**,** 13-27.

Boeuf, S., Kunz, P., Hennig, T., Lehner, B., Hogendoorn, P. C. W., Bovée, J. & Richter, W. (2008). A chondrogenic gene expression signature in mesenchymal stem cells is a classifier of conventional central chondrosarcoma. *The Journal of Pathology,* 216**,** 158-166.

Bovée, J. V. M. G., Cleton-Jansen, A.-M., Taminiau, A. H. M. & Hogendoorn, P. C. W. (2005). Emerging pathways in the development of chondrosarcoma of bone and implications for targeted treatment. *The Lancet Oncology,* 6**,** 599-607.

Bradbury, E. J., Moon, L. D. F., Popat, R. J., King, V. R., Bennett, G. S., Patel, P. N., Fawcett, J. W. & Mcmahon, S. B. (2002). Chondroitinase ABC promotes functional recovery after spinal cord injury. *Nature,* 416**,** 636-640.

Brittberg, M., Lindahl, A., Nilsson, A., Ohlsson, C., Isaksson, O. & Peterson, L. (1994). Treatment of deep cartilage defects in the knee with autologous chondrocyte transplantation. *N Engl J Med,* 331**,** 889-895.

Bullwinkel, J., Baron-Lühr, B., Lüdemann, A., Wohlenberg, C., Gerdes, J. & Scholzen, T. (2006). Ki-67 protein is associated with ribosomal RNA transcription in quiescent and proliferating cells. *Journal of Cellular Physiology,* 206**,** 624-635.

Bunce, C. M., Mountford, J. C., French, P. J., Mole, D. J., Durham, J., Michell, R. H. & Brown, G. (1996). Potentiation of myeloid differentiation by anti-inflammatory agents, by steroids and by retinoic acid involves a single intracellular target, probably an enzyme of the aldoketoreductase family. *Biochimica et Biophysica Acta (BBA) - Molecular Cell Research,* 1311**,** 189-198.

Calabuig-Fariñas, S., Gil Benso, R., Szuhai, K., Machado, I., López-Guerrero, J. A., De Jong, D., Peydró, A., San Miguel, T., Navarro, L., Pellín, A. & Llombart-Bosch, A. (2012). Characterization of a new human cell line (CH-3573) derived from a grade II chondrosarcoma with matrix production. *Pathol Oncol Res,* 18**,** 793-802.

Campo, E., Swerdlow, S. H., Harris, N. L., Pileri, S., Stein, H. & Jaffe, E. S. (2011). The 2008 WHO classification of lymphoid neoplasms and beyond: evolving concepts and practical applications. *Blood,* 117**,** 5019-5032.

Caplan, A. I. (1991). Mesenchymal stem cells. *Journal of Orthopaedic Research,* 9**,** 641-650.

Caplan, A. I. & Dennis, J. E. (2006). Mesenchymal stem cells as trophic mediators. *Journal of Cellular Biochemistry,* 98**,** 1076-1084.

Caplan, A. I. (2008). All MSCs Are Pericytes? *Cell Stem Cell,* 3**,** 229-230.

Caplan, A. I. (2010). What's in a name? *Tissue Eng Part A,* 16**,** 2415-2417.

Caplan, A. I. & Correa, D. (2011a). PDGF in bone formation and regeneration: New insights into a novel mechanism involving MSCs. *Journal of Orthopaedic Research,* 29**,** 1795-1803.

Caplan, Arnold i. & Correa, D. (2011b). The MSC: An Injury Drugstore. *Cell Stem Cell,* 9**,** 11-15.

Caplan, A. I. & Ricordi, C. (2013). The Rule of Science. *CellR4,* 1**,** e385.

Carmeliet, G., Nys, G. & Bouillon, R. (1997). Microgravity Reduces the Differentiation of Human Osteoblastic MG-63 Cells. *Journal of Bone and Mineral Research,* 12**,** 786-794.

Centeno, C. J., Schultz, J. R., Cheever, M., Freeman, M., Faulkner, S., Robinson, B. & Hanson, R. (2011). Safety and complications reporting update on the re-implantation of culture-expanded mesenchymal stem cells using autologous platelet lysate technique. *Curr Stem Cell Res Ther,* 6**,** 368-378.

Chailakhyan, R. K., Fridenshtein, A. Y. & Vasil'ev, A. V. (1970). Clone formation in monolayer cultures of bone marrow and spleen. *Bulletin of Experimental Biology and Medicine,* 69**,** 188-191.

Chamberlain, G., Fox, J., Ashton, B. & Middleton, J. (2007). Concise Review: Mesenchymal Stem Cells: Their Phenotype, Differentiation Capacity, Immunological Features, and Potential for Homing. *Stem Cells,* 25**,** 2739-2749.

Chan, A. C., Heathman, T. J., Coopman, K. & Hewitt, C. (2014). Multiparameter flow cytometry for the characterisation of extracellular markers on human mesenchymal stem cells. *Biotechnology Letters,* 36**,** 731-741.

Chen, Q., Shou, P., Zhang, L., Xu, C., Zheng, C., Han, Y., Li, W., Huang, Y., Zhang, X., Shao, C., Roberts, A. I., Rabson, A. B., Ren, G., Zhang, Y., Wang, Y., Denhardt, D. T. & Shi, Y. (2014). An Osteopontin-Integrin Interaction Plays a Critical Role in Directing Adipogenesis and Osteogenesis by Mesenchymal Stem Cells. *STEM CELLS,* 32**,** 327-337.

Chi, Y., Du, W. J., Cui, J. J., Chen, F., Han, Z. B., Ma, F. X., Li, X., Yang, S. G., Lu, S. H. & Han, Z. C. (2013). [Effect of 15-deoxy-Delta(12), 14-prostaglandin J2 on the cytokines in the culture supernatant of bone marrow mesenchymal stem cells]. *Zhongguo Shi Yan Xue Ye Xue Za Zhi,* 21**,** 1557-1562.

Cho, H. H., Park, H. T., Kim, Y. J., Bae, Y. C., Suh, K. T. & Jung, J. S. (2005). Induction of osteogenic differentiation of human mesenchymal stem cells by histone deacetylase inhibitors. *Journal of Cellular Biochemistry,* 96**,** 533-542.

Choudhery, M. S., Badowski, M., Muise, A., Pierce, J. & Harris, D. T. (2014). Donor age negatively impacts adipose tissue-derived mesenchymal stem cell expansion and differentiation. *J Transl Med,* 12**,** 8.

Choy, E., Hornicek, F., Macconaill, L., Harmon, D., Tariq, Z., Garraway, L. & Duan, Z. (2012). High-throughput genotyping in osteosarcoma identifies multiple mutations in phosphoinositide-3-kinase and other oncogenes. *Cancer,* 118**,** 2905-2914.

Činčárová, L., Zdráhal, Z. & Fajkus, J. (2013). New perspectives of valproic acid in clinical practice. *Expert Opinion on Investigational Drugs,* 22**,** 1535-1547.

Cohnheim, J. (1867). Ueber Entzündung und Eiterung. *Archiv für pathologische Anatomie und Physiologie und für klinische Medicin,* 40**,** 1-79.

Cook, D. A., Fellgett, S. W., Pownall, M. E., O'shea, P. J. & Genever, P. G. (2014). Wnt-dependent osteogenic commitment of bone marrow stromal cells using a novel GSK3β inhibitor. *Stem Cell Research,* 12**,** 415-427.

Couffinhal, T., Dufourcq, P. & Duplàa, C. (2006). β-Catenin Nuclear Activation: Common Pathway Between Wnt and Growth Factor Signaling in Vascular Smooth Muscle Cell Proliferation? *Circulation Research,* 99**,** 1287-1289.

Cox, G., Boxall, S. A., Giannoudis, P. V., Buckley, C. T., Roshdy, T., Churchman, S. M., Mcgonagle, D. & Jones, E. (2011). High abundance of CD271+ multipotential stromal cells (MSCs) in intramedullary cavities of long bones. *Bone*.

Crisan, M., Yap, S., Casteilla, L., Chen, C.-W., Corselli, M., Park, T. S., Andriolo, G., Sun, B., Zheng, B., Zhang, L., Norotte, C., Teng, P.-N., Traas, J., Schugar, R., Deasy, B. M., Badylak, S., Bűhring, H.-J., Giacobino, J.-P., Lazzari, L., Huard, J. & Péault, B. (2008). A Perivascular Origin for Mesenchymal Stem Cells in Multiple Human Organs. *Cell Stem Cell,* 3**,** 301-313.

Curl, W. W., Krome, J., Gordon, E. S., Rushing, J., Smith, B. P. & Poehling, G. G. (1997). Cartilage injuries: a review of 31,516 knee arthroscopies. *Arthroscopy,* 13**,** 456-460.

D'ippolito, G., Diabira, S., Howard, G. A., Menei, P., Roos, B. A. & Schiller, P. C. (2004). Marrow-isolated adult multilineage inducible (MIAMI) cells, a unique population of postnatal young

and old human cells with extensive expansion and differentiation potential. *J Cell Sci,* 117**,** 2971-2981.

D'ippolito, G., Diabira, S., Howard, G. A., Roos, B. A. & Schiller, P. C. (2006). Low oxygen tension inhibits osteogenic differentiation and enhances stemness of human MIAMI cells. *Bone,* 39**,** 513-522.

Daar, A. S. & Greenwood, H. L. (2007). A proposed definition of regenerative medicine. *Journal of Tissue Engineering and Regenerative Medicine,* 1**,** 179-184.

Dahlen, A., Debiec-Rychter, M., Pedeutour, F., Domanski, H. A., Hoglund, M., Bauer, H. C., Rydholm, A., Sciot, R., Mandahl, N. & Mertens, F. (2003). Clustering of deletions on chromosome 13 in benign and low-malignant lipomatous tumors. *Int J Cancer,* 103**,** 616-623.

Dang, L., White, D. W., Gross, S., Bennett, B. D., Bittinger, M. A., Driggers, E. M., Fantin, V. R., Jang, H. G., Jin, S., Keenan, M. C., Marks, K. M., Prins, R. M., Ward, P. S., Yen, K. E., Liau, L. M., Rabinowitz, J. D., Cantley, L. C., Thompson, C. B., Vander Heiden, M. G. & Su, S. M. (2009). Cancer-associated IDH1 mutations produce 2-hydroxyglutarate. *Nature,* 462**,** 739-744.

De La Fuente, R., Bernad, A., Garcia-Castro, J., Martin, M. C. & Cigudosa, J. C. (2010). Retraction: Spontaneous Human Adult Stem Cell Transformation. *Cancer Research,* 70**,** 6682-6682.

De Ruijter, A. J., Van Gennip, A. H., Caron, H. N., Kemp, S. & Van Kuilenburg, A. B. (2003). Histone deacetylases (HDACs): characterization of the classical HDAC family. *Biochem J,* 370**,** 737-749.

Dimarino, A. M., Caplan, A. I. & Bonfield, T. L. (2013). Mesenchymal stem cells in tissue repair. *Front Immunol,* 4**,** 201.

Dominici, M., Le Blanc, K., Mueller, I., Slaper-Cortenbach, I., Marini, F., Krause, D., Deans, R., Keating, A., Prockop, D. & Horwitz, E. (2006). Minimal criteria for defining multipotent mesenchymal stromal cells. The International Society for Cellular Therapy position statement. *Cytotherapy,* 8**,** 315-317.

Dulamea, A. O., Sirbu-Boeti, M.-P., Bleotu, C., Dragu, D., Moldovan, L., Lupescu, I. & Comi, G. (2015). Autologous mesenchymal stem cells applied on the pressure ulcers had produced a surprising outcome in a severe case of neuromyelitis optica. *Neural Regeneration Research,* 10**,** 1841-1845.

Enzmann, G. U., Benton, R. L., Woock, J. P., Howard, R. M., Tsoulfas, P. & Whittemore, S. R. (2005). Consequences of noggin expression by neural stem, glial, and neuronal precursor cells engrafted into the injured spinal cord. *Experimental Neurology,* 195**,** 293-304.

Erices, A., Conget, P. & Minguell, J. J. (2000). Mesenchymal progenitor cells in human umbilical cord blood. *British Journal of Haematology,* 109**,** 235-242.

European Parliament, C. O. T. E. U. (2007). Regulation (EC) No 1394/2007 of the European Parliament and of the Council of 13 November 2007 on advanced therapy medicinal products and amending Directive 2001/83/EC and Regulation (EC) No 726/2004 (Text with EEA relevance) *Official Journal of the European Union,* 50**,** 121-137.

Evans, M. J. & Kaufman, M. H. (1981). Establishment in culture of pluripotential cells from mouse embryos. *nature,* 292**,** 154-156.

Eyrich, D., Brandl, F., Appel, B., Wiese, H., Maier, G., Wenzel, M., Staudenmaier, R., Goepferich, A. & Blunk, T. (2007). Long-term stable fibrin gels for cartilage engineering. *Biomaterials,* 28**,** 55-65.

Falah, M., Nierenberg, G., Soudry, M., Hayden, M. & Volpin, G. (2010). Treatment of articular cartilage lesions of the knee. *Int Orthop,* 34**,** 621-630.

Falanga, V., Iwamoto, S., Chartier, M., Yufit, T., Butmarc, J., Kouttab, N., Shrayer, D. & Carson, P. (2007). Autologous bone marrow-derived cultured mesenchymal stem cells delivered in a fibrin spray accelerate healing in murine and human cutaneous wounds. *Tissue Eng,* 13**,** 1299-1312.

Farley, J. R., Hall, S. L., Herring, S., Tarbaux, N. M., Matsuyama, T. & Wergedal, J. E. (1991). Skeletal alkaline phosphatase specific activity is an index of the osteoblastic phenotype in subpopulations of the human osteosarcoma cell line SaOS-2. *Metabolism,* 40**,** 664-671.

Fekete, N., Gadelorge, M., Fürst, D., Maurer, C., Dausend, J., Fleury-Cappellesso, S., Mailänder, V., Lotfi, R., Ignatius, A., Sensebé, L., Bourin, P., Schrezenmeier, H. & Rojewski, M. T. (2012a). Platelet lysate from whole blood-derived pooled platelet concentrates and apheresis-derived platelet concentrates for the isolation and expansion of human bone marrow mesenchymal stromal cells: production process, content and identification of active components. *Cytotherapy,* 14**,** 540-554.

Fekete, N., Rojewski, M. T., Fürst, D., Kreja, L., Ignatius, A., Dausend, J. & Schrezenmeier, H. (2012b). GMP-Compliant Isolation and Large-Scale Expansion of Bone Marrow-Derived MSC. *PLoS ONE,* 7**,** e43255.

Fenton, S. L., Drayson, M. T., Hewison, M., Vickers, E., Brown, G. & Bunce, C. M. (1999). Clofibric acid: a potential therapeutic agent in AML and MDS. *British Journal of Haematology,* 105**,** 448-451.

Fenton, S. L., Luong, Q. T., Sarafeim, A., Mustard, K. J. W., Pound, J., Desmond, J. C., Gordon, J., Drayson, M. T. & Bunce, C. M. (2003). Fibrates and medroxyprogesterone acetate induce apoptosis of primary Burkitt's lymphoma cells and cell lines: potential for applying old drugs to a new disease. *Leukemia,* 17**,** 568-575.

Féron, F., Perry, C., Cochrane, J., Licina, P., Nowitzke, A., Urquhart, S., Geraghty, T. & Mackay-Sim, A. (2005). Autologous olfactory ensheathing cell transplantation in human spinal cord injury. *Brain,* 128**,** 2951-2960.

Fogh, J. & Trempe, G. (1975). New Human Tumor Cell Lines. *In:* FOGH, J. (ed.) *Human Tumor Cells in Vitro.* Springer US.

Fogh, J., Fogh, J. M. & Orfeo, T. (1977). One hundred and twenty-seven cultured human tumor cell lines producing tumors in nude mice. *Journal of the National Cancer Institute,* 59**,** 221-226.

Forman, B. M., Tontonoz, P., Chen, J., Brun, R. P., Spiegelman, B. M. & Evans, R. M. (1995). 15-Deoxy-delta 12, 14-prostaglandin J2 is a ligand for the adipocyte determination factor PPAR gamma. *Cell,* 83**,** 803-812.

Frantz, S. (2012). Embryonic stem cell pioneer Geron exits field, cuts losses. *Nat Biotech,* 30**,** 12-13.

Friedenstein, A. J., Petrakova, K. V., Kurolesova, A. I. & Frolova, G. P. (1968). Heterotopic of bone marrow. Analysis of precursor cells for osteogenic and hematopoietic tissues. *Transplantation,* 6**,** 230-247.

Friedenstein, A. J., Chailakhjan, R. K. & Lalykina, K. S. (1970). The development of fibroblast colonies in monolayer cultures of guinea-pig bone marrow and spleen cells. *Cell Tissue Kinet,* 3**,** 393-403.

Friedenstein, A. J., Chailakhyan, R. K., Latsinik, N. V., Panasyuk, A. F. & Keiliss-Borok, I. V. (1974a). Stromal cells responsible for transferring the microenvironment of the hemopoietic tissues. Cloning in vitro and retransplantation in vivo. *Transplantation,* 17**,** 331-340.

Friedenstein, A. J., Deriglasova, U. F., Kulagina, N. N., Panasuk, A. F., Rudakowa, S. F., Luria, E. A. & Ruadkow, I. A. (1974b). Precursors for fibroblasts in different populations of hematopoietic cells as detected by the in vitro colony assay method. *Exp Hematol,* 2**,** 83-92.

Friedenstein, A. J. (1980). Stromal mechanisms of bone marrow: cloning in vitro and retransplantation in vivo. *Haematol Blood Transfus,* 25**,** 19-29.

Friedenstein, A. J., Latzinik, N. W., Grosheva, A. G. & Gorskaya, U. F. (1982). Marrow microenvironment transfer by heterotopic transplantation of freshly isolated and cultured cells in porous sponges. *Exp Hematol,* 10**,** 217-227.

Friedenstein, A. J., Chailakhyan, R. K. & Gerasimov, U. V. (1987). Bone marrow osteogenic stem cells: in vitro cultivation and transplantation in diffusion chambers. *Cell Tissue Kinet,* 20**,** 263-272.

Gabarra-Niecko, V., Schaller, M. & Dunty, J. (2003). FAK regulates biological processes important for the pathogenesis of cancer. *Cancer and Metastasis Reviews,* 22**,** 359-374.

Garcia, S., Martín, M. C., De La Fuente, R., Cigudosa, J. C., Garcia-Castro, J. & Bernad, A. (2010). Pitfalls in spontaneous in vitro transformation of human mesenchymal stem cells. *Experimental Cell Research,* 316**,** 1648-1650.

Gaur, T., Lengner, C. J., Hovhannisyan, H., Bhat, R. A., Bodine, P. V. N., Komm, B. S., Javed, A., Van Wijnen, A. J., Stein, J. L., Stein, G. S. & Lian, J. B. (2005). Canonical WNT Signaling Promotes Osteogenesis by Directly Stimulating Runx2 Gene Expression. *Journal of Biological Chemistry,* 280**,** 33132-33140.

Gelderblom, H., Hogendoorn, P. C. W., Dijkstra, S. D., Van Rijswijk, C. S., Krol, A. D., Taminiau, A. H. M. & Bovée, J. V. M. G. (2008). The Clinical Approach Towards Chondrosarcoma. *The Oncologist,* 13**,** 320-329.

Gibbs, C. P., Kukekov, V. G., Reith, J. D., Tchigrinova, O., Suslov, O. N., Scott, E. W., Ghivizzani, S. C., Ignatova, T. N. & Steindler, D. A. (2005). Stem-like cells in bone sarcomas: implications for tumorigenesis. *Neoplasia,* 7**,** 967-976.

Gibson, A. J., Mcdonnell, S. M. & Price, A. J. (2006). Matrix-Induced Autologous Chondrocyte Implantation. *Operative Techniques in Orthopaedics,* 16**,** 262-265.

Glass, G. G. (2006). Osteoarthritis. *Disease-a-Month,* 52**,** 343-362.

Gluckman, E., Broxmeyer, H. E., Auerbach, A. D., Friedman, H. S., Douglas, G. W., Devergie, A., Esperou, H., Thierry, D., Socie, G., Lehn, P., Cooper, S., English, D., Kurtzberg, J., Bard, J. & Boyse, E. A. (1989). Hematopoietic Reconstitution in a Patient with Fanconi's Anemia by Means of Umbilical-Cord Blood from an HLA-Identical Sibling. *New England Journal of Medicine,* 321**,** 1174-1178.

Goldring, Chris e. P., Duffy, Paul a., Benvenisty, N., Andrews, Peter w., Ben-David, U., Eakins, R., French, N., Hanley, Neil a., Kelly, L., Kitteringham, Neil r., Kurth, J., Ladenheim, D., Laverty, H., Mcblane, J., Narayanan, G., Patel, S., Reinhardt, J., Rossi, A., Sharpe, M. & Park, B. K. (2011). Assessing the Safety of Stem Cell Therapeutics. *Cell Stem Cell,* 8**,** 618-628.

Gómez-Barrena, E., Rosset, P., Lozano, D., Stanovici, J., Ermthaller, C. & Gerbhard, F. (2015). Bone fracture healing: Cell therapy in delayed unions and nonunions. *Bone,* 70**,** 93-101.

Gore, A., Li, Z., Fung, H.-L., Young, J. E., Agarwal, S., Antosiewicz-Bourget, J., Canto, I., Giorgetti, A., Israel, M. A., Kiskinis, E., Lee, J.-H., Loh, Y.-H., Manos, P. D., Montserrat, N., Panopoulos, A. D., Ruiz, S., Wilbert, M. L., Yu, J., Kirkness, E. F., Belmonte, J. C. I., Rossi, D. J., Thomson, J. A., Eggan, K., Daley, G. Q., Goldstein, L. S. B. & Zhang, K. (2011). Somatic coding mutations in human induced pluripotent stem cells. *Nature,* 471**,** 63-67.

Grey, J. E., Harding, K. G. & Enoch, S. (2006). Pressure ulcers. *BMJ,* 332**,** 472-475.

Guidelines., C. F. S. C. M. C. P. (2001). Pressure ulcer prevention and treatment following spinal cord injury: a clinical practice guideline for health-care professionals. *J Spinal Cord Med,* 24 Suppl 1**,** S40-101.

Gurvich, N., Tsygankova, O. M., Meinkoth, J. L. & Klein, P. S. (2004). Histone deacetylase is a target of valproic acid-mediated cellular differentiation. *Cancer Res,* 64**,** 1079-1086.

Haleem, A. M., Singergy, A. a. E., Sabry, D., Atta, H. M., Rashed, L. A., Chu, C. R., Shewy, M. T. E., Azzam, A. & Aziz, M. T. A. (2010). The Clinical Use of Human Culture–Expanded Autologous Bone Marrow Mesenchymal Stem Cells Transplanted on Platelet-Rich Fibrin Glue in the Treatment of Articular Cartilage Defects: A Pilot Study and Preliminary Results. *Cartilage,* 1**,** 253-261.

Harding, K. G., Morris, H. L. & Patel, G. K. (2002). Healing chronic wounds. *BMJ,* 324**,** 160-163.

Hass, R., Kasper, C., Bohm, S. & Jacobs, R. (2011). Different populations and sources of human mesenchymal stem cells (MSC): A comparison of adult and neonatal tissue-derived MSC. *Cell Commun Signal,* 9**,** 12.

Hausser, H.-J. & Brenner, R. E. (2005). Phenotypic instability of Saos-2 cells in long-term culture. *Biochemical and Biophysical Research Communications,* 333**,** 216-222.

Hayashi, N., Nakamori, S., Hiraoka, N., Tsujie, M., Xundi, X., Takano, T., Amino, N., Sakon, M. & Monden, M. (2004). Antitumor effects of peroxisome proliferator activate receptor gamma ligands on anaplastic thyroid carcinoma. *Int J Oncol,* 24**,** 89-95.

Heathman, T. R. J., Nienow, A. W., Mccall, M. J., Coopman, K., Kara, B. & Hewitt, C. J. (2015a). The translation of cell-based therapies: clinical landscape and manufacturing challenges. *Regenerative Medicine,* 10**,** 49-64.

Heathman, T. R. J., Stolzing, A., Fabian, C., Rafiq, Q. A., Coopman, K., Nienow, A. W., Kara, B. & Hewitt, C. J. (2015b). Serum-free process development: improving the yield and consistency of human mesenchymal stromal cell production. *Cytotherapy,* 17**,** 1524-1535.

Heathman, T. R. J., Rafiq, Q. A., Chan, A. K. C., Coopman, K., Nienow, A. W., Kara, B. & Hewitt, C. J. (2016a). Characterization of human mesenchymal stem cells from multiple donors and the implications for large scale bioprocess development. *Biochemical Engineering Journal,* 108**,** 14-23.

Heathman, T. R. J., Stolzing, A., Fabian, C., Rafiq, Q. A., Coopman, K., Nienow, A. W., Kara, B. & Hewitt, C. J. (2016b). Scalability and process transfer of mesenchymal stromal cell production from monolayer to microcarrier culture using human platelet lysate. *Cytotherapy,* 18**,** 523-535.

Hocking, A. M. & Gibran, N. S. (2010). Mesenchymal stem cells: Paracrine signaling and differentiation during cutaneous wound repair. *Experimental Cell Research,* 316**,** 2213-2219.

Horan, P. K. & Slezak, S. E. (1989). Stable cell membrane labelling. *Nature,* 340**,** 167-168.

Horwitz, E. M., Le Blanc, K., Dominici, M., Mueller, I., Slaper-Cortenbach, I., Marini, F. C., Deans, R. J., Krause, D. S. & Keating, A. (2005). Clarification of the nomenclature for MSC: The International Society for Cellular Therapy position statement. *Cytotherapy,* 7**,** 393-395.

Hourd, P., Chandra, A., Medcalf, N. & Williams, D. J. (2008). Regulatory challenges for the manufacture and scale-out of autologous cell therapies. *StemBook.* Cambridge (MA): Harvard Stem Cell Institute

Howlett, C. R., Cave, J., Williamson, M., Farmer, J., Ali, S. Y., Bab, I. & Owen, M. E. (1986). Mineralization in in vitro cultures of rabbit marrow stromal cells. *Clin Orthop Relat Res***,** 251-263.

Huang, K. T., Chen, Y. H. & Walker, A. M. (2004). Inaccuracies in MTS assays: major distorting effects of medium, serum albumin, and fatty acids. *Biotechniques,* 37**,** 406, 408, 410-402.

Huang, Y., Dai, H. & Guo, Q.-N. (2012). TSSC3 overexpression reduces stemness and induces apoptosis of osteosarcoma tumor-initiating cells. *Apoptosis,* 17**,** 749-761.

Hussein, S. M., Batada, N. N., Vuoristo, S., Ching, R. W., Autio, R., Narva, E., Ng, S., Sourour, M., Hamalainen, R., Olsson, C., Lundin, K., Mikkola, M., Trokovic, R., Peitz, M., Brustle, O., Bazett-Jones, D. P., Alitalo, K., Lahesmaa, R., Nagy, A. & Otonkoski, T. (2011). Copy number variation and selection during reprogramming to pluripotency. *Nature,* 471**,** 58-62.

In 'T Anker, P. S., Scherjon, S. A., Kleijburg-Van Der Keur, C., De Groot-Swings, G. M., Claas, F. H., Fibbe, W. E. & Kanhai, H. H. (2004). Isolation of mesenchymal stem cells of fetal or maternal origin from human placenta. *Stem Cells,* 22**,** 1338-1345.

Jaiswal, N., Haynesworth, S. E., Caplan, A. I. & Bruder, S. P. (1997). Osteogenic differentiation of purified, culture-expanded human mesenchymal stem cells in vitro. *Journal of Cellular Biochemistry,* 64**,** 295-312.

Janicki, P., Boeuf, S., Steck, E., Egermann, M., Kasten, P. & Richter, W. (2011). Prediction of in vivo bone forming potency of bone marrow-derived human mesenchymal stem cells. *Eur Cell Mater,* 21**,** 488-507.

Javazon, E. H., Beggs, K. J. & Flake, A. W. (2004). Mesenchymal stem cells: paradoxes of passaging. *Experimental Hematology,* 32**,** 414-425.

Jaye, D. L., Bray, R. A., Gebel, H. M., Harris, W. a. C. & Waller, E. K. (2012). Translational Applications of Flow Cytometry in Clinical Practice. *The Journal of Immunology,* 188**,** 4715-4719.

Jia, S.-F., Worth, L. & Kleinerman, E. (1999). A nude mouse model of human osteosarcoma lung metastases for evaluating new therapeutic strategies. *Clinical & Experimental Metastasis,* 17**,** 501-506.

Jiang, Y., Jahagirdar, B. N., Reinhardt, R. L., Schwartz, R. E., Keene, C. D., Ortiz-Gonzalez, X. R., Reyes, M., Lenvik, T., Lund, T., Blackstad, M., Du, J., Aldrich, S., Lisberg, A., Low, W. C., Largaespada, D. A. & Verfaillie, C. M. (2002). Pluripotency of mesenchymal stem cells derived from adult marrow. *Nature,* 418**,** 41-49.

Johnstone, B., Hering, T. M., Caplan, A. I., Goldberg, V. M. & Yoo, J. U. (1998). In VitroChondrogenesis of Bone Marrow-Derived Mesenchymal Progenitor Cells. *Experimental Cell Research,* 238**,** 265-272.

Keirstead, H. S., Nistor, G., Bernal, G., Totoiu, M., Cloutier, F., Sharp, K. & Steward, O. (2005). Human embryonic stem cell-derived oligodendrocyte progenitor cell transplants remyelinate and restore locomotion after spinal cord injury. *J Neurosci,* 25**,** 4694-4705.

Khanim, F. L., Hayden, R. E., Birtwistle, J., Lodi, A., Tiziani, S., Davies, N. J., Ride, J. P., Viant, M. R., Gunther, U. L., Mountford, J. C., Schrewe, H., Green, R. M., Murray, J. A., Drayson, M. T. & Bunce, C. M. (2009). Combined Bezafibrate and Medroxyprogesterone Acetate: Potential Novel Therapy for Acute Myeloid Leukaemia. *PLoS ONE,* 4**,** e8147.

Kim, J.-S., Kim, E.-J., Kim, H.-J., Yang, J.-Y., Hwang, G.-S. & Kim, C.-W. (2011). Proteomic and metabolomic analysis of H2O2-induced premature senescent human mesenchymal stem cells. *Experimental Gerontology,* 46**,** 500-510.

Kim, S.-J. & Shettey, A. A. (2011). (ii) Stem cell research in orthopaedic and trauma surgery. *Orthopaedics and Trauma,* 25**,** 168-173.

Kim, Y.-T., Caldwell, J.-M. & Bellamkonda, R. V. (2009). Nanoparticle-mediated local delivery of methylprednisolone after spinal cord injury. *Biomaterials,* 30**,** 2582-2590.

Kohli, N., Wright, K. T., Sammons, R. L., Jeys, L., Snow, M. & Johnson, W. E. (2015). An In Vitro Comparison of the Incorporation, Growth, and Chondrogenic Potential of Human Bone Marrow versus Adipose Tissue Mesenchymal Stem Cells in Clinically Relevant Cell Scaffolds Used for Cartilage Repair. *Cartilage,* 6**,** 252-263.

Kondo, M., Shibata, T., Kumagai, T., Osawa, T., Shibata, N., Kobayashi, M., Sasaki, S., Iwata, M., Noguchi, N. & Uchida, K. (2002). 15-Deoxy-Delta(12,14)-prostaglandin J(2): the endogenous electrophile that induces neuronal apoptosis. *Proc Natl Acad Sci U S A,* 99**,** 7367-7372.

Kuroda, R., Ishida, K., Matsumoto, T., Akisue, T., Fujioka, H., Mizuno, K., Ohgushi, H., Wakitani, S. & Kurosaka, M. (2007). Treatment of a full-thickness articular cartilage defect in the femoral condyle of an athlete with autologous bone-marrow stromal cells. *Osteoarthritis Cartilage,* 15**,** 226-231.

Laval, F. (1980). Effect of uncouplers on radiosensitivity and mutagenicity in x-irradiated mammalian cells. *Proc Natl Acad Sci U S A,* 77**,** 2702-2705.

Lee, S. J., Kim, M. S., Park, J. Y., Woo, J. S. & Kim, Y. K. (2008). 15-Deoxy-Δ12,14-prostaglandin J2 induces apoptosis via JNK-mediated mitochondrial pathway in osteoblastic cells. *Toxicology,* 248**,** 121-129.

Lin, M. S., Chen, W. C., Bai, X. & Wang, Y. D. (2007). Activation of peroxisome proliferator-activated receptor gamma inhibits cell growth via apoptosis and arrest of the cell cycle in human colorectal cancer. *J Dig Dis,* 8**,** 82-88.

Lin, P. P., Wang, Y. & Lozano, G. (2011). Mesenchymal Stem Cells and the Origin of Ewing's Sarcoma. *Sarcoma,* 2011**,** 1-8.

Ling, L., Nurcombe, V. & Cool, S. M. (2009). Wnt signaling controls the fate of mesenchymal stem cells. *Gene,* 433**,** 1-7.

Lister, R., Pelizzola, M., Kida, Y. S., Hawkins, R. D., Nery, J. R., Hon, G., Antosiewicz-Bourget, J., O/'Malley, R., Castanon, R., Klugman, S., Downes, M., Yu, R., Stewart, R., Ren, B., Thomson,

J. A., Evans, R. M. & Ecker, J. R. (2011). Hotspots of aberrant epigenomic reprogramming in human induced pluripotent stem cells. *Nature,* 471**,** 68-73.

Lowe, S. W. & Lin, A. W. (2000). Apoptosis in cancer. *Carcinogenesis,* 21**,** 485-495.

Lu, D., Chen, B., Liang, Z., Deng, W., Jiang, Y., Li, S., Xu, J., Wu, Q., Zhang, Z., Xie, B. & Chen, S. (2011). Comparison of bone marrow mesenchymal stem cells with bone marrow-derived mononuclear cells for treatment of diabetic critical limb ischemia and foot ulcer: A double-blind, randomized, controlled trial. *Diabetes Research and Clinical Practice,* 92**,** 26-36.

Lu, P. & Tuszynski, M. H. (2005). Can bone marrow-derived stem cells differentiate into functional neurons? *Experimental Neurology,* 193**,** 273-278.

Luo, X., Chen, J., Song, W.-X., Tang, N., Luo, J., Deng, Z.-L., Sharff, K. A., He, G., Bi, Y., He, B.-C., Bennett, E., Huang, J., Kang, Q., Jiang, W., Su, Y., Zhu, G.-H., Yin, H., He, Y., Wang, Y., Souris, J. S., Chen, L., Zuo, G.-W., Montag, A. G., Reid, R. R., Haydon, R. C., Luu, H. H. & He, T.-C. (2008). Osteogenic BMPs promote tumor growth of human osteosarcomas that harbor differentiation defects. *Lab Invest,* 88**,** 1264-1277.

Lurati, A., Laria, A., Mazzocchi, D., Angela, R. K., Marrazza, M. & Scarpellini, M. (Article in press, 2014). Effects of Hyaluronic Acid (HA) viscosupplementation on peripheral Th cells in knee and hip osteoarthritis. *Osteoarthritis and Cartilage*.

Luyten, F. P., Tylzanowski, P. & Lories, R. J. (2009). Wnt signaling and osteoarthritis. *Bone,* 44**,** 522-527.

Machado, I., Noguera, R., Pellin, A., Lopez-Guerrero, J. A., Piqueras, M., Navarro, S. & Llombart-Bosch, A. (2009). Molecular diagnosis of Ewing sarcoma family of tumors: a comparative analysis of 560 cases with FISH and RT-PCR. *Diagn Mol Pathol,* 18**,** 189-199.

Mackay-Sim, A., Féron, F., Cochrane, J., Bassingthwaighte, L., Bayliss, C., Davies, W., Fronek, P., Gray, C., Kerr, G., Licina, P., Nowitzke, A., Perry, C., Silburn, P. a. S., Urquhart, S. & Geraghty, T. (2008). Autologous olfactory ensheathing cell transplantation in human paraplegia: a 3-year clinical trial. *Brain,* 131**,** 2376-2386.

Mackay, A. M., Beck, S. C., Murphy, J. M., Barry, F. P., Chichester, C. O. & Pittenger, M. F. (1998). Chondrogenic differentiation of cultured human mesenchymal stem cells from marrow. *Tissue Eng,* 4**,** 415-428.

Marlovits, S., Zeller, P., Singer, P., Resinger, C. & Vécsei, V. (2006). Cartilage repair: Generations of autologous chondrocyte transplantation. *European Journal of Radiology,* 57**,** 24-31.

Martin, G. R. (1981). Isolation of a pluripotent cell line from early mouse embryos cultured in medium conditioned by teratocarcinoma stem cells. *Proc Natl Acad Sci U S A,* 78**,** 7634-7638.

Martinez, C., Hofmann, T. J., Marino, R., Dominici, M. & Horwitz, E. M. (2007). Human bone marrow mesenchymal stromal cells express the neural ganglioside GD2: a novel surface marker for the identification of MSCs. *Blood,* 109**,** 4245-4248.

Matsuoka, F., Takeuchi, I., Agata, H., Kagami, H., Shiono, H., Kiyota, Y., Honda, H. & Kato, R. (2013). Morphology-Based Prediction of Osteogenic Differentiation Potential of Human Mesenchymal Stem Cells. *PLoS ONE,* 8**,** e55082.

Mayshar, Y., Ben-David, U., Lavon, N., Biancotti, J.-C., Yakir, B., Clark, A. T., Plath, K., Lowry, W. E. & Benvenisty, N. (2010). Identification and Classification of Chromosomal Aberrations in Human Induced Pluripotent Stem Cells. *Cell Stem Cell,* 7**,** 521-531.

Megas, P. (2005). Classification of non-union. *Injury,* 36**,** S30-S37.

Mendez-Ferrer, S., Michurina, T. V., Ferraro, F., Mazloom, A. R., Macarthur, B. D., Lira, S. A., Scadden, D. T., Ma/'Ayan, A., Enikolopov, G. N. & Frenette, P. S. (2010). Mesenchymal and haematopoietic stem cells form a unique bone marrow niche. *Nature,* 466**,** 829-834.

Metcalfe, A. D. & Ferguson, M. W. J. (2007). Tissue engineering of replacement skin: the crossroads of biomaterials, wound healing, embryonic development, stem cells and regeneration. *Journal of The Royal Society Interface,* 4**,** 413-437.

Miao, Z., Jin, J., Chen, L., Zhu, J., Huang, W., Zhao, J., Qian, H. & Zhang, X. (2006). Isolation of mesenchymal stem cells from human placenta: Comparison with human bone marrow mesenchymal stem cells. *Cell Biology International,* 30**,** 681-687.

Mitsiades, N., Poulaki, V., Mitsiades, C. & Tsokos, M. (2001). Ewing's Sarcoma Family Tumors Are Sensitive to Tumor Necrosis Factor-related Apoptosis-inducing Ligand and Express Death Receptor 4 and Death Receptor 5. *Cancer Research,* 61**,** 2704-2712.

Mohseny, A. B., Szuhai, K., Romeo, S., Buddingh, E. P., Briaire-De Bruijn, I., De Jong, D., Van Pel, M., Cleton-Jansen, A.-M. & Hogendoorn, P. C. W. (2009). Osteosarcoma originates from mesenchymal stem cells in consequence of aneuploidization and genomic loss of Cdkn2. *The Journal of Pathology,* 219**,** 294-305.

Molyneux, E., Merrick, B., Khanim, F. L., Banda, K., Dunn, J. A., Iqbal, G., Bunce, C. M. & Drayson, M. T. (2014). Bezafibrate and medroxyprogesterone acetate in resistant and relapsed endemic Burkitt lymphoma in Malawi; an open-label, single-arm, phase 2 study (ISRCTN34303497). *British Journal of Haematology,* 164**,** 888-890.

Monderer, D., Luseau, A., Bellec, A., David, E., Ponsolle, S., Saiagh, S., Bercegeay, S., Piloquet, P., Denis, M. G., Lode, L., Redini, F., Biger, M., Heymann, D., Heymann, M.-F., Le Bot, R., Gouin, F. & Blanchard, F. (2013). New chondrosarcoma cell lines and mouse models to study the link between chondrogenesis and chemoresistance. *Lab Invest,* 93**,** 1100-1114.

Morosetti, R., Servidei, T., Mirabella, M., Rutella, S., Mangiola, A., Maira, G., Mastrangelo, R. & Koeffler, H. P. (2004). The PPARgamma ligands PGJ2 and rosiglitazone show a differential ability to inhibit proliferation and to induce apoptosis and differentiation of human glioblastoma cell lines. *Int J Oncol,* 25**,** 493-502.

Muff, R., Nigg, N., Gruber, P., Walters, D., Born, W. & Fuchs, B. (2007). Altered Morphology, Nuclear Stability and Adhesion of Highly Metastatic Derivatives of Osteoblast-like SAOS-2 Osteosarcoma Cells. *Anticancer Research,* 27**,** 3973-3979.

Murphy, M. B., Moncivais, K. & Caplan, A. I. (2013). Mesenchymal stem cells: environmentally responsive therapeutics for regenerative medicine. *Exp Mol Med,* 45**,** e54.

Murray, J. A., Khanim, F. L., Hayden, R. E., Craddock, C. F., Holyoake, T. L., Jackson, N., Lumley, M., Bunce, C. M. & Drayson, M. T. (2010). Combined bezafibrate and medroxyprogesterone acetate have efficacy without haematological toxicity in elderly and relapsed acute myeloid leukaemia (AML). *Br J Haematol,* 149**,** 65-69.

Mutsaers, A. J. & Walkley, C. R. (2014). Cells of origin in osteosarcoma: Mesenchymal stem cells or osteoblast committed cells? *Bone,* 62**,** 56-63.

Nakata, S., Yoshida, T., Shiraishi, T., Horinaka, M., Kouhara, J., Wakada, M. & Sakai, T. (2006). 15-Deoxy-Δ12,14-prostaglandin J2 induces death receptor 5 expression through mRNA stabilization independently of PPARγ and potentiates TRAIL-induced apoptosis. *Molecular Cancer Therapeutics,* 5**,** 1827-1835.

Ng, T. L., Gown, A. M., Barry, T. S., Cheang, M. C. U., Chan, A. K. W., Turbin, D. A., Hsu, F. D., West, R. B. & Nielsen, T. O. (2004). Nuclear beta-catenin in mesenchymal tumors. *Mod Pathol,* 18**,** 68-74.

Niehage, C., Steenblock, C., Pursche, T., Bornhäuser, M., Corbeil, D. & Hoflack, B. (2011). The Cell Surface Proteome of Human Mesenchymal Stromal Cells. *PLoS ONE,* 6**,** e20399.

Nikitakis, N. G., Siavash, H., Hebert, C., Reynolds, M. A., Hamburger, A. W. & Sauk, J. J. (2002). 15-PGJ2, but not thiazolidinediones, inhibits cell growth, induces apoptosis, and causes downregulation of Stat3 in human oral SCCa cells. *Br J Cancer,* 87**,** 1396-1403.

Nishida, K., Furumatsu, T., Takada, I., Kawai, A., Yoshida, A., Kunisada, T. & Inoue, H. (2002). Inhibition of human chondrosarcoma cell growth via apoptosis by peroxisome proliferator-activated receptor-γ. *British Journal of Cancer,* 86**,** 1303-1309.

Noble, L. J., Donovan, F., Igarashi, T., Goussev, S. & Werb, Z. (2002). Matrix metalloproteinases limit functional recovery after spinal cord injury by modulation of early vascular events. *The Journal of neuroscience,* 22**,** 7526-7535.

Noth, U., Steinert, A. F. & Tuan, R. S. (2008). Technology Insight: adult mesenchymal stem cells for osteoarthritis therapy. *Nat Clin Pract Rheum,* 4**,** 371-380.

Orozco, L., Soler, R., Morera, C., Alberca, M., Sanchez, A. & Garcia-Sancho, J. (2011). Intervertebral disc repair by autologous mesenchymal bone marrow cells: a pilot study. *Transplantation,* 92**,** 822-828.

Orozco, L., Munar, A., Soler, R., Alberca, M., Soler, F., Huguet, M., Sentis, J., Sanchez, A. & Garcia-Sancho, J. (2013). Treatment of knee osteoarthritis with autologous mesenchymal stem cells: a pilot study. *Transplantation,* 95**,** 1535-1541.

Orozco, L., Munar, A., Soler, R., Alberca, M., Soler, F., Huguet, M., Sentis, J., Sanchez, A. & Garcia-Sancho, J. (2014). Treatment of knee osteoarthritis with autologous mesenchymal stem cells: two-year follow-up results. *Transplantation,* 97**,** e66-68.

Owen, M. & Friedenstein, A. J. (1988). Stromal stem cells: marrow-derived osteogenic precursors. *Ciba Found Symp,* 136**,** 42-60.

Owen, M. E., Cave, J. & Joyner, C. J. (1987). Clonal analysis in vitro of osteogenic differentiation of marrow CFU-F. *J Cell Sci,* 87 (Pt 5)**,** 731-738.

Park, J. H., Kim, D. Y., Sung, I. Y., Choi, G. H., Jeon, M. H., Kim, K. K. & Jeon, S. R. (2012). Long-term results of spinal cord injury therapy using mesenchymal stem cells derived from bone marrow in humans. *Neurosurgery,* 70**,** 1238-1247; discussion 1247.

Pautke, C., Schieker, M., Tischer, T., Kolk, A., Neth, P., Mutschler, W. & Milz, S. (2004). Characterization of Osteosarcoma Cell Lines MG-63, Saos-2 and U-2 OS in Comparison to Human Osteoblasts. *Anticancer Research,* 24**,** 3743-3748.

Pera, M. F. (2011). Stem cells: The dark side of induced pluripotency. *Nature,* 471**,** 46-47.

Peroni, D., Scambi, I., Pasini, A., Lisi, V., Bifari, F., Krampera, M., Rigotti, G., Sbarbati, A. & Galiè, M. (2008). Stem molecular signature of adipose-derived stromal cells. *Experimental Cell Research,* 314**,** 603-615.

Perry, B. C., Zhou, D., Wu, X., Yang, F. C., Byers, M. A., Chu, T. M., Hockema, J. J., Woods, E. J. & Goebel, W. S. (2008). Collection, cryopreservation, and characterization of human dental pulp-derived mesenchymal stem cells for banking and clinical use. *Tissue Eng Part C Methods,* 14**,** 149-156.

Pevsner-Fischer, M., Levin, S. & Zipori, D. (2011). The Origins of Mesenchymal Stromal Cell Heterogeneity. *Stem Cell Reviews and Reports,* 7**,** 560-568.

Phinney, D. G., Kopen, G., Righter, W., Webster, S., Tremain, N. & Prockop, D. J. (1999). Donor variation in the growth properties and osteogenic potential of human marrow stromal cells. *J Cell Biochem,* 75**,** 424-436.

Phinney, D. G. & Prockop, D. J. (2007). Concise Review: Mesenchymal Stem/Multipotent Stromal Cells: The State of Transdifferentiation and Modes of Tissue Repair—Current Views. *STEM CELLS,* 25**,** 2896-2902.

Phinney, D. G., Galipeau, J., Krampera, M., Martin, I., Shi, Y. & Sensebe, L. (2013). MSCs: science and trials. *Nat Med,* 19**,** 812-812.

Pierantozzi, E., Gava, B., Manini, I., Roviello, F., Marotta, G., Chiavarelli, M. & Sorrentino, V. (2011). Pluripotency Regulators in Human Mesenchymal Stem Cells: Expression of NANOG But Not of OCT-4 and SOX-2. *Stem Cells and Development* 20**,** 915-923.

Pittenger, M. F. (1999). Multilineage Potential of Adult Human Mesenchymal Stem Cells. *Science,* 284**,** 143-147.

Polak, D. J. M. (2009). Regenerative medicine: A primer for paediatricians. *Early Human Development,* 85**,** 685-689.

Popovich, P., Guan, Z., Mcgaughy, V., Fisher, L., Hickey, W. & Basso, D. (2002). The neuropathological and behavioral consequences of intraspinal microglial/macrophage activation. *Journal of Neuropathology & Experimental Neurology,* 61**,** 623-633.

Prasad, V. K., Lucas, K. G., Kleiner, G. I., Talano, J. a. M., Jacobsohn, D., Broadwater, G., Monroy, R. & Kurtzberg, J. (2011). Efficacy and Safety of Ex Vivo Cultured Adult Human Mesenchymal

Stem Cells (Prochymal™) in Pediatric Patients with Severe Refractory Acute Graft-Versus-Host Disease in a Compassionate Use Study. *Biology of Blood and Marrow Transplantation,* 17**,** 534-541.

Prockop, D. J. (1997). Marrow Stromal Cells as Stem Cells for Nonhematopoietic Tissues. *Science,* 276**,** 71-74.

Prockop, D. J. & Keating, A. (2012). Relearning the Lessons of Genomic Stability of Human Cells During Expansion in Culture: Implications for Clinical Research. *STEM CELLS,* 30**,** 1051-1052.

Ra, J. C., Shin, I. S., Kim, S. H., Kang, S. K., Kang, B. C., Lee, H. Y., Kim, Y. J., Jo, J. Y., Yoon, E. J., Choi, H. J. & Kwon, E. (2011). Safety of intravenous infusion of human adipose tissue-derived mesenchymal stem cells in animals and humans. *Stem Cells Dev,* 20**,** 1297-1308.

Ramer, M., Harper, G. & Bradbury, E. (2000). Progress in spinal cord research-a refined strategy for the International Spinal Research Trust. *Spinal cord,* 38**,** 449-472.

Ramírez-Zacarías, J. L., Castro-Muñozledo, F. & Kuri-Harcuch, W. (1992). Quantitation of adipose conversion and triglycerides by staining intracytoplasmic lipids with oil red O. *Histochemistry,* 97**,** 493-497.

Rasini, V., Dominici, M., Kluba, T., Siegel, G., Lusenti, G., Northoff, H., Horwitz, E. M. & Schäfer, R. (2013). Mesenchymal stromal/stem cells markers in the human bone marrow. *Cytotherapy,* 15**,** 292-306.

Rastegar, F., Shenaq, D., Huang, J., Zhang, W., Zhang, B. Q., He, B. C., Chen, L., Zuo, G. W., Luo, Q., Shi, Q., Wagner, E. R., Huang, E., Gao, Y., Gao, J. L., Kim, S. H., Zhou, J. Z., Bi, Y., Su, Y., Zhu, G., Luo, J., Luo, X., Qin, J., Reid, R. R., Luu, H. H., Haydon, R. C., Deng, Z. L. & He, T. C. (2010). Mesenchymal stem cells: Molecular characteristics and clinical applications. *World J Stem Cells,* 2**,** 67-80.

Ray, D. M., Akbiyik, F. & Phipps, R. P. (2006). The Peroxisome Proliferator-Activated Receptor γ (PPARγ) Ligands 15-Deoxy-Δ12,14-Prostaglandin J2 and Ciglitazone Induce Human B Lymphocyte and B Cell Lymphoma Apoptosis by PPARγ-Independent Mechanisms. *The Journal of Immunology,* 177**,** 5068-5076.

Reddy, M., Gill, S. S. & Rochon, P. A. (2006). Preventing pressure ulcers: a systematic review. *Jama,* 296**,** 974-984.

Riggi, N., Suvà, M.-L., Suvà, D., Cironi, L., Provero, P., Tercier, S., Joseph, J.-M., Stehle, J.-C., Baumer, K., Kindler, V. & Stamenkovic, I. (2008). EWS-FLI-1 expression triggers a Ewing's sarcoma initiation program in primary human mesenchymal stem cells. *Cancer research,* 68**,** 2176-2185.

Roberts, S., Mccall, I. W., Darby, A. J., Menage, J., Evans, H., Harrison, P. E. & Richardson, J. B. (2003). Autologous chondrocyte implantation for cartilage repair: monitoring its success by magnetic resonance imaging and histology. *Arthritis Res Ther,* 5**,** R60-73.

Rodan, S. B., Imai, Y., Thiede, M. A., Wesolowski, G., Thompson, D., Bar-Shavit, Z., Shull, S., Mann, K. & Rodan, G. A. (1987). Characterization of a Human Osteosarcoma Cell Line (Saos-2) with Osteoblastic Properties. *Cancer Research,* 47**,** 4961-4966.

Rosenthal, N. (2003). Prometheus's Vulture and the Stem-Cell Promise. *New England Journal of Medicine,* 349**,** 267-274.

Rosland, G. V., Svendsen, A., Torsvik, A., Sobala, E., Mccormack, E., Immervoll, H., Mysliwietz, J., Tonn, J. C., Goldbrunner, R., Lonning, P. E., Bjerkvig, R. & Schichor, C. (2009). Long-term Cultures of Bone Marrow-Derived Human Mesenchymal Stem Cells Frequently Undergo Spontaneous Malignant Transformation. *Cancer Research,* 69**,** 5331-5339.

Roughley, P. J. & Mort, J. S. (2014). The role of aggrecan in normal and osteoarthritic cartilage. *Journal of Experimental Orthopaedics,* 1**,** 8.

Rubio, D., Garcia-Castro, J., Martín, M. C., Fuente, R. D. L., Cigudosa, J. C. & Lloyd, A. C. (2005). Spontaneous human adult stem cell transformation. *Cancer research,* 65**,** 3035-3039.

Rubio, D., Garcia, S., De La Cueva, T., Paz, M. F., Lloyd, A. C., Bernad, A. & Garcia-Castro, J. (2008a). Human mesenchymal stem cell transformation is associated with a mesenchymal–epithelial transition. *Experimental Cell Research,* 314**,** 691-698.

Rubio, D., Garcia, S., Paz, M. F., De La Cueva, T., Lopez-Fernandez, L. A., Lloyd, A. C., Garcia-Castro, J. & Bernad, A. (2008b). Molecular characterization of spontaneous mesenchymal stem cell transformation. *PLoS One,* 3**,** e1398.

Rumi, M. A., Sato, H., Ishihara, S., Kawashima, K., Hamamoto, S., Kazumori, H., Okuyama, T., Fukuda, R., Nagasue, N. & Kinoshita, Y. (2001). Peroxisome proliferator-activated receptor gamma ligand-induced growth inhibition of human hepatocellular carcinoma. *Br J Cancer,* 84**,** 1640-1647.

Saberi, H., Moshayedi, P., Aghayan, H.-R., Arjmand, B., Hosseini, S.-K., Emami-Razavi, S.-H., Rahimi-Movaghar, V., Raza, M. & Firouzi, M. (2008). Treatment of chronic thoracic spinal cord injury patients with autologous Schwann cell transplantation: An interim report on safety considerations and possible outcomes. *Neuroscience Letters,* 443**,** 46-50.

Sarasua, J. G., Lopez, S. P., Viejo, M. A., Basterrechea, M. P., Rodriguez, A. F., Gutierrez, A. F., Gala, J. G., Menendez, Y. M., Augusto, D. E., Arias, A. P. & Hernandez, J. O. (2011). Treatment of pressure ulcers with autologous bone marrow nuclear cells in patients with spinal cord injury. *J Spinal Cord Med,* 34**,** 301-307.

Sasaki, M., Abe, R., Fujita, Y., Ando, S., Inokuma, D. & Shimizu, H. (2008). Mesenchymal Stem Cells Are Recruited into Wounded Skin and Contribute to Wound Repair by Transdifferentiation into Multiple Skin Cell Type. *The Journal of Immunology,* 180**,** 2581-2587.

Scharstuhl, A., Schewe, B., Benz, K., Gaissmaier, C., Bühring, H.-J. & Stoop, R. (2007). Chondrogenic Potential of Human Adult Mesenchymal Stem Cells Is Independent of Age or Osteoarthritis Etiology. *Stem Cells,* 25**,** 3244-3251.

Schindeler, A., Mcdonald, M. M., Bokko, P. & Little, D. G. (2008). Bone remodeling during fracture repair: The cellular picture. *Seminars in Cell & Developmental Biology,* 19**,** 459-466.

Schmitz, N., Laverty, S., Kraus, V. B. & Aigner, T. (2010). Basic methods in histopathology of joint tissues. *Osteoarthritis and Cartilage,* 18, Supplement 3**,** S113-S116.

Schulze-Tanzil, G. (2009). Activation and dedifferentiation of chondrocytes: implications in cartilage injury and repair. *Ann Anat,* 191**,** 325-338.

Seita, J. & Weissman, I. L. (2010). Hematopoietic stem cell: self-renewal versus differentiation. *Wiley Interdiscip Rev Syst Biol Med,* 2**,** 640-653.

Sensebé, L., Tarte, K., Galipeau, J., Krampera, M., Martin, I., Phinney, Donald g. & Shi, Y. (2012). Limited Acquisition of Chromosomal Aberrations in Human Adult Mesenchymal Stromal Cells. *Cell Stem Cell,* 10**,** 9-10.

Shen, Z.-N., Nishida, K., Doi, H., Oohashi, T., Hirohata, S., Ozaki, T., Yoshida, A., Ninomiya, Y. & Inoue, H. (2005). Suppression of chondrosarcoma cells by 15-deoxy-Δ12,14-prostaglandin J2 is associated with altered expression of Bax/Bcl-xL and p21. *Biochemical and Biophysical Research Communications,* 328**,** 375-382.

Si, Y.-L., Zhao, Y.-L., Hao, H.-J., Fu, X.-B. & Han, W.-D. (2011). MSCs: Biological characteristics, clinical applications and their outstanding concerns. *Ageing Research Reviews,* 10**,** 93-103.

Siclari, V. & Qin, L. (2010). Targeting the osteosarcoma cancer stem cell. *Journal of Orthopaedic Surgery and Research,* 5**,** 78.

Siddappa, R., Licht, R., Van Blitterswijk, C. & De Boer, J. (2007). Donor variation and loss of multipotency during in vitro expansion of human mesenchymal stem cells for bone tissue engineering. *Journal of Orthopaedic Research,* 25**,** 1029-1041.

Smith, D. (2014). *Process monitoring and control using live cell imaging for the manufacturing of cell therapies.* Ph.D., Loughborough University.

Soler, R., Orozco, L., Munar, A., Huguet, M., López, R., Vives, J., Coll, R., Codinach, M. & Garcia-Lopez, J. (2016). Final results of a phase I–II trial using ex vivo expanded autologous

Mesenchymal Stromal Cells for the treatment of osteoarthritis of the knee confirming safety and suggesting cartilage regeneration. *The Knee*.

Southam, A. D., Khanim, F. L., Hayden, R. E., Constantinou, J. K., Koczula, K. M., Michell, R. H., Viant, M. R., Drayson, M. T. & Bunce, C. M. (2015). Drug Redeployment to Kill Leukemia and Lymphoma Cells by Disrupting SCD1-Mediated Synthesis of Monounsaturated Fatty Acids. *Cancer Research,* 75**,** 2530-2540.

Sridharan, G. & Shankar, A. A. (2012). Toluidine blue: A review of its chemistry and clinical utility. *J Oral Maxillofac Pathol,* 16**,** 251-255.

Sun, D., Yuan, D. & Zhang, X. (2011). A new hypothesis on the mechanism of atrophic non-union. *Medical Hypotheses,* 77**,** 69-70.

Suva, M. L., Riggi, N., Stehle, J. C., Baumer, K., Tercier, S., Joseph, J. M., Suva, D., Clement, V., Provero, P., Cironi, L., Osterheld, M. C., Guillou, L. & Stamenkovic, I. (2009). Identification of Cancer Stem Cells in Ewing's Sarcoma. *Cancer Research,* 69**,** 1776-1781.

Takada, I., Yogiashi, Y. & Kato, S. (2012). Signaling Crosstalk between PPARγ and BMP2 in Mesenchymal Stem Cells. *PPAR Research,* 2012**,** 7.

Takahashi, K. & Yamanaka, S. (2006). Induction of Pluripotent Stem Cells from Mouse Embryonic and Adult Fibroblast Cultures by Defined Factors. *Cell,* 126**,** 663-676.

Takahashi, K., Tanabe, K., Ohnuki, M., Narita, M., Ichisaka, T., Tomoda, K. & Yamanaka, S. (2007). Induction of Pluripotent Stem Cells from Adult Human Fibroblasts by Defined Factors. *Cell,* 131**,** 861-872.

Thomas, D. M., Carty, S. A., Piscopo, D. M., Lee, J.-S., Wang, W.-F., Forrester, W. C. & Hinds, P. W. (2001). The Retinoblastoma Protein Acts as a Transcriptional Coactivator Required for Osteogenic Differentiation. *Molecular Cell,* 8**,** 303-316.

Tilghman, R. W. & Parsons, J. T. (2008). Focal adhesion kinase as a regulator of cell tension in the progression of cancer. *Seminars in Cancer Biology,* 18**,** 45-52.

Tirino, V., Desiderio, V., D'aquino, R., De Francesco, F., Pirozzi, G., Galderisi, U., Cavaliere, C., De Rosa, A. & Papaccio, G. (2008). Detection and Characterization of $CD133^+$ Cancer Stem Cells in Human Solid Tumours. *PLoS ONE,* 3**,** e3469.

Toimela, T., Tahti, H. & Ylikomi, T. (2008). Comparison of an automated pattern analysis machine vision time-lapse system with traditional endpoint measurements in the analysis of cell growth and cytotoxicity. *Altern Lab Anim,* 36**,** 313-325.

Toma, C., Pittenger, M. F., Cahill, K. S., Byrne, B. J. & Kessler, P. D. (2002). Human Mesenchymal Stem Cells Differentiate to a Cardiomyocyte Phenotype in the Adult Murine Heart. *Circulation,* 105**,** 93-98.

Torsvik, A., Røsland, G. V., Svendsen, A., Molven, A., Immervoll, H., Mccormack, E., Lønning, P. E., Primon, M., Sobala, E., Tonn, J.-C., Goldbrunner, R., Schichor, C., Mysliwietz, J., Lah, T. T. & Motaln, H. (2010). Spontaneous Malignant Transformation of Human Mesenchymal Stem Cells Reflects Cross-Contamination: Putting the Research Field on Track – Letter. *Cancer Research,* 70**,** 6393-6396.

Toussaint, O., Medrano, E. E. & Von Zglinicki, T. (2000). Cellular and molecular mechanisms of stress-induced premature senescence (SIPS) of human diploid fibroblasts and melanocytes. *Experimental Gerontology,* 35**,** 927-945.

Trattnig, S., Ba-Ssalamah, A., Pinker, K., Plank, C., Vecsei, V. & Marlovits, S. (2005). Matrix-based autologous chondrocyte implantation for cartilage repair: noninvasive monitoring by high-resolution magnetic resonance imaging. *Magnetic Resonance Imaging,* 23**,** 779-787.

Trivedi, A., Olivas, A. D. & Noble-Haeusslein, L. J. (2006). Inflammation and spinal cord injury: Infiltrating leukocytes as determinants of injury and repair processes. *Clinical Neuroscience Research,* 6**,** 283-292.

Tzioupis, C. & Giannoudis, P. V. (2007). Prevalence of long-bone non-unions. *Injury,* 38, Supplement 2**,** S3-S9.

Van Oosterwijk, J. G., De Jong, D., Van Ruler, M. A., Hogendoorn, P. C., Dijkstra, P. D., Van Rijswijk, C. S., Machado, I., Llombart-Bosch, A., Szuhai, K. & Bovee, J. V. (2012). Three new chondrosarcoma cell lines: one grade III conventional central chondrosarcoma and two dedifferentiated chondrosarcomas of bone. *BMC cancer,* 12**,** 375.

Waites, K. B. & Talkington, D. F. (2004). Mycoplasma pneumoniae and Its Role as a Human Pathogen. *Clinical Microbiology Reviews,* 17**,** 697-728.

Wakitani, S., Saito, T. & Caplan, A. I. (1995). Myogenic cells derived from rat bone marrow mesenchymal stem cells exposed to 5-azacytidine. *Muscle Nerve,* 18**,** 1417-1426.

Wakitani, S., Nawata, M., Tensho, K., Okabe, T., Machida, H. & Ohgushi, H. (2007). Repair of articular cartilage defects in the patello-femoral joint with autologous bone marrow mesenchymal cell transplantation: three case reports involving nine defects in five knees. *Journal of Tissue Engineering and Regenerative Medicine,* 1**,** 74-79.

Walter, M. N. M., Wright, K. T., Fuller, H. R., Macneil, S. & Johnson, W. E. B. (2010). Mesenchymal stem cell-conditioned medium accelerates skin wound healing: An in vitro study of fibroblast and keratinocyte scratch assays. *Experimental Cell Research,* 316**,** 1271-1281.

Wang, H.-S., Hung, S.-C., Peng, S.-T., Huang, C.-C., Wei, H.-M., Guo, Y.-J., Fu, Y.-S., Lai, M.-C. & Chen, C.-C. (2004). Mesenchymal Stem Cells in the Wharton's Jelly of the Human Umbilical Cord. *STEM CELLS,* 22**,** 1330-1337.

Weinreb, M., Shinar, D. & Rodan, G. A. (1990). Different pattern of alkaline phosphatase, osteopontin, and osteocalcin expression in developing rat bone visualized by in situ hybridization. *Journal of Bone and Mineral Research,* 5**,** 831-842.

Whitfield, M. J., Lee, W. C. J. & Van Vliet, K. J. (2013). Onset of heterogeneity in culture-expanded bone marrow stromal cells. *Stem Cell Research,* 11**,** 1365-1377.

Willerth, S. M. & Sakiyama-Elbert, S. E. (2008). Cell therapy for spinal cord regeneration. *Advanced Drug Delivery Reviews,* 60**,** 263-276.

Wittenburg, L. A., Bisson, L., Rose, B. J., Korch, C. & Thamm, D. H. (2011). The histone deacetylase inhibitor valproic acid sensitizes human and canine osteosarcoma to doxorubicin. *Cancer Chemother Pharmacol,* 67**,** 83-92.

Wozniak, M. A., Modzelewska, K., Kwong, L. & Keely, P. J. (2004). Focal adhesion regulation of cell behavior. *Biochimica et Biophysica Acta (BBA) - Molecular Cell Research,* 1692**,** 103-119.

Wright, K. A., Nadire, K. B., Busto, P., Tubo, R., Mcpherson, J. M. & Wentworth, B. M. (1998). Alternative delivery of keratinocytes using a polyurethane membrane and the implications for its use in the treatment of full-thickness burn injury. *Burns,* 24**,** 7-17.

Wright, K. T., Griffiths, G. J. & Johnson, W. E. B. (2010). A Comparison of High-Content Screening versus Manual Analysis to Assay the Effects of Mesenchymal Stem Cell-Conditioned Medium on Neurite Outgrowth In Vitro. *Journal of Biomolecular Screening,* 15**,** 576-582.

Wright, K. T., Masri, W. E., Osman, A., Chowdhury, J. & Johnson, W. E. B. (2011). Concise Review: Bone Marrow for the Treatment of Spinal Cord Injury: Mechanisms and Clinical Applications. *Stem Cells,* 29**,** 169-178.

Yamaguchi, T., Toguchida, J., Wadayama, B., Kanoe, H., Nakayama, T., Ishizaki, K., Ikenaga, M., Kotoura, Y. & Sasaki, M. S. (1996). Loss of heterozygosity and tumor suppressor gene mutations in chondrosarcomas. *Anticancer Res,* 16**,** 2009-2015.

Yen, C. C., Hsiao, C. D., Chen, W. M., Wen, Y. S., Lin, Y. C., Chang, T. W., Yao, F. Y., Hung, S. C., Wang, J. Y., Chiu, J. H., Wang, H. W., Lin, C. H., Chen, T. H., Chen, P. C., Liu, C. L., Tzeng, C. H. & Fletcher, J. A. (2014). Cytotoxic effects of 15d-PGJ2 against osteosarcoma through ROS-mediated AKT and cell cycle inhibition. *Oncotarget,* 5**,** 716-725.

Zanella, F., Lorens, J. B. & Link, W. (2010). High content screening: seeing is believing. *Trends in Biotechnology,* 28**,** 237-245.

Zanini, C., Bruno, S., Mandili, G., Baci, D., Cerutti, F., Cenacchi, G., Izzi, L., Camussi, G. & Forni, M. (2011). Differentiation of Mesenchymal Stem Cells Derived from Pancreatic Islets and Bone Marrow into Islet-Like Cell Phenotype. *PLoS ONE,* 6**,** e28175.

Zhao, S., Lin, Y., Xu, W., Jiang, W., Zha, Z., Wang, P., Yu, W., Li, Z., Gong, L., Peng, Y., Ding, J., Lei, Q., Guan, K.-L. & Xiong, Y. (2009). Glioma-Derived Mutations in IDH1 Dominantly Inhibit IDH1 Catalytic Activity and Induce HIF-1α. *Science,* 324**,** 261-265.

Zhao, W., Phinney, D. G., Bonnet, D., Dominici, M. & Krampera, M. (2014). Mesenchymal stem cell biodistribution, migration, and homing in vivo. *Stem Cells Int,* 2014**,** 292109.

Ziegler, U. & Groscurth, P. (2004). *Morphological Features of Cell Death*.

Appendix

7.1 Chapter 3: Supplementary figures and data

7.1.1 HCS imaging protocol development, image analysis and data presentation

MSC, SAOS2 and MG63 cells were seeded in monoculture within 96 well multiwell plates (detailed in section 2.1.8), allowed to adhere and cultured for 24hrs, formalin fixed (section 2.3), then ICC stained for biomarkers of interest (section 2.11). Following this, HCS analysis was performed (section 2.12). The following figures detail the protocol development stages.

Figure 7.1 shows a typical plate layout for ICC staining for biomarkers of interest on SAOS2 cells. Control wells were imaged where the 1^0Ab was excluded (designated -1^0Ab control cells). Following image collection of fluorescent immunoreactive cells, the appropriate plate, wells and cells were inspected (Figure 7.2) for image pre-processing (Figure 7.3) and analysis protocol development (Figure 7.4 through Figure 7.8).

Images were initially processed where background was removed (Figure 7.3). Figure 7.4 shows a typical screenshot of Hoechst 33342 (Ch1) and Ki67 antigen immunoreactive GFP (Ch2) labelled SAOS2 cells. Primary objects are initially identified based on Hoechst 33342 staining and then excluded if the location of the nucleus is touching the boarder of the cells or the area of the cell is smaller or greater than set thresholds (Figure 7.5). Following primary object selection, a circ or ring ROI was applied to Ch2 and Ch3 images where the fluorescent intensity for these channels can be measured within this nuclear (circ) or cytoplasmic (ring) ROI respectively. Pixels with a fluorescent intensity which was higher than a threshold value within the circ (circ spots) or ring (ring spots) were identified (Figure 7.6) and then counted as positive relative to the total number of cells identified within the ROI. Figure 7.7 and Figure 7.8 show the identification and selection of immunoreactive circ spots and ring spots within Ki67 antigen and B-catenin immunoreactive SAOS2 cells.

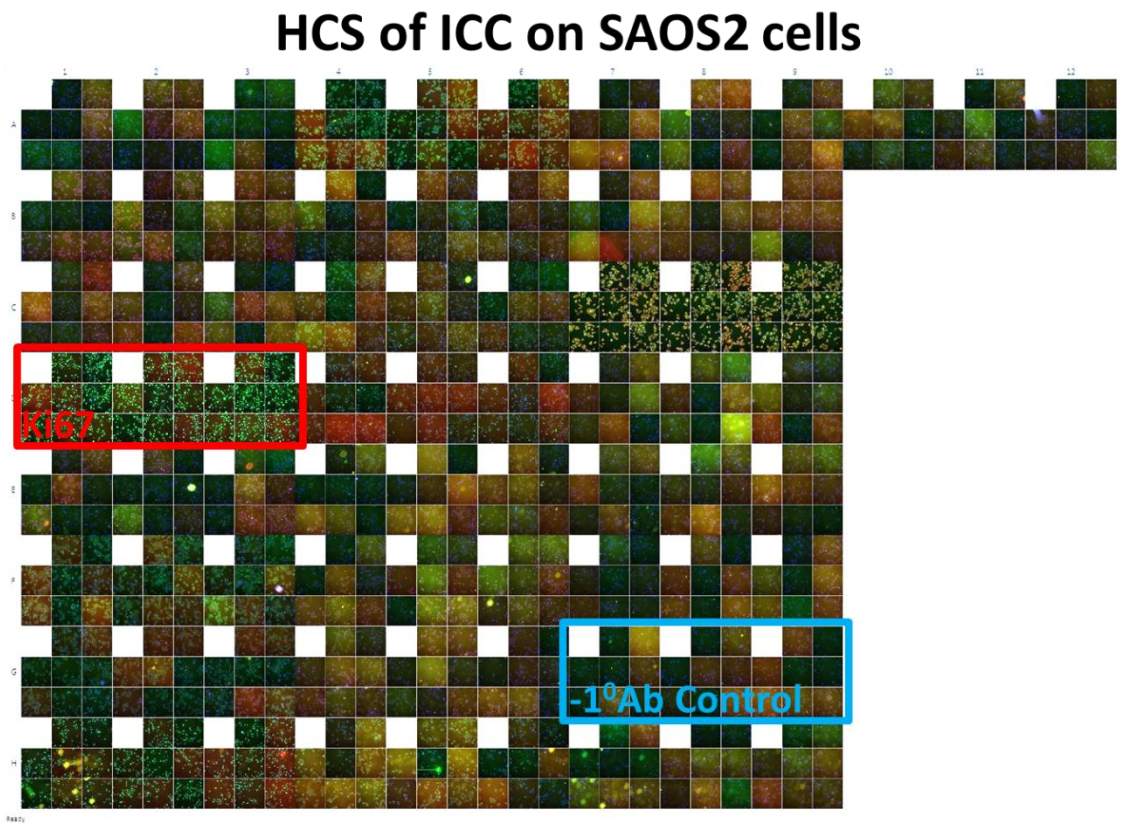

Figure 7.1: HCS plate layout and imaging

Screenshot of a 96 well multiwell plate seeded with SAOS2 cells, where cells have been fixed and fluorescently marked following ICC for selected markers. 75/96 wells were imaged, showing 8 raw images obtained per well. The RED rectangle indicates wells which were ICC immunoreactive for the Ki67 antigen. The BLUE rectangle indicates wells which were the ICC -1^0Ab control. ICC for all biomarkers presented within this thesis were performed on triplicate wells as shown.

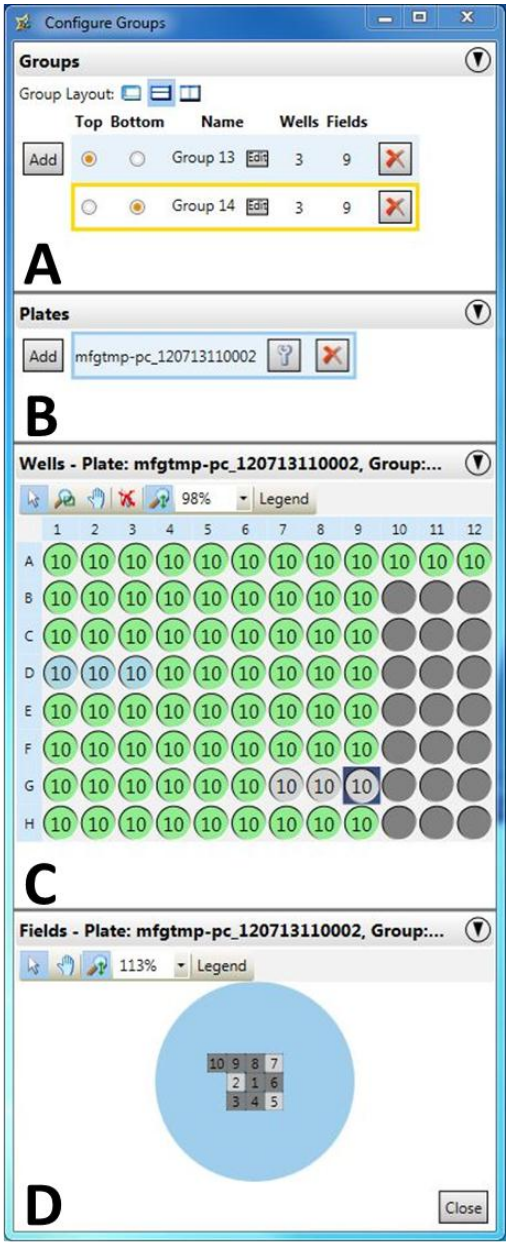

Figure 7.2: Image selection for processing and data analysis.

Screenshot showing the selected plate (B), plate layout (C), well groups (A) and selection of images being viewed within each well (D) using the Cellomics Array Scan HCS software. Here images of Ki67 antigen ICC immunoreactive stained cells are being compared to the -1^0Ab control images.

Figure 7.3: Image pre-processing.

The figure shows fluorescent images of ICC immunoreactivity for the Ki67 antigen within SAOS2 cells taken using a GFP filter, designated as channel 2. A single ROI raw image (left) is compared to the same ROI image with the background removed (right).

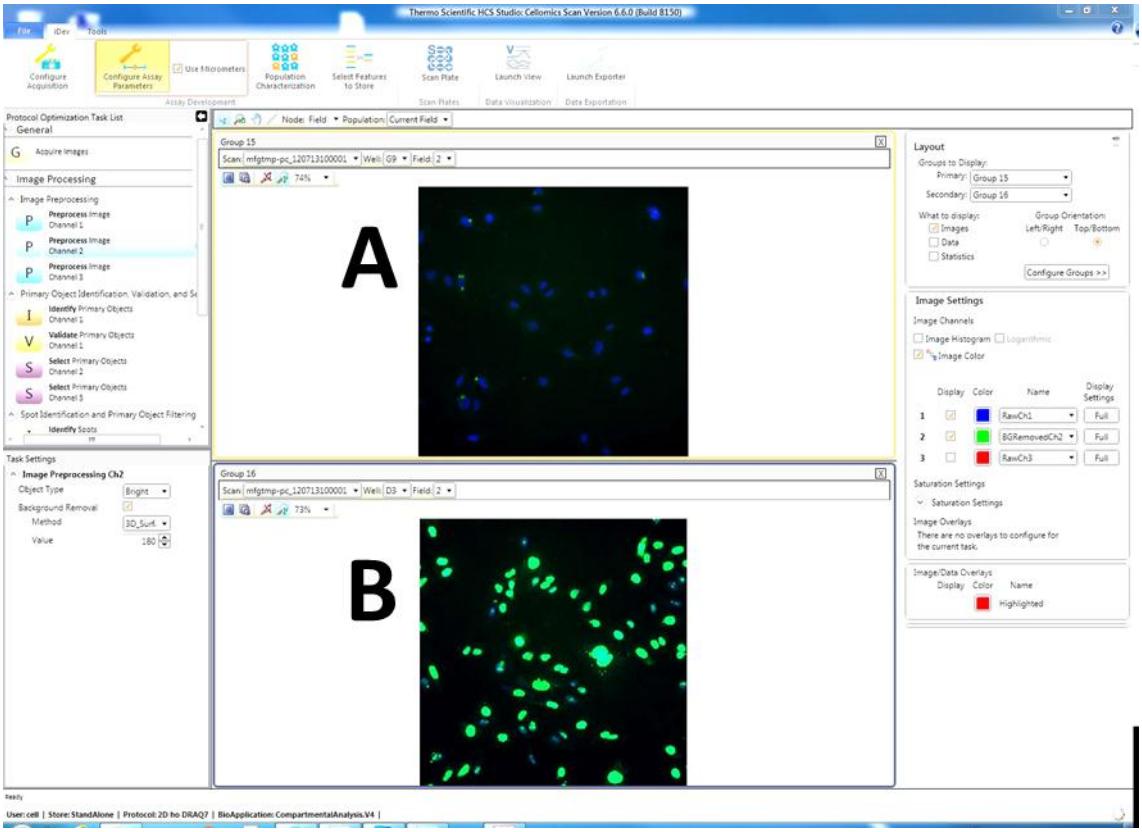

Figure 7.4: Screenshot of Thermo Scientific HCS Studio: Cellomics Scan Version 6.6.0.

The screen shot shows the comparison of a single ROI of Ki67 antigen ICC immunoreactivity within SAOS2 (B) compared to a single ROI of the -1^0Ab control (A). Images show Hoechst 33342 stained nuclei (designated to Ch1 - blue) with nuclear Ki67 antigen ICC (designated to Ch2 – green).

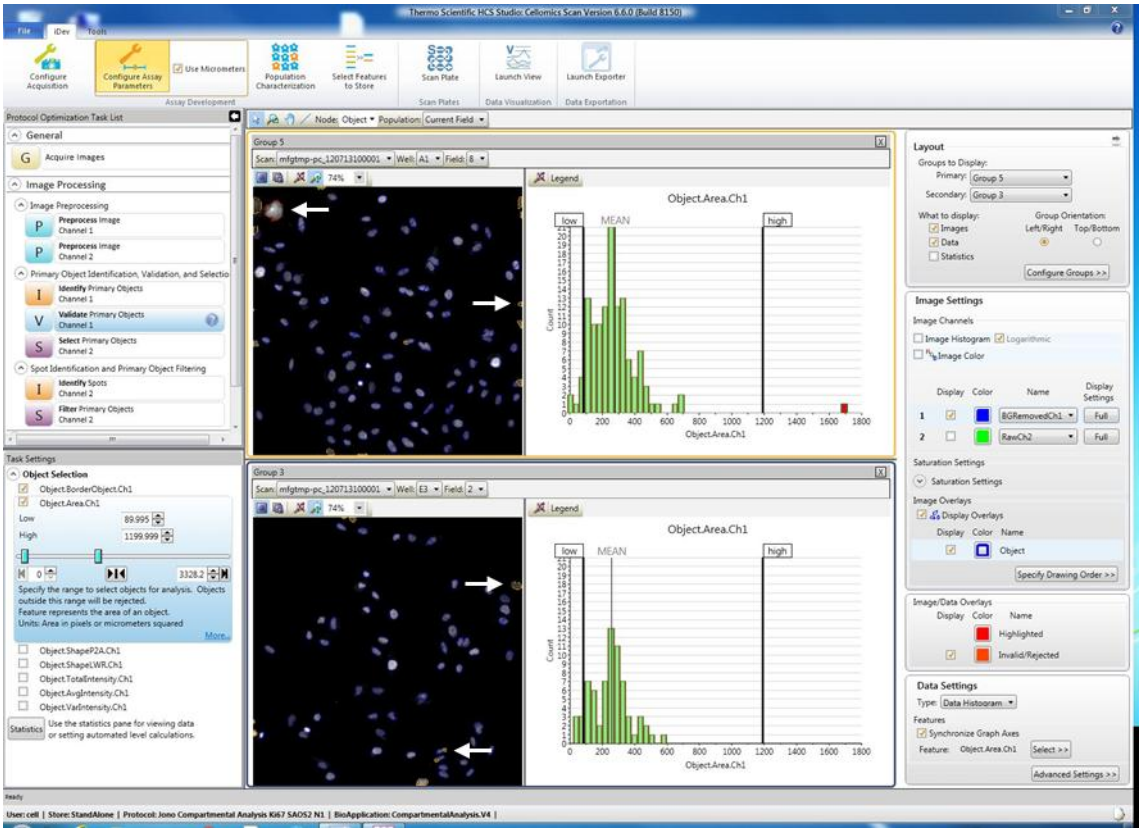

Figure 7.5: Screenshot of primary object selection

The screen shot shows the selection within two ROI images of cells based on Hoechst 33342 stained nuclei (designated to Ch1) in -1^{0}Ab control cells (top left image) and Ki67 antigen ICC stained cells (bottom left image). Only Ch1 nuclear staining is shown. Objects highlighted by the white arrows indicate cells which have been rejected due to the location of the nucleus on the boarder of the ROI, or the area of the object is smaller or larger than the designated threshold (left panel).

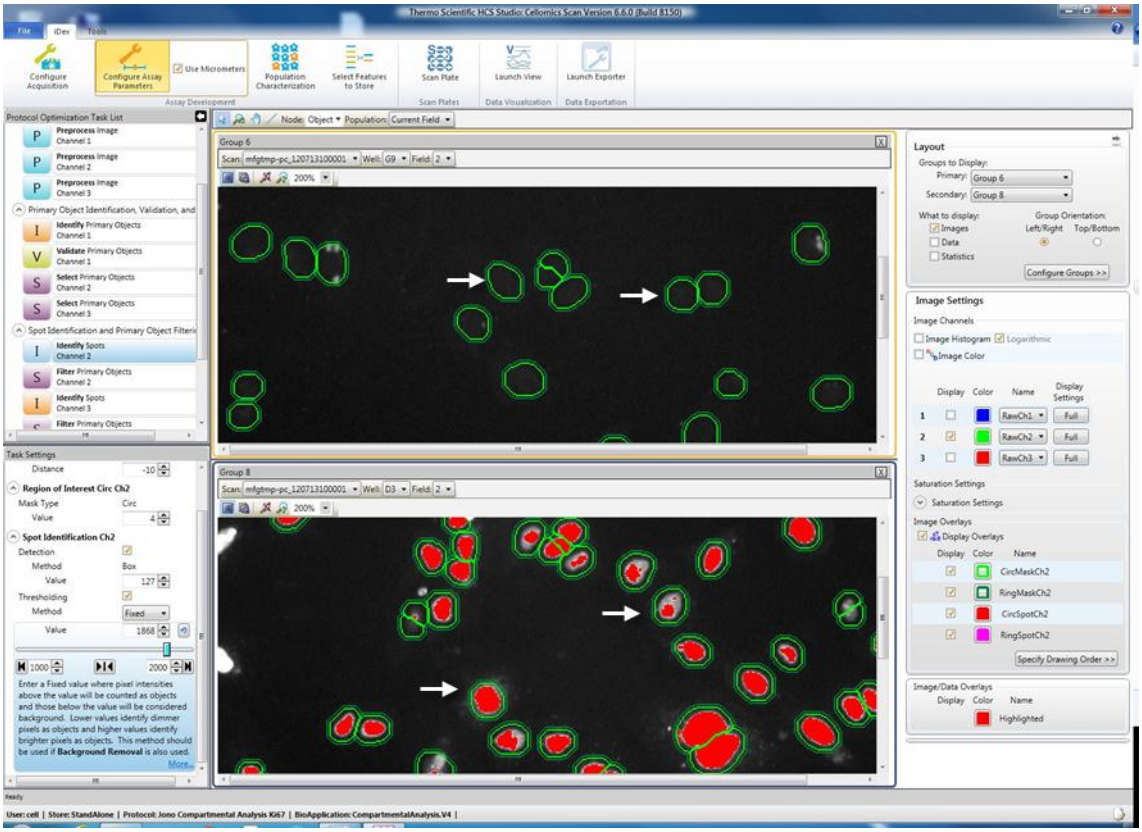

Figure 7.6: Screenshot of nuclear (circ) spot object identification

The screenshot shows the nuclear (circ) ROI for SAOS2 cells based on Hoechst 33342 staining (designated to Ch1) with overlaid RED indicating pixels within the circ which have a fluorescent intensity in Ch2 (GFP) which is greater than the set threshold value shown in the panel to the right. White arrows highlight -1^0Ab control SAOS2 cells (top panel image) and Ki67 antigen ICC immunoreactive SAOS2 cells (bottom panel image) with and without bright fluorescent spots within the nucleus.

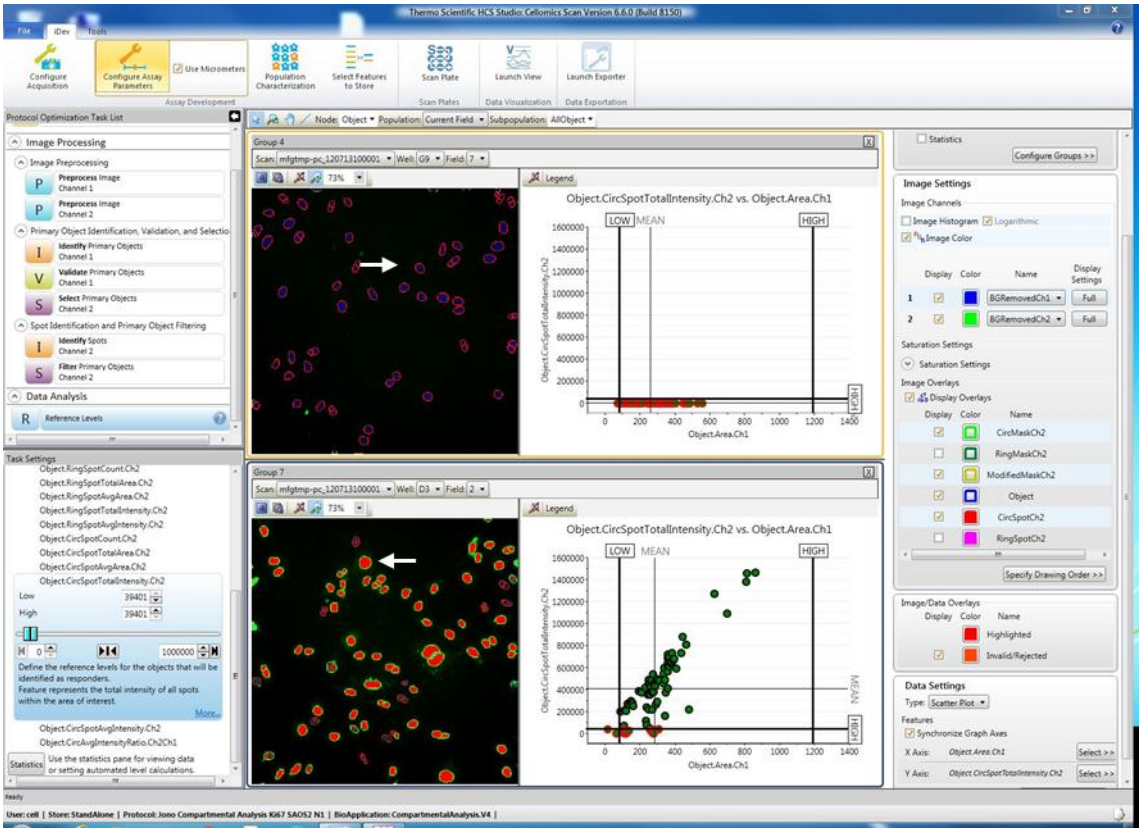

Figure 7.7: Screenshot of nuclear (circ) spot object selection.

The screen shot shows the nuclear (circ) ROI selection within two images of cells based on Hoechst 33342 stained nuclei (designated to Ch1 - blue) in -1^0Ab control cells (top left image) and Ki67 antigen ICC stained cells (bottom left image; designated to Ch2 - green). The white arrow in the top panel image indicates cells which have been rejected (red circle) due to the fluorescent nuclear spot intensity to be lower than that of a threshold (right panel). The white arrow in the bottom panel image indicates cells which have been selected (highlighted in red) and counted as positive for immunoreactive staining within the nuclear area. The graphs (right panels) show the circ spot total intensity versus the object area where selected cells (green spot with black circle) within the threshold parameters are counted, compared to rejected (green spot with red circle) cells.

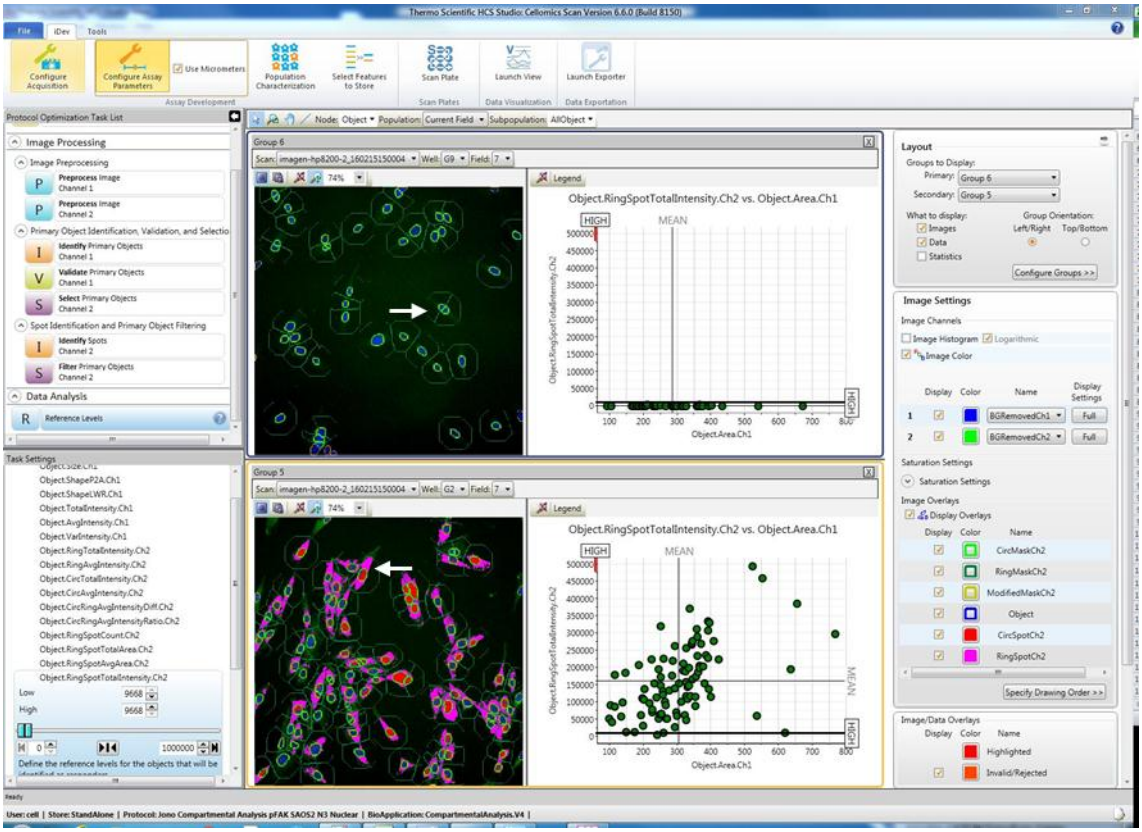

Figure 7.8: Screenshot of cytoplasmic (ring) spot object selection

The screen shot shows the cytoplasmic (ring) ROI selection within two images of cells based on Hoechst 33342 stained nuclei (designated to Ch1 - blue) in -1^{0}Ab control cells (top left image) and B-catenin ICC stained cells (bottom left image; designated to Ch2 - green). The white arrow in the top panel image indicates cells which have been rejected (red circle) due to the fluorescent nuclear spot intensity to be lower than that of a threshold (right panel). The white arrow in the bottom panel image indicates cells which have been selected (highlighted in red) and counted as positive for immunoreactive staining within the cytoplasmic area. The graphs (right panels) show the ring spot total intensity versus the object area where cells are included or excluded based on threshold parameters (right panel).

7.1.2 HCS image analysis and raw data

The average fluorescent intensities (Figure 7.9 and Figure 7.13), sum fluorescent intensities (Figure 7.10 and Figure 7.14), average spot fluorescent intensities (Figure 7.11 and Figure 7.15) and sum fluorescent spot intensities (Figure 7.12 and Figure 7.16) of fluorescent immuno-labelled biomarkers located within the nuclear or cytoplasmic regions of interest respectively, of MSCs, SAOS2 and MG63 cells are shown.

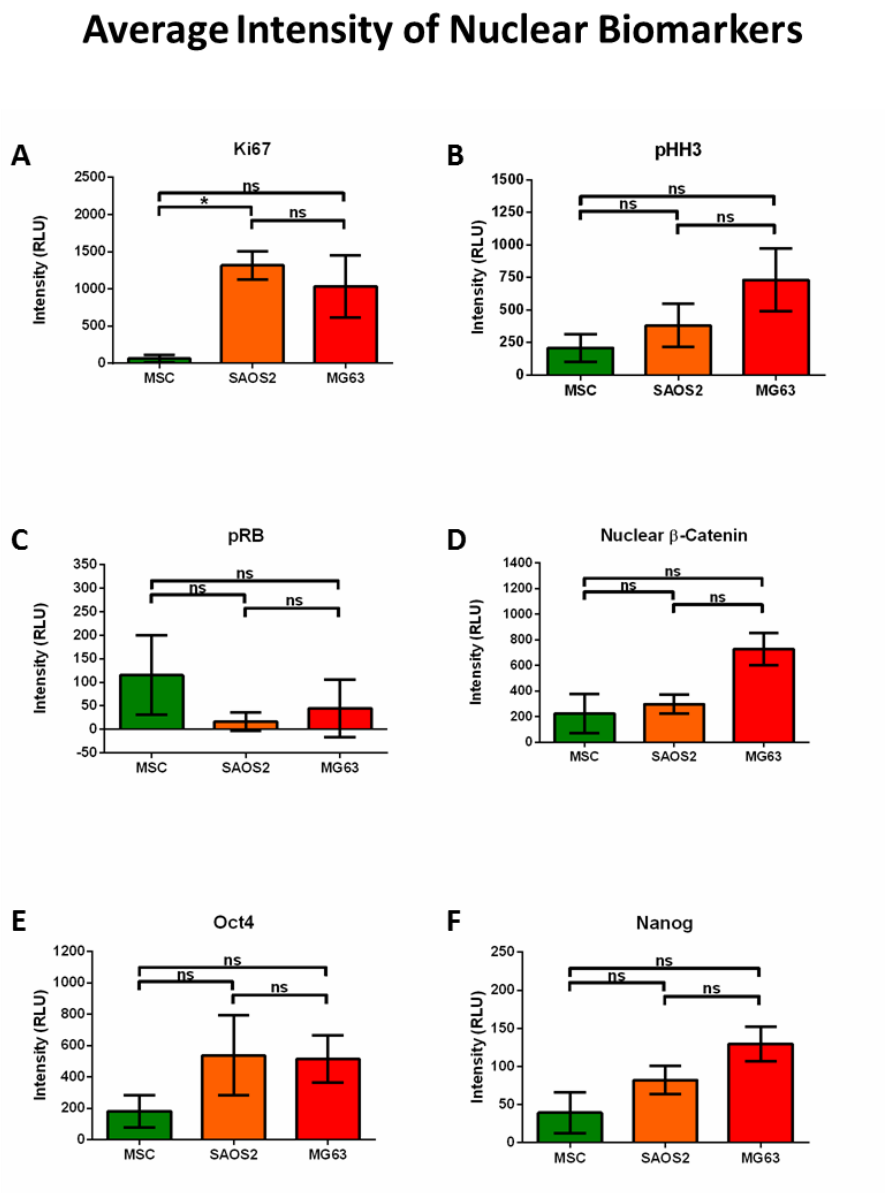

Figure 7.9: Average fluorescent intensity of biomarkers located within the nuclear (circ) region of interest.

The average fluorescent intensity (RLU) of the nuclear biomarkers; Ki67, pHH3, pRB, nuclear β-catenin, Oct4 and nanog were quantitated and shown for MSCs (green), SAOS2 (orange) and MG63 cells (red). Data shown are Mean ± SEM from n=3 donor MSCs analysed along with SAOS2 and MG63 cells over 3 independent experiments. All; two-way ANOVA with a Tukey's post-test, ns indicates no significant difference, *$p \leq 0.05$, **$p \leq 0.01$, ***$p \leq 0.001$.

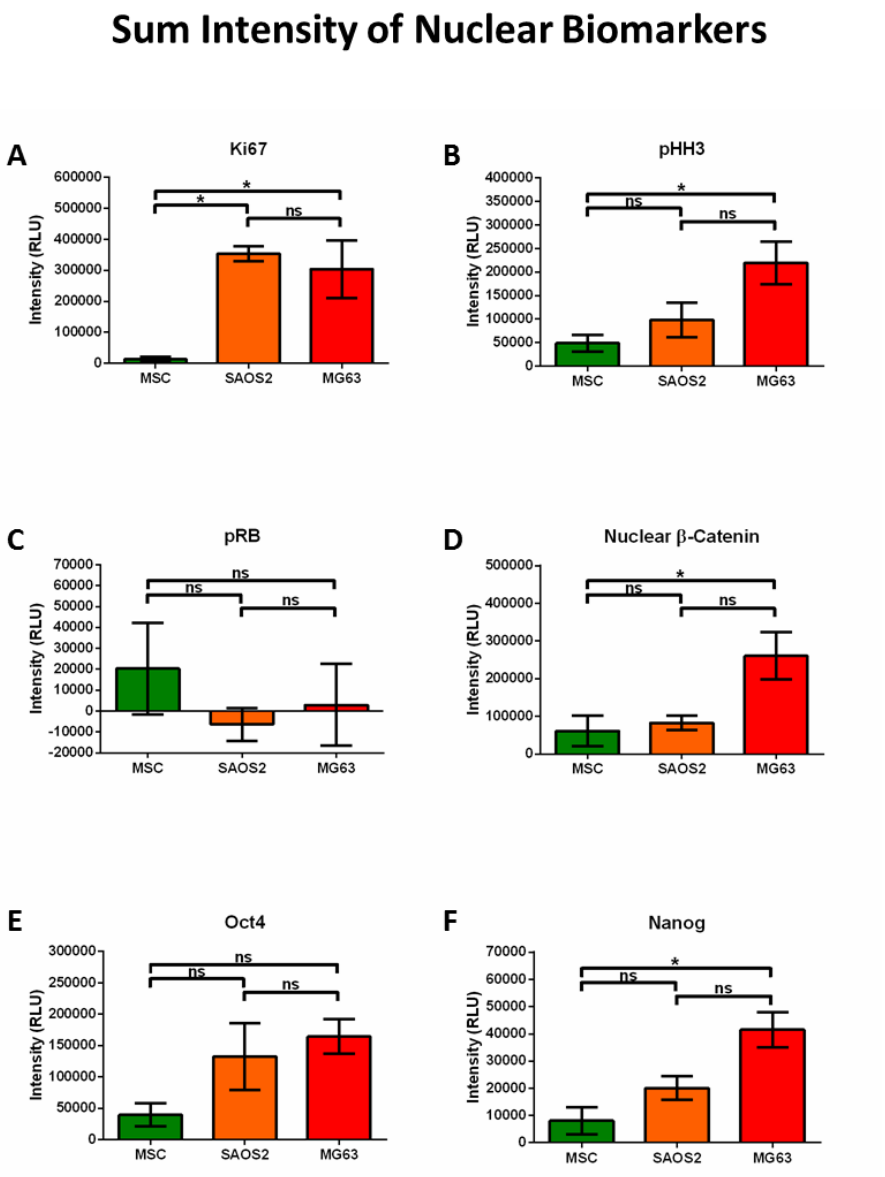

Figure 7.10: Sum fluorescent intensity of biomarkers located within the nuclear (circ) region of interest.

The sum fluorescent intensity (RLU) of the nuclear biomarkers; Ki67, pHH3, pRB, nuclear β-catenin, Oct4 and nanog were quantitated and shown for MSCs (green), SAOS2 (orange) and MG63 cells (red). Data shown are Mean ± SEM from n=3 donor MSCs analysed along with SAOS2 and MG63 cells over 3 independent experiments. All; two-way ANOVA with a Tukey's post-test, ns indicates no significant difference, *$p \leq 0.05$, **$p \leq 0.01$, ***$p \leq 0.001$.

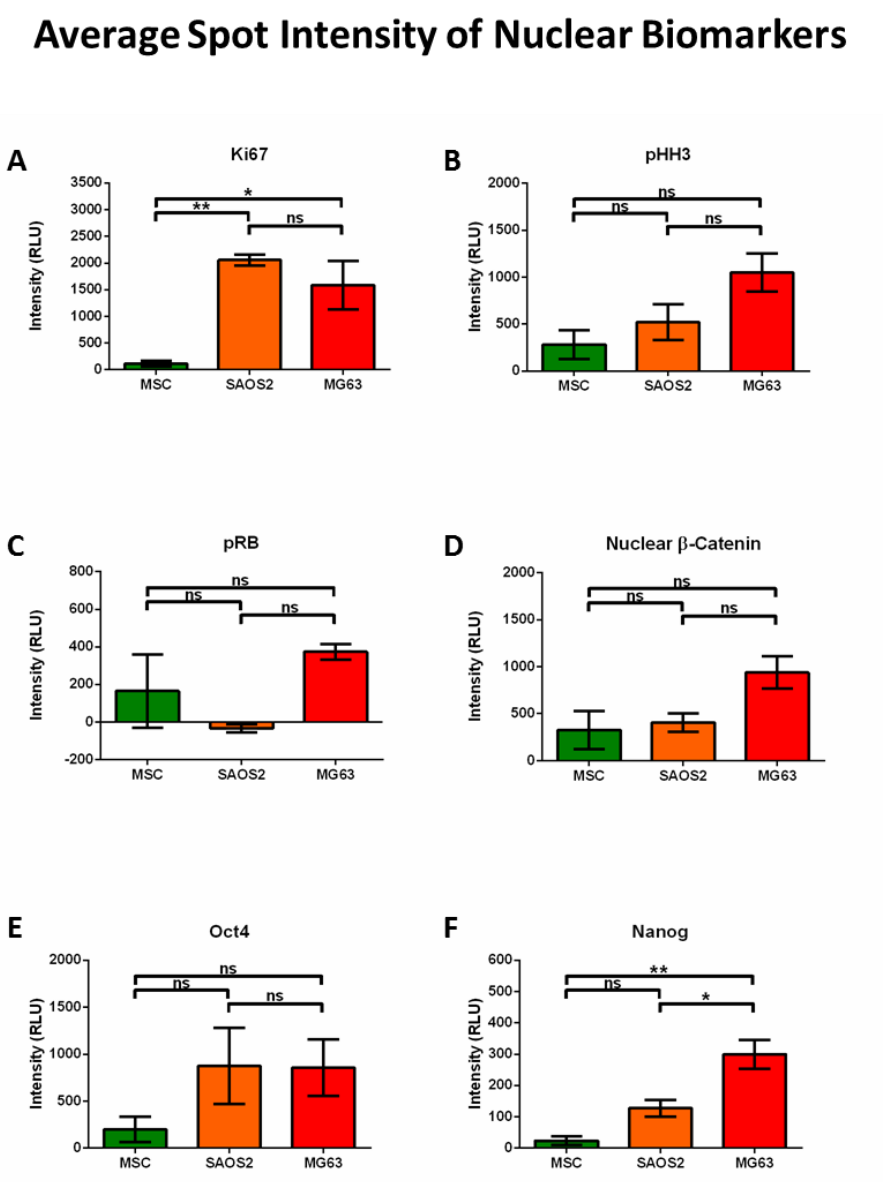

Figure 7.11: Average fluorescent spot intensity of biomarkers located within the nuclear (circ) region of interest.

The average fluorescent spot intensity (RLU) of the nuclear biomarkers; Ki67, pHH3, pRB, nuclear β-catenin, Oct4 and nanog were quantitated and shown for MSCs (green), SAOS2 (orange) and MG63 cells (red). Data shown are Mean ± SEM from n=3 donor MSCs analysed along with SAOS2 and MG63 cells over 3 independent experiments. All; two-way ANOVA with a Tukey's post-test, ns indicates no significant difference, *$p \leq 0.05$, **$p \leq 0.01$, ***$p \leq 0.001$.

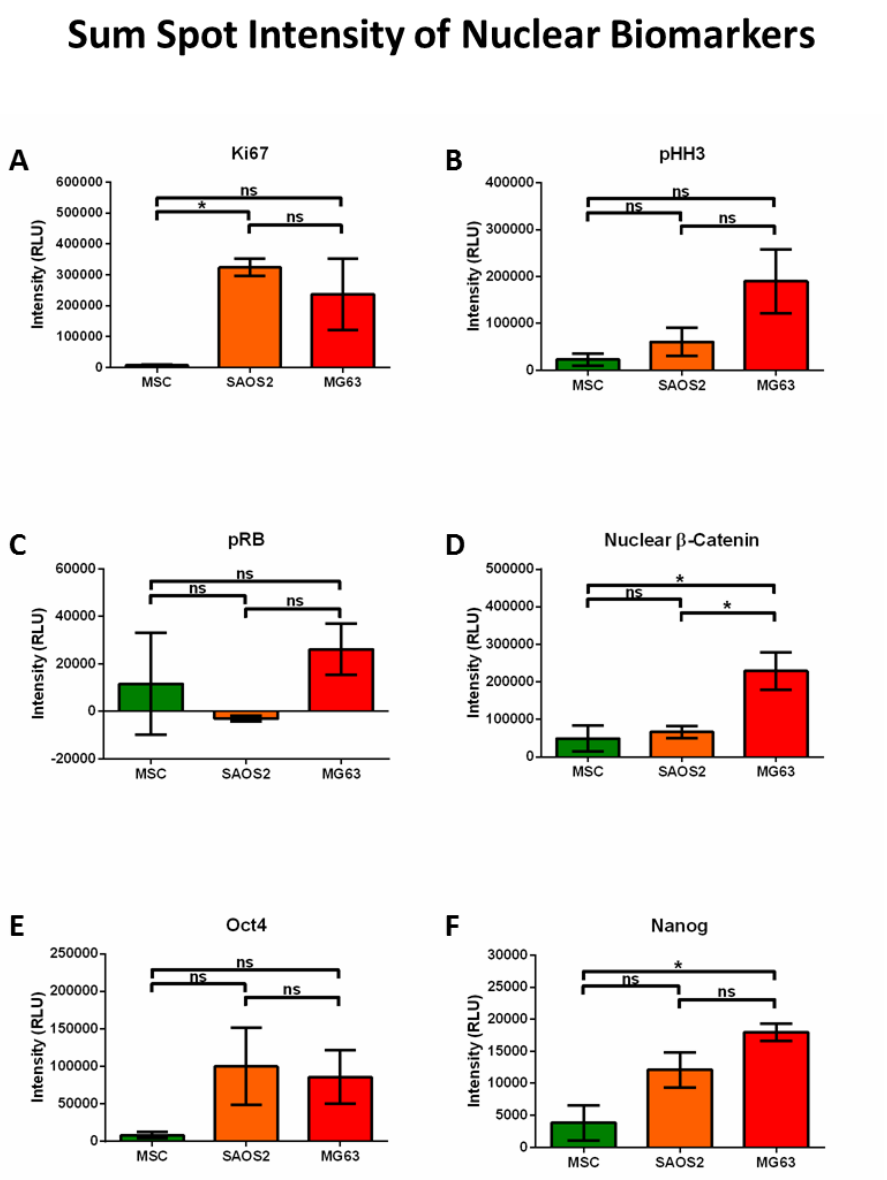

Figure 7.12: Sum fluorescent spot intensity of biomarkers located within the nuclear (circ) region of interest.

The sum fluorescent spot intensity (RLU) of the nuclear biomarkers; Ki67, pHH3, pRB, nuclear β-catenin, Oct4 and nanog were quantitated and shown for MSCs (green), SAOS2 (orange) and MG63 cells (red). Data shown are Mean ± SEM from n=3 donor MSCs analysed along with SAOS2 and MG63 cells over 3 independent experiments. All; two-way ANOVA with a Tukey's post-test, ns indicates no significant difference, *$p \leq 0.05$, **$p \leq 0.01$, ***$p \leq 0.001$.

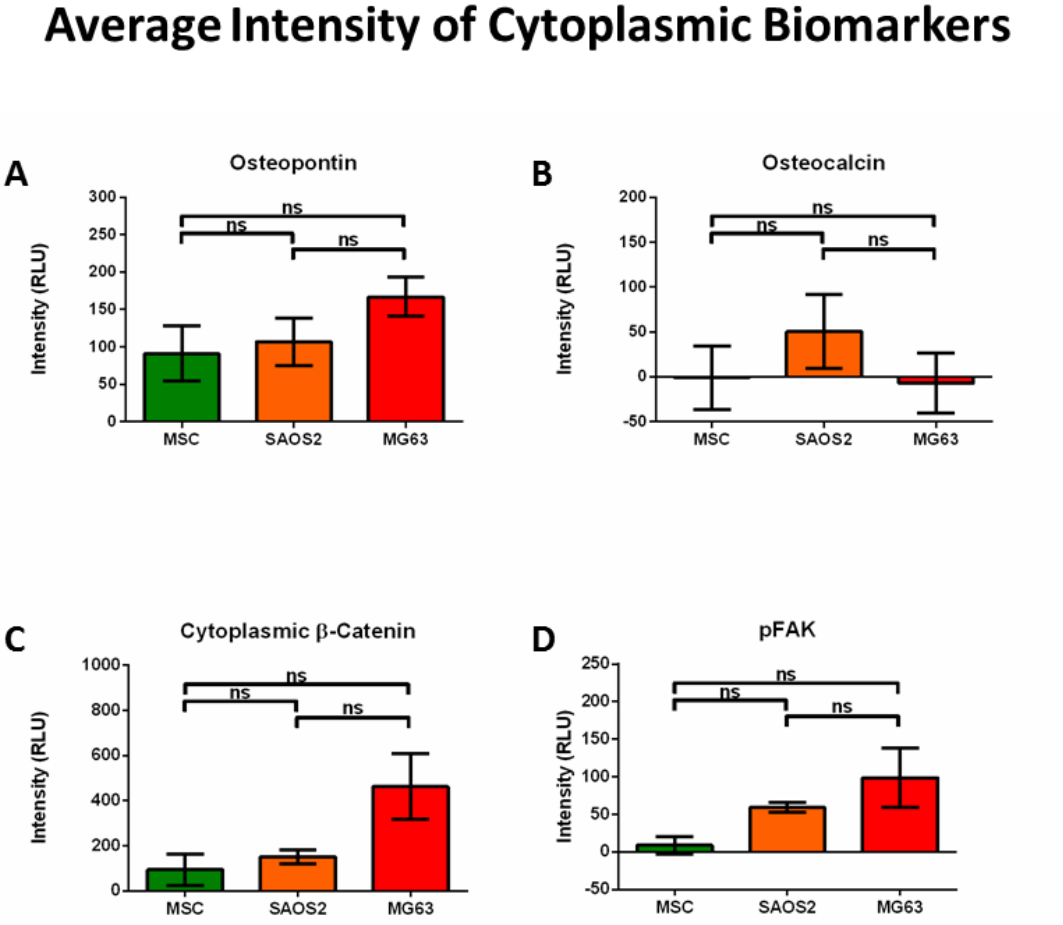

Figure 7.13: Average fluorescent intensity of biomarkers located within the cytoplasmic (ring) region of interest.

The average fluorescent intensity (RLU) of the cytoplasmic biomarkers; osteopontin, osteocalcin, cytoplasmic β-catenin and pFAK were quantitated and shown for MSCs (green), SAOS2 (orange) and MG63 cells (red). Data shown are Mean ± SEM from n=3 donor MSCs analysed along with SAOS2 and MG63 cells over 3 independent experiments. All; two-way ANOVA with a Tukey's post-test, ns indicates no significant difference, *$p \leq 0.05$, **$p \leq 0.01$, ***$p \leq 0.001$.

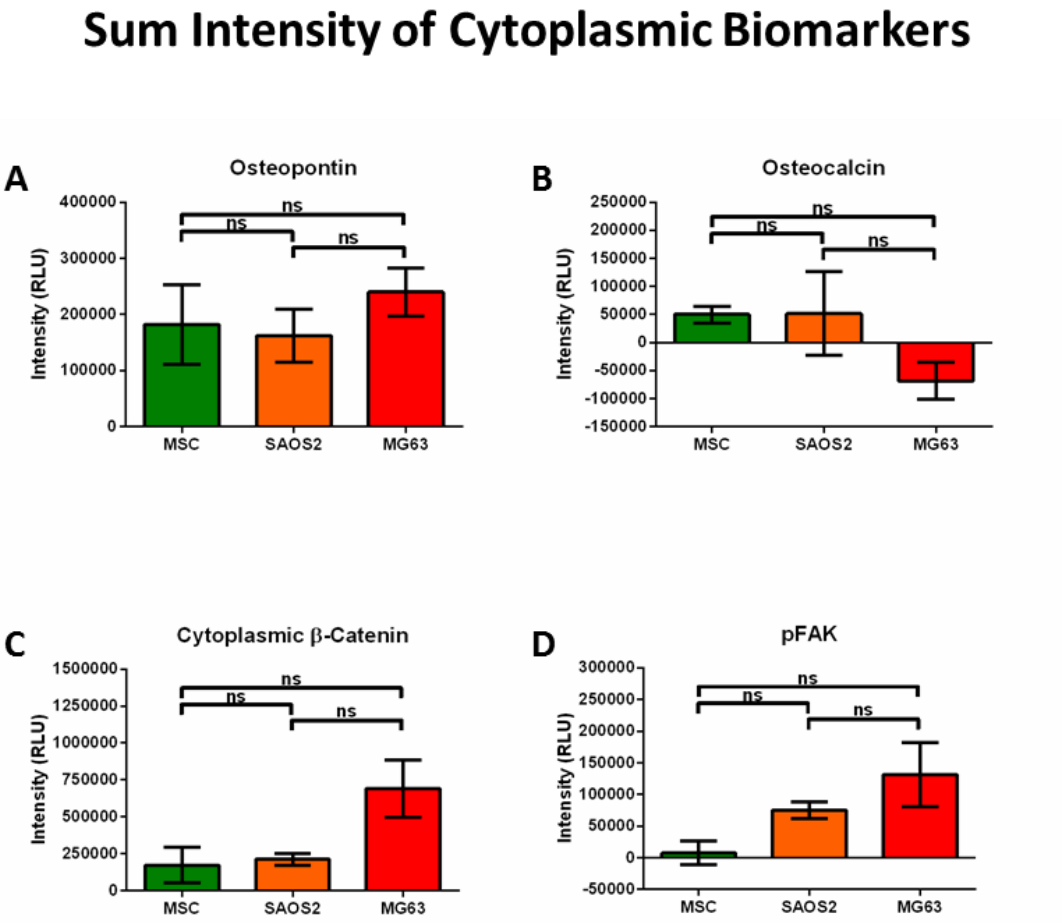

Figure 7.14: Sum fluorescent intensity of biomarkers located within the cytoplasmic (ring) region of interest.

The sum fluorescent intensity (RLU) of the cytoplasmic biomarkers; osteopontin, osteocalcin, cytoplasmic β-catenin and pFAK were quantitated and shown for MSCs (green), SAOS2 (orange) and MG63 cells (red). Data shown are Mean ± SEM from n=3 donor MSCs analysed along with SAOS2 and MG63 cells over 3 independent experiments. All; two-way ANOVA with a Tukey's post-test, ns indicates no significant difference, *$p \leq 0.05$, **$p \leq 0.01$, ***$p \leq 0.001$.

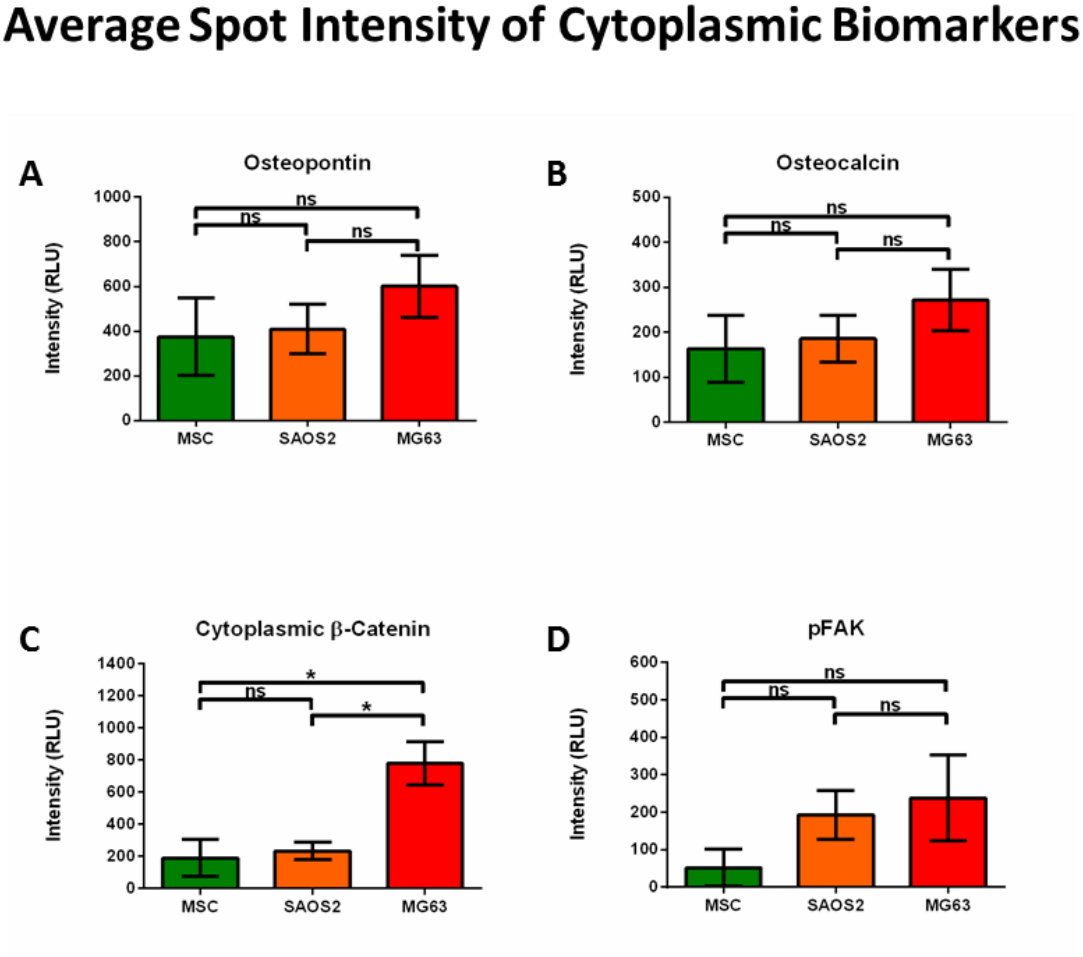

Figure 7.15: Average fluorescent spot intensity of biomarkers located within the cytoplasmic (ring) region of interest.

The average fluorescent spot intensity (RLU) of the cytoplasmic biomarkers; osteopontin, osteocalcin, cytoplasmic β-catenin and pFAK were quantitated and shown for MSCs (green), SAOS2 (orange) and MG63 cells (red). Data shown are Mean ± SEM from n=3 donor MSCs analysed along with SAOS2 and MG63 cells over 3 independent experiments. All; two-way ANOVA with a Tukey's post-test, ns indicates no significant difference, *$p \leq 0.05$, **$p \leq 0.01$, ***$p \leq 0.001$.

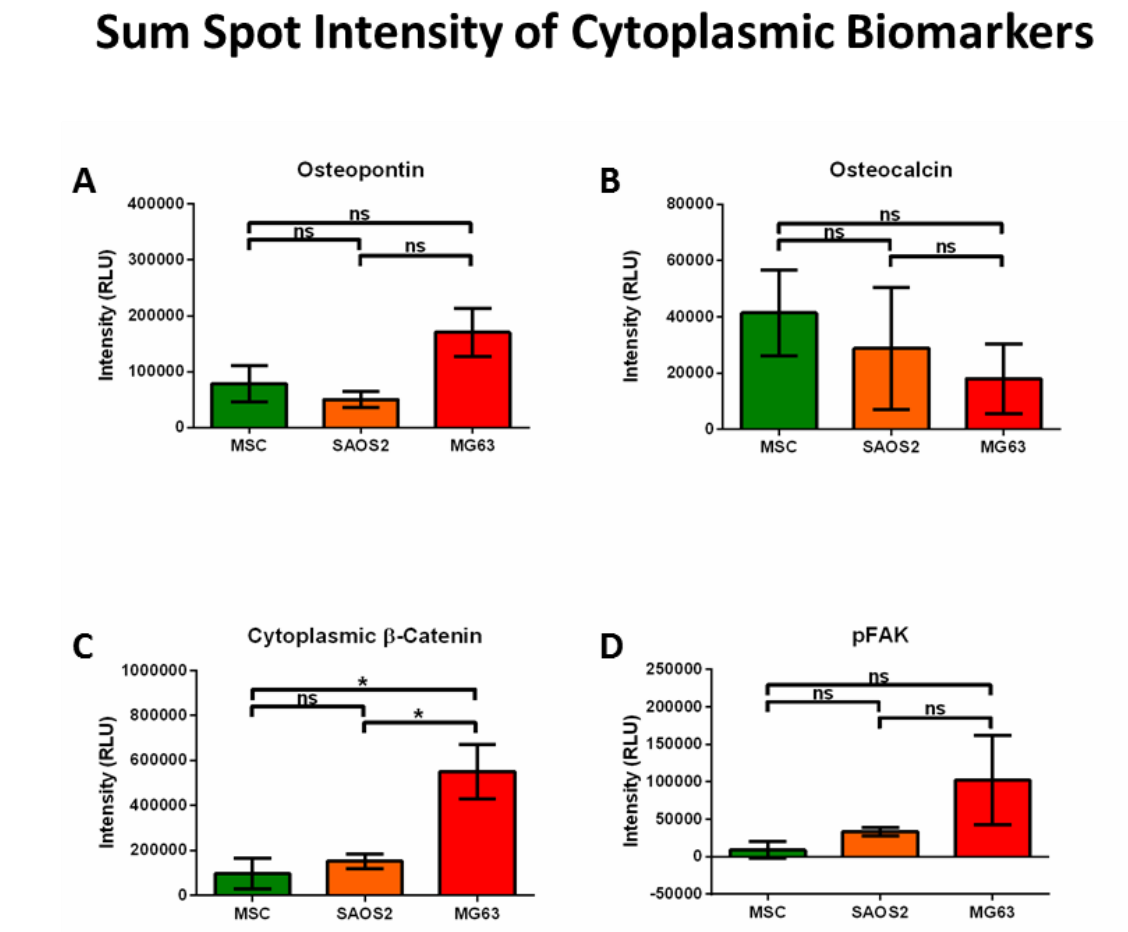

Figure 7.16: Sum fluorescent spot intensity of biomarkers located within the cytoplasmic (ring) region of interest.

The sum fluorescent spot intensity (RLU) of the cytoplasmic biomarkers; osteopontin, osteocalcin, cytoplasmic β-catenin and pFAK were quantitated and shown for MSCs (green), SAOS2 (orange) and MG63 cells (red). Data shown are Mean ± SEM from n=3 donor MSCs analysed along with SAOS2 and MG63 cells over 3 independent experiments. All; two-way ANOVA with a Tukey's post-test, ns indicates no significant difference, *$p \leq 0.05$, **$p \leq 0.01$, ***$p \leq 0.001$.

7.1.3 IN CELL Analyzer Multi Target Analysis method

Following ALP enzymatic activity staining (section 2.4), HCS of cells was performed using the IN CELL Analyzer 1000 platform (GE Healthcare, Buckinghamshire, UK). Similarly to the Cellomics ArrayScan, 9 images were taken from the centre through a spiral pattern outward towards the edge of the well with no less than 5000 cells imaged within the 9 images. Images were taken in two channels: channel 1 ($386nm_{EM}$), channel 2 (bright field). These images were then analysed through the standard bio-application analysis protocol to measure the pixel intensity for the 'Ring' regions of interest on a per cell basis. The software reported the mean cytoplasmic intensity on a per cell basis, designated here as relative light units (RLU, an arbitrary annotation). The inverse of the intensity was then calculated and plotted.

7.1.4 Alkaline phosphatase enzymatic activity in MSCs, SAOS2 and MG63 cells

Representative bright-field, monochromatic images of alkaline phosphatase (ALP) enzymatic activity are shown in Figure 7.17 A. As shown, SAOS2 cells showed dark cytoplasmic and nuclear ALP staining activity. In contrast, few MSCs and MG63 cells were stained by the ALP activity. The graph in Figure 7.17 B shows the mean intensity of ALP activity within three donor MSCs compared to SAOS2 and MG63 cells. As shown, quantitation of the staining for ALP activity inSAOS2 (158.4 ± 13.7 AU) was 12 fold higher than that for ALP activity in MSCs (13.0 ± 1.4 AU) and approximately 10 fold greater than staining for ALP activity in MG63 cells (16.1 ± 3.0 AU). Staining intensity of the SAOS2 cells was significantly higher than both MSCs and MG63 cells ($p<0.001$; one-way ANOVA with a Tukey's post-test).

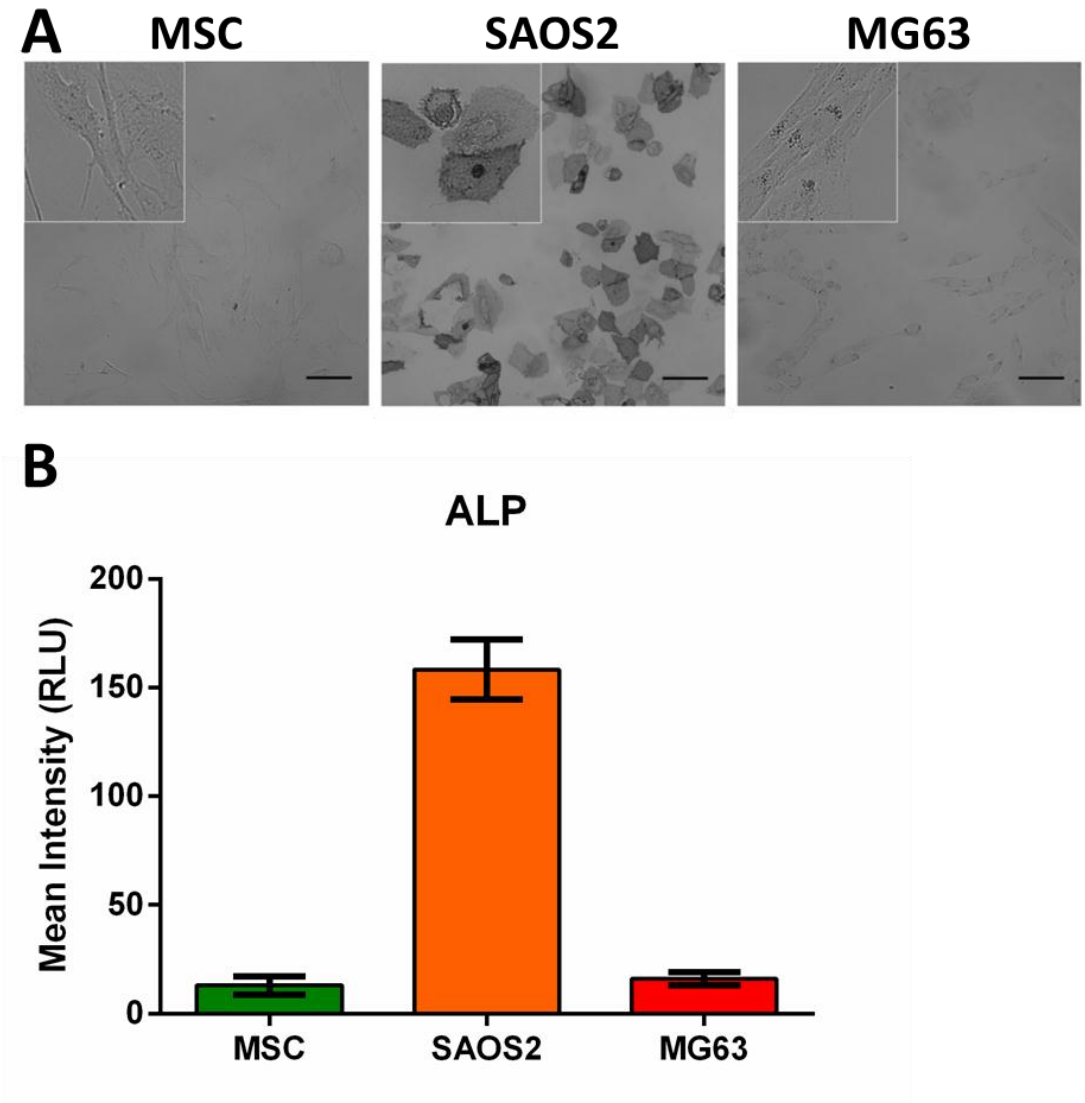

Figure 7.17: Increased activity of the differentiation associated marker Alkaline Phosphatase (ALP) distinguished primary human MSCs from SAOS2 cells, but not MG63 cells.

(A) Representative images showing increased ALP activity in MSC, SAOS2 and MG63 cells (Bar = 100µm). Inset is 3x magnified. (B) Quantitation of the mean cytoplasmic intensity of ALP within MSCs, SAOS2 and MG63 cells, determined using the IN CELL Analyser© HCS platform. Data shown are means ± SD from n=1 experiment.

7.2 Chapter 4: Supplementary figures and data

7.2.1 Live-cell imaging protocol development, image analysis and data presentation.

Cell-IQ Analyser™ software analysis must be performed in a stepwise process prior to the production of results. Initially images are segmented using a threshold, where an image is segmented by parameters determined for distances between cells, area of cells as well as cell symmetry (Figure 7.18). Segmentation parameter settings were initially used to identify all cells within the population (**Error! Reference source not found.**); however, these were later fine-tuned or cell type specific segmentation aiming towards better cell type identified. Images of two MSC samples, SAOS2 and MG63 cells cultured in monoculture at 48hrs post seeding, were initially used to define cell type specific segmentation parameters.

The cell type specific segmentation parameters were then used for the next step of cell classification. The classification step groups the segments of the images into separate classes based on a user built sample library. Prior to adding samples, a predefined 'Recognition window size' must be selected (Figure 7.19). During cell sample collection, only a single recognition window size can be used whilst adding samples to the sample library (Figure 7.22), therefore several recognition windows were selected and protocols formed (Table 8). When the recognition area was specified, samples/stamps of each cell type were added to the cell classes, the cell counting segmentation parameters were set (Figure 7.21), then the protocol algorithms were written and the images of the MSC, SAOS2 and MG63 cell monocultures were analysed. Figure 7.22 shows phase contrast images of two MSC samples, SAOS2 and MG63 cells at 48hrs post seeding, in their original form (top row), following segmentation with RED dots indicating identified points of interest (middle row), then following classification of the segmented dots into cell classes (bottom row) and the protocol used in the bottom left corner of the image. The number of events identifying a specific cell type in monoculture was then calculated relative to incorrect identification events and graphed

as identification (% of total) as shown in Figure 7.23. It can be seen that Protocol 5 was most accurate for identifying MSC (BMS003) (68%), Protocol 1 for MSC (BMS006) (68%), Protocol 5 for SAOS2 cells (92%) and Protocol 6 for MG63 cells (94%).

These protocols were then enhanced where cell samples were added taken from images collected through the full culture period. Analysis was of the monocultures was performed and the results can be seen in Figure 7.24.

Images of MSC, SAOS2 and MG63 cell monocultures, showing the identification points were examined and incorrect identification of cells was noted. The events where cells were misidentified were noted and the cell sample library was adjusted appropriately where possible. Figure 7.25 shows the identification of MSCs, SAOS2 and MG63 cells at 72 and 96hrs post seeding, where the inserts show incorrect identification with a RED box and correct identification by a GREEN box. Misidentification of MSCs and SAOS2 cells as MG63 cells can be seen in inserts b, d, f and n. This is due to the phase bright 'halo' seen around the cells, a distinctive characteristic of the MG63 cells throughout their growth cycles. Misidentification of the spaces between MSCs as MG63 cells seen in insert j, is similarly due to the phase bright 'halo' effect. This was counteracted by teaching the library to identify these areas as background. Misidentification of the MG63 cell as an MSC seen in inserts h and p may have been identification of the cell based on the large flat cytoplasm with less punctate markings within and around the nucleus. Misidentification of MSCs as SAOS2 cells seen in insert l is not clear and may be due to the particular cytoplasmic pattern displayed at that time.

Since many of these misidentifications were due to similarities between cell morphology, there was little that could be changed within the identification library; therefore, to address these, the sample size of each cell type class was increased, ensuring samples had distinctive differences.

Review of the analysed images, as shown in, highlighted areas of incorrect identification of cell types within the monocultures. As shown; inset images with a green boarder highlight cells which

have been correctly identified, inset images with a red boarder highlight cells which have been incorrectly identified.

The process of protocol development was continued, where images of identified cells were reviewed and the sample library adjusted accordingly. Similarly the cell segmentation parameters were adjusted. Analysis was re-run and the results reviewed. This was performed several times whilst including images and samples taken from repeat experiments. Videos showing the Cell Finder tool analysis of representative ROIs of two culture expanded MSCs, SAOS2 and MG63 cells can be seen on the supplementary DVD (Appendix 7.4).

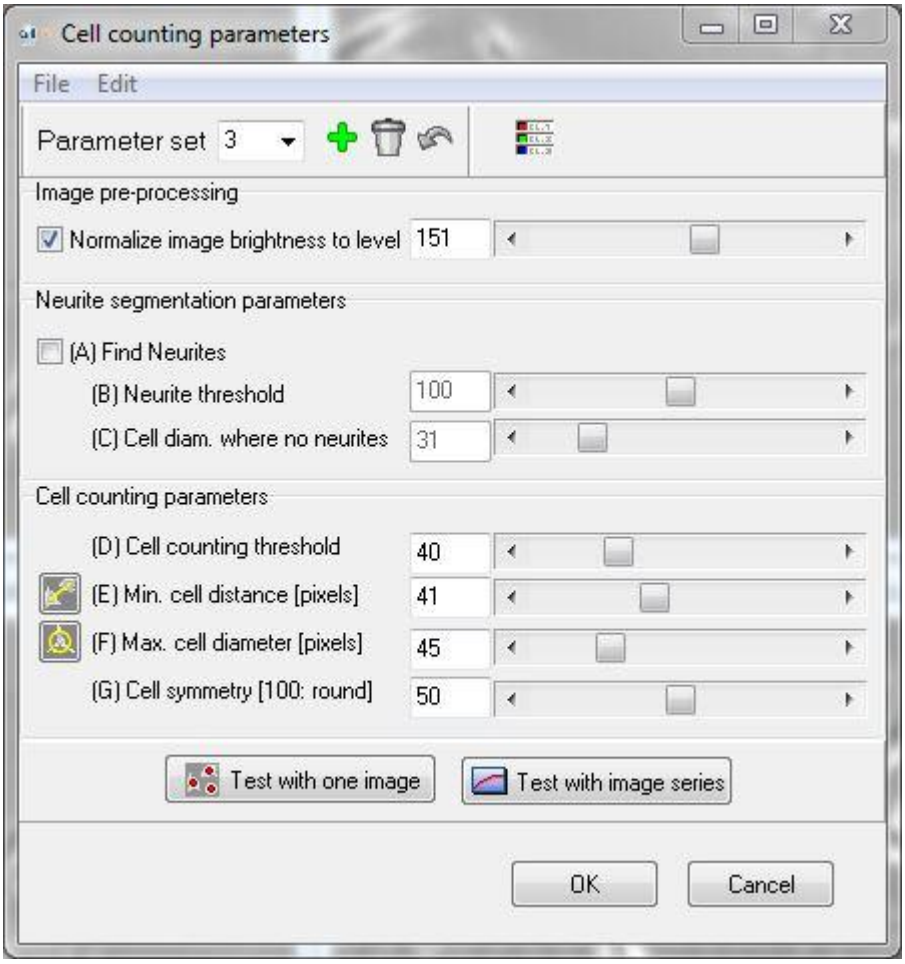

Figure 7.18: Cell counting segmentation parameters.

This screenshot illustrates the option for adding multiple parameter settings, then applying those settings towards the analysis and classification of cells within the images collected. Settings D through G which were manipulated specific to MSCs, SAOS2 and MG63 cells are shown in Table 4.

Table 7: Table showing the cell counting parameter settings for segmentation of images for analysis during protocol development.

Cell Type	Parameter set ID	Parameter A	Parameter B	Parameter C	Parameter D	Parameter E	Parameter F	Parameter G
MSC (BMS003)	1	-	-	-	50	50	65	20
MSC (BMS006)	2	-	-	-	50	50	65	20
SAOS2	3	-	-	-	40	40	45	50
MG63	4	-	-	-	45	45	55	20

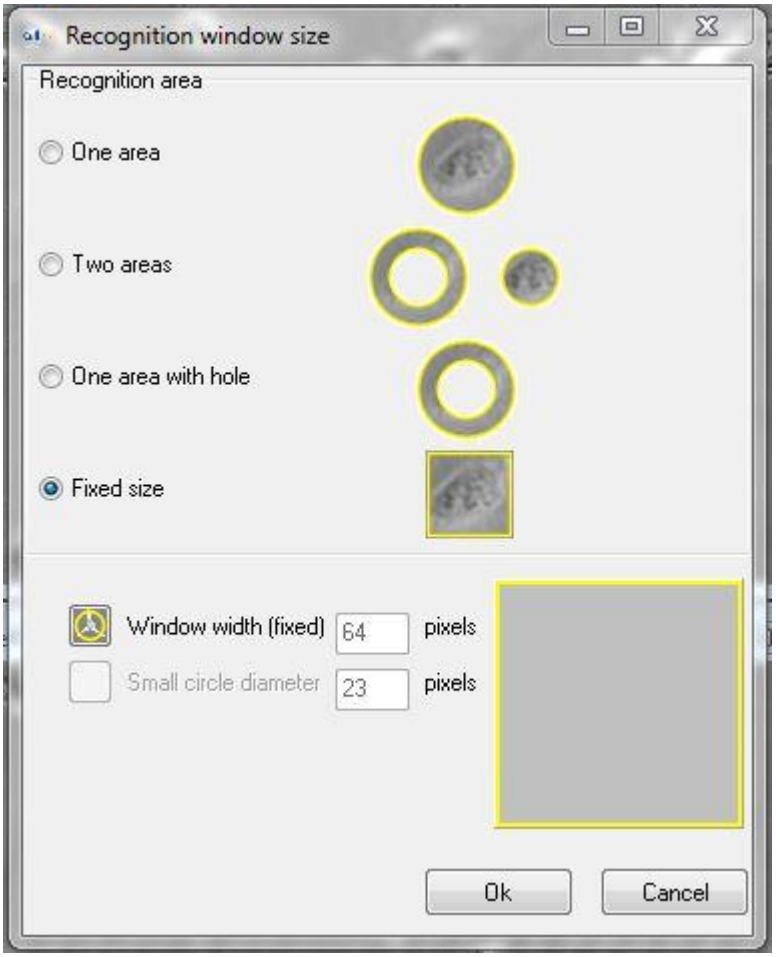

Figure 7.19: Cell-IQ Analyser™ Recognition window settings.

The recognition window options shown above allow for variability during the selection process for stamps used towards the collection and composition of a library. Within this thesis, the Two Areas recognition window was used.

Table 8: Table showing the cell counting parameter settings for recognition windows used during protocol development.

Protocol	Recognition Area	Window Size (Outer Circle)	Window Size (Inner Circle)
Protocol 1	One Area	130	
Protocol 2	Two Areas	130	50
Protocol 3	One Area	100	
Protocol 4	Two Areas	100	50
Protocol 5	One Area	120	
Protocol 6	Two Areas	120	45

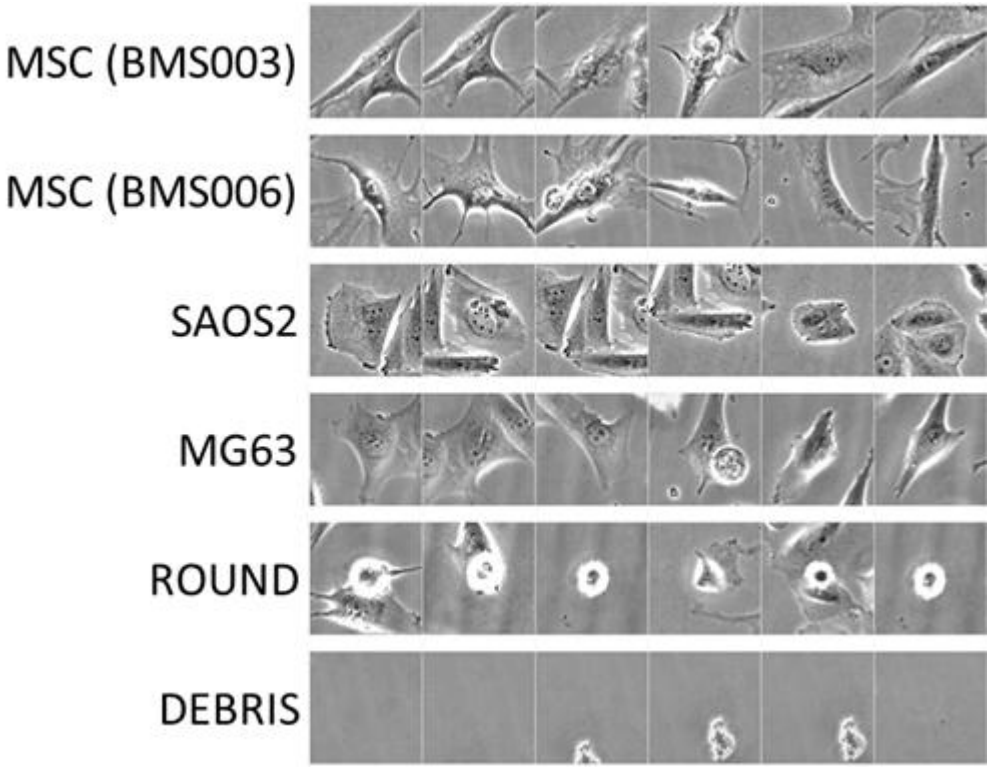

Figure 7.20: Sample images used to form the cell sample library which classifies cells following segmentation.

Stamps of specific cell morphologies are collected and classified by the user. Following stamp collection, the library images and categories are digitized into a pattern recognition algorithm which is then used to analyse and classify the cells within other images collected.

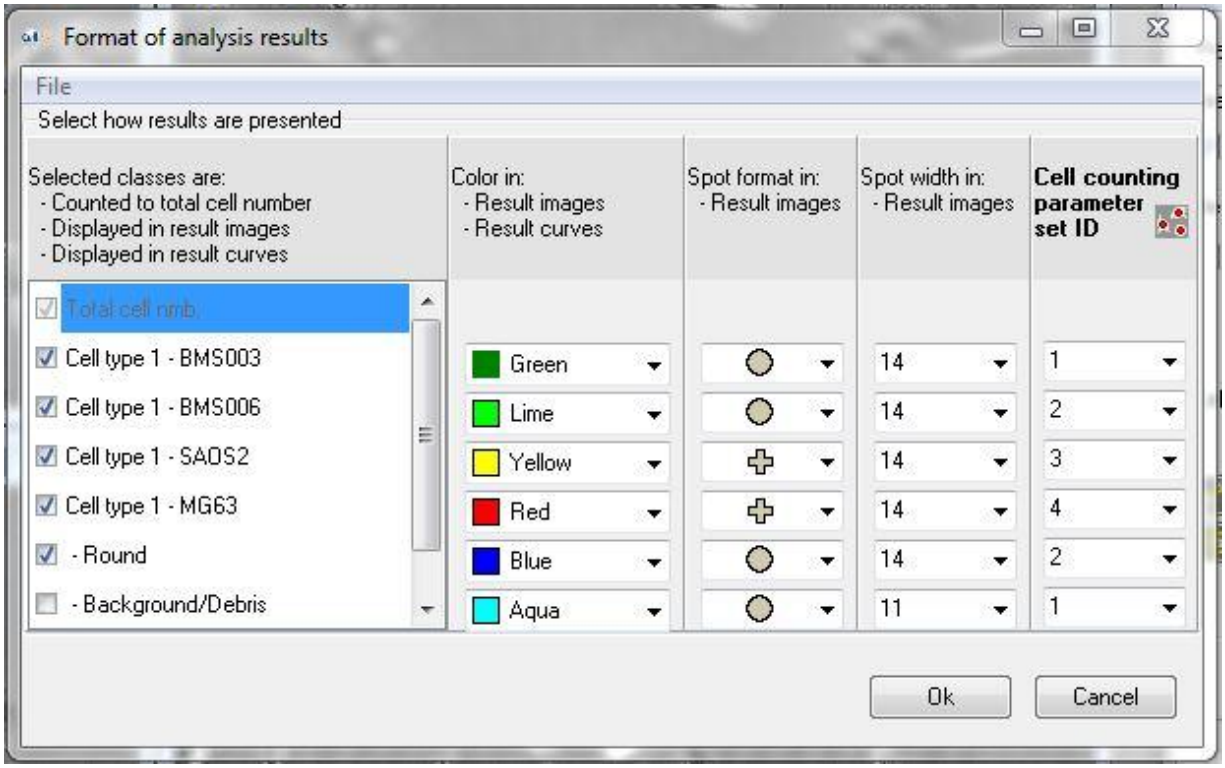

Figure 7.21: Details of cell identification analysis for Cell-IQ Analyser™ protocols.

The screenshot shows the development process for the identification and classification of two MSC samples (BMS003 and BMS006), SAOS2, MG63 and Round cells, as well as background/debris. Each class is designated a colour, shape, shape size and the cell counting and classification parameters can be set.

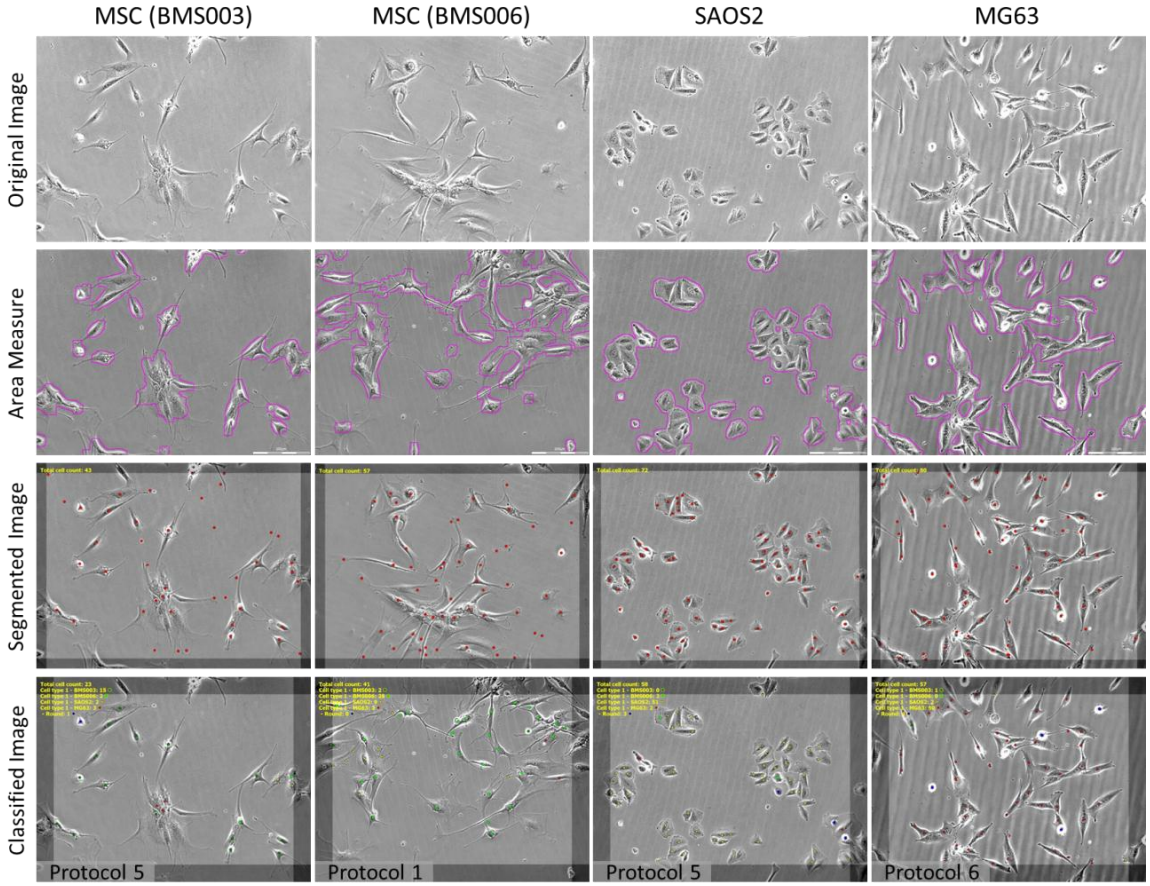

Figure 7.22: Images of cells 48hrs post seeding prior to and after segmentation using Cell-IQ Analyser™.

Images show the development process of the pattern recognition process where original images were collected and then the area of the cells was determined based on threshold analysis. Following this, cell counting with variable parameters and accuracy was performed. Finally, classification of the counted cells was performed.

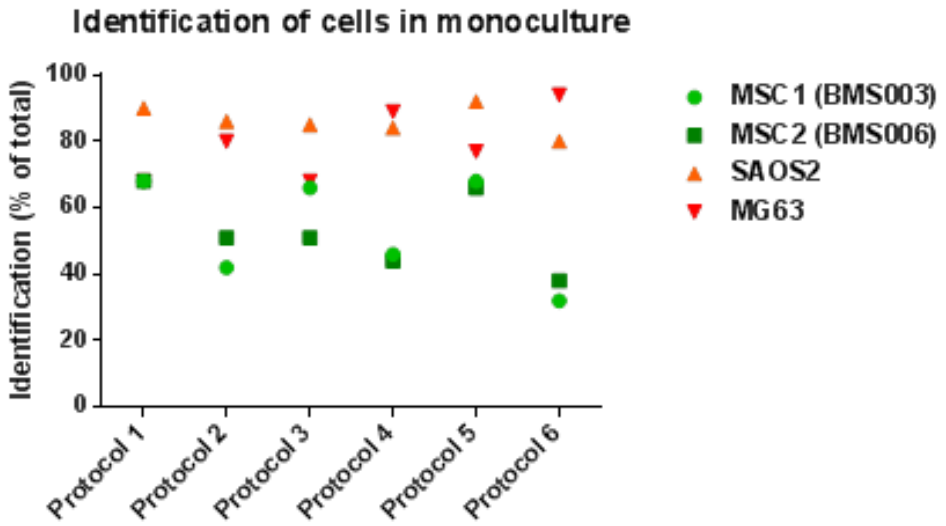

Figure 7.23: Graph showing the percentage of correct identification of cells in monoculture according to different protocols.

During the development of the image recognition algorithm, several protocols were established and tested for their efficiency to recognise and categorise two MSCs, SAOS2 and MG63 cells cultured in monocultures at a single time point. The percentage (%) identification of the cells relative to the total is shown for each protocol and call type.

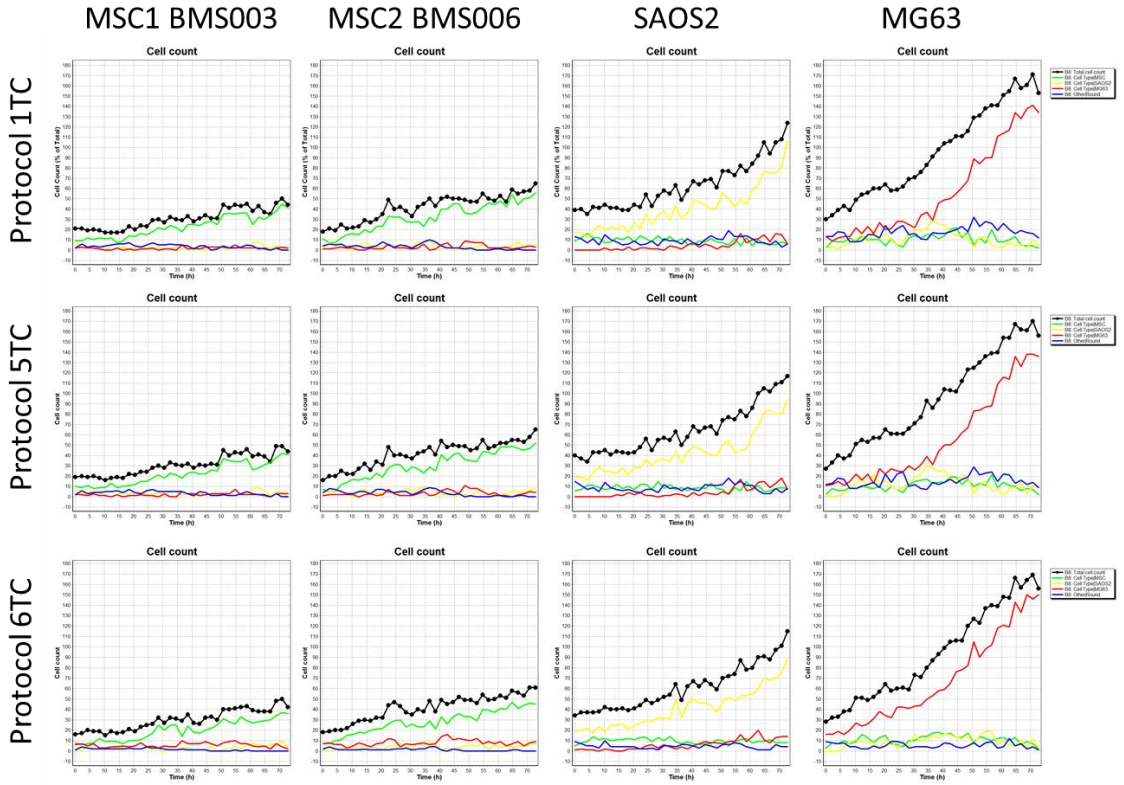

Figure 7.24: Analysis using 1TC, 5TC and 6TC protocols for identification of MSC, SAOS2 and MG63 cells.

Graphs illustrate the efficiency of three protocols to count and classify two MSCs, SAOS2 and MG63 cells over 120hrs of monoculture. The total number of cells (black line), MSCs, (green line), SAOS2 cells (yellow line), MG63 cells (red line) and debris (blue line) are shown within each graph from 0hrs of imaging (left of the graph) through 120hrs of imaging (right of the graph).

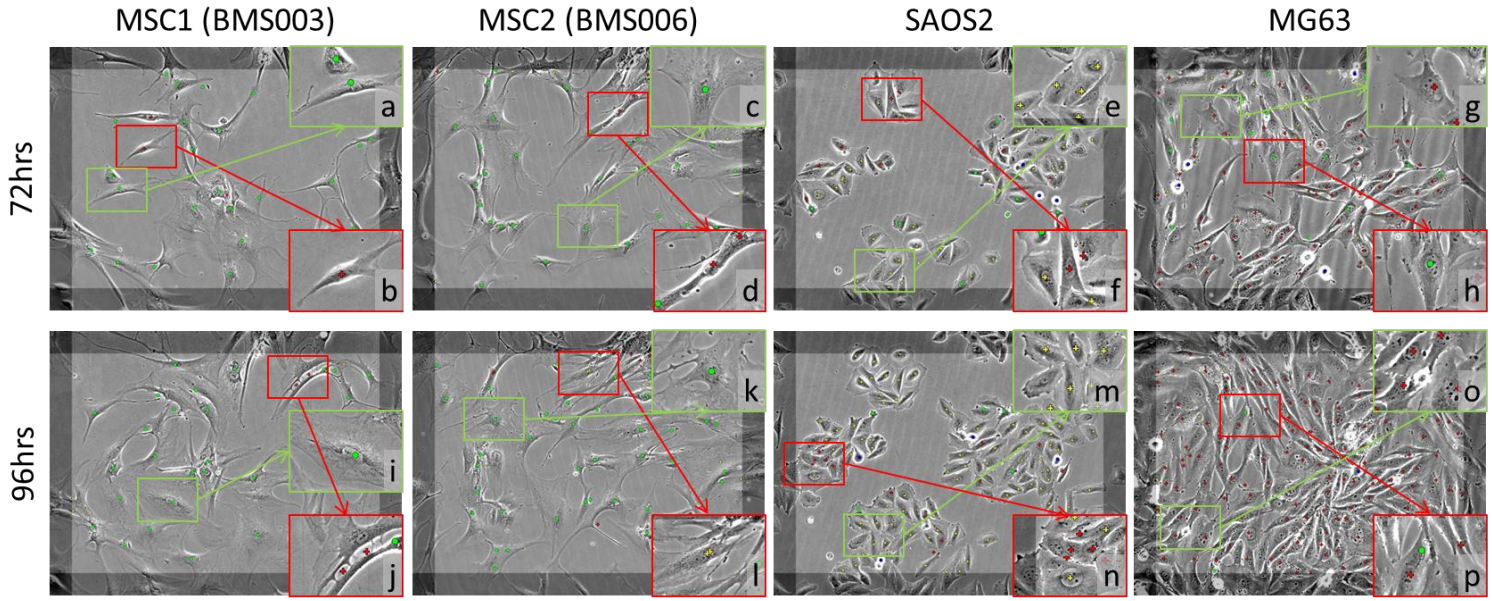

Figure 7.25: Correct and incorrect identification of MSCs, SAOS2 and MG63 cells.

The identification and classification of cells seen in images of MSC1 (left column), MSC2 (second left column), SAOS2 cells (third left column) and MG63 cells (right column) grown in monoculture are shown at 72hrs post seeding (top row) and 96hrs post seeding (bottom row). Inserts highlight cells and areas which have been correctly identified (green box - a, c, e, g, I, k, m, o) according to that cell type, or misidentified (red box - b, d, f, h, j, l, n, p) as an alternative cell type.

7.2.2 Chondrosarcoma diagnosis and treatment

The image in Figure 7.26 A shows a tomogram from a computerised tomography (CT) scan of the patient's upper left humerus. As shown, the tissue within the medullar cavity of the upper left humerus presented with a non-uniform pattern, where bright spots were seen (top arrow). The density of the bone was also seen to be variable above the deltoid tuberosity (bottom arrow). The image in Figure 7.26 B shows a magnetic resonance imaging (MRI) scan. As shown, the suspected lesion was seen as a large dark area (arrow) within the medullar cavity of the left upper proximal humerus. The image in Figure 7.26 C shows a dynamic contrast MRI scan. As shown, the lesion appeared as a large bright area (arrow) within the medullar cavity of the upper left proximal humerus. The lesion was measured by radiologists to be greater than 8.5cm in length. The initial diagnosis was a suspected tumour encased within the bone cavity, without signs of metastasis.

A biopsy of tissue was removed for histological analysis. Histological staining of the biopsy confirmed diagnosis of the tumour as a low grade I chondrosarcoma. Representative images of haematoxylin and eosin (H&E) staining of the cancerous lesion biopsy are shown in Figure 7.27 A-D. Cartilaginous tissues were stained blue with haematoxylin, and bone tissue stained pink with eosin. The lesion was identified and diagnosed as a well differentiated hyaline cartilaginous lesion. The image in Figure 7.27 A shows malignant permeating tumour cells encompassed within the host bony trabeculae (arrow). The image in Figure 7.27 B shows entrapment of host bone by cartilaginous tumour (arrow). The image in Figure 7.27 C shows the formation of a distinctive low cellular enchondromatic nodule (arrow). The image in Figure 7.27 D shows endochondral ossification within areas of the cancerous lesion (bracket and arrow). This appearance was considered consistent with diagnosis as a grade I chondrosarcoma.

The surgical procedure detailing the excision of an infected humerus, irradiation and re-implantation of the post-irradiated humerus packed with bone cement, can be seen in Figure 7.28. As shown, the central section of the humerus (a) was excised from the left arm (b). The tumour was curettaged from the medulla cavity of the excised bone fragment (c). A sample of tumour tissue was taken directly from the curettaged tissue (d). This sample has been referred to as the non-radio sample. A second sample of curettaged tumour tissue (e) and the bone fragment (f) were then treated with a single fraction of 90Gy deep X-ray therapy (DXT). This second sample has been referred to as the post-radio sample. Following irradiation, the bone fragment was packed with non-vascularised bone cement and fixed back into place within the left arm (g). The weight of the non-radio and post-radio therapy treated samples were 0.860g and 1.103g respectively.

H&E staining of the curettage confirmed diagnosis of the tumour as a low grade I chondrosarcoma, shown in Figure 7.29. As shown, the curettaged tissue presented as a well differentiated hyaline cartilaginous lesion. Areas of interest within Figure 7.29 A are highlighted and presented in Figure 7.29 B-D, showing malignant permeating tumour cells encompassed within host bone (Figure 7.29 B), a distinctive low cellular enchondromatic nodule (Figure 7.29 C), and endochondral ossification (Figure 7.29 D).

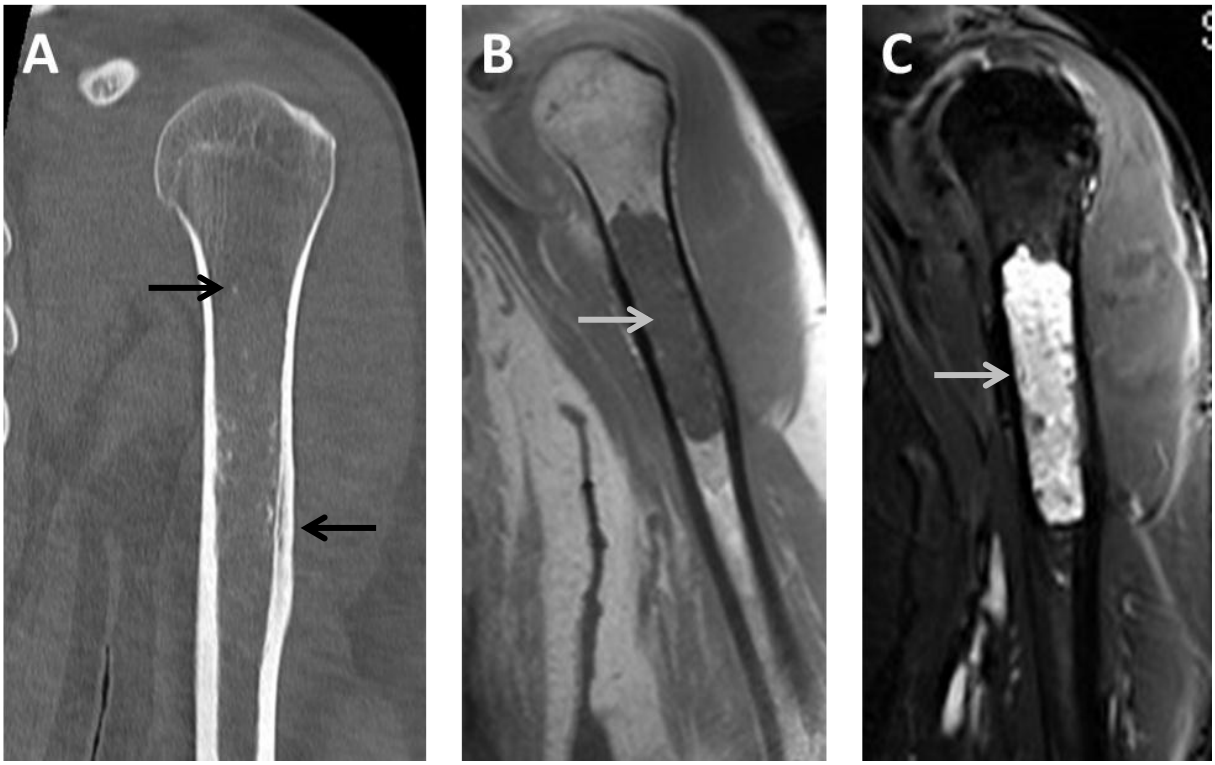

Figure 7.26: Radiological examination identified the chondroid lesion.

Radiological examination by CT (A), MRI (B) and dynamic contrast MRI (C) scans were used to identify the chonroid lesion, and offer a more definitive opinion on how to manage the patient's lesion. The lesion was measured to be greater than 8.5 cm in length and described as a low grade chondrosarcoma contained within the host bone, as indicated by the arrows. Patient's scans were provided by ROH.

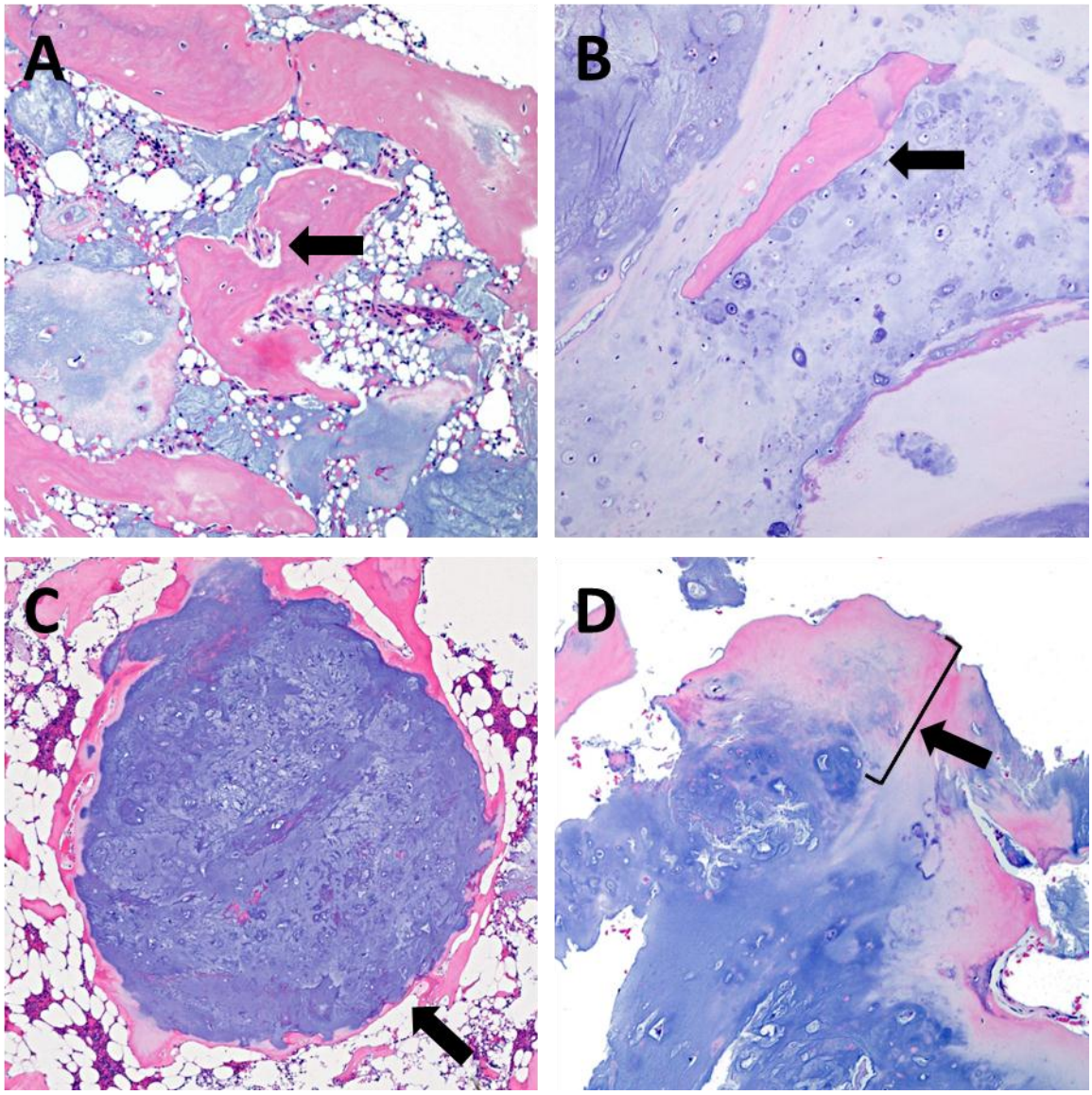

Figure 7.27: Histological analysis of the biopsy diagnosed the chondroid lesion as a low grade I chondrosarcoma.

Biopsy and imaging were consistent with a well differentiated cartilaginous lesion suspected to be a grade I chondrosarcoma. Examination of cartilage stained with haematoxylin (blue) and bone stained with eosin (pink) on sections of the biopsy material shows well differentiated hyaline cartilaginous lesions consisting of (A) malignant permeating tumour cells (arrow) permeating host bony trabeculae (4x), (B) entrapment of host bone by the tumour (10x), (C) distinctive low cellularity enchondromatic nodule formation (4x) and (D) endochondral ossification (10x).

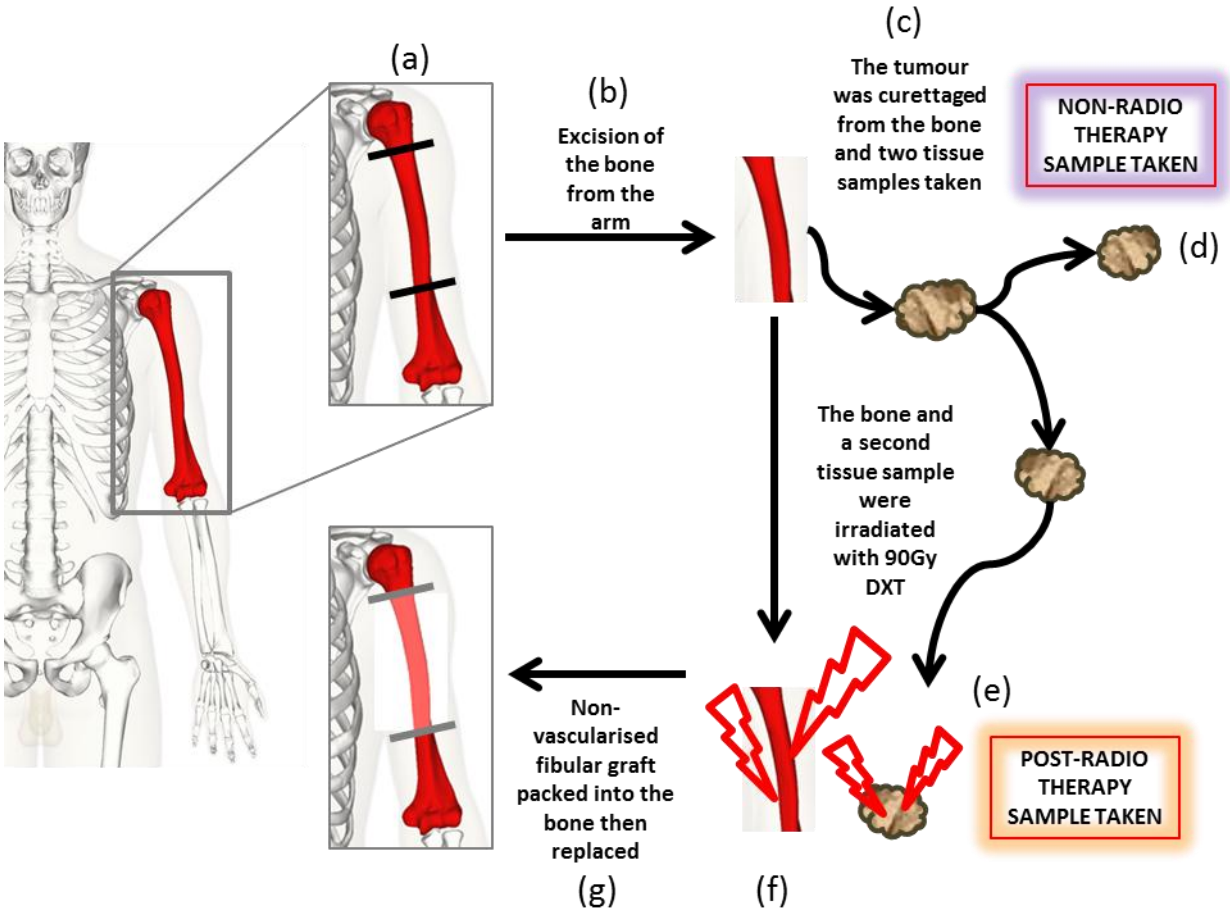

Figure 7.28: A schematic diagram showing the surgical procedure of excision, irradiation and re-implantation.

Clockwise from left. The central section of the humerus (a) was excised from the left arm (b) and the tumour was curettaged from the medulla cavity of the excised bone fragment (c). A sample of tumour tissue was taken from the curettaged fragment (d). This sample is referred to as the non-radio therapy sample. The bone fragment and another sample of tumour tissue were treated with a single fraction of 90Gy deep X-ray therapy (DXT) (e-f). This sample is referred to as the post-radio therapy sample. Following irradiation, the bone fragment was packed with non-vascularised bone cement and fixed back into place (g). Image adapted from www.lifesciencedb.jp

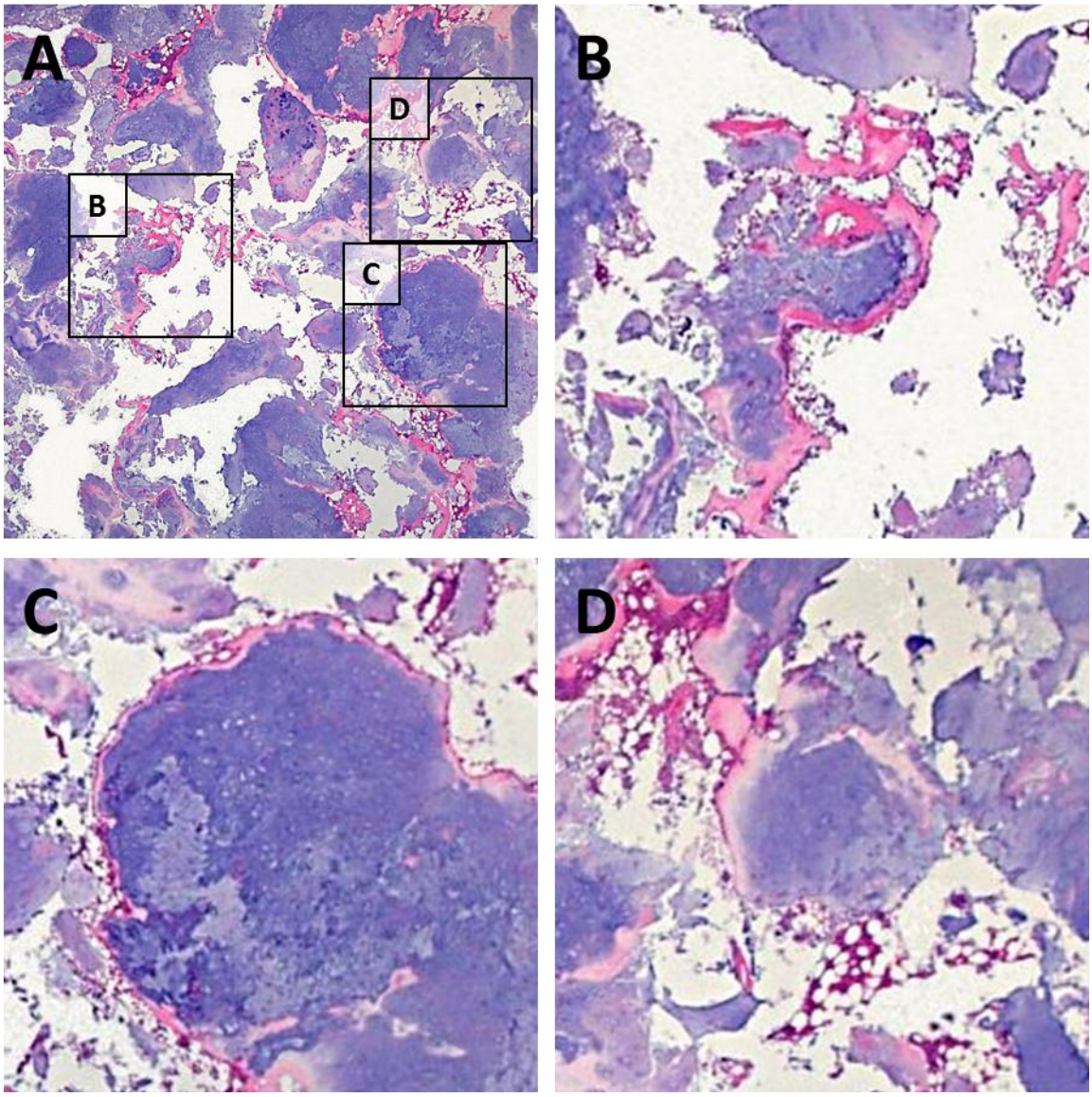

Figure 7.29: Histological analysis of the curettaged chondrosarcoma confirmed diagnosis and showed similar histological material to the pre-operative biopsy.

Examination of cartilage stained with haematoxylin (blue) and bone stained with eosin (pink) on (A) a curettage chondrosarcoma section (2x) show well differentiated hyaline cartilaginous lesions consisting of (B) malignant permeating tumour cells, (C) a low cellularity enchondromatic nodule and (D) minor endochondral ossification. Images B-D are 3.2x magnified insets from image A.

7.2.3 Manual cell lineage tracking of MSCs, SAOS2 and MG63 cells distinguishes donor to donor variability, as well as distinguishes between cell types

Data obtained from the Manual Lineage Tracking is shown in Figure 7.30 where the average divisions (A), trajectory length (B) and speed via trajectory (C) are presented for each cell type, specifically detailing the patient to patient and sample variability of 5 primary human MSCs, SAOS2, MG63 and CS cells. It can be seen that MG63 cells divided most compared to the other cell types (A); two of the five MSCs and MG63 cells migrated the furthest with high trajectory lengths (B) and these same samples had the greatest speed via trajectory.

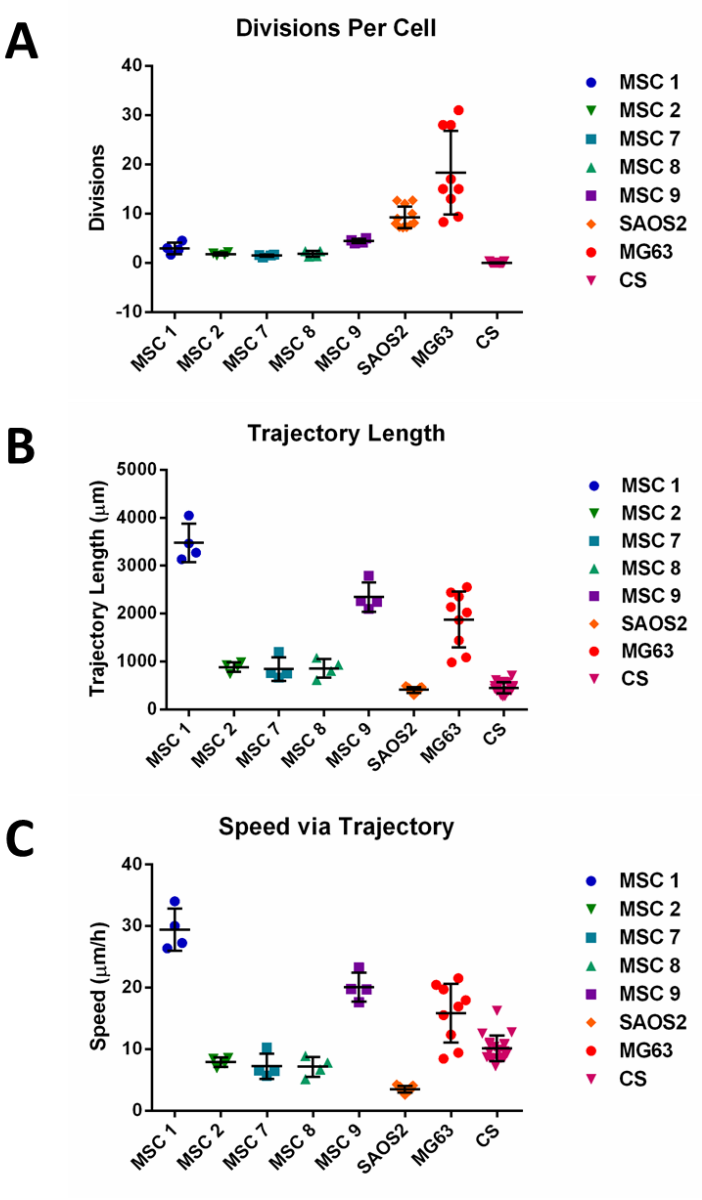

Figure 7.30: Manual cell lineage tracking of live-cells distinguishes between five primary human MSCs, SAOS2, MG63 and chondrosarcoma derived cells based on the average number of cell divisions, trajectory length and speed via trajectory.

Cells from five human MSCs, SAOS2, MG63 and CS cells were tracked with the Manual Cell Lineage tracking tool. The average number of divisions, trajectory length and speed via trajectory were recorded and reported. Data shown for all call types are mean ± SD since individual donor measurements are shown. SAOS2 and MG63 cell data are from n=3 independent experiments. CS data are from n=1 sample, imaged and analysed over n=3 independent experiments.

7.3 Chapter 5: Supplementary figures and data

7.3.1 Donor to donor variability response to BEZ, MPA, VPA, BAP and V-BAP treatments according to MTT assay

Within the MSC cultures, marked donor to donor variation in response to the treatments were seen (Figure 7.31) where; BEZ inhibited the growth of MSC8 cells more than other MSCs; MPA enhanced cell growth of MSC1 and MSC9 cells, whilst inhibiting MSC7 and MSC8 cells, with little effect to MSC2 cells; whilst VPA inhibited MSC8 cells and enhancing the cell growth of MSC2 cells.

In terms of combined treatment effects on the MSCs, similar donor to donor variability was seen (Figure 7.32); yet, viability of all MSCs decreased at the highest concentration of BAP and V-BAP. However, four of five MSCs (MSC1, MSC2, MSC7, and MSC9) remained viable ≥85% following treatment with ≤[0.5mM/5.0µM] BAP and ≤[0.5mM/5.0µM/0.6mM] V-BAP. The viability of MSC8 was similar to that of SAOS2 and MG63 cells.

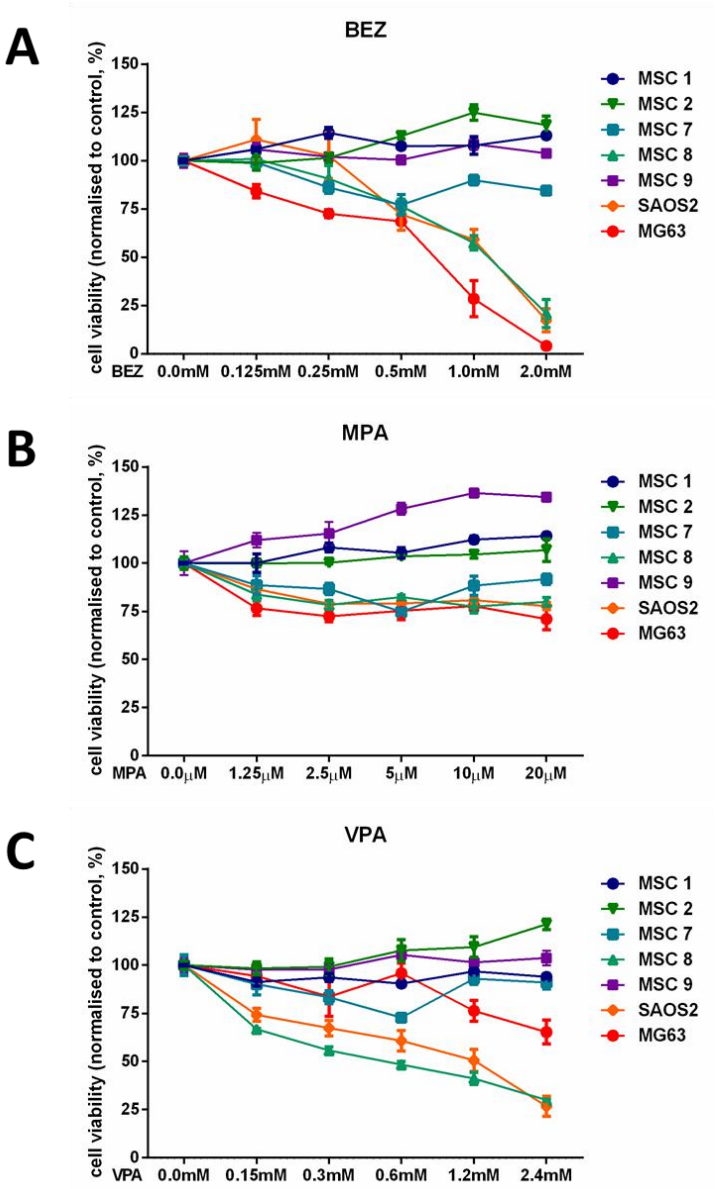

Figure 7.31: BEZ, MPA and VPA affected the viability of five primary human MSCs, SAOS2 and MG63 cells in a concentration-dependent manner according to MTT assay.

The cell viability normalised to the percentage of the carrier-alone control is shown. Five human MSCs, SAOS2 and MG63 osteosarcoma cell lines were treated for 5 days with two-fold increasing doses of BEZ (A), MPA (B) or VPA (C). Cells were seeded and assayed in triplicate wells. MSC data shown are mean ± SD since individual donor measurements are shown. Osteosarcoma data shown are mean ± SEM from n=3 independent experiments.

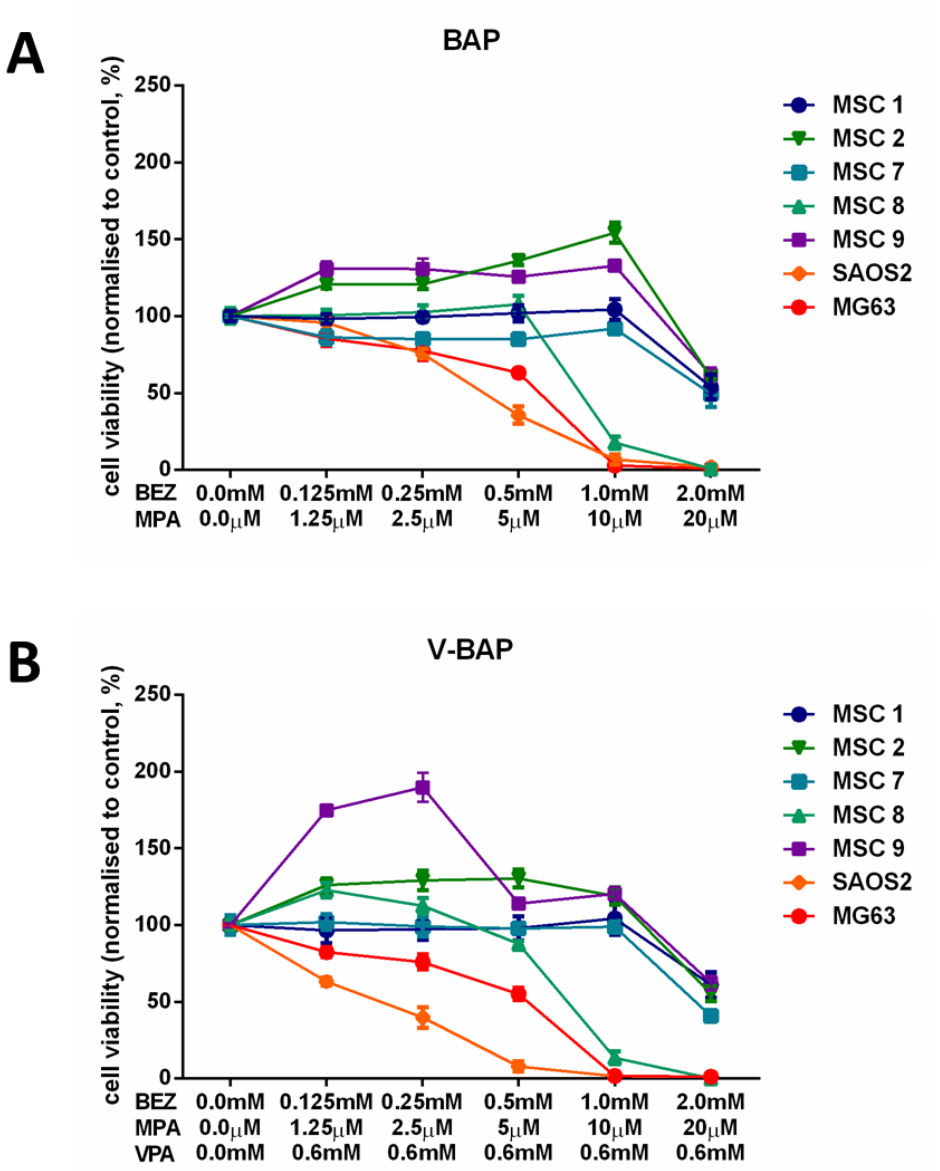

Figure 7.32: BAP and V-BAP affected the viability of five primary human MSCs, SAOS2 and MG63 cells in a concentration-dependent manner according to MTT assay.

The cell viability normalised to the percentage of the carrier-alone control is shown. Five human MSCs, SAOS2 and MG63 osteosarcoma cell lines were treated for 5 days with two-fold increasing doses of BAP (A) or V-BAP (B). Cells were seeded and assayed in triplicate wells. MSC data shown are mean ± SD since individual donor measurements are shown. Osteosarcoma data shown are mean ± SEM from n=4 independent experiments.

7.4 Digital content on accompanying DVD

#1 Live-Cell Imaging Protocols: Cell-IQ live-cell imaging Cell Finder protocols used in Chapter 4 for counting and classifying MSCs, SAOSs, MG63 and CS cells.

#2 Live-Cell Imaging Videos:

#2.1 Cell-IQ Original Images: Videos of original ROI images showing the culture expansion of MSCs, SAOS2 and MG63 cells prior to analysis obtained using the Cell-IQ live-cell imaging platform.

#2.2 Cell-IQ Area Measure tool: Videos of the above ROIs of culture expanded MSCs, SAOS2 and MG63 cells following analysis with the Cell-IQ Area Measure tool.

#2.3 Cell-IQ Cell Finder tool: Videos of ROIs of culture expanded MSCs, SAOS2 and MG63 cells following analysis and classification with the Cell-IQ Cell Finder tool used during the protocol development process detailed in Appendix 7.2.1.

#2.4 Cell-IQ Imaging of CS cells: Videos of ROIs of culture expanded CS cells following passage.

#2.5 Cell-IQ Imaging of Control and V-BAP treatments: Videos of ROIs of culture expanded MSCs, SAOS2 and MG63 cells following culture in control and V-BAP culture conditions.